# THE REGULATION OF THE SERUM RESPONSE NETWORK BY THE RGS-RHOGEFS IS CRITICAL FOR YAP1 ACTIVITY AND CELL FATE DECISIONS

Brandon S. Lane

Submitted to the faculty of the University Graduate School
in partial fulfillment of the requirements
for the degree
Doctor of Philosophy
in the Department of Biochemistry and Molecular Biology,
Indiana University
July 2017

Accepted by the Graduate Faculty, of Indiana University, in partial fulfillment of the requirements for the degree of Doctor of Philosophy.

Clark D. Wells, Ph.D., Chair

Doctoral Committee

Theresa Guise, M.D.

Lindsey D. Mayo, Ph.D.

November 17, 2016

Lawrence Quilliam, Ph.D.

## DEDICATION

I dedicate this dissertation to my family, especially my parents, Susan R. Lane and Randal S. Lane, as they valued my education and pushed me to strive for perfection during my academic career. I would also like to dedicate this dissertation to my close friends, Tim Rayne, Kate Ruddell, Michael Vinci, Mikal Coppage, Kristen Holcomb, Brittany Cardinal, Lauren Bringman, Nick Renier and Jessica Vogel. None of this would have been possible without their support, adventurous spirits, companionship, and the dedication they showed in their own line of work. They are all truly inspirational in their own right and I thank them for being supportive through the good, the bad and the ugly. However to be frank, they also contributed to prolonging my stay, by my estimation, for an extra year or two.

## ACKNOWLEDGMENTS

I would first and foremost like to thank my mentor Dr. Clark D. Wells. He allowed me to pursue my own independent project, and pushed me to ask the necessary and tough questions to see it through. He further instilled in me a scientific acumen that was second to none. His dedication to my success over the past 6 years was paramount to my success in this program and to all my future endeavors. For that I am forever grateful.

I would also like to thank my committee members Dr. Lindsey Mayo, Dr. Theresa Guise, and Dr. Lawrence Quilliam, as they all provided valuable feedback both scientifically and professionally, and unwavering support throughout this entire process. I would especially like to thank Dr. Lawrence Quilliam, for being our lab neighbor, and always engaging in strong scientific discussions both experimentally and conceptually. His scientific knowledge was extremely valuable to my success as I often consulted with him about new ideas and he always provided insightful feedback.

When I first began in the lab of Dr. Clark Wells, Dr. Lauren Bringman also began at the same time. Through our struggles becoming accustomed to the rigors of graduate school, we developed a life-long bond of friendship. She has seen me at my highs and lows throughout this process, as I have with her. It is that shared struggle that pushed me to finish this project, and for that I thank her.

I would also like to thank my close friends Dr. Tom Baird, Dr. Sara Young, and Dr. Aarti Chawla. They also shared in my struggles and achievements, and were invaluable sources to bounce scientific ideas off of over occasional beers. To all of you I would like to say one final THANK YOU!

And finally I would like to say thank you to the entire office staff of the Department of Biochemistry and Molecular Biology. They were always helpful in circumventing our IT problems, scheduling classes, and ordering reagents. Without them much of the nuisances of graduate school would not be possible. Thank you all for your time and patience.

Brandon S. Lane

THE REGULATION OF THE SERUM RESPONSE NETWORK BY THE RGS-RHOGEFS IS CRITICAL FOR YAP1 ACTIVITY AND CELL FATE DECISIONS

The growth of mammary epithelial cells is regulated by interactions with neighboring cells and by exposure to soluble factors including hormones and growth factors. These cues are integrated within the cell, perpetuating changes onto the organization of the actin cytoskeleton, resulting in altered transcriptional programs. Rho family GTPases regulates actin dynamics that facilitate transcriptional reprogramming. In particular, RhoA induces the formation of actin stress fibers to promote the transcriptional co-activator YAP1 to translocate from the cytosol into the nucleus. There, it co-activates TEAD family transcription factors to drive the expression of pro-growth and survival genes. Rho family members are activated by guanine exchange factors (GEF) and inhibited by GTPase activating proteins (GAP). Here, we determined the relative effects of expression of 67 RhoGEFs and RhoGAPs on the activation of TEAD. This revealed that regulator of G-protein signaling (RGS) domain containing ArhGEF1, ArhGEF11 and ArhGEF12 all promoted YAP1 dependent activation of TEAD. These RhoGEFs mediate signaling from heptahelical receptors that are stimulated by lipid mitogens to activate the heterotrimeric G-proteins $G\alpha_{12}$ and $G\alpha_{13}$. Consistently, loss of expression of ArhGEF12 and to a lesser degree ArhGEF11 prevented actin stress fiber accumulation and activation of YAP1 mediated signaling by serum. Conversely, several complementary experiments revealed that ArhGEF1 dominantly limits $G\alpha_{13}$ selective activation of YAP1 and the mitogen activated protein kinase (MAPK) cascades. Furthermore excessive $G\alpha_{13}$ activity results in both high levels of filamentous actin and

arrest cells in the $G_{1/0}$ phase of the cell cycle. This is likely due to the systemic inhibition of cell cycle promoting signaling and a loss of protein translation. Further, YAP1 was found to be essential for the survival of ArhGEF1 silenced cells. Together, these studies define a circuit whereby the rgRhoGEFs regulate $G\alpha_{12/13}$-RhoA signaling flux to regulate cellular growth that is promoted by serum factors.

Clark D. Wells, Ph.D., Chair

## TABLE OF CONTENTS

## LIST OF FIGURES

## LIST OF ABBREVIATIONS

| | |
|---|---|
| AJ | Adherens junctions |
| Amot | Angiomotin |
| Amot130 | 130KDa Amot protein product |
| ARG1 | ArhGEF1 |
| ARG11 | ArhGEF11 |
| ARG12 | ArhGEF12 |
| ATCC | American Type Culture Collection |
| BCA | Bicinchoninic acid |
| CDC42 | Cell Division Control protein 42 |
| cDNA | Complimentary DNA |
| Crb | Crumb |
| CTGF | Connective tissue growth factor |
| Cyr61 | Cysteine-rich angiogenic inducer 61 |
| DAPI | 4', 6 diamidino 2 phenylindole |
| DH | dbl homology domain |
| DMEM | Dulbecco's Modified Eagle Medium |
| E2 | Estradiol |
| EGF | Epidermal growth factor |
| EGFR | Epidermal growth factor receptor |
| Elk1 | Ets-like gene 1 |
| ER | Estrogen receptor |
| ERK | Extracellular signal-regulated kinase |
| FBS | Fetal bovine serum |
| GAP | GTPase Activating Protein |
| GEF | Guanine nucleotide exchange factor |
| GPCR | G-Protein Coupled Receptors |
| Grb2 | Growth factor receptor-bound protein 2 |
| GTP | Guanosine triphosphate |
| Her2 | Human Epidermal Growth Factor Receptor 2 |
| IDC | Invasive ductal carcinoma |
| LPA | Lysophosphatidic acid |
| Lats | Large tumor suppressor |
| lrECM | Laminin-rich extracellular matrix |
| MAPK | Mitogen-activated protein kinase |
| MEK | MAPK/ERK kinase |
| Mst | Mammalian STE20-like protein kinase |
| PALS1 | Protein associated with Lin Seven 1 |
| PAR | Protease activated receptor |
| PAR3 | Partitioning defective 3 |
| PAR6 | Partitioning defective 6 |
| PATJ | PALS1-associated tight junction protein |
| PBS | Phosphate buffered saline |
| PCNA | Proliferating cell nuclear antigen |
| PDZ | Post-synaptic density, Discs large, Zonula occludens |

| | |
|---|---|
| PEI | Polyethylenimine |
| PR | Progesterone receptor |
| PTEN | Phosphatase and tensin homolog |
| qRTPCR | Quantitative real time polymerase chain reaction |
| Rac1 | Ras-related C3 Botulinum toxin substrate 1 |
| Ras | Rat sarcoma |
| RGS | Regulator of G-protein Signaling |
| RIPA | Radioimmunoprecipitation assay buffer |
| RT | Reverse transcriptase |
| RTK | Receptor tyrosine kinase |
| SDS-PAGE | Sodium-dodecyl sulfate polyacrylamide gel electrophoresis |
| SH2 | Src Homology 2 |
| SOS | Son of sevenless |
| S1P | Sphingosine-1-phosphate |
| SRF | Serum response factor |
| STAT | Signal transducers and activators of transcription |
| Taz | Transcriptional co-activator with PDZ-binding motif |
| TEAD | Tea-domain |
| TEAD | TEA-domain containing |
| TGF | Transforming growth factor |
| TJ | Tight junction |
| Yap | Yes-associated protein |
| ZO1 | Zona occluden 1 |
| ZONAB | ZO-1-associated nucleic acid binding protein |

# CHAPTER 1. INTRODUCTION

## 1.1 Organization of the Mammary Organ and the Origins of Breast Cancer

The growth of living organisms is dictated by the availability of nutrients as well as interactions with the surrounding environment. The responses to these factors exists along a continuum from the macroscopic level, the world with which we live, down to the microscopic level, the world with which our cells are maintained in the human body. The human body maintains inherent growth control via mechanisms that are both biochemical or biophysical in nature (1). Malfunctions in the ability to sense alterations in biochemical cues or changes in tissue architecture, is a major contributor to the development of diseases such as cancer (1). The mammary gland is prime example of how biochemical and biophysical signals dictate tissue homeostasis. The structure of the mammary organ changes throughout the life cycle of a female and is mediated by remodeling events that are induced by temporal hormonal activity (2). These continued alterations in growth control mechanism make this organ highly susceptible to the development of hyperplastic growth. This makes studying normal and cancerous mammary cell lines an ideal model for studying signaling mechanisms that regulate cellular growth control.

The mammary organ remains relatively naïve in structure and function during prepubescent growth, whereas it undergoes drastic remodeling events during puberty, pregnancy, lactation, and menopause (3). These events require the reorganization of the tissue, which is orchestrated by changes in cellular size, location and growth patterns (4). The mature mammary organ is composed of support tissues and glandular epithelium. The supporting material is comprised of adipose tissue, blood vessels, and underlying pectoral muscles. The glandular tissue secretes and transports milk to support the growth

of a mother's offspring. The development of glandular tissue begins during puberty and becomes fully functional during lactation. The continued remodeling of the glandular tissue and its composition makes it susceptible to perturbations that may result in unwarranted hyperplasia (4).

Post pubescent but pre menopausal mammary glandular tissue contains a network of hollow tubes that facilitate the secretion and movement of milk during lactation. These tubes are organized into 10-20 lobules that are comprised of 10-100 alveoli structures (5). Each lobule has a hollow duct; termed the lactiferous duct that drains the secreted milk into the opening of the nipple. The ducts and lobules are surrounded by a layer of myoepithelial cells, which upon stimulation by the hormone oxytocin, contract. The consequent squeezing of the epithelial cell layer promotes milk flow through the lumens of the lobules and lactiferous ducts (6). The structural component of lactiferous ducts and lobule trees are the mammary cuboidal epithelial cells. Mammary cuboidal epithelial cells are asymmetrically organized into a baso-lateral domain and an apical domain. The baso-lateral domain facilitates attachment to the basement membrane and neighboring cells (2). The apical domain facilitates milk secretion consistent with it facing the hollow lumen of the ducts and lobules. The asymmetric organization of mammary epithelial cells is not only essential to maintain proper structure and function of both the ducts and lobules, it also fundamentally acts to prevent unwanted growth (2). Ductal epithelial cells are overwhelming the origin of breast cancers as perturbations in the organization of this cell type elicits pro-growth effects (Figure 1-1A).

Hyperplasia's that arise from the epithelial cells that line the lactiferous ductal structure can be either invasive or non-invasive. Non-invasive hyperplasia and its more

advanced form, diagnosed as ductal carcinoma in situ (DCIS) are considered pre-cancerous due to the lack of cells that have infiltrated the surrounding supporting tissue (7). DCIS is characteristic of the mammary epithelial cells severing attachments with the basement membrane and actively proliferating into the hollow lumen of the lactiferous duct. Once the cells break through the underlying basement membrane, they are considered cancerous, as they invade into the surrounding supporting stroma. This phenotype is diagnosed as invasive ductal carcinoma (IDC) (7). These cells can then infiltrate supporting blood and lymph vessels to metastasize throughout the body (Figure 1-2A). Such spreading is the primary cause of patient mortality.

Breast cancer is the second leading cause of cancer related deaths among women. According to the American Cancer Society. In the United States it is expected that roughly 300,000 new cases of breast cancer will be diagnosed in 2016. Of these cases, 60,000 will be classified as pre-cancerous DCIS, while 240,000 will be classified as IDC. DCIS is considered the lowest malignant type of tumor (Stage I) with an expected 5-year relative survival rate of nearly 100%. As the disease progresses to Stages II-IV, it is based upon acquiring an IDC phenotype. The expected five year relative survival rate declines with each successive stage: 93%, 72%, and 22%, respectively. It is therefore essential to understand the mechanisms by which mammary epithelial cells transition into growth activating states of DCIS and then through increasing grades of IDC.

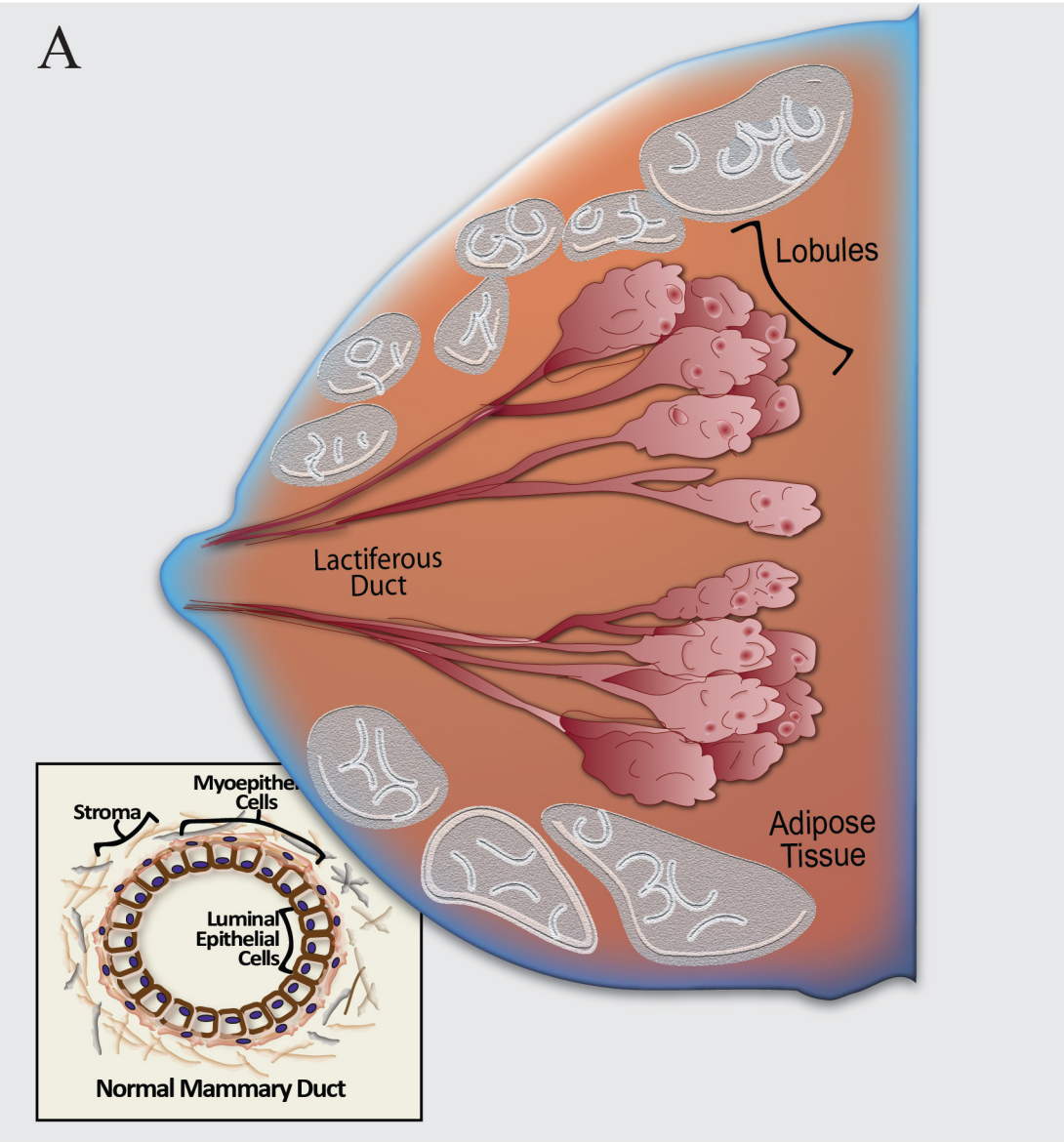


**Figure 1-1: Structure of the Mammary Organ**.

**A.** The breast is composed of supporting and functional tissue. The supporting tissue is comprised of adipose tissue, stroma and a network of connective tissue. The lactiferous duct and lobules comprise the functional tissue that facilitates the secretion and transportation of milk. The subset (lower left) is a cross-sectional view of a lactiferous duct. The lactiferous duct is made up of cuboidal mammary epithelial cells and surrounded by supporting myoepithelial cells and underlying stroma. These cells give rise to the structure and secretory function of lactiferous duct. (Figure Adapted from J. Adler).

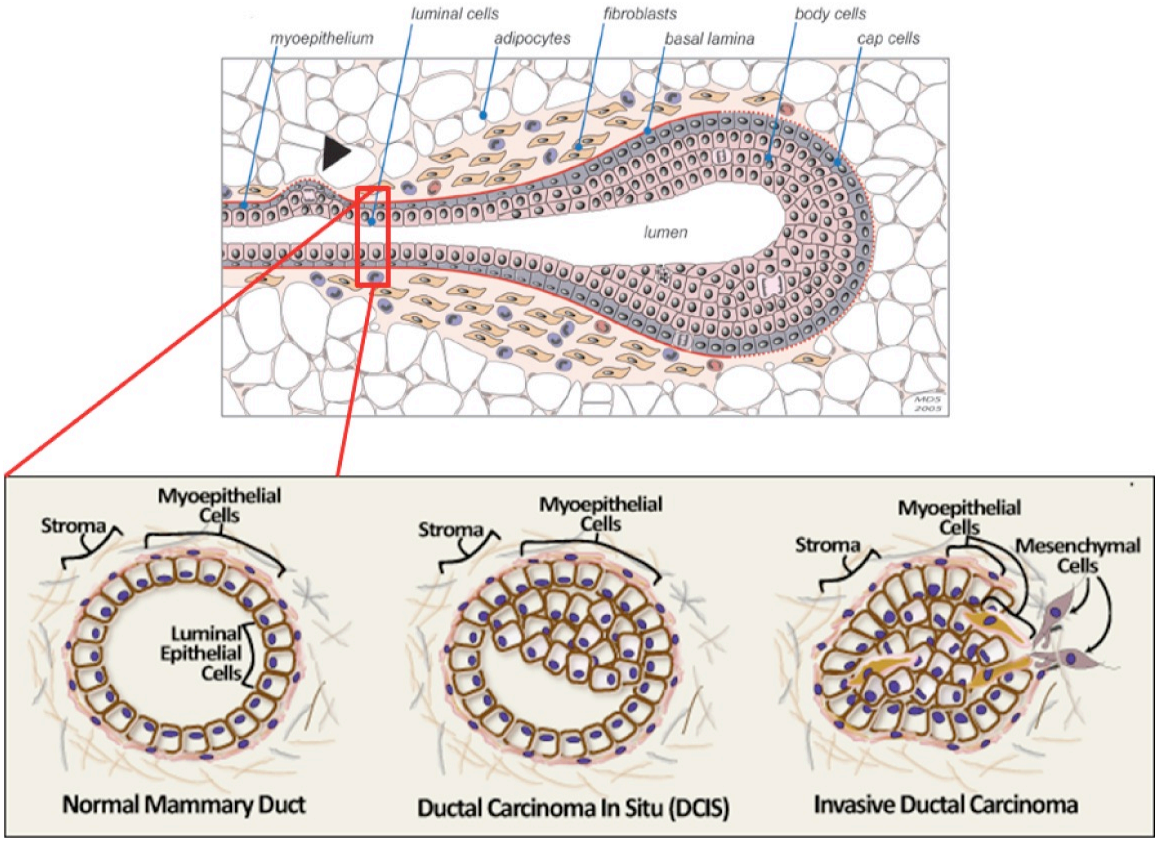


**Figure 1-2: Progression of Invasive Ductal Carcinoma in Breast.**

Representation of a "normal" mammary duct and the supporting cells and stroma (above). Below is a cross-sectional reference that highlights the progression of cancer within the ductal system. In normal mammary ducts, epithelial cells are growth arrested through contact-dependent growth inhibition providing a barrier between the hollow lumen and surround stromal tissue. The development of ductal carcinoma in situ (DCIS) results in the loss of contact inhibition of growth and the proliferation of cells into the hollow lumen. Advancement of this precancerous state to a cancerous state involves the proliferating epithelial cells penetrating the basement membrane; this is termed invasive ductal carcinoma (IDC). (Figure Adapted from W.Ranahan).

## 1.2 Cell Cycle Regulation in Epithelial Cells is Dependent on Biochemical and Biophysical Stimuli

Normal mammalian epithelial cells can either be actively proliferating, held in a non-proliferative state that is readily induced to proliferate (quiescence), or terminally differentiated. Mammalian cells actively grow when nutrients and space to grow are plentiful, otherwise they arrest at the "restriction point (8)." Studies of a variety of cell types, highlight the lack of nutrients causes cells to enter a quiescent state, and the subsequent re-introduction to those nutrients, enhances DNA synthesis (9-12) and induces synchronized growth, as measured by thymidine incorporation, and cell division (10). If cells experience prolonged stress, such as extended periods without essential nutrients, they are unable to exit the restriction point through an unidirectional extension of quiescence known as senescence (13). Differentiated epithelial cells also, typically, do not exit the restriction point as long as interactions with the surrounding environment reinforce this state. Cancers cells, by circumventing these mechanisms for growth control, are able to exit a normal restriction point and progress through the cell cycle (8).

The "cell cycle" describes the process whereby eukaryotic cells duplicate their genomes and separate into two daughter cells (14). In eukaryotes, the cell cycle is a product of three temporal periods: interphase, mitosis, and cytokinesis. During early interphase the cell actively acquires nutrients and carries out protein synthesis to grow in size while concurrently facilitating normal functions. This also prepares it for duplication of its genome during late interphase. Interphase is comprised of three unidirectional stages that are monitored by checkpoints to ensure their integrity. The initial stage of interphase is called Gap 1 ($G_1$). During $G_1$ the cell acquires nutrients and produces the

protein machinery necessary for undertaking DNA replication (9-12). The second stage of interphase is Synthesis (S), during which the cell duplicates its entire genome. The final stage of interphase is Gap 2 ($G_2$). During $G_2$ the cell checks the integrity of the replicated genome and produces lipids and proteins that are necessary for mitosis. During mitosis the duplicated cellular genome condenses into sister chromatids, which following their separation into sister chromosomes, are transported to opposite ends of the dividing cell. Cell division commences during cytokinesis, which creates two daughter cells with replicate, semi-conserved genomes. The cell then either initiates another round of the cell cycle or it exits the cell cycle and enters dormancy, this is considered $G_0$. In normal cells improper duplication of the genome or division of the cell is sensed by specific checkpoints that pause mitosis and initiate corrective measures (15, 16). If these measures cannot restore integrity, cell clearing is initiated through various forms of cell death. Cancer cells often acquire mutations that override integrity checkpoints to evade cell death and to facilitate cell growth (16).

Cell cycle activity is regulated by a variety of proteins that monitor the integrity of the duplicating genome (14). Principle amongst these are the cyclins whose expression and subsequent degradation oscillate with the stages of the cell cycle (Figure 1-3A) (17). In mammals 16 cyclins either control the progression through the cell cycle or have independent roles in regulating transcription, DNA repair, promoting differentiation or apoptosis. Cyclins contain a cyclin box domain that signals their destruction upon phosphorylation by members of the cyclin-dependent kinases (Cdk) family. Exit from $G_0$ requires at least one of the three D-type cyclins (18) to be stabilized in response to the presence of nutrients (14). This allows D-type cyclins to associate with the cyclin-

dependent kinases (Cdk) 4 or 6 to couple them to hyper-phosphorylate Retinoblastoma tumor suppressive protein (Rb) (19). This prevents Rb from interacting and inhibiting members of the E2F family of transcription factors. This further allows E2F proteins to activate genes involved in DNA synthesis and cell cycle progression, including E, and A-type cyclins. The inhibition of Rb by cyclin D-Cdk4/6 protein complexes is essential for cells to by-pass multiple restriction points and thereby progress into S, $G_2$, and M phase. E-type cyclins are required for $G_1$ to S phase transition (20), where their transcription in response to E2F activity increases at mid $G_1$ phase and is maintained through the middle of S phase (21). E2F activity also promotes the transcription of A-type cyclins (21), when associated with Cdk2 and mediates the entry of the cell into S-phase. During latter stages of S phase, A-type cyclins associate with Cdk1 to facilitate S phase completion (22, 23) and the transition into mitosis. Finally, B-type cyclins associate with Cdk1 and are required for $G_2$ exit (Figure 1-3B) (24). The regulation of these cyclin complexes by both biochemical and biophysical stimuli thereby controls the growth of normal mammary epithelial cells.

The activity of the cell cycle of mammary epithelial cells is highly impacted by the relative level of attachment of a cell to neighboring cells versus the basement membrane. Many lines of evidence conclusively show that non-transformed cells experience growth inhibition when they contact other cells (25). This underlies the ability of mammary epithelial cells to form the highly organized structures in a gland. Contact-dependent growth inhibition occurs when cells fill a space and therefore physically associate with other cells at all lateral points (26). Early studies on murine fibroblasts in culture identified this as the “saturation point”; where DNA synthesis and cell division

are drastically reduced (27). These cells have exited the cell cycle and remain in the $G_0$ phase. However, these cells can readily re-enter the cell cycle if their microenvironment changes in a way that unoccupied adjacent space becomes available, e.g. a confluent cell culture is subject to a "wound" (27). Subsequent studies have identified the molecular mechanism by which cell polarity proteins restrict cell growth in response to intercellular contact.

The asymmetric organization of epithelial cells can fundamentally repress cell cycle progression (28). Differentiated epithelial cells form a lumen facing apical domain and baso-lateral domain that is attached to the basement membrane. The PAR and Crumbs polarity complexes localize to and establish the apical domain (29). The Scribble protein complex distributes to and establishes the baso-lateral domain (30). Within the baso-lateral domain, the Scribble complex recruits machineries that effect cell-cell and cell-extracellular matrix interactions, many of which directly regulate key components of the cell cycle (31). Several junctional complexes connect cells from the apical to basal axis. The tight junction, which is composed of a belt of transmembrane strand proteins, is the most apical junction (32). The tight junction both acts as a fence to prevent diffusion between the apical and basal membranes as well as a permeability barrier between cells (32). The adherence junction, which lies below the tight junction, is mainly comprised of the cadherin-catenin protein complexes (33). The adherence junction provides the majority of the mechanical strength that keeps cells attached to each other (34). Both the tight junction and the adherence junction scaffold proteins on their cytosolic faces that bind the actin cytoskeleton. This produces isotension across the cell and tissue that is essential to maintain overall structural integrity. Furthermore the loss of

these junctions releases pro-growth transcription factors that are otherwise sequestered there. For instance, beta-catenin binds to E-Cadherin in the adherens junction. The breakdown of the adherens junction causes β-Catenin to release from E-Cadherin and enter the cytosol. If β-Catenin is not degraded, its accumulation results in its translocation into the nucleus where it trans-activates lymphoid enhancing factors (LEF-1-4) (35). This activates LEF-1 dependent transcription of many pro-growth genes including Cyclin D1 which is a master regulator of cellular proliferation (36). Tight-junctions are mainly comprised of the transmembrane claudins, which form strands that encircle the cell and also contain other transmembrane proteins including occludins, junctional adhesion molecules and Nectins. These transmembrane proteins bind their counterparts on neighboring cells to form a seal between cells that prevents paracellular diffusion (32). The zona occludin family of tight junction associated proteins, bind to the cytosolic domain of the claudins and to the actin cytoskeleton. The formation of tight junctions is well established to inhibit Cyclin D1, to prevent a $G_1$-to-S phase cell cycle transition (37, 38). This is only one of many known examples whereby intercellular interactions mediate extracellular to intracellular signaling cascades that control cell cycle progression.

Regulation of cell cycle progression by biophysical stimuli is likely secondary to biochemical stimuli. The cell needs large quantities of macronutrients to facilitate doubling in size. Not only does it have to duplicate its entire genome it also must duplicate a vast majority of cellular organelles and its lipid bilayer. This requires a spike in translation to facilitate protein synthesis that mediates many of these processes (11). In studies of cells at high density, growth restriction was released when the system was flooded with serum or amino acids (8). This suggests that nutrient availability is a

dominant regulator of cell cycle progression. In addition, potent mitogens in serum by activating intracellular kinase cascades promote Cyclin D1 transcription and other proteins that regulate progression through the cell cycle.

The loss of cell-cycle checkpoints that prevent the transition from $G_1$ to S phase, often results in hyperplastic cell growth and eventually cancers. For instance, DNA translocations that activate the Cyclin D1 gene are responsible for the development of parathyroid adenomas (39) and B-cell lymphomas (40, 41). Furthermore amplification of the Cyclin D1 gene or increases in Cyclin D1 protein are found in subsets of breast (42), colorectal (43), and neuroblastomas (44). Identifying how biophysical and biochemical stimuli facilitate cell cycle regulation is essential to understanding how cancers induce hyperplastic growth.

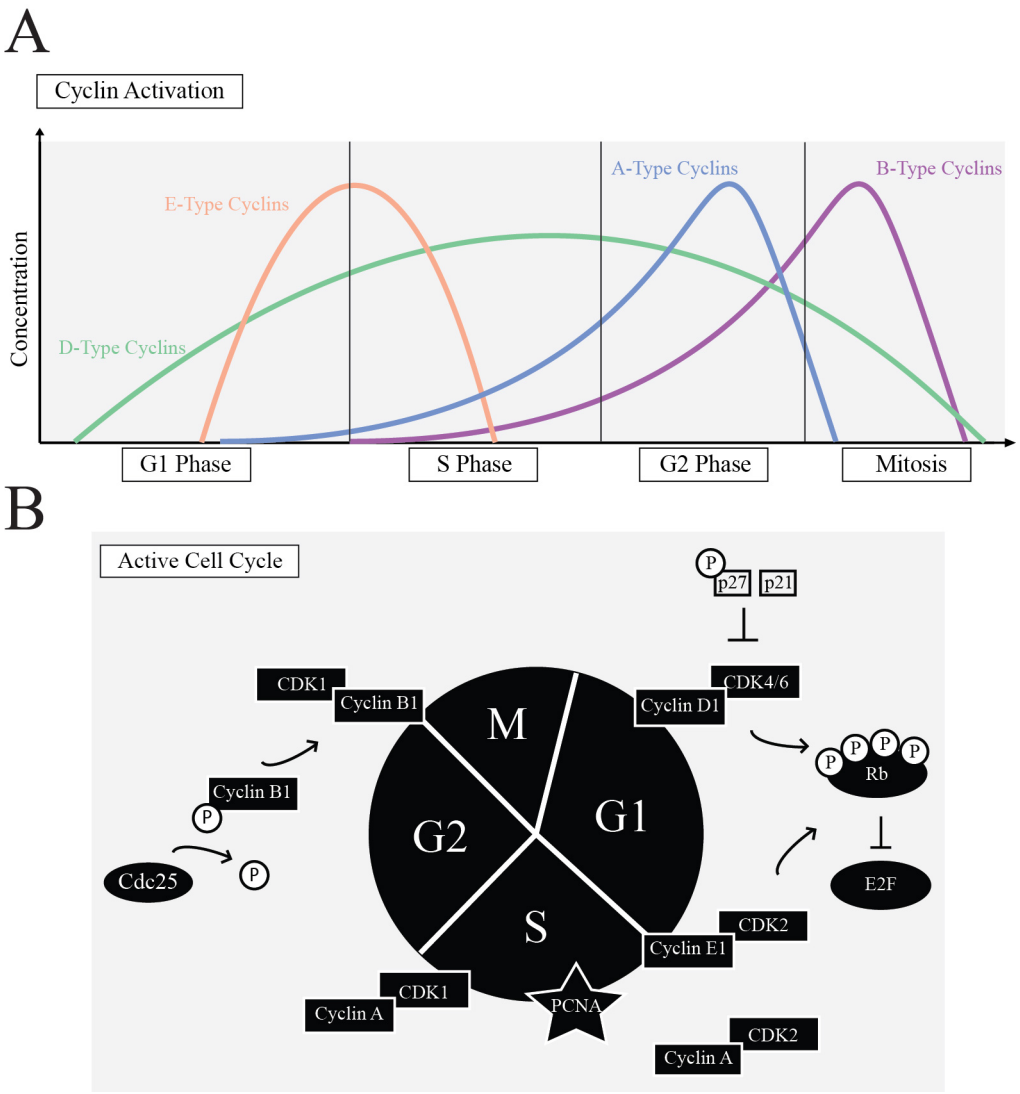


**Figure 1-3: Cyclin Activity During the Cell Cycle, Regulated by Epithelial Cell Differentiation.**

**A.** Relative levels of expression of the different families of cyclins throughout the various stages of the cell cycle. **B.** Schematic of the requirements of the different Cyclin and Cyclin Dependent Kinases for each stage of the cell cycle. Cyclin D1-CDK4/6 is required to initiate $G_0$ to $G_1$ phase transition as they phosphorylate and inhibit the negative regulator of the cell cycle Retinoblastoma (Rb). Cyclin E1-CDK complex is required for the transition from $G_1$ to S phase. Cyclin A-CDK2 complex is required for S phase, and Cyclin A association with CDK1 in late stage S phase is required for $G_2$ transition. PCNA is a processivity factor for polymerase. Cyclin B1-CDK1 complex is required for the transition from $G_2$ to M and is positively regulated by its dephosphorylation by the Cdc25 phosphatase.

## 1.3 Serum Response Network and Its Role in Epithelial Cellular Growth and Cancer

Breast cancer results from reprogramming that deregulates normal growth control mechanisms in differentiated growth arrested cells. Many biochemical stimuli that promote this transformation are transmitted through the blood or through extracellular fluid onto the target cells. These stimuli are often referred to as mitogens as they induce mitosis. Mitogens typically function by activating cell surface receptors to facilitate outward-inward cellular signaling that induces cell growth and proliferation (45). Lipid and protease mitogens in the serum fraction from blood activate G-protein coupled receptors. The most potent bioactive lipid mitogens are lysophosphatidic acid (LPA) and sphingosine-1-phosphate (S1P). Typically they are produced by platelets (46, 47) in response to wound healing, inflammatory responses, or by tumor-stromal interactions. LPA and SIP, stimulate epithelial cell growth by agonizing G-protein coupled receptors (GPCR) (43). In breast cancer, endothelial differentiation gene (EDG) receptors for LPA and S1P mediate progression and metastasis to bone (48-50). Overexpression of EDG receptors also induces hyperplasia in mammary murine glands (51).

Mitogenic proteases including thrombin, tryptase and trypsin also act through GPCRs. Thrombin activates the protease-activated receptors (PAR) 1,3, and 4 by cleaving the N-terminus to expose a tethered ligand, which in-turn is free to bind and self-activate the second loop of the receptor. Stimulation of PAR1 promotes growth and invasion, and is often found in late stage breast cancers (52). PAR2 activity is stimulated by tryptase and trypsin to promote invasive capacity of breast cancer cells (53). Together bioactive lipids and cleaved peptides, explain many of the effects of serum in promoting

epithelial cell proliferation and the induction of hyperplasia in the mammary organ through their activation of GPCRs.

GPCRs represent the largest family of cell-surface proteins and are the targets of an estimated 50-60% of currently used drugs (54). GPCRs function in a variety of signaling pathways that mediate development, differentiation, angiogenesis, cell proliferation and cell survival. GPCRs contain an N-terminal extracellular ligand binding domain, attached to 7 trans-membrane hydrophobic alpha-helices followed by a C-terminal domain that binds to specific heterotrimeric GTPases (55, 56). GPCRs upon agonist dependent activation undergo internal conformational changes that result in their stimulation of nucleotide exchange on specific types of G-proteins. Heterotrimeric GTPases are comprised of a Gα, Gβ, and Gγ subunit. The association of the Gα subunit with Guanine Triphosphate (GTP) causes its dissociation from the Gβ/Gγ subunits. The Gα-GTP and the G-βγ subunits then activate or inhibit downstream effectors. The Gα subunit hydrolyzes the terminal phosphodiester bond of GTP to inorganic phosphate (57), which is released, forming Guanine diphosphate (GDP), that remains bound to the Gα subunit. This promotes Gα to rebind the Gβ/Gγ subunits.

There are four classes of heterotrimeric G-proteins, $G\alpha_s$, $G\alpha_i$, $G\alpha_q$, and $G\alpha_{12/13}$ (58). Serum agonists including LPA, S1P, and thrombin all activate receptors that couple to the $G\alpha_{12/13}$ subclass. $G\alpha_{12/13}$, as well as $G\alpha_{s,}$ are the only subclasses to be identified as oncogenes based on their ability to transform fibroblast when overexpressed (59, 60). $G\alpha_{12/13}$, also promote the invasion and metastasis of prostate (61), oral (62), ovarian (63) and breast cancer (64) cells. $G\alpha_{12/13}$ primarily regulate actin dynamics via their activation of the RGS-RhoGEFs, which then activate the small GTPase RhoA (Figure 1-4A). The

RGS-RhoGEFs include ArhGEF1, ArhGEF11 and ArhGEF12. They are all RhoA specific GEFs that also contain an N-terminal GAP domain for heterotrimeric G-proteins, coined the Regulator of G-protein Signaling (RGS) domain. The RGS-RhoGEFs are recruited to the plasma membrane by activated GPCRs through an interaction of the RGS domain with $G\alpha_{12/13}$ subunit (65-67). This allows their dbl homology (DH) domain, which is the region responsible for GEF activity for RhoA, to be activated by a secondary low affinity interaction with the Gα subunit (67). Conversely, their ability to GAP $G\alpha_{12/13}$ allows them to control the length of time over which they can be activated (68). The RGS-RhoGEFs along with many other Rho GEFs were identified by their ability to transform NIH3T3 fibroblasts when overexpressed (69-71). This activity was later attributed to their dbl homology (DH) domains (72, 73). Likewise, ArhGEF1 and ArhGEF12 are implicated in driving transformation and/or contributing to cancer progression, respectively. Overexpression of a mutant of ArhGEF1 that is fused with the CAAX motif from RAF transforms NIH3T3 fibroblasts (74). ArhGEF12, is also known as Leukemia Associated RhoGEF, as its fusion to the *MLL* gene is the main driving mutation in the development of acute myeloid leukemia (75, 76).

The RGS-RhoGEFs also mediate mitogenic lipid signaling (77, 78) onto the activation of RhoA induced actin dynamics that facilitates the induction of an "immediate early" pro-growth transcriptional program (Figure 1-4B). This specifically involves both the breakdown of cortical actin structures that support cell-to-cell contacts, and the coordinated increases in stress fiber actin. "Immediate early" gene induction is in part due to the reduction of globular actin (G-actin) as it assembles into filamentous actin (F-actin). This prevents the sequestration of Myocardin Related Transcription Factor

(MRTF) in the cytosol, which occurs otherwise as it binds g-actin. MRTF upon its liberation from g-actin, translocates into the nucleus where it binds and co-activates Serum Response Factor (SRF) (79-83) (Figure 1-4C). SRF sits on Serum Response Elements (SRE) in the promoters of "immediate early" response genes (84-86), including cFOS, a component of the AP-1 transcription factor complex (85-88). This gene product when translated combines with cJUN to form the AP-1 transcription factor complex, which is an essential element for the transcription of cell cycle factors including Cyclin D1. Immediate early genes also activate transcriptional programs that promote cell survival, invasion and proliferation.

The serum response network induces transcriptional programs that facilitate cell growth and survival. Under normal physiological conditions the activation of this network is transient, however cancer cells override "fail-safe" checkpoints to allow its chronic activation to induce autocrine and paracrine signaling that promotes hyperplastic cell growth (89, 90).

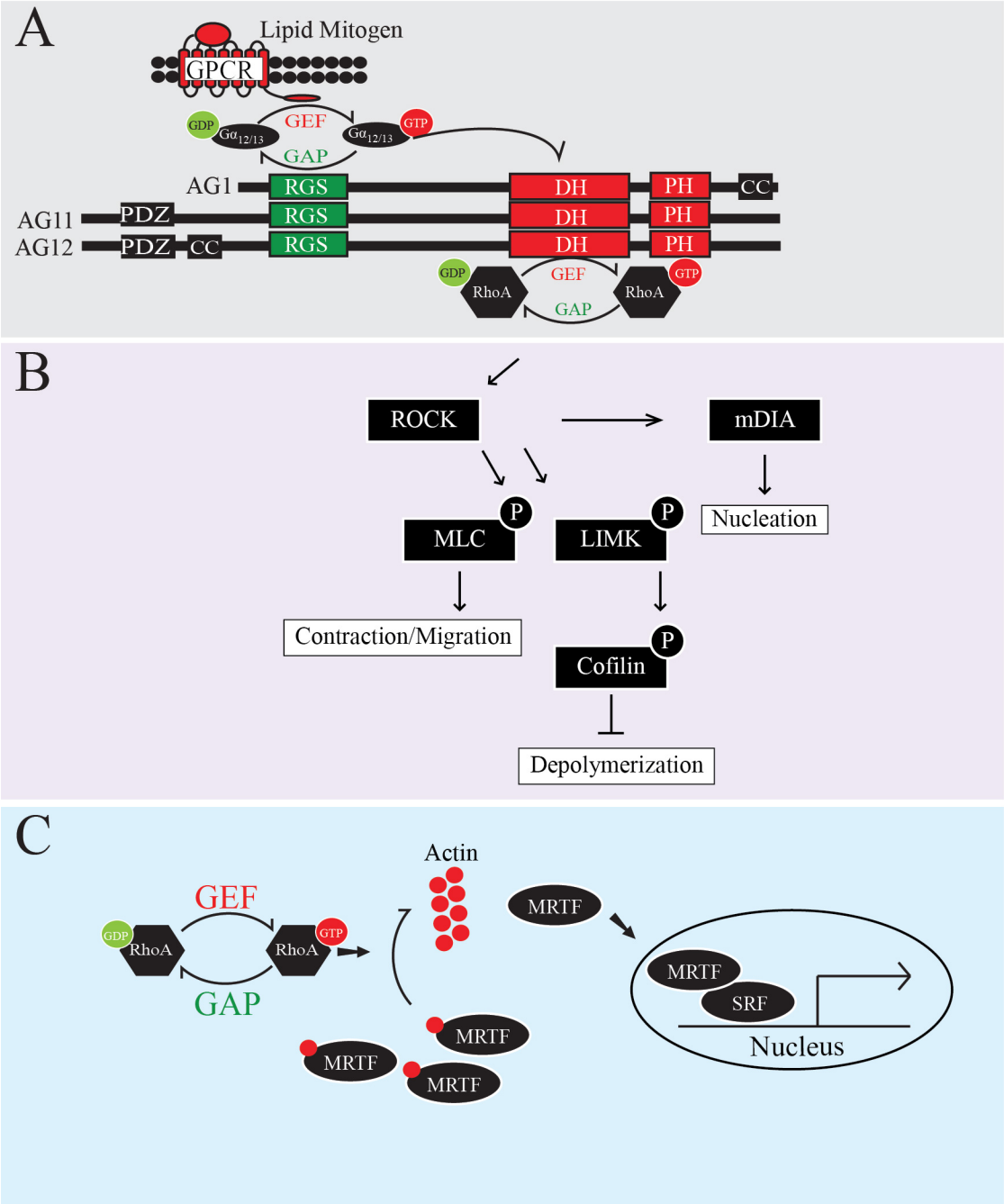


**Figure 1-4: Classical Activation of Serum Response Network.**

**A.** Schematic of lipid mitogen activation of the GPCR/$G\alpha_{12/13}$/RGS-RhoGEFs/RhoA signaling axis. **B.** RhoA activation of ROCK results in the phosphorylation of downstream effectors that contribute to actin formation, stability and contraction. **C**. RhoA dependent actin filament formation induces MRTF translocation to the nucleus where it binds the transcriptional co-activators SRF to drive gene transcription.

## 1.4 Regulation of the MAPK Network by $G\alpha_{12}$ and $G\alpha_{13}$

Mitogen activated protein kinases (MAPK) transmit external to internal signaling to promote cellular growth. The activation of MAPK proteins usually occurs in a bi-phasic manner, with an initial burst of activity that does not materially impact the cell cycle and a less efficacious longer-term stimulation that strongly activates the cell cycle (91). However, chronic MAPK simulation can also induce cellular senescence or apoptosis if certain survival factors are not concomitantly activated (91). These "fail-safe" mechanisms in nonmalignant cells are fundamentally important to prevent cancer (92). Malignancy occurs when cells circumvent these "fail-safe" mechanisms to couple MAPK cascades to growth propagating effects that promote tumor formation (92). Consistent with $G\alpha_{12}$ and $G\alpha_{13}$ being implicated in promoting cancer, they both activate MAPK signaling.

All MAPK signaling is activated by a receptor tyrosine kinase (RTK) binding to a growth factor peptide, stress lipopolysaccharide or inflammatory cytokines (93). Binding to these ligands causes RTKs to dimerize and auto-phosphorylate their c-terminal cytoplasmic region. This initiates the sequential activation of the MAP Kinase Kinase Kinase (MAP3K), MAP Kinase Kinase (MAP2K), and a MAP Kinase (MAPK) cascade. This results in dual phosphorylation of either serine sites on MAPKK or of a threonine and tyrosine near their activation loop on MAPK (93). Typically to achieve activation of the MAP2K or MAPK an incoming signal must be high enough to saturate both phosphorylation sites. MAP3Ks are less concentrated than their upstream MAP2K. However MAPKs and their cognate MAP2K have roughly equal concentrations within the cell. This allows signal amplification at each successive step within the kinase

cascade (94). It may also suggest why a variety of cancers harbor activating mutations in receptors or MAP3K proteins, as this allows signal propagation, versus a mutation in the downstream MAPK.

Canonical mammalian MAPK signaling consists of three well-characterized pathways; the ERK1/2, JNK1/2 and p38 cascades (Figure 1-5A) (93). External stimuli that activate ERK1 and ERK2 generally elicit transcriptional programs that activate the cell cycle. Stimulation of a RTK by an agonist, such as epidermal growth factor (EGF), elicits the autophosphorylation of the RTK, Grb2, an adaptor protein, is then recruited to the membrane through binding the phosphorylated tyrosine via its SH2 domain. Grb2 may also be recruited indirectly by phosphorylated Shc2; an adaptor protein that binds to the autophosphorylated RTK. Son of Sevenless, (SOS) is then recruited by Grb2 to allow its GEF domain to facilitate the exchange of GDP for GTP on rat sarcoma (RAS) GTPases. Activated RAS binds the N-terminal domain of one of three isoforms of Raf (a, b, and c also known as 1) which results in their activation (95). Consequently, Raf binds and phosphorylates MEK1/2 at both serine/threonine (96, 97) residues near the activation loop. This activates the dual specificity kinase activity of MEK, resulting in its phosphorylation of ERK1/2 on threonine 183 and subsequently on tyrosine 185 (98). The dual phosphorylation of ERK1/2 increases its activity by >1000 fold (91). Initial mitogenic stimulation results in an early phase activation of a large fraction of ERK1/2 within 5 minutes. Following this spike in activity, a second phase involving much lower levels of ERK1/2 phosphorylation can occur over several hours (91). This sustained ERK1/2 activation can drive sufficient cyclin activity to promote the cell to enter S phase (91) while also promoting translation (99) committing the cell to growth (100). Activated

ERK1/2 translocates to the nucleus (101) and phosphorylates a variety of pro-growth transcription factors, such as Elk-1. Elk-1, contains a N-terminal ETS DNA binding domain (102, 103), that upon phosphorylation by ERK1/2 (104) binds to the transcription factor SRF to form a ternary complex factor (TCF). The TCF/SRF complex binds to SREs in the promoter of the proto-oncogene, cFOS, and drives its transcription (105, 106). cFOS combined with cJUN facilitates passage through the $G_1$ restriction point via the induction of Cyclin D1 transcription (107, 108).

JNK 1/2 signaling also occurs in a biphasic manner in which the initial phase promotes cell growth and survival while the secondary prolonged phase induces apoptosis (109). Inflammatory cytokines and biophysical stresses activate the upstream JNK pathway MAP3K, termed transforming growth factor-beta activated kinase-1 (TAK1). Activated TAK1 then phosphorylates serine residues near the activation loop of the MAP2Ks MEKK4/7. MEKK4/7 then sequentially phosphorylate threonine and tyrosine residues within the activation loop of JNK. Chronic phosphorylation of these residues induces JNK to direct the E3 ubiquitin ligase Itch to mediate proteosomal degradation of the caspase-8 inhibitor $cFLIP_L$ to result in cell death (110). Furthermore, stress activated JNK can phosphorylate histone H2A variant, H2AX at serine 139, resulting in DNA fragmentation and apoptosis (111). JNK also mediates stress alleviating effects through its downstream target, the transcription factor cJUN. cJUN was originally isolated as the cellular homolog to v-Jun, the oncogene that causes Avian Sarcoma Virus 17 (112). cJUN was first transcription factor identified to have transforming potential. cJUN is phosphorylated by JNK within its transactivation domain at serine 63 and serine 73, in response to a variety of stimuli including UV-light, and receptor tyrosine kinases

via HRAS (113). The neutralization of cJUN by microinjected anti-cJUN antibodies prevents the transition of cells from $G_1$ to S phase (114). The dominant roles cJUN and cFOS in cell cycle progression underlies the utilization of MAPK cascades by cancerous cells to mediate neoplastic growth.

MAPK cascades are also activated by $G\alpha_{12}$ and $G\alpha_{13}$. Both $G\alpha_{12}$ and $G\alpha_{13}$ activate a variety of small GTPases including RAS, Rac1, Cdc42, and RhoA to stimulate the JNK1 cascade (Figure 1-5B). $G\alpha_{12}$ activates JNK through MEKK7, which phosphorylates JNK1 at threonine 187. Conversely, $G\alpha_{13}$ activates MEKK4, which then phosphorylates JNK1 at tyrosine 185. Together, phosphorylation at both sites allows the full activation of JNK1. Evidence for the importance of the crosstalk between the serum response network and MAPK signaling is highlighted by the requirement of ArhGEF1 for RhoA-dependent activation of JNK in P19 cells (115). Further, ectopic expression of $G\alpha_{12}$ facilitates the activation or inhibition of ERK1/2 depending on cell-type (116). Because the mutations in proteins involved in these pathways contribute to breast cancer initiation and progression (117), it is essential to understand how these pathways integrate and contribute to normal physiological growth.

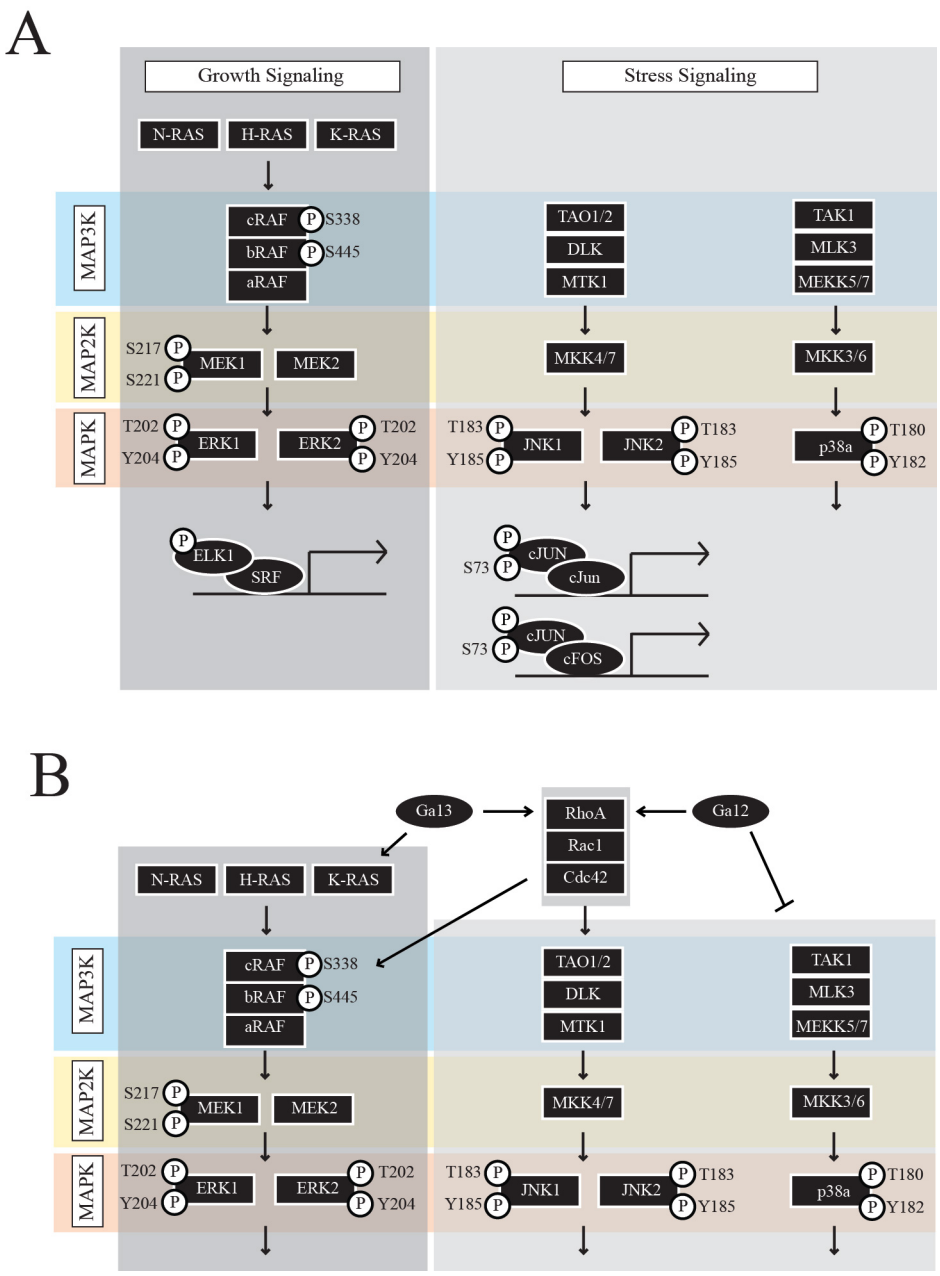


**Figure 1-5: Classical and Non-Classical Activation of the MAPK Cascades.**

**A.** Classic activation of the canonical MAPK pathways. The pro-growth growth factor response pathway that ends in ERK1/2 phosphorylation (Left panel) and the stress response MAPK pathways that ends in JNK1/2 and p38 phosphorylation (Right Panel). Upstream kinases MAP2K (Yellow) and MAP3K (Blue). **B.** Role $G\alpha_{12}$ and $G\alpha_{13}$ play in activating the MAPK cascades in response to activation of G-protein coupled receptors.

## 1.5 Integration of HIPPO Signaling in Epithelial Polarity, Serum Response Network and MAPK

Over the past decade the HIPPO signaling pathway has emerged as a mediator of growth control and stem-like features in response to biochemical and biophysical interactions. (118, 119). Initial discoveries elucidated the role of HIPPO signaling in organ size control in response to cell-to-cell contacts (Figure 1-6A) (120, 121). More recently, the regulation of HIPPO signaling by the Serum Response Network and MAPK cascades was also appreciated (122, 123). Many of these studies highlight the co-dependencies of these pathways to drive aberrant growth in cancer cells. This dependency suggest that under normal physiological conditions there are a multitude of checks and balances integrated among various canonical signaling pathways to maintain cellular and tissue homeostasis. However, the mechanisms and complete functional relationship between the integration of the HIPPO pathway, Serum Response Network, and MAPK Cascades in contributing to cellular growth in epithelial cells is still largely not understood.

Discovered in *Drosophila melanogaster* by genetic mosaic screens, mammalian homologues of the Drosophila HIPPO pathway have since been discovered. Mammalian STE-like (MST) 1/2 and Large Tumor Suppressor (LATS) 1/2 kinases are activated by cell-to-cell contacts . This allows them to phosphorylate and thereby inactivate the potent oncogenes transcriptional co-activator Yes-Associated Protein 1 (YAP1) and its homolog WWTR1 (TAZ). Phosphorylation of YAP1 at serine 127 or TAZ at serine 89 promotes their binding to 14-3-3, which results in cytosolic sequestration. If cells are not engaged with one another, the LATS1/2 kinases are inactive which allows YAP1 to translocate to

the nucleus where it co-activates transcriptional events (120). Further regulation of YAP1 occurs through its degradation via an Angiomotin dependent process that is initiated by LATS1/2 phosphorylation of serine 175 on Angiomotin in response to serum deprivation (124, 125). Upregulation of YAP1 occurs in a variety of cancers including hepatocellular carcinoma, uveal melanoma (126), colorectal (127), pancreatic ductal adenocarcinoma (128), lung adenocarcinoma (129), neurofibromatosis, and malignant mesothelioma (130).

YAP1 and TAZ are dynamic transcriptional co-activators that have no inherent DNA binding domain. They mediate their transcriptional effects by binding to a variety of transcription factors including RUNX2, p73 and most notable the TEA domain containing (TEAD) family. Mammalian TEAD family members consists of 4 highly conserved and ubiquitously expressed transcription factors that are conserved from yeast (131). All TEADs bind YAP1 and TAZ (132-134). The N-terminal domain of YAP1 binds the carboxyl-terminal domain of TEAD (135, 136). The transcriptional activity of the YAP1/TEAD complex is facilitated by the recognition of M-CAT motifs (5′-TCATTCCT-3′) (137) in the promoter of a variety of growth inducing genes. The YAP1/TEAD/DNA complex is functionally activated when tethered, via the acidic carboxyl terminus of YAP1, to RNA Polymerase II (132). The YAP1/TEAD transcription factor complex drives transcription of a variety of genes, the most notable being the CCN family of genes (134, 138).

The CCN family of genes are named for the first three members identified: Cysteine Rich, Angiogenic Inducer, 61 (**C**yr1 or CCN1), Connective Tissue Growth Factor (**C**TGF or CCN2), nephroblastoma overexpressed (**N**OV or CCN3) and CCN4-6.

The CCN proteins are secreted into the stromal matrix where they activate cell growth by manipulating the cells interactions with the surrounding microenvironment. CTGF and Cyr61 activate extracellular matrix metalloprotease-2 and the integrin network to promote cell growth and survival signaling by activating integrin linked kinase and ERK1/2 (139, 140). Overall, the facilitation of autocrine and paracrine signaling by YAP1 is critical for cellular homeostasis and fate decisions.

Regulation of the actin cytoskeleton network is a fundamental requirement for YAP1 nuclear translocation. Activation of RhoA by mitogen stimulated $G\alpha_{12/13}$ heterotrimeric G-proteins induces the formation of stress fibers (Figure 1-6A). Stress fiber formation is required for YAP1 nuclear translocation. However if this occurs in a LATS1/2 dependent or independent manner is still an area of controversy. The use of a RhoA specific inhibitor, the exoenzyme bostulum C3 toxin (141), or using latrunculin A, a drug that binds 1:1 with monomeric actin and inhibits polymerization prevents a mutant of YAP1 that is insensitive to LATS1/2 phosphorylation from localizing to the nucleus (142). However, activation of $G\alpha_{12/13}$ by lipid mitogens also reduces the phosphorylation of LATS1/2 to promote YAP1 nuclear translocation (122). LATS1/2 phosphorylation and YAP1 cytosolic sequestration are also increased upon treatment of cells with C3. It is therefore likely that the serum response network regulates YAP1 by both LATS1/2 dependent and independent modes depending on the context of actin dynamics.

Activation of the MRTF/SRF and AP-1 transcription factor complexes is required for many YAP1/TEAD mediated effects. For instance, in glioblastoma cells lines, YAP1/TEAD synergistically function with MRTF/SRF to activate the transcription of Cyr61, a known YAP1 target in response to activation of GPCRs by S1P (143). The

transcription of Cyr61 in this scenario is abrogated by the independent knockdown of either YAP1 or MRTF. Furthermore, in a "normal" transformed breast cancer cell line, MCF10A, YAP1 synergizes with AP-1 transcription factor complex to promote cell growth in 3D tissue culture models as well as in vivo orthotropic transplantation (144). Together these studies highlight how the serum response network and the HIPPO pathway are integrated to control cellular growth.

MAPK cascades further regulate YAP1 activity and cell growth potential. Treatment of the mammary epithelial cell line MCF10As with Epidermal Growth Factor (EGF) causes dissociation of the HIPPO kinases and YAP1 activation (123). Further, activation of the Ajuba family protein WTIP by RAS in response to the loss of cortical actin tension enhances its association with LATS1/2 . This prevents LATS1/2 phosphorylation of YAP1 to promote its nuclear localization (145, 146). A requirement of YAP1 and MAPK signaling is also evident in pancreatic cancers. Ninety percent of pancreatic cancers tumors exhibit constitutively activated KRAS mutants (147). In these cancers YAP1 is dispensable for initiation events, however it is required for progression (128). The requirement of YAP1 activity for the functionality of MAPK cascade signaling highlights the importance of YAP1 in dictating cellular fate decisions.

Further elucidation of how the serum response network, MAPK cascades, and the HIPPO pathway convert external biophysical and biochemical stimuli into regulated growth is needed. For it is the deregulation of these pathways, not in solidarity, but in the integrated network, that cancers can by-pass inherent fail-safe mechanism to propagate unwarranted growth (90, 92).

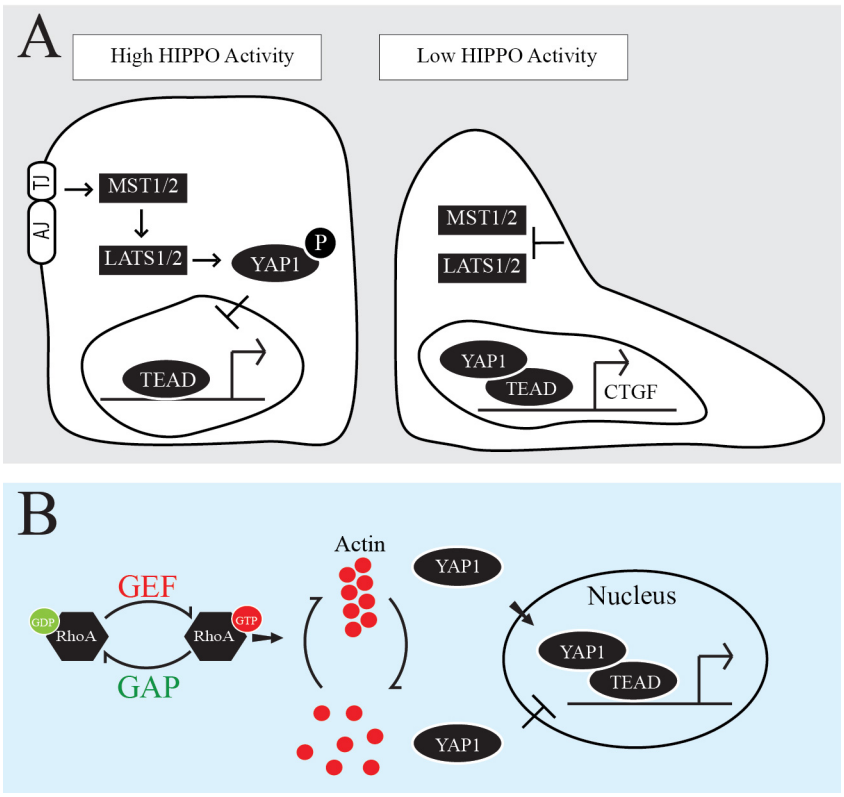


**Figure 1-6: Integration of Serum Response Network and HIPPO Signaling.**

**A.** High HIPPO: Differentiated epithelial cells, upon cell-to-cell contact at junctions, initiate the sequential activation of the HIPPO kinases MST1/2 and LATS1/2, respectively. LATS1/2 then phosphorylates YAP1 at serine 127 and it is further sequestered from the nucleus by 14-3-3. **B.** A model of RhoA dependent actin stress fiber formation that results in the translocation of YAP1 to the nucleus.

## 1.6 Model Systems Justification

Mammary tumors are typically a heterogeneous group that utilizes a wide variety of hormone and growth factor signal transduction pathways to mediate cell growth (148, 149). Tumor subtypes are classified by the presence or lack of the hormone responsive estrogen and progesterone receptors, and the growth factor receptor HER2 (150). Estrogen or progesterone receptor positive tumors are typically treated with anti-hormone therapy, while tumors that present with HER2 are treated with a HER2 antagonist. As breast cancers progress they become refractory to treatment (151). The varying receptor profiles of breast cancers, as they are diagnosed or as they progress, suggest that many cancers can re-wire internal signal transduction circuitry to adapt and mediate cell growth needs (90, 150). It is therefore necessary to exploit specific breast cancers models to accurately represent the tumor type under investigation. Furthermore, studying signaling pathway in a broad range of cell lines may lead to a better understanding of how breast cancers develop and progress through subsequent stages.

BT474 are estrogen (ER+), progesterone receptor (PR+) and HER2 positive. This cell line was derived from a 60-year-old Caucasian female. In this study, BT474 cells were used to initially identify RhoGEFs and RhoGAPs that modulate YAP1 dependent TEAD activity. MCF7 cells are estrogen receptor (ER+) and progesterone receptor (PR+) positive cell lines, but they lack overexpression of HER2 (HER2-). These cells represent an IDC luminal tumor type and are derived from a pleural effusion of a 69-year old Caucasian woman. MDA-MB-231 cells are derived from a metastatic site within a 51-year-old Caucasian female. The cells are triple negative meaning they lack estrogen receptors (ER-), progesterone receptors (PR-), and HER2 (HER2-). Signaling regulating

$G\alpha_{12/13}$ was primarily elucidated in MCF7 and MDA-MB-231 cells lines. Human Embryonic Kidney (HEK) 293T cells were derived from human embryonic kidneys and transformed with fragments of adenovirus type 3 and contain the SV40 T-antigen (152, 153). These cells were used to produce the lentiviruses used in this study.

Biochemical and biophysical microenvironmental cues are major drivers of cell fate decisions under physiological conditions (154). Cell grown on 2D plastic surfaces alter cellular signaling in comparison to the connective tissue rich environment within the mammary organ. Therefore plastic tissue culture dishes may not be an optimal environment for studying cell signaling. To address these concerns, results in 2D were validated in a representative 3D environment. Cells were grown in a laminin rich extracellular matrix known as Matrigel® (155). This substance best represents the soft, connective tissue environment that comprises the breast tissue.

## 1.7 Rationale and Central Focus

The overall goal of this dissertation is to understand how the integration of the serum response and HIPPO signaling networks facilitates cell fate decisions. Growth is a finite process at both the organismal and cellular level. The integration of growth signaling pathways inherently provides a system of checks and balances to maintain cellular homeostasis. In the context of epithelial cells, these checks and balances are mediated by biophysical interactions with surrounding cells and the basement membrane, as well as biochemical stimulation through serum mitogens. Recent studies have highlighted how these biophysical and biochemical stimuli regulate the HIPPO pathway and its downstream effector YAP1 to mediate cell fate decisions (122, 142). Aberrant regulation of this pathway leads to cell growth and tumorigenesis (156). Through cell-to-cell contact or serum deprivation, YAP1 is phosphorylated and retained in the cytosol or degraded (125, 156). Conversely, the loss of cell-to-cell contacts, the activation of the serum response network by LPA and/or S1P, or the activation of MAPK signaling by EGF promotes YAP1 nuclear localization (122, 123, 145). However, even though these major signaling pathways are known to independently regulate YAP1 nuclear localization, nothing is known about how they spatially and temporally cooperate to regulate YAP1 and subsequent cellular fate decisions.

Recent work has highlighted the requirement of RhoA-dependent actin stress fiber formation, independent of LATS1/2 for YAP1 nuclear translocation (142). RhoA is a small GTPase whose activity is modulated by GEFs and GAPs that respond to upstream extracellular signals, such as LPA and SIP (77). RhoA however, functions at various cellular locations, driving both stress fiber formation activating YAP1, and participating

in cortical actin formation (157), which is hypothesized to inhibit YAP1 activity. RhoA can also be active in the nucleus. These seemingly contradictory functions have muddled the understanding of how RhoA regulates YAP1 dependent cell fate decisions.

A key to the selective spatial and temporal regulation of RhoA is the GEFs and GAPs that facilitate its GDP/GTP cycle (158-162). To date, only a handful of GEFs and GAPs are implicated in the regulation of YAP1, via the activation or inhibition of their corresponding G-protein (126, 163). It is therefore hypothesized that the regulation of RhoA by specific GEFs and GAPs is critical for understanding YAP1 nuclear activity.

The central focus of this dissertation is the mechanisms for the integration of canonical growth regulatory signaling with HIPPO signaling to control cell growth and survival. The central focus was tested by: (1) the discovery of the RGS-RhoGEFs as major regulators of YAP1-dependent transcription. (2) The characterization of the RGS-RhoGEFs, ArhGEF1, ArhGEF11 and ArhGEF12, in contributing to serum induced RhoA-dependent YAP1 activation. This characterization further highlighted that ArhGEF12, and to a more modest extent ArhGEF11, mainly mediates GDP/GTP exchange activity for RhoA, whereas ArhGEF1 is essential to GAP $G\alpha_{13,}$ which was further identified as the primary transducer of serum instigated YAP1 transcriptional activity. (3). Furthermore, all of the RGS-RhoGEFs were found to be required for cellular growth in 2D and 3D model systems. However, ArhGEF1 was found to be essential for cell growth via a novel mechanism involving the induction of expression of proteins involved in cell cycle activation and protein translation (4) Finally, we describe the requirement of YAP1 in maintaining cell survival in hyper-activated growth signaling and high tensile environments. The loss of ArhGEF1 was found to sensitize cells to $G\alpha_{13}$

serum signaling, however this did not initiate cellular growth. The combined knockout of ArhGEF1 and YAP1 results in a synthetic activation of apoptosis. These discoveries address a flawed presumption in the field that stress fiber induced YAP1 nuclear translocation always results in cell growth. This work dissects how the RGS-RhoGEFs fine-tune YAP1 functionality by coordinating a variety of signaling cascades that typically mediate cellular growth, to maintain an optimal range of cellular homeostasis that is defined by biochemical and biophysical interactions. However, when these pathways are aberrantly activated and cellular homeostasis is disrupted, YAP1 functionality switches to promote survival.

# CHAPTER 2. MATERIALS & METHODS

2.1. Methods of Cell Culture

Cells were maintained in a 37$^{o}$C incubator at 5% $CO_2$. Cells were passaged as follows: Media was aspirated from the plate and cells were washed with sterile PBS. Upon aspiration of the PBS, 1 mL of 2.5 g/L trypsin (Sigma) supplemented with 5 mM EDTA (Sigma) was added and cells were placed back in the 37$^{o}$C incubator. After 2-10 minutes, varying among cell types, cells were visually inspected for cellular detachment from the plate. Upon detachment, 3 mLs of media was added to kill the trypsinization process, and cells were pipetted into 15 mL conical tubes (Falcon), using p1000 filter tips (FisherBrand). Cells were centrifuged at 1500 RPM for 1.5 minutes in an Eppendorf Centrifuge (5702). Upon retrieval cells were resuspended by pipetting 15 times using 1 mL of media, and subsequently seeded at desired density and/or cell number.

Cell types used in this study include the mammary breast cancer cell lines MCF7, MCF10As, MDA-MB-231 (Mayo Lab), MDA-MB-231 Metastatic (Guise Lab,) BT474, SKBR3s, and the human embryonic kidney cell line, HEK293Ts. All cell lines were obtained from ATCC unless otherwise noted. MCF7s, MDA-MB-231, MDA-MB-231 Metastatic, SKBR3s, and HEK293Ts were cultured in complete media which consists of Dulbecco's Modified Eagles Serum (DMEM)/High Glucose (ThermoFisher) supplemented with 10% Fetal Bovine Serum (FBS) (Atlanta Biologics) and 1% penicillin-streptomycin solution (Hyoclone). BT474s were cultured in RPMI-1640 (ThermoFisher) supplemented with 10% FBS (Atlanta Biologics).

Cell treatments consist of basal, serum starved (SS), or serum add back (4) conditions, unless otherwise noted. Under basal conditions, cells were seeded into complete media containing 10% FBS. Under serum starved conditions, cells were seeded

into complete media, and after 24 hours the media was replaced with media lacking 10% FBS. Serum add back consisted of replacing the serum starved after 24 hours with complete media containing 10% FBS for indicated time points.

2.2. Stable Cell Line Generation Using Lentivirus

Second generation lenti viral constructs were used to transduce cell lines with either MISSION® pLKO.1 shRNA, from Sigma Aldrich, or with a mammalian lent viral expression plasmid, to create a stable cell population with either a silenced or overexpression gene of interest. Four million HEK293Ts were plated into a 10 cm dish and grown overnight (Day 1). The following day lenti viral packaging vectors were transfected along with either the pLKO.1 shRNA or mammalian lent viral expression plasmid (Day 2). For the transfection, 6 ug of pCMV-VSVG, 5 ug of psRSV-REV, 10 ug of pMDLg-pRRE, and 20 ug of indicated plasmid were vortexed at medium speed in 1 mL of serum free media while adding 25 uL of PEI (2mg/mL), dropwise. The mixture was allowed to sit for 5 minutes in the biosafety hood. The transfection master mix was then added drop wise to an 80% confluent 10 cm plate of HEK293Ts prepared the night before. The following morning, the transfection media was removed and replaced with complete medium (Day 3). Twenty-four hours later, the viral containing medium was collected into a 15 mL Falcon Tube (Day 4). If desired, another round of medium was added to the 10 cm plate and collected on Day 5. After collection of the virus, the supernatant was passed through a .45 uM filter to remove any debris. Hexadimethrine Bromide, also known as Polybrene (5mg/mL), was then added, 1:500, and allowed to mix with the viral supernatant for 10 minutes. Virus can be stored at $4^{o}$C for up to two weeks.

Target cell lines, those being infected, can be plated out on Day 2 or at anytime up to two weeks after collection of the virus. The target cell lines in this study, MCF7 and MDA-MB-231 were seeded at 2 million and 4 million cells, respectively in a 10 $cm^2$ dish. Twenty-four hours after seeding cells were incubated with 6 mLs of viral supernatant that was diluted 1:2 unless otherwise indicated. After 4-6 hour incubation, medium was changed to complete media. Target cells were given 48 hours to incorporate the lenti transduced DNA and then split for an assay.

## 2.3. Method of Transient Transfection

Forward and reverse transient transfection methods were performed depending on cell type. Forward transfections were done in HEK293Ts. HEK293Ts cells were seeded so that the following day they would be 70-80% confluent. 1 ug of cDNA was transfected per 100,000 cells seeded. The cDNA was added to serum free medium in glass disposable culture tubes (FisherBrand), the total volume of which did not exceed 5% of the total volume of complete medium on the cells. Polyethylenimine (PEI) (2mg/mL) was then added at a ratio of 1uL of 2mg/mL PEI/1ug cDNA drop wise to the transfection mixture, and allowed to sit for 5 minutes. The final mixture with the transfection reagents was then added drop wise to the plates of cells.

For a reverse transfection cells were counted and seeded. The same procedure for creating the transfection mixture, as highlighted above, was undertaken. The transfection mixture was then added drop wise prior to the cells adhering to the plate.

2.4. Plasmids, Antibodies, and Lysis Buffers

**Expression Plasmids:** cDNA expression plasmids used to screen YAP1-TEAD dependent transcription activity are located in **Appendix A**. Lenti viral packaging (psRSV-Rev, pMDLg-RRE, and pCMV-VSVG) and shRNA scramble control (1864) vectors were acquired from Addgene. 5XGal4-luc, Gal4-TEAD4, (gifts from L. Quilliam). 3x-Flag $G\alpha_{13}$WT, 3x-Flag $G\alpha_{13}$WT R232E, 3x-Flag $G\alpha_{13}$QL, and 3x-Flag $G\alpha_{12}$WT were cloned by B.Heller (originals were obtained from Philip Wedegaertner and Tohru Kazasa).

**Primary Antibodies used for immunoblots:** M2 (Sigma, F3165) 1:10000, 9E10 (in house) 1:1000, p115 (in house (65)) 1:1000, ARHGEF11 (Santa Cruz, sc-67023) 1:1000, ARHGEF12 (Santa Cruz,sc-25638) 1:1000, pERK (Santa Cruz, sc-7382) 1:1000, pERK ( Cell Signaling, 9106S) 1:1000, ERK (Cell Signaling, 9102S) 1:1000, GAPDH (Millipore, MAB374) 1:10000, pYAP1 (Cell Signaling, #4911) 1:1000, YAP1 (Abnova, H00010413-M01) 1:1000, AIP4 1:1000, cMYC (Cell Signaling, D84C12) 1:1000, U1 snRNP70 (Santa Cruz, sc-9571).

**Secondary antibodies for immunoblotting** were all used at a dilution of 1:20,000 and applied in the absence of light at room temperature for 30 minutes. These antibodies include goat anti-Mouse IRDye 800CW (LI-COR), goat anti-Rabbit IRDye 680CW (LI-COR), and donkey anti-goat DyLight 800 (Pierce).

**Primary antibodies used for immunofluorescent fixed cell imaging:** p115 (in house) 1:1000, ARHGEF11 (Bethyl, A301-952A) 1:250, ARHGEF12 (Bethyl, A301-959A) 1:250, M2 (Sigma, F3165) 1:10000, YAP1 (Abnova, H00010413-M01).

**Secondary antibodies for immunofluorescent fixed cell imaging**: Secondary's were all diluted to 1:500 and applied for 30 minutes in the absence of light. Goat-anti

Rabbit IgG CFL 488 (Santa Cruz, sc-362262), Goat-anti Mouse IgG Alex Fluor 488 (Invitrogen A11001), Goat-anti Rabbit IgG-CFL 594 (Santa Cruz, sc-362282), Goat-anti Mouse-IgG CFL 594 (Santa Cruz, sc362277).

**RIPA Lysis buffer:** (in water: 150 mM NaCl, .1% SDS, 50 mM of pH 8.0m Tris, 2mM EDTA, 1% TritonX-100). **PLC Lysis Buffer:** (in water: 50 mM pH 7.5 HEPES, 150 mM NaCl, 10% Glycerol, 1% TritonX-100, 1.5 mM MgCl2, 1 mM EGTA). **Passive Lysis Buffer (Promega):** Proprietary. **Nuclear Fractionation Buffer A:** (in water: 10 mM HEPES pH 7.9, 1.5 mM $MgCl_2$, 10 mM KCl, and .05% IGEPAL).

2.5. Method of Immunoblot and Western Analysis

**Protein Extraction and Quantitation from 2D:** After treatment, cells were removed from the incubator and placed immediately on ice. Serum was then aspirated, and cells were washed once with cold PBS, which was subsequently removed. RIPA Lysis Buffer supplemented with protease cocktail inhibitor, was then added. An appropriate volume, taking into account cell density and plate size was added. 100% confluent 6 cm and 10 cm plates were lysed in 200 uL and 1 mL of RIPA, respectively. 50% confluent 6 cm and 10 cm plates were lysed in 100 uL and 500 uL of RIPA Lysis, respectively. Using a scraper, cells were removed from the plate and placed into a 1.7 mL microcentrifuge tube and placed on ice for 10 minutes. Lysates were then clarified by being spun down in an Eppendorf Centrifuge (5417R) at 14,000 RPM for 10 minutes at $4^oC$. A Bicinchoninic acid (BCA) assay was used to determine the protein concentration of cell lysates. Lysates were normalized to contain the same protein concentration, with a

total of 30-40 ug of protein per 20 uL. Normalized protein samples were then boiled in 1x SDS sample buffer.

**Protein Extraction and Quantitation from 3D:** Protein was extracted from Matrigel® through a combined method of chemical and physical means. Cells in Matrigel® were removed from the incubator and placed on ice. Cells were washed 1x with ice cold PBS, careful not to perturb the Matrigel®. 150 uL of RIPA lysis9 buffer, supplemented with appropriate protease inhibitors was then added to the dish. The Matrigel® was scraped off using a cell scraper and placed into a 1.7 mL microcentrifuge tube. Using a p200, the Matrigel® was vigorously broken up into a homogenous solution, and snap frozen on dry ice for 10 minutes. Lysates were then hand-thawed, and subjected to p200 pipetting. Lysates were clarified through a 4$^{o}$C spin for 10 minutes at a speed of 14,000 RPM in an Eppendorf Centrifuge (5417R). The clarified supernatant was then boiled in 1x SDS sample buffer for 5-10 minutes at 100$^{o}$C. It is important to note that a BCA assay cannot be run on these samples as the Matrigel® will interfere with the assay. The standard practice for normalizing protein concentration for these samples is to run a GAPDH blot and perform a densimetric analysis using ImageJ to adjust the ratio of sample loading for future blots.

**Resolution and Transfer:** Resolution of proteins was achieved via sodium dodecyl sulfate polyacrylamide gel electrophoresis (SDS-PAGE). 6-12% polyacrylamide gels were made depending on the size of protein being resolved. For proteins in the range of 30-115 kD an 8% polyacrylamide gel was prepared. For proteins that exceeded 115 kD in size, a 6% polyacrylamide gel was prepared, and for anything smaller that 30 kD a 12% gel was created. Polyacrylamide gels were placed at 4$^{o}$C overnight. 20 uL of each

sample was loaded into the appropriate percentage 15 well polyacrylamide gel. Protein was then resolved in running buffer for 1 hour and 30 minutes at 120 volts using a BioRad Powerpack. Proteins were then transferred to Protran BA85 nitrocellulose membranes via a Genie-Blotter. Conditions under which different percentage polyacrylamide gels were transferred were as follows: 6% gels were transferred at 24 volts for 2 hours with 10% methanol added to the transfer buffer; 8% gels were transferred at 12 volts for 1 hour and 30 minutes with 20% methanol added to the transfer buffer; 12% gels were transferred at 12 volts for 45 minutes in buffer that had no SDS and supplemented with 20% methanol. Upon completion of the transfer, nitrocellulose membranes were placed on an orbital shaker and blocked in 5% (w/v) low-fat milk dissolved in TBS for 20 minutes at room temperature. Membranes were washed 3X in TBS that contained .1% (v/v) Tween20. Membranes were transferred to a hybridization bag and encased with 6-7 mL of primary antibody diluted in TBS/T. Hybridization bags were placed on a nutator at $4^{o}$C for a minimum of 1 hour for most primary antibody incubations, unless primary antibodies against ARHGEF1/11/2 or YAP1 were used and those incubations were done overnight. Membranes were then removed from the hybridization bags and washed 3x in TBS/T. Incubation with the appropriate secondary antibody was done in the dark at room temperature for 30 minutes. Membranes were then washed 3x in TBS/T and imaged using Li-COR® Odyssey scanner.

## 2.6. Method of Nuclear Fractionation

4 million MCF7s were seeded into 10 cm plates and allowed to reach 90% confluence. Upon treatment cells were removed from the incubator and placed on ice.

Cells were then washed 2x in ice cold PBS. 1 mL of Nuclear Fractionation Buffer A, supplemented with appropriate protease inhibitors, was added to the cells and using a cell scraper they were gently removed from the plate and pipetted into a 1.7 mL microcentrifuge tube. Lysates were set on ice for 10 minutes and then spun down at 3000 RPM for 10 minutes in 4$^{o}$C Eppendorf centrifuge (5417R). 100 uL of the supernatant was then removed and labeled as the "Cytosolic Fraction." The rest of the supernatant was discarded. The pellet, milky in color, was washed in 1 mL of Nuclear Fractionation Buffer A by **GENTLY** pipetting up and down 3 times causing slight dissociation of the pellet. The lysate was then spun down at 3000 RPM for 1 minute, and this process of washing the nuclear pellet was repeated two more times. After the final wash the supernatant is discarded and the pellet is vigorously resuspended in 100 uL of RIPA supplemented with protease inhibitors. The lysate is then incubated on ice for 10 minutes followed by a spin at 14,000 RPM in an Eppendorf centrifuge (5417R) at 4$^{o}$C. The supernatant is removed and labeled as the "Nuclear Fraction." Protein concentrations were then determined by BCA assay. Normalized samples were boiled in 1x SDS sample buffer at 100$^{o}$C and resolved as described in section 2.5.

2.7. BCA Assay for Protein Concentration

Pierce® BCA Protein Assay Kit was purchased and used as directed by manufacturer. 2 uL of clarified protein lysate from one sample was added per well of a 96 well plate. A mastermix of Pierce® BCA Protein Assay Reagent A and Pierce® BCA Protein Assay Reagent B was created by adding Reagent B to Reagent A at 1:50 dilution. 198 uL of the mastermix was added to each well containing clarified protein lysate and

the plate was sealed, and allowed to incubate in 37$^{o}$C water bath for 15 minutes. Upon retrieval, the bottom of the plate was dried and placed into a 96 well SpectraMax 250 (Molecular Devices) plate reader. The plate was read under the BCA assay program. A standard curve was created using 2, 4, 8, 12, 16, and 32 uL of 1ug/uL BSA.

## 2.8. Short Hairpin RNA Information

Stable cell lines for silenced gene expression were made using a combination of the Sigma Mission® shRNA pLKO.1-puro vectors with lenti viral packaging vectors as described in section 2.2. After infection, cells were given 2 Days to produce optimal gene knockdown and were split into assays. Mission shRNAs used in this study include: shARHGEF1 (TRCN0000033566), shARHGEF1 (TRCN0000033568), shARHGEF11 (TRCN0000047465), shARHGEF12 (TRCN0000298941), shARHGEF12 (TRCN0000298942), shYAP1 (TRCN0000107267) and for a control a pLKO.1 shScramble purchased from Addgene (1864)

## 2.9. RNA Extraction, cDNA Synthesis, and Quantitative Real Time PCR

**RNA Extraction from 2D:**Treated cells were removed from the incubator and placed at room temperature. The media was aspirated and 500 uL of TRIZOL® was added per 6 cm plate. Using a cell scraper, cells were collected and pipetted into a 1.7 mL microcentrifuge tube. Samples sat at room temperature for 10 minutes, and then 100 uL of Chloroform was added. Samples were vortexed until the solution was homogenous and allowed to sit again at room temperature for 10 minutes. Samples were then spun down in an Eppendorf centrifuge (5417R) for 10 minutes at 14,000 RPM and 4oC.

200 uL of the aqueous layer was then removed and added to 150 uL of isopropanol to precipitate the RNA. Samples were incubated at room temperature for 10 minutes and then spun down at 4 $^{o}$C at 14,000 RPM for 10 minutes. The RNA pellet was washed in 75% ice-cold ethanol, to remove excess salt, and spun down at 9,500 RPM for 5 minutes. This step was then repeated. After the second wash the majority of ethanol was aspirated and the remainder was removed using a p200. The RNA was allowed to air dry for 5 minutes and then dissolved in 20 uL of ddH2O.

**RNA Extraction from 3D:** Treated cells were removed from the incubator and placed at room temperature. The media was aspirated and 1mL of TRIZOL® was added per 3.5 cm plate. Using a cell scraper, only the Matrigel® was removed, leaving a ring of 2D cells left on the plate. The Matrigel®/Trizol mixture was added to a 1.7 mL microcentrifuge tube and incubated at room temperature for 10 minutes. Two hundred microliters of Chloroform was then added. Samples were vortexed until the solution was homogenous and allowed to sit again at room temperature for 10 minutes. Samples were then spun down in an Eppendorf centrifuge (5417R) for 10 minutes at 14,000 RPM and 4$^{o}$C.

600 uL of the aqueous layer was then removed and added to 450 uL of isopropanol to precipitate the RNA. The mixture was incubated at room temperature for 10 minutes. Samples were then spun down at 14,000 RPM at 4$^{o}$C for 10 minutes. The RNA pellet was washed in 75% ice-cold ethanol, to remove excess salt, and spun down at 9,500 RPM for 5 minutes, and repeated. After the second wash the ethanol was aspirated and a p200 was used to remove the remaining ethanol. The RNA was allowed to air dry for 5 minutes and dissolved in 20 uL of ddH2O.

**Generation of complimentary DNA (cDNA):** 8 uL of RNA (~8ug) from the above extractions was added to 2 uL of 50 uM Oligo dT (164) and 4 uL of 10 uM dNTPs (Bio Basic Canada). 16 uL of ddH2O was added for a final volume of 24 uL, and the mixture was incubated at 65$^{o}$C for 5 minutes. Tubes were removed from heat source and 10 uL of ddH2O, 4 uL of 10x Reverse Transcriptase (RT) buffer MulVI (New England BioLabs), and 2 uL of in-house reverse transcriptase was added to each tube.. The samples were then incubated at 50$^{o}$C for 45 minutes and immediately spun in 4$^{o}$C at 9,500 RPM for 10 minutes. cDNA concentration was determined using a ND-1000 Spectrophotometer (Nanodrop).

**Quantitative Real Time PCR (qRTPCR):** The cDNA made in the above section was diluted to 400 ng/uL in ddH2O and qRTPCR was run per manufacturers instructions on an Eppendorf Realplex2 epGradient Mastercycler. Each reaction consisted of 5 uL of diluted cDNA , 3 uL of ddH2O, 1 uL of the appropriate Sense and Antisense primers, and 10 uL of 2x SensiMix SYBR No-ROX Mastermix (BioLine) for a total volume of 20 uL. Samples were loaded into MicroAmp® Fast Optical 96-Well Reaction Plates (Applied Biosystems). PCR was performed following a 2-step cycling method: 1 Cycle at 95$^{o}$C for 2 minutes followed by 40 cycles of 95$^{o}$C for 5 seconds and 60$^{o}$C for 30 seconds. Deltadelta CT ($\Delta\Delta$CT) values were calculated for each sample, using GAPDH as the normalizing control. Comparison of the variable $\Delta\Delta$CT to control $\Delta\Delta$CT was then performed to determine the relative change in mRNA expression. Sequence sets for the primers of specific mRNA targets are found in Appendix B.

## 2.10. Three-Dimensional Growth Assay Procedure

Matrigel® was purchased from Corning. At -20$^{o}$C Matrigel® is frozen, at 0$^{o}$C the material becomes a liquid, and at 37$^{o}$C it polymerizes to form a laminin enriched extracellular matrix. Frozen Matrigel® was placed on ice for 4 hours prior to use to allow the material to liquefy. Once in liquid state, 150 uL of Matrigel® was spread out into a 35 mm$^{2}$ tissue culture dish, not allowing it to touch the edges of the dish. The dishes were then covered and placed into the 37$^{o}$C tissue culture incubator for at least 15 minutes to induce polymerization. During the polymerization phase MCF7s and MDA-MB-231 breast cancer cells were trypsinized and counted. 300,000K cells were then resuspended in 2 mLs of media. Upon polymerization cells were evenly seeded onto the Martrigel®, this is considered Day 0. Four images were captured of each condition using a Nikon SMZ1500 stereomicroscope at 10x magnification starting on Day 1 and ending on either Day 4 or Day 5. Colony size was determined by assessing the cross-sectional area using the Adobe Photoshop® Quick Selection tool. Relative colony growth was determined by comparing colony size of Day 1 to Day 4 or Day 5.

## 2.11. Cell Accumulation Assay

On Day 0, 100,000 control and variable cells, were seeded in triplicate in 12 well dishes. The following day, Day 1, 3 samples of control and each variable condition were trypsinized and counted using a hemocytometer to determine cell counts. The same procedure was repeated for Days 2-4. Growth rates for both the control and variable conditions were then determined as a percent growth normalized to Day 1.

2.12. Cell Proliferation Assay (MTT Assay)

Cells were seeded into 96 well plates at two different densities and allowed to grow for 3 days. MCF7s and MDA-MB-231 were seeded at 10,000 and 20,000 per well in 100 uL. On Day 3, 15 uL of MTT (3-(4,5-Dimethylthiazol-2-yl)-2,5-Diphenyltetrazolium Bromide), dissolved in water, at a stock concentration of 5 mg/mL, was added to each well for 4 hours. Cells were permeabilized and the converted formazan was solubilized by 100 uL of MTT Solvent Buffer (4 mM HCl, .1% Nondet P-40, in isopropanol) for 1 hour. The 96 well plate was then read by a SpectraMax 250 (Molecular Devices) plate reader, at a wavelength of 570 nm. Absorbance was then normalized to control.

2.13. Scratch Wound Assay

On Day 0, 1 million cells were seeded into a 35 $mm^2$ plate (100% confluence). The following day, Day 1 a scratch was introduced using a p200 filter tip from one edge of the plate to the other (Time 0). Images were obtained at Time 0, 12, and 24 hours using Brightfield Microscopy, as described in section 2.20. Percent wound closure was calculated using the Adobe Photoshop® Quick Selection Tool, calculating the area from one edge of the wound to the other. Each hour time point was normalized to Time 0.`

2.14. TEAD Reporter Assay

**Set up & lysate collection:** 400,000 BT474 cells were seeded into 12 well plates and cultured for 18 hours before being transfected with 0.04 μg TK_Renilla (V3605), 0.05 μg TEAD4_ GAL (Addgene 24640), 0.4 μg GAL-Luciferase Reporter (V3105),

0.23 μg 3xFLAG YAP1, and 1 μg of the indicated plasmid. 18 hours post transfection cells were washed in PBS three times and then 250 uL of Passive Lysis Buffer (Promega) was added. Plates were placed on an orbital shaker for 15 minutes to dislodge adherent cells. Lysates were then collected and cooled on ice for 10 minutes. Lysates were clarified through a $4^{o}$C spin for 10 minutes at a speed of 14,000 RPM in an Eppendorf centrifuge (5417R). 50 uL was aliquoted into 1.7 mL microcentrifuge tubes.

**Dual Luciferase Assay:** The Dual-Luciferase Assay System (Promega) was used in tandem with a $20/20^{n}$ Luminometer (Turner Biosystems) to detect luminescence. For each reaction 50 uL of LAR II was added and luciferase was measured. 50 uL of Stop & Glo substrate was then added and subsequent luciferase measurement was taken. The ratio of LAR II/Stop & Glo luciferase units was then calculated. All data was derived from at least three separate experiments that were performed in three biological replicates. Error bars represent standard deviation of mean.

2.15. CTGF Reporter Construct Cloning

Original CTGF 4.5 kb and $1^{st}$ SRF mutant luciferase coupled promoter as described in (165) were obtained from Dr. Margarete Goppelt-Struebe. These promoters were inserted into the MCS of pGL3-basic vector using a 5' KpnI and 3' XhoI restriction enzyme sites. Within the CTGF promoter there are two MluI restriction enzyme sites, one that lies ~600 bp 3' to the 5' KPNI and one that lies ~4000 kbp from the 5' KpnI restriction enzyme site. Using PCR based cloning we designed primers to ablate the 5' MluI site and reintroduce a 5' KpnI site to be used for insertion into the MCS. The CTGF reporter made from this strategy is considered the long form encompassing ~3.7 kbp.

From this construct the short ~700 bp CTGF promoter was made through restriction digest with MluI and XhoI, which was then ligated into an empty MCS of a basic-pGL3 vector. Site directed mutagenesis of SRF binding sites (2-3) (TAT→CCC) (165) and TEAD binding sites (1-2) (AAT→GCG)(134) were conducted by the Stratagene method using the primers listed in Supplemental Table 2. A gBlock was synthesized by IDT that contained the desired mutations for TEAD5-7 binding sites. This gBlock was inserted into the short and long promoter using a 5'MluI (the reason for ablating the original MluI site in the long promoter) and a 3' SacII restriction enzyme sites, following IDT protocol (Figure 2-1). All clones were sequences verified using GeneScript DNA Sequencing. Primer List in Appendix B.

2.16. CTGF Reporter Assay

HEK293Ts were plated at 200K per well of a 12 well plate. 24 hours later cells were transfected with 0.5 ug of indicated CTGF promoter luciferase construct and 0.5 ug of control TK_Renilla construct. The same procedure for "Dual Luciferase Assay" in section 2.14 was followed to collect luciferase data.

2.17. Reverse Phase Protein Array

MCF7s were transduced with either a shScramble or shARHGEF1 and serum starved for 24 hours. Following a 30 minute treatment with complete media cells, were lysed in RIPA lysis buffer. Protein concentration was measured by BCA assay, and lysates were adjusted to contain a final concentration of 1.0 ug/uL, in 1x SDS. 50 uL of lysate were transferred to a new 1.7 mL microcentrifuge, and 2 uL of β-mercaptoethanol

was added. Lysates were frozen and shipped to the Functional Proteomics RPPA Core Facility at MD Anderson Center. **Complete results are in Appendix C**.

2.18. Propidium Iodide Flow Cytometry

MCF7 cells were trypsinized and spun down at 1500 RPM for 1.5 minutes in an Eppendorf 5702 tabletop centrifuge. Cells were then washed in PBS and spun down for a second time. PBS was removed and cells were resuspended using a p1000 in 100 uL of PBS. 1 mL of 70% freshly prepared ice cold Ethanol was added drop-wise while vortexing at medium speed (4-5) to prevent cell aggregation. After drop-wise addition of 1 mL 70% ethanol, another 1 mL of ice cold ethanol was added and cells were placed on the nutator at 4$^{o}$C for overnight incubation. After fixation was complete the following morning cells were removed from 4$^{o}$C and stored at -20$^{o}$C until analysis. On the day of analysis cell were washed in PBS, spun down, and incubated in 500uL FxCycle PI/RNase Staining Solution (Life Technologies) for 30 minutes in the dark. PI fluorescence was then measured with a 590/40-emission filter (BL2) on an Attune Acoustic Focusing Flow Cytometer (Life Technologies). Live cells were gated based on forward (FSC) and side (SSC) scattering light area. 100,000 live events were captured and characterized for each sample. Appropriate cell populations were calculated using Attune Cytometric software and presented as a percentage of total live cells.

2.19. Cell Fixation for Immunofluorescence

MCF7 cells were plated onto glass coverslips in a 12 well dish. Following indicated perturbations, cells were washed in PBS and fixed with 4% Paraformaldehyde

for 5 minutes at 4°C. Cells were then washed again with PBS and blocking buffer was added for at least an hour and up to 24 hours. Primary antibodies were incubated at indicated concentrations in section 2.4 for 1 hour, followed with a PBS wash. Secondary antibodies were applied at 1:500 for 30 minutes. Cells were then washed in blocking buffer 3 times and if phalloidin was used to stain for F-actin it was applied for 20 minutes after being diluted 1:4000 in blocking buffer. Cells were again washed in blocking buffer and then nuclei were stained with Hoechst (1:3000) for 7 minutes. Coverslips were then dipped into ddH2O and mounted onto slides using 10 uL of ProLong® Gold antifade reagent (Life Technologies), and allowed to dry overnight.

## 2.20. Immunofluorescence, Brightfield and Stereomicroscopy

**Immunofluorescence:** Epifluorescent confocal images of fixed cells, as described in section 2.19, were acquired using structured light via an Apotome on a Zeiss Axio ObserverZ1. Staining dilutions of antibodies used and duration of incubation are specified in sections 2.4 and 2.19, respectively. Quantification of pixel intensity and co-localization was calculated using Zeiss Zen software. Images were processed with Adobe Photoshop®.

**Brightfield:** Brightfield images were obtained using the Zeiss Axio ObserverZ1 under the Dapi filter at 450 nm. The transmitted light was elevated to the level that saturated the fluorescent signal. Images were then taken under a phase contrast (ph) 1 or 2 setting. Phase two was used to limit the "Halo" effect seen in ph 1 images. Images were processed with Adobe Photoshop®.

**Stereomicroscopy:** Images were taken at a 10x magnification with a Nikon SMZ1500 stereomicroscope. Images were processed with Adobe Photoshop®.

2.21. Illumina HiSeq

Total transcriptional analysis was performed using a Illumina HiSeq sequencing platform. MCF7 cells were infected with either shScramble or shArhGEF1 using lenti viral transduction to create stable cell lines. Each condition was expanded to an N=4. 1 Day post seeding, cells total RNA was collected using RNeasy Kit from Qiagen. Total RNA was frozen at -70$^{o}$C and then shipped to IU Bloomington for sequencing.

2.22. Statistical Analysis

Relative levels of mRNA, cell proliferation, cell-accumulation, cell viability, total cross-sectional area/acini are presented as the means standard deviation. P-values were calculated by an unpaired two-tailed t-test.

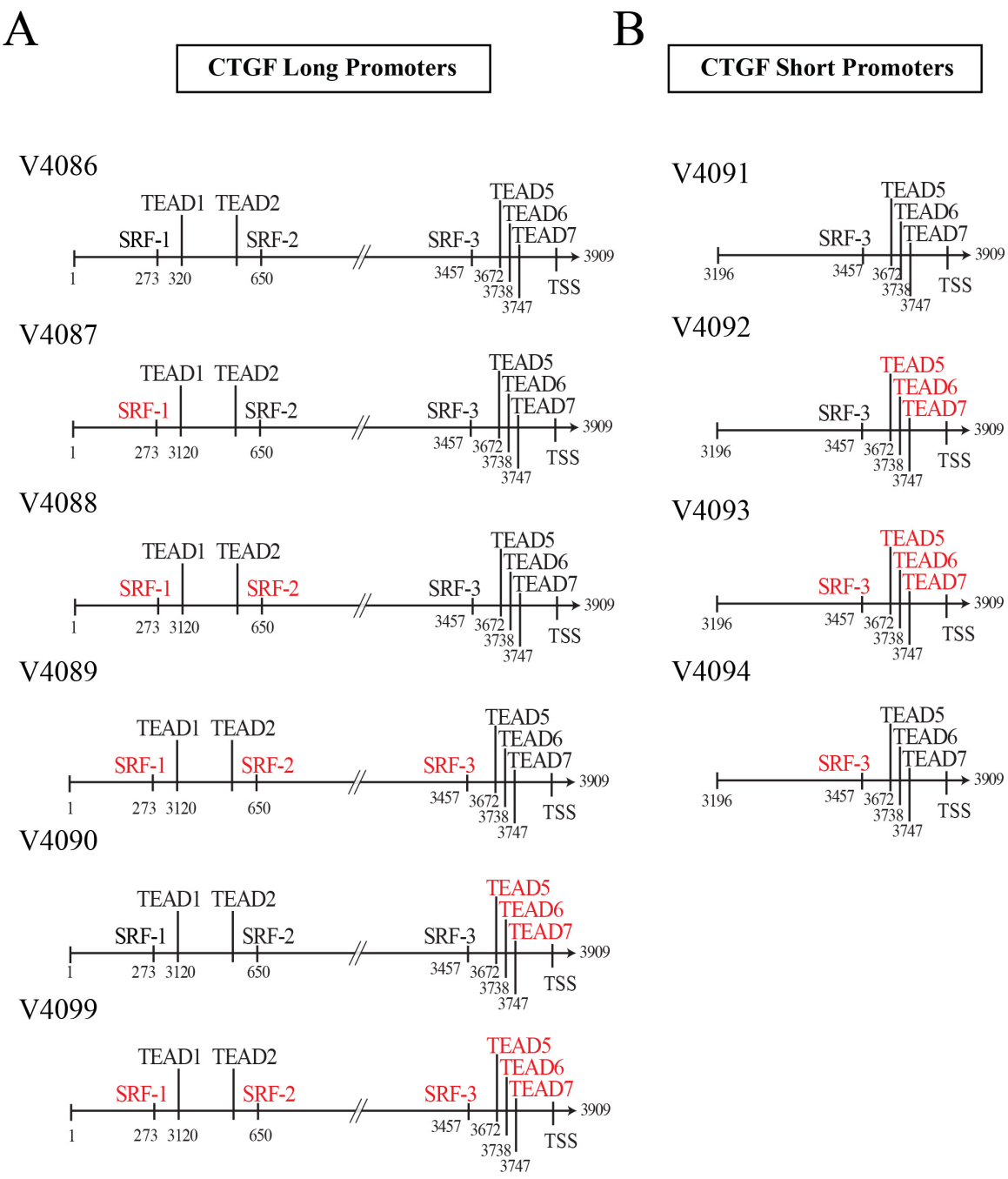


**Figure 2-1: CTGF Promoter Luciferase Reporter Constructs Cloned.**

**A.** Schematic of all long form CTGF promoters cloned. **B.** Schematic of all short form CTGF promoters cloned. Red indicates mutated SRF or TEAD response element as described in materials and methods. TEAD responsive sites 3 and 4 are located at the dashed lines and were not mutated in any of the reporters above.

# CHAPTER 3. THE RGS-RHOGEFS COORDINATE SERUM INITIATED SIGNALING ONTO THE REGULATION OF RHOA DEPENDENT YAP1 ACTIVITY

## 3.1 INTRODUCTION

Both the state of cellular adhesion (120) and the activity of multiple ligand receptor systems (122, 166-168) feed onto the HIPPO signaling pathway to control transcriptional programs that drive cell growth and survival. The core HIPPO pathway consists of MST1/2 kinase, which phosphorylates and thereby activates LATS1/2 kinase (120, 156). LATS1/2 mainly functions to phosphorylate the transcriptional co-activators YAP1 and TAZ (120, 156) as well as the family of Amot adaptor proteins (125). These phosphorylation events result in the inhibition of YAP1 transcriptional activity by sequestrating it in the cytosol (169) or promoting its degradation. Nuclear YAP1 binds and co-activates multiple transcription factors, most notably TEAD1-4 (134), that control the expression of extracellular matrix-associated growth factors such as CTGF and Cyr61. These factors in turn are essential for wound healing and organ growth (120, 169), while their deregulation promotes many diseases including various cancers. The activation of HIPPO signaling by the formation of intercellular contacts is a cornerstone in limiting these processes in normal tissues. Conversely, connections to the extracellular matrix that produce mechanical loading and consequently increased formation of actin stress fibers are necessary for YAP1 to enter the nucleus (170).

Growth factors have been found to alter the activity of the HIPPO kinases, the stability of YAP1, and/or modulate the proclivity of YAP1 to enter the nucleus and be active. For example, activation of the PI3-Kinase pathway via EGFR, inhibits the HIPPO pathway in an AKT independent manner resulting in the activation of YAP1 transcriptional activity (123). Conversely, LIFR activates HIPPO signaling to prevent YAP1 dependent migration and invasion of breast cancer cells (168). Signaling by

GPCRs that couple to $G\alpha_{12/13,}$ $G\alpha_{11}$, $G\alpha_{i}$, $G\alpha_{O}$ and $G\alpha_{q}$ also have important roles in activating YAP1 (171). This is particularly evident for serum lipid mitogens including lysophasphatidic acid (LPA) and spingosine-1 phosphate (S1P), which agonize $G\alpha_{12/13}$ (122, 166). While these discoveries highlight the importance of soluble factors in controlling YAP1, the signaling that mediates their effects are still not fully understood.

While growth factors impact HIPPO signaling in many ways, in all cases, actin filament formation is essential for the nuclear translocation of YAP1 (142). The Rho family of GTPases, RhoA, Rac1 and Cdc42 have fundamental roles in cytoskeletal dynamics and cell growth mainly as reusable switches. Rho GTPases are active when bound to GTP and carry out little or no signaling when bound to GDP. Guanine Exchange Factors (GEFs) stimulate nucleotide release to enable binding to the more prevalent GTP. Conversely, when GTPases bind GTPase Activating Proteins (GAPs) their intrinsic GTPase activity enhances the hydrolysis of GTP to GDP (172, 173). Both RhoA (142) and Cdc42 (174), through their control of actin dynamics play key roles in regulating HIPPO signaling. To understand how growth factors control different subpopulations of Rho GTPases that are committed to regulating HIPPO signaling, it is important to understand the temporal and localized activation of the GEFs and GAPs within the cell. Because only a handful of Rho family GEFs and GAPs are implicated in regulating YAP1 localization or activity (126, 163, 175), this study investigated the relative effects of expression of 67 Rho family GEFs and GAPs (representing every major subclass of these proteins) on YAP1 dependent transcription. This and subsequent characterization revealed that the RGS-RhoGEFs, ARHGEF1, ARHGEF11, and

ARHGEF12 robustly modulate YAP1 dependent transcription via the $G\alpha_{12/13}$ signaling axis.

## 3.2 RESULTS

### 3.2.1 Defining the Elements of CTGF Promoter that are Required for Serum Induced Transcription

YAP1 through its co-activation of TEAD family transcription factors is a fundamental determinant of organ size control and oncogenesis (133, 134). Connective tissue growth factor is a key target of TEAD transcription and its levels often correspond closely to TEAD activity (134). Consequently, measurements of the relative levels of CTGF transcript have become the most common way to infer YAP1/TEAD activity. However, RhoA induced formation of actin fibers can also drive the transcription of CTGF via the depletion of monomeric globular actin, which frees MRTF to translocate into the nucleus and dimerize with SRF (Figure 3-1A) (82, 83). This, in certain contexts, is also necessary and sufficient for CTGF expression (165). However, to our knowledge, the relative requirement for SRF versus TEAD in the direct transcriptional activation of CTGF by RhoA/Actin has not been defined (Figure 3-1B).

The role of TEAD and SRF response elements in RhoA induced activation of both a long (~3.9 kb) (Figure 3-1C) and a short (700 bp) (Figure 3-1C) version of the CTGF promoter. The long CTGF promoter encodes three predicted SRF and seven TEAD binding elements (Figure 3-1C). The SRF site most distal to the transcription start site (TSS) was found to be necessary for this promoter to be activated by actin polymerization (165). Whereas, the short version of the CTGF promoter which contains 1 SRF and 3 TEAD response elements requires the TEAD elements to be activated by YAP1 or TEAD (Figure 3-1D) (134). Expression of the constitutively active RhoA

(Q63L) mutant stimulated the transcription of the reporter plasmids with the long CTGF promoter (long wild-type) or a variant in which all 3 SRF elements had been ablated (long 3X-SRF) by 2-fold. However, a reporter with a mutated long promoter that lacked 5 of the TEAD binding sites (long 5X-TEAD) was refractory to activation by RhoA (Q63L) expression (Figure 3-1E). Similarly, the expression of RhoA (Q63L) activated transcription of the reporter plasmids with the short wild-type CTGF promoter (short wild-type) or short CTGF promoter with a mutant SRF element (short 1X-SRF), but not the reporter with mutations in all three TEAD binding elements (short 3X TEAD) (Figure 3-1F). Consistently, treatment of cells with the drug verteporfin, which competitively blocks the interaction of YAP1 with TEAD (176), abolished the induction of CTGF transcript by serum treatment (Figure 3-1G). These results strongly point to the importance of TEAD but not SRF response elements in mediating the activation of transcription of CTGF by RhoA induced actin fiber formation.

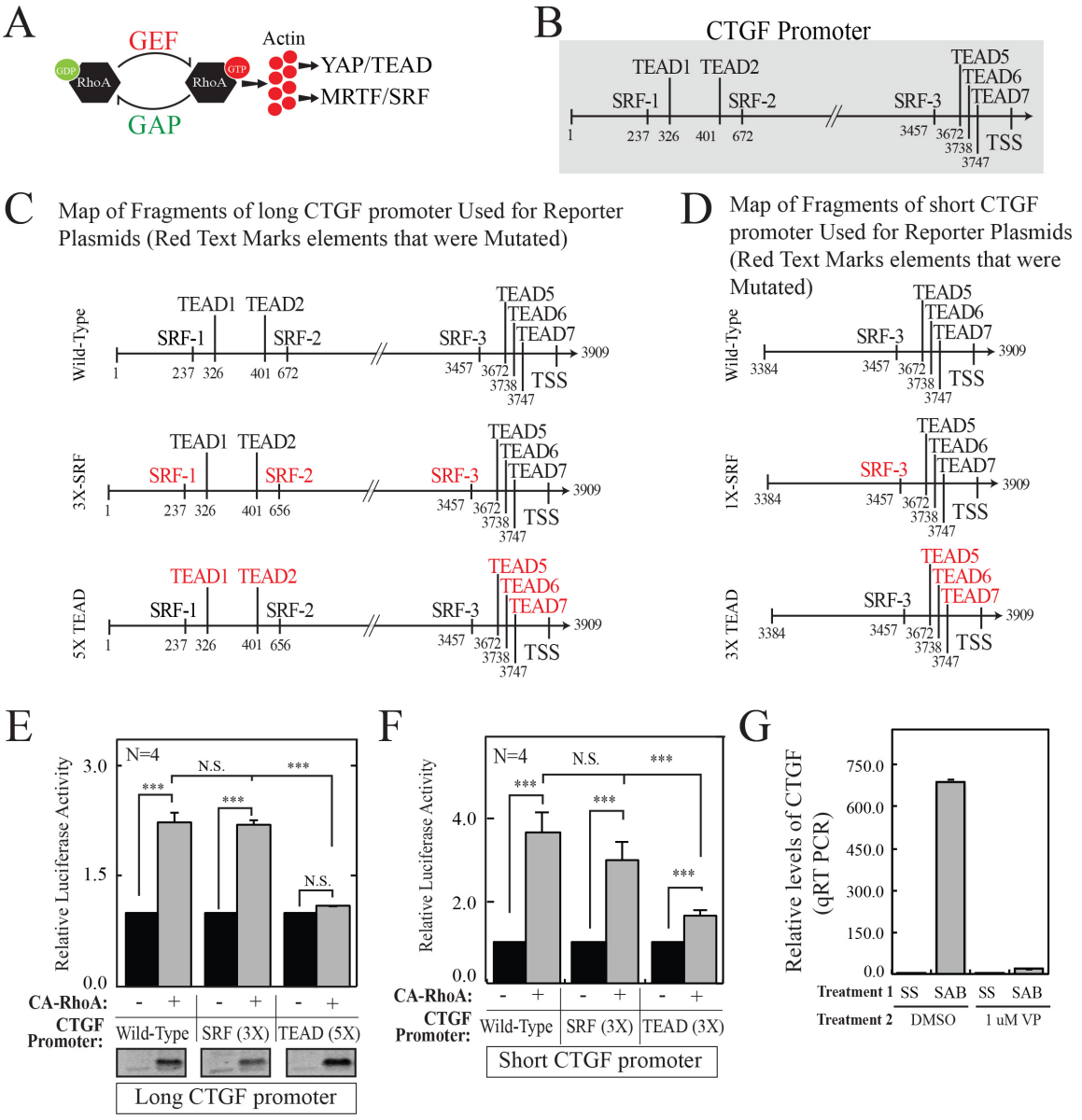


**Figure 3-1: Delineating the Requirements of TEAD vs. SRF in RhoA-Dependent CTGF Transcription.**

**A.** A model for the role of RhoA induced stress fiber formation that is coupled to the activation of MRTF and YAP1. **B.** Depiction of the ~4kb CTGF promoter with the SRF and TEAD binding elements. **C.** Schematic of the long forms of the CTGF wild-type long, 3x-SRF long, and 5x-TEAD long promoters. (Red indicates mutated response element) **D.** Schematic of the short forms of the CTGF wildtype short, 1x-SRF short, and 3x-TEAD short promoters (Red indicates mutated response element). **E.** Graph of the fold-activation of transcriptional reporters with the indicated variants of the 4 kb promoter of CTGF in MCF7 cells expressing CA-RhoA (Q63L) versus a control plasmid. All raw luciferase values were initially normalized to activity of TK-Renilla. SRF (3x) indicates 3 SRF response elements mutated, while TEAD (5X) indicates 5 TEAD response elements are mutated **F.** Graph of the fold-activation of transcriptional reporters with the indicated variants of the 700 bp promoter of CTGF in MCF7 cells expressing CA-RhoA (Q63L) versus a control plasmid. All raw luciferase values were initially normalized to activity of TK-

Renilla. SRF (3x) indicates 3 SRF response elements mutated, while TEAD (3X) indicates 3 TEAD response elements are mutated **G.** CT value of CTGF mRNA transcript was measured by qRT-PCR of MCF7 treated with 1uM of Verteporfin following 24 hours serum starvation and 30 minute treatment of 10% serum**.** Relative level of CTGF mRNA fold change (ΔΔCT) was then calculated for each sample compared to control expressing MCF7 cells.

### 3.2.2 Calibration of YAP1-Dependent TEAD Luciferase Assay

To identify which GEFs and GAPs regulate YAP1-dependent transcription the TEAD4-β-galactosidase coupled luciferase system was enlisted to identify the dynamic range of YAP1 activity in relevant models. Initial optimization studies of this assay, scanned a panel of breast cancer cell lines to determine their transfection efficiency, practicality in cell lysing, and whether TEAD dependent transcription required YAP1 activity. Among a panel of breast cancer cell lines, BT474 and MCF10A cells showed a 2-fold and 5-fold increase, respectively, in TEAD4 activity after transfection with wild type YAP1 for 24 hours (Figure 3-2A). The remaining breast cancer cell lines showed little to no response. BT474 were further chosen as the model system, due in part for their practicality in being lysed in Passive Lysis Buffer that was supplied by Promega Dual Luciferase Reporter kit, as MCF10A were refractory to this procedure. Identifying the dynamic range of maximal YAP1-dependent TEAD transcription was then further characterized over numerous time points in BT474s. Wild type 3x-Flag tagged YAP1 WT and 3x-Flag tagged YAP1 S127A, which cannot be regulated by LATS1/2 dependent phosphorylation were transiently transfected along with the TEAD4-β−galactosidase and Gal4-Reporter constructs into BT474 cells. Subsequently, lysates were collected at indicated time points. The maximal difference in TEAD transcriptional activity between YAP1 WT and YAP1 S127A, was observed between 15 and 20 hours (Figure 3-2B). To ensure maximal dependence on YAP1, assays were conducted on lysates that were collected following 18 hours of transfection. To ensure the effects of 3x-Flag tagged YAP1 WT were linearly dependent on the amount of DNA transfected, , increasing amount of 3x-Flag tagged YAP1 WT were transfected and lysates were collected at 18

hours. This produced a linear dose response with an $R^2$ value of .97 (Figure 3-2C). To validate that the YAP1-dependent activation of TEAD4-β−galactosidase were dependent on RhoA and not Rac1 or Cdc42, constitutive active mutants of all three GTPase were transfected separately into BT474 cells with the reporter constructs. This revealed that only RhoA significantly increased in TEAD4 transcription (Figure 3-2D). This tightly calibrated reporter system was then used to screen 67 GEFs and GAPs for their ability to regulated YAP1-dependent transcription.

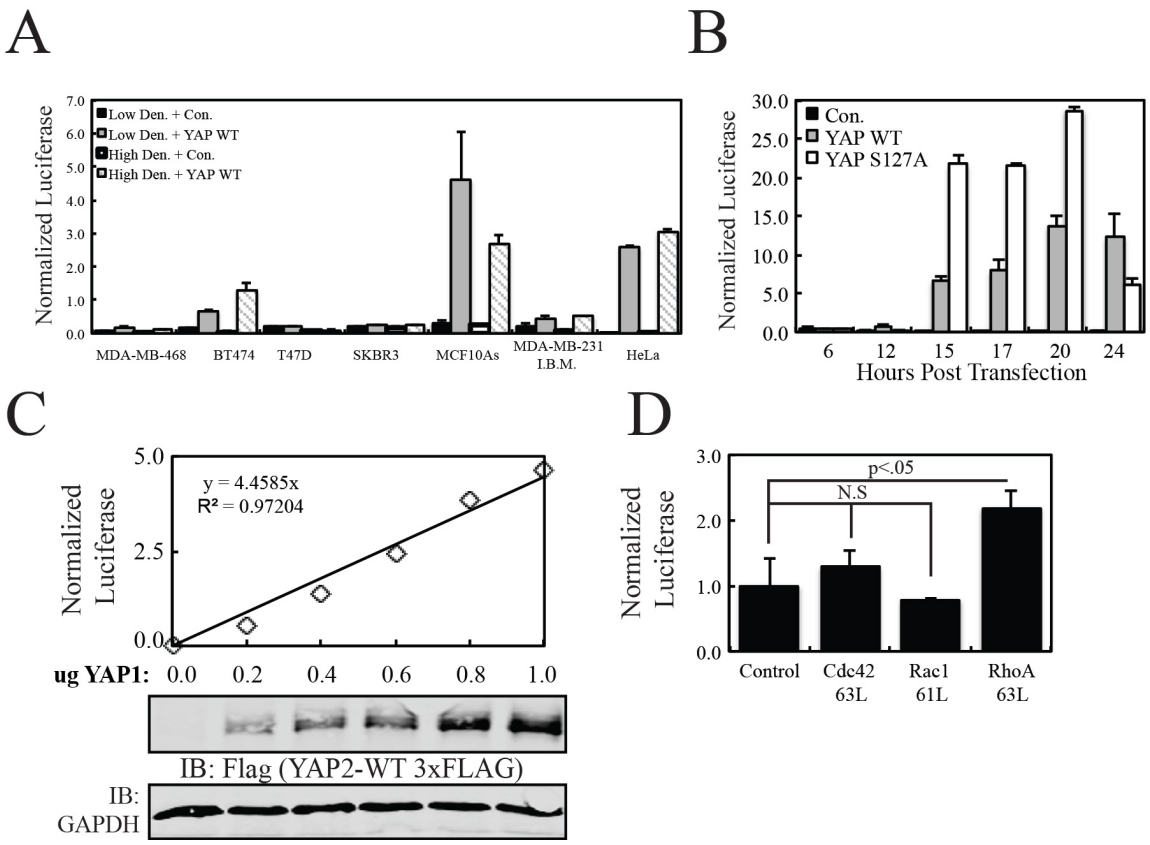


**Figure 3-2: Calibration of YAP1-Dependent TEAD4x-Gal Luciferase Activity.**

**A.** A graph of the fold change activation of TEAD4-Gal coupled 5xGal4-luciferase reporter to TK_Renilla reporter, after 18 hour transient overexpression of YAP1 in various breast cancer cell lines at high (400,000 cells) and low density (200,000 cells). **B.** A graph of the fold change activation of TEAD-Gal coupled 5xGal4-luciferase to TK_Renilla reporter, after transient overexpression of wild-type flag-tagged YAP1, flag-tagged mutant YAP1 (S127A), or control at indicated time points post transfection in BT474. **C.** A graph comparing dose dependent transient expression of flag-tagged YAP1 on the activation of TEAD-Gal coupled 5xGal4-luciferase normalized by TK_Renilla reporter in BT474s (Upper panel). Expression of flag-tagged proteins was detected by immunoblot with the M2 antibody (Bottom Panel). **D.** A graph measuring the activation of TEAD-Gal coupled 5xGal4-luciferase reporter normalized to TK_Renilla reporter for transient overexpression of RhoA (Q63L), Rac1 (Q61L), and Cdc42 (Q63L) in BT474.

### 3.2.3 Identification of Rho GEFs & GAPs that Regulate YAP1-Dependent Transcription

The effects of heterologous expression of 67 Rho GEFs and GAPs described in (177) on the activity of a TEAD4-β−galactosidase coupled luciferase reporter was determined. All 67 RhoGEFs and RhoGAPs were ordered based on their impact on the activity of the TEAD reporter (average of at least 3 separate experiments of 3 biological replicates each) (Figure 3-3A). This revealed that proteins with a DH domain with RhoGEF activity were 3 times more likely to activate the TEAD reporter versus proteins with a RhoGAP domain. Further, only proteins with a RhoGEF domain stimulated TEAD reporter activity over 2-fold (Figure 3-3B). Of these, ArhGEFs1/11/12 (74, 178-180), Plekhg6 (158), and Ect2 (181) are reported to stimulate the exchange of nucleotide for RhoA. Only, Vav1 (182) and Prex1 (183) are selective for Rac1. ArhGEF2 exhibits specificity towards RhoA and Rac1 (184). While Intersectin1 was the only GEF that is specific for Cdc42 (185) ( Figure 3-3B). Taken together, RhoGEFs with activity against RhoA were the most prevalent and efficacious activators of the TEAD reporter.

Conversely, inhibitors of the TEAD reporter, while more likely to encode a RhoGAP domain, also comprised many proteins with RhoGEF domains. Of the 13 proteins that inhibited TEAD activity more than 2-fold (top inhibitors), seven encode a GAP domain (STARD8, STARD13, ArhGAP26, ArhGAP8, ArhGAP1, HMHA1 and SYDE1), 5 a DH domain (ArhGEF39, ArhGEF16, ArhGEF7, ArhGEF9, ArhGEF25) and DOCK6 encodes a DOCK homology region 2 domain. STARD8 and STARD13, which are members of the Deleted in Liver Cancer family (DLC), were further validated as inhibitors by showing that their transient expression significantly reduced the levels of endogenous CTGF transcript (Figure 3-3C). While SYD1, HMA1 and ArhGEF39 have

no reported GTPase selectivity; the remaining top inhibitors are all known to act on Cdc42 (Figure 3-3B). This is consistent with previous reports that Cdc42 is a significant player in HIPPO signaling (174). Interestingly, all of the RhoGAPs identified as top inhibitors have been reported to accelerate the GTPase activity of RhoA (162, 186). However, amongst the GEFs, that inhibited the TEAD reporter, only ArhGEF25 is reported to have exchange activity towards RhoA. Dock6, ArhGEF25, and ArhGEF7 have GEF activity for Rac1 (Figure 3-3B). Overall, the five top inhibitors with a RhoGEF domain have exchange activity for Cdc42 (Figure 3-3B). Four of these also act on Rac1 and in a single case also on RhoA. Whereas, RhoGAPs with strong inhibitory activity all act on RhoA as well as on Cdc42.

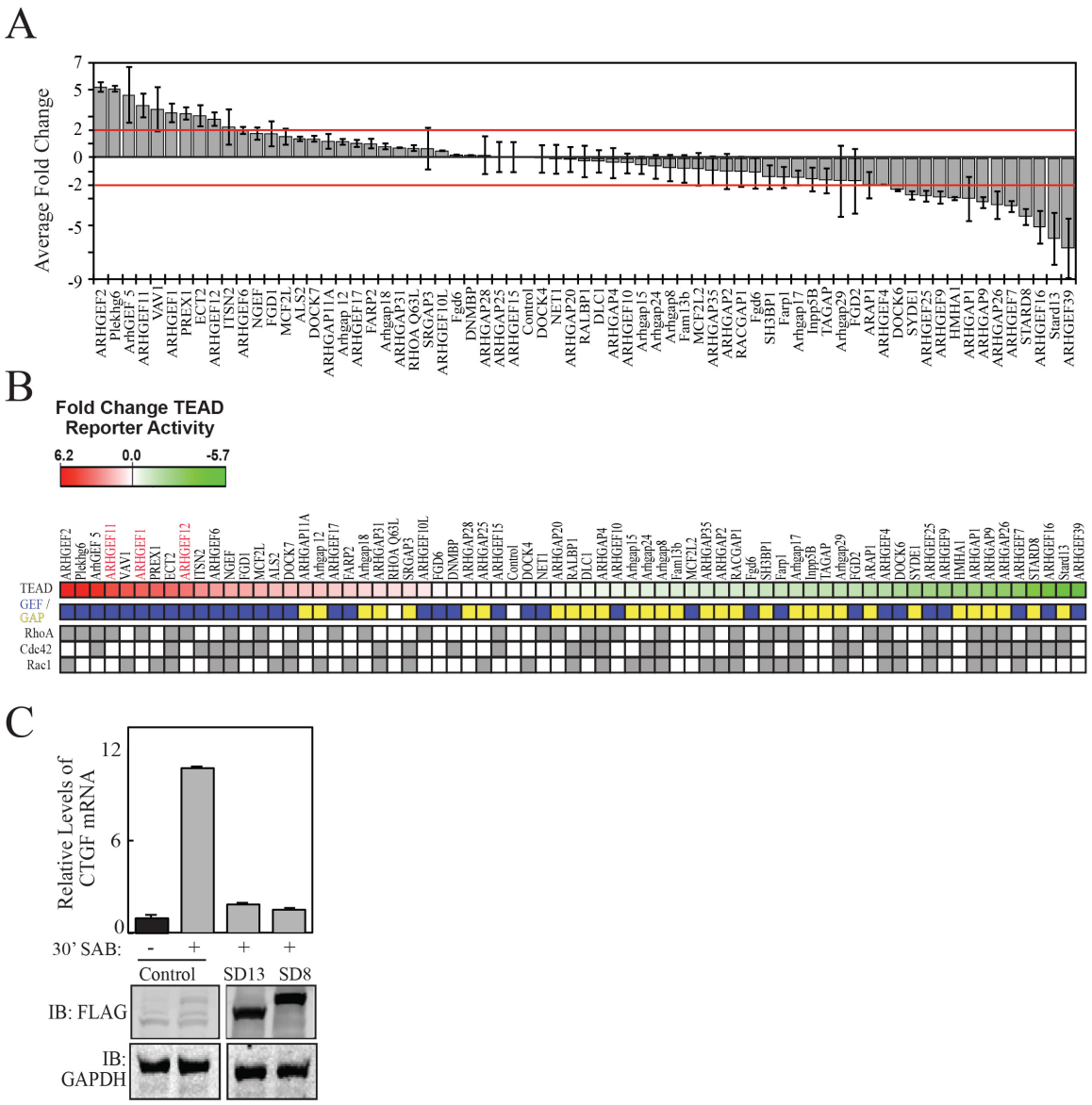


**Figure 3-3: Identification of GEFs and GAPs that Activate or Inhibit YAP1-Dependent TEAD Transcription.**

**A.** A graph measuring the fold activation of a TEAD-Gal coupled 5xGal4-luciferase reporter normalized to TK_Renilla in response to the transient overexpression of indicated flag-tagged GEF or GAP along with 0.23 μg of flag-tagged YAP1 in BT474 cells. All samples were normalized to blank control. **B.** A heat map showing the relative luciferase activity expressed in a YAP1 dependent manner from a TEAD-Gal coupled 5xGal4-luciferase reporter in BT474 cells grown under basal conditions (10% FBS), expressing the indicated RhoGEF or RhoGAP versus BT474 cell with a control plasmid. In B, every condition represents > 9 biologic replicates. Error bars represent Standard Deviation of Mean. P-values * < 0.05; ** < 0.01; *** < 0.001. **C.** CT value of CTGF mRNA transcript was measured by qRT-PCR in MCF7 cells transiently overexpressing of flag-tagged SD13 or SD8 compared to empty vector control following a 24-hour serum starvation and 10% serum treatment for 30 minutes (Upper Panel). Expression of flag-tagged proteins was detected by immunoblot with the M2 antibody (Bottom Panel).

### 3.2.4 RGS-RhoGEFs Mediate Signaling from $G\alpha_{12/13}$ onto Induction of CTGF by RhoA

Given the importance of the RGS-RhoGEFs in signaling from lipid mitogens onto the activation of RhoA, further investigations focused on their role in transmitting serum cues onto the regulation of YAP1/TEAD to control CTGF expression. All three RGS-RhoGEFs activate RhoA (74, 178-180) through a Dbl homology (DH) domain and encode an N-terminal RGS domain that exhibits GAP activity towards $G\alpha_{12}$ and/or $G\alpha_{13}$ (68, 187). Factors in serum including lipids such as LPA and thrombin proteases agonize G-protein coupled Receptors (GPCR) that recruit and activate the heterotrimeric G-proteins $G\alpha_{12}$ and $G\alpha_{13}$ (77, 188). The RGS-RhoGEFs consequently are recruited by the activated G-protein at the membrane mainly through interactions with their RGS domain (65). This enables a secondary low affinity interaction between $G\alpha_{13}$ and the DH domain that enhances exchange activity (189, 190) (Figure 3-4A). Induction of CTGF transcript levels by serum after 1 hour was significantly lower in MCF7 cells transiently expressing the RGS domain of ArhGEF1, which selectively inhibits $G\alpha_{12}$ and $G\alpha_{13}$ (187), versus cells expressing a control plasmid (Figure 3-4B). This is consistent with previous work showing that serum strongly requires $G\alpha_{12}$ and/or $G\alpha_{13}$ to activate YAP1/TEAD (171). The significantly reduced levels of CTGF transcript in MC7 cells expressing the $G\alpha_{13}$ (R232E) mutant, which binds to the RGS-RhoGEFs but cannot stimulate their exchange activity (67), versus wild-type $G\alpha_{13}$ denotes that the RGS-RhoGEFs are required for serum induced activation of YAP1/TEAD (Figure 3-4C). The modest induction of CTGF by the $G\alpha_{13}$ (R232E) mutant may result from $G\alpha_{13}$ (R232E) affecting the RGS-RhoGEFs independently of direct stimulation of exchange activity, e.g. recruitment to the membrane (191). Together, the activation of RhoA by $G\alpha_{12}$ and $G\alpha_{13}$ through the RGS-

RhoGEFs is found to constitute a primary pathway for the activation of YAP1 dependent transcription of CTGF by serum.

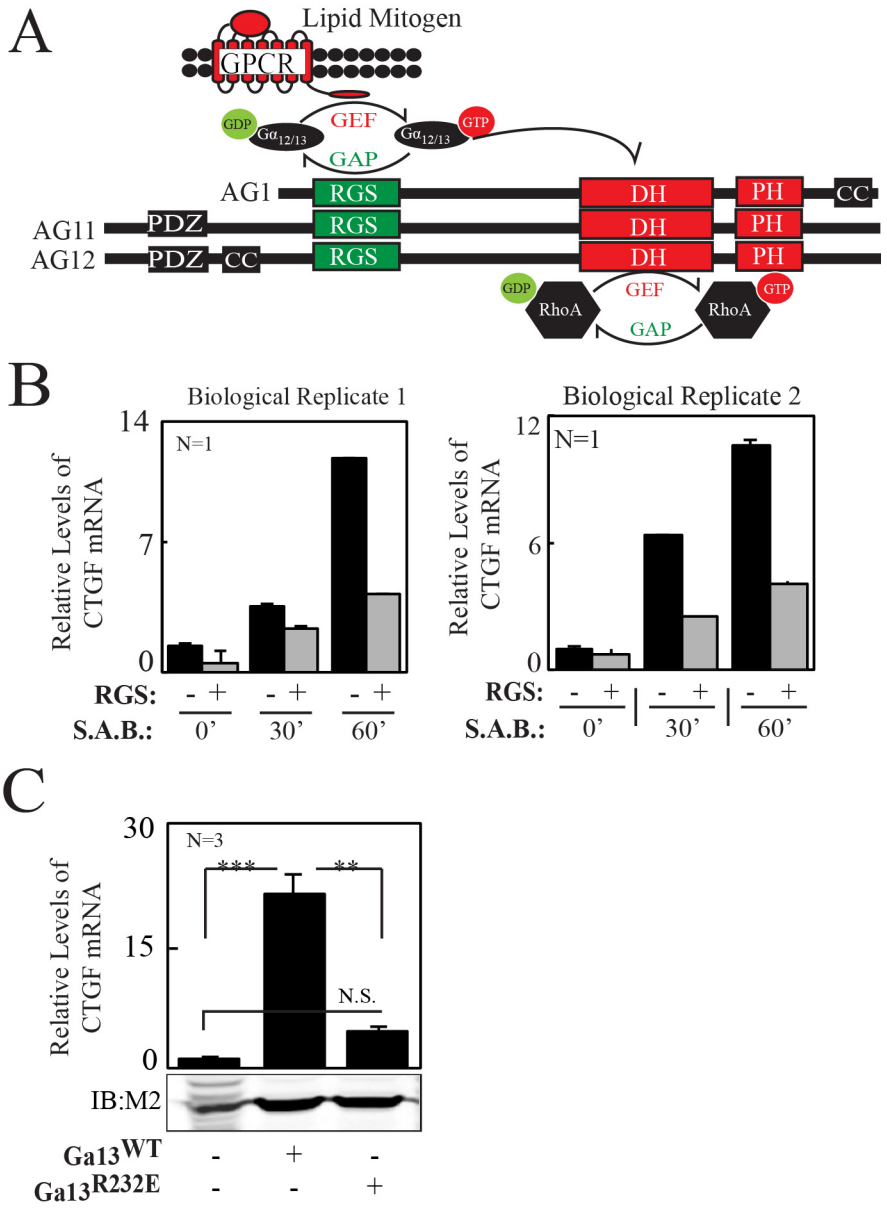


**Figure 3-4: $G\alpha_{13}$ Signaling through the RGS-RhoGEFs Induces CTGF Transcript Levels.**

**A.** Model for the activation of $G\alpha_{12/13}$ heterotrimeric g-proteins and their consequent bi-directional signaling with ArhGEF1, 11, 12. **B.** CT value of CTGF mRNA transcript was measured by qRT-PCR in MCF7 cells transiently expressing either the RGS domain of ArhGEF1 or a control plasmid. MCF7 cells were also incubated without serum for 24-hours and then with 10% FBS (Serum Add Back; S.A.B.) for the indicated times. Relative level of CTGF mRNA fold change (ΔΔCT) was then calculated for each sample compared to control expressing MCF7 cells at time 0'. Biological replicates side by side. **C.** CT value of CTGF mRNA transcript was measured by qRT-PCR in MCF7 cells transduced by lentivirus for the expression of Flag-tagged $G\alpha_{13}$ wild-type or the Flag-tagged $G\alpha_{13}$ (R232E) mutant, which cannot stimulate exchange activity of bound RGS-RhoGEF (Top Graph) Relative level of CTGF mRNA fold change (ΔΔCT) was then calculated for each sample compared to control expressing MCF7 cells.

Expression of flag-tagged proteins was detected by immunoblot with the M2 antibody (Bottom Panel).

### 3.2.5 ArhGEF11 and ArhGEF12 Transmit $G\alpha_{12/13}$ Signaling onto the Activation of YAP1/TEAD

While heterologous expression of all of the RGS-RhoGEFs resulted in the YAP1 dependent activation of the TEAD reporter, the physiologic circumstances for these activities are unclear. The lack of induction of the levels of CTGF transcript in cells expressing either ArhGEF11 or ArhGEF12 in combination with the exoenzyme C3 transferase exotoxin (a selective inhibitor of RhoA) confirms that they require RhoA activity to activate YAP1 (Figure 3-5A). A more dominant role of ArhGEF12 in this pathway, in MCF7 cells, is supported by the ~ 80 % decrease in the levels of CTGF transcript following serum treatment of ArhGEF12 silenced cells versus a 50 % decrease in cells silenced for ArhGEF11 (Figure 3-5B). While LPA is the most studied agonists for GPCRs that couple to $G\alpha_{12/13}$, several other factors including Sphingosine-1-phosphate, thrombin proteases, and calcium activate these GTPases (188, 192). Along these lines, the induction of CTGF transcript levels in cells treated with LPA or with a peptide agonists for the Protease Activated Receptor (PAR) 2 but not a peptide agonist for PAR1 were significantly less in cells silenced for ArhGEF12 expression versus control cells (Figure 3-5D). Similarly, induction of CTGF transcript levels upon expression of $G\alpha_{12}$ (Figure 3-5E) or $G\alpha_{13}$ (Figure 3-5F) was diminished by over 80 % if the cells were also silenced for ArhGEF12. Whereas, cells silenced for ArhGEF11 reduced CTGF transcription by 50% after LPA treatment, versus control cells, but retained similar levels of CTGF transcription after treatment with the peptide agonists for the PAR1 or PAR2 receptors (Figure 3-5G). Upon stable expression of $G\alpha_{12}$ (Figure 3-5H) or $G\alpha_{13}$ (Figure 3-5I), knockdown of ArhGEF11, like ArhGEF12, showed an ~80%

reduction in CTGF transcript levels. ArhGEF12 therefore appears to mediate the majority of signaling onto YAP1 activation that is initiated by the LPA and PAR receptors versus ArhGEFF11. Consistent with these data, cells silenced for ArhGEF12 (Figure 3-5K) expression showed profoundly greater losses of actin fibers and a rounded morphology versus cells silenced for ArhGEF11 (Figure 3-5L).

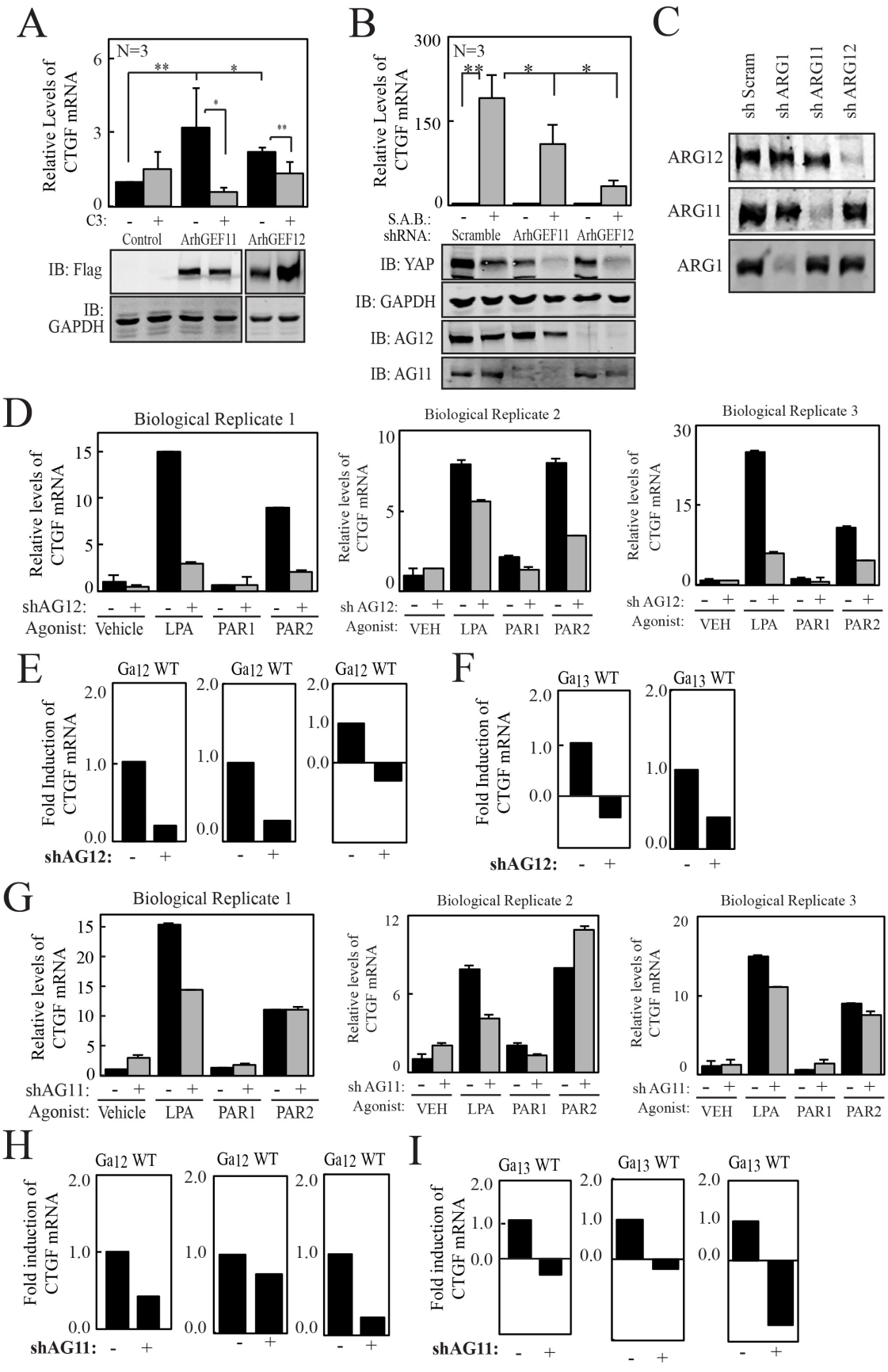
A
N=3
Relative Levels of CTGF mRNA
C3:
Control
ArhGEF11
ArhGEF12
IB: Flag
IB: GAPDH
B
N=3
Relative Levels of CTGF mRNA
S.A.B.:
shRNA:
Scramble
ArhGEF11
ArhGEF12
IB: YAP
IB: GAPDH
IB: AG12
IB: AG11
C
sh Scram
sh ARG1
sh ARG11
sh ARG12
ARG12
ARG11
ARG1
D
Biological Replicate 1
Biological Replicate 2
Biological Replicate 3
Relative levels of CTGF mRNA
shAG12:
Agonist:
Vehicle
LPA
PAR1
PAR2
VEH
E
Gα12 WT
Fold Induction of CTGF mRNA
shAG12:
F
Gα13 WT
Fold Induction of CTGF mRNA
shAG12:
G
Biological Replicate 1
Biological Replicate 2
Biological Replicate 3
Relative levels of CTGF mRNA
shAG11:
Agonist:
Vehicle
LPA
PAR1
PAR2
VEH
H
Gα12 WT
Fold induction of CTGF mRNA
shAG11:
I
Gα13 WT
Fold induction of CTGF mRNA
shAG11:

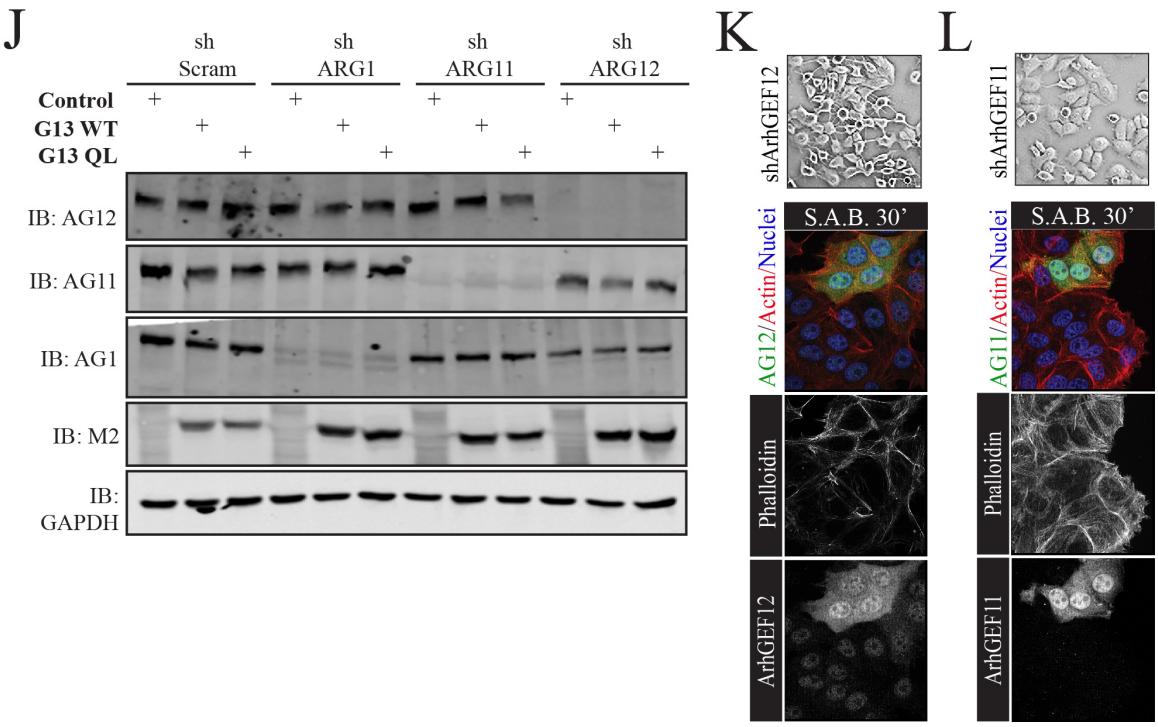


**Figure 3-5: ARHGEF11 and ARHGEF12 are Essential for the Induction of CTGF by $G\alpha_{12}$ and $G\alpha_{13}$ Dependent Signaling.**

**A.** CT value of CTGF mRNA transcript was measured by qRT-PCR in MCF7 cells that transiently expressed Flag-Tagged tagged ArhGEF11 or Flag-tagged ArhGEF12 in combination with transient expression of C3 exotoxin plasmid or a control (Top Graph). Relative level of CTGF mRNA fold change (ΔΔCT) was then calculated for each sample compared to control expressing MCF7 cells. Immunoblot with antibodies against Flag-tag (M2) or GAPDH (bottom panels) **B.** CT value of CTGF mRNA transcript was measured by qRT-PCR in MCF7 cells stably silenced through lenti viral transduction of shScramble, shArhGEF11 or shArhGEF12 and subject to 24 hour serum starvation followed with a 30 minute treatment of 10% FBS (S.A.B.) (Top Graph). Relative level of CTGF mRNA fold change (ΔΔCT) was then calculated for each sample compared to control expressing serum starved MCF7 cells. The relative levels of YAP1, ArhGEF11 (ARG11), ArhGEF12 (ARG12) and GAPDH were detected by immunoblot (Bottom Panels) **C.** Immunoblot of endogenous protein expression in MCF7 cells knocked down for ArhGEF1, ArhGEF11, and ArhGEF12 using lenti viral delivered shRNA. **D.** CT value of CTGF mRNA transcript was measured by qRT-PCR in MCF7 cells stably silenced through lenti viral transduction of shRNA for ArhGEF12 (shAG12) or with control shRNA and serum starved for 24 hours before incubation with agonists of the LPA (1uM), PAR1 (TFLLR-$NH_2$: 10 uM) or PAR2 receptors (2-furoyl-LIGRLO-$NH_2$ 5 uM). Relative level of CTGF mRNA fold change (ΔΔCT) was then calculated for each sample compared to serum starved MCF7 cells not stimulated by agonist. (3 Biological Replicates) **E.** CT value of CTGF mRNA transcript was measured by qRT-PCR in MCF7 upon lenti viral transduced stable expression of Flag-tagged $G\alpha_{12}$ versus Flag control, between cells stable silenced for ArhGEF12 (shARG12) or a control shRNA using lentiviral transduction. Relative level of CTGF mRNA fold change (ΔΔCT) was then calculated for each sample compared to serum starved MCF7 cells not stimulated by agonist. (3 Biological Replicates) **F.** CT value of CTGF mRNA transcript was measured by qRT-PCR in MCF7 upon lentiviral transduced stable expression of Flag-tagged $G\alpha_{13}$ versus Flag control, between cells stable silenced for ArhGEF12 (shARG12) or a control shRNA using lentiviral

transduction. Relative level of CTGF mRNA fold change (ΔΔCT) was then calculated for each sample compared to serum starved MCF7 cells not stimulated by agonist. (2 Biological Replicates **G.** CT value of CTGF mRNA transcript was measured by qRT-PCR in MCF7 cells silenced for ArhGEF11 (shAG11) or control shRNA, using lentiviral transduction, and serum starved for 24 hours before incubation with agonists of the LPA (1uM), PAR1 (TFLLR-$NH_2$: 10 uM) or PAR2 receptors (2-furoyl-LIGRLO-$NH_2$ 5 uM). (3 Biological Replicates) **H.** CT value of CTGF mRNA transcript was measured by qRT-PCR in MCF7 cells following stable by lentiviral transduction expression of Flag-tagged $G\alpha_{12}$ (versus expression of Flag control between cells infected with sahAG11 or control shRNA. (3 Biological Replicates). **I.** CT value of CTGF mRNA transcript was measured by qRT-PCR in MCF7 cells following stable by lentiviral transduction expression of flag-tagged $G\alpha_{13}$ (Right Panel) versus expression of flag control between cells infected with sahAG11 or control shRNA. (3 Biological Replicates). **J.** Immunoblot of endogenous expression of RGS-RhoGEFs and Flag-tagged $G\alpha_{13}$ (M2 antibody) in MCF7 cells stably expression $G\alpha_{13}$, $G\alpha_{13}$ QL, or control cells in combination with stably silenced RGS-RhoGEF. **K.** Brightfield imaging of MCF7 cells stably silenced for ArhGEF12 (Top Panel) through lentiviral delivery of shRNA. Stably silenced cells MCF7 were serum starved and treated with 10% serum for 30 minutes then fixed and immunostained for ArhGEF12 and YAP1 merged with nuclei stained with Hoechst dye (Bottom Panel). **L.** Brightfield imaging of MCF7 cells stably silenced for ArhGEF11 (Top Panel) through lentiviral mediated delivery of shRNA. Stably silenced MCF7 cells were serum starved and treated with 10% serum for 30 minutes then fixed and immunostained for ArhGEF11 and YAP1 then merged with nuclei stained with Hoechst dye (Bottom Panel).

### 3.2.6 ArhGEF1 Dampens $G\alpha_{12/13}$ Signaling Initiated by Mitogens in Serum

The role of ArhGEF1 in transducing the effects of serum onto YAP1/TEAD activation was compared to those of ArhGEF11 and ArhGEF12. Surprisingly, MCF7 cells stably silenced for the expression of ArhGEF1 had elevated levels of CTGF at 2, 4 and 5 hours in comparison to control cells following the add back of serum (Figure 3-6A). This effect likely requires RhoA activation as the expression of ArhGEF1 with C3-toxin had similar levels of CTGF as control cells (Figure 3-6B). Given the disparity of these two results and with the original observation that ArhGEF1 overexpression enhances TEAD4 transcriptional activity, the impact of ArhGEF1 expression on the induction of CTGF transcript levels by serum was determined. Similar to the candidate expression screen, MCF7 cells stably expressing ArhGEF1 grown in the absence of serum for 24-hours produced a 2-fold induction of CTGF transcript versus control MCF7 cells (Figure 3-6C). Conversely, significantly lower levels of CTGF transcript was observed in cells following a 30 minute exposure to media with 10 % serum versus control (Figure 3-6C). The effects of ArhGEF1 loss on CTGF transcript levels were also highly impacted by cell density. ArhGEF1 silenced MCF7 cells grown at low density or at very high density exhibited similar or only modestly higher levels of CTGF transcript versus control MCF7 cells grown to a corresponding density after serum treatment (Figure 3-6D). These data highlight the ability of ArhGEF1 to limit serum induction of CTGF transcription in a manner that is highly sensitive to RhoA activity and cell density.

Given our findings that TEAD elements are primarily mediating the activation of the CTGF promoter by RhoA, the role of YAP1 in mediating the affects of ArhGEF1 onto the induction of CTGF was investigated. Consistent with YAP1 activation,

immunoblot analysis revealed that the ratio of S-127 phosphorylated YAP1 over total YAP1 decreased in lysates from ArhGEF1 silenced MCF7 cells following a serum starvation serum, add back treatment versus MCF7 cells infected with a control shRNA (Figure 3-6E). This was further confirmed by the enhanced distribution of YAP1 in the nucleus of cells (grown to intermediate density) with the highest degree of ArhGEF1 silencing (Figure 3-6F), compared to its exclusion in control MCF7 cells. This effect was not evident in cells at low density where YAP1 almost exclusively localized in the nucleus (Figure 3-6G), nor in cells grown at high density where YAP1 was overwhelmingly localized in the cytosol (Figure 3-6H). A requirement for YAP1 activation for enhanced induction of CTGF transcript by serum in MCF7 cells silenced for ArhGEF1, is strongly indicated by loss of this effect in cells simultaneously silenced for YAP1 by as little as 50 % (Figure 3-6I). Overall, these results demonstrate that ArhGEF1 limits the effects of serum signaling onto CTGF transcription by preventing YAP1 activation in cells that are in the processes of forming intercellular contacts (intermediate density).

The knockdown of ArhGEF1 enhances serum induced YAP1 dependent CTGF transcription; the role of how actin dynamics regulate this process was further investigated. By increasing the multiplicity of infection of MCF7 cells with lenti virus containing shRNA against ArhGEF1, moderate (50-60 %), high (80-90 %) and complete (undetectable) loss of protein expression of ArhGEF1 was achieved, as measured by western blot. While cells with high and complete levels of ArhGEF1 silencing showed similar levels of induction of CTGF following treatment with serum, complete silencing resulted in significantly higher levels of CTGF transcript (albeit much lower than in cells

after serum-add back) under serum starved conditions versus cells with even 90 % loss of ArhGEF1 expression (Figure 3-7A). Cells with complete silencing also showed an extreme flattened morphology (Figure 3-7B) and a drastic increase in filamentous actin (Figure 3-7C) versus cells with high or moderate levels of ArhGEF1 silencing. Because a certain level of filamentous actin is required for YAP1 to enter the nucleus (142, 170), a partial loss of ArhGEF1 is proposed to increase the formation of f-actin and thereby sensitize cells to the activation of YAP1 by serum. Interestingly an almost complete loss ArhGEF1 results in a dramatic shift in morphology resulting in YAP1 activation in cells grown in the absence of serum for 24-hours. These data indicate that only modest levels of ArhGEF1 are needed to maintain control of YAP1 nuclear translocation.

The dominant role of ArhGEF1 in blocking serum signaling onto YAP1 activation may be explained by its RGS domain accelerating the GTPase activity of $G\alpha_{12}$ and/or $G\alpha_{13}$ (187, 189). However, it is not clear whether ArhGEF1 in cells functions selectively in response to different receptors that couple to $G\alpha_{12/13}$. It is also not clear whether ArhGEF1 functions similarly towards $G\alpha_{12}$ and $G\alpha_{13}$ in cells. Consistent with results from serum, the induction of CTGF transcript in MCF7 cells stably silenced for ArhGEF1 was significantly greater after treatment with LPA or a peptide that specifically activates PAR2 versus cells that express normal levels of ArhGEF1. However, loss of ArhGEF1 expression had no impact on the induction of CTGF by a peptide that only activates PAR1 (Figure 3-8A). Further, cells silenced for ArhGEF1 exhibited an over 5-fold increase in the levels of CTGF transcript following transient expression of $G\alpha_{13}$ but reduced CTGF induction in cells expressing $G\alpha_{12}$ when compared to non-silenced cells expressing these respective GTPases. Similarly, ArhGEF1 silencing suppressed the

induction of CTGF by the expression of the GTPase deficient $G\alpha_{13}$ mutant $G\alpha_{13}$ (QL) (Figure 3-8B). ArhGEF1 in cells therefore appears to mainly function as a GAP against $G\alpha_{13}$ but not $G\alpha_{12}$ following receptor activation. Further, if ArhGEF1 cannot act as a GAP, it then appears to be stimulated by $G\alpha_{12/13}$ to transmit signaling that activates YAP1 dependent transcription of CTGF, as evident when silenced in a $G\alpha_{13}$QL stable overexpression background.

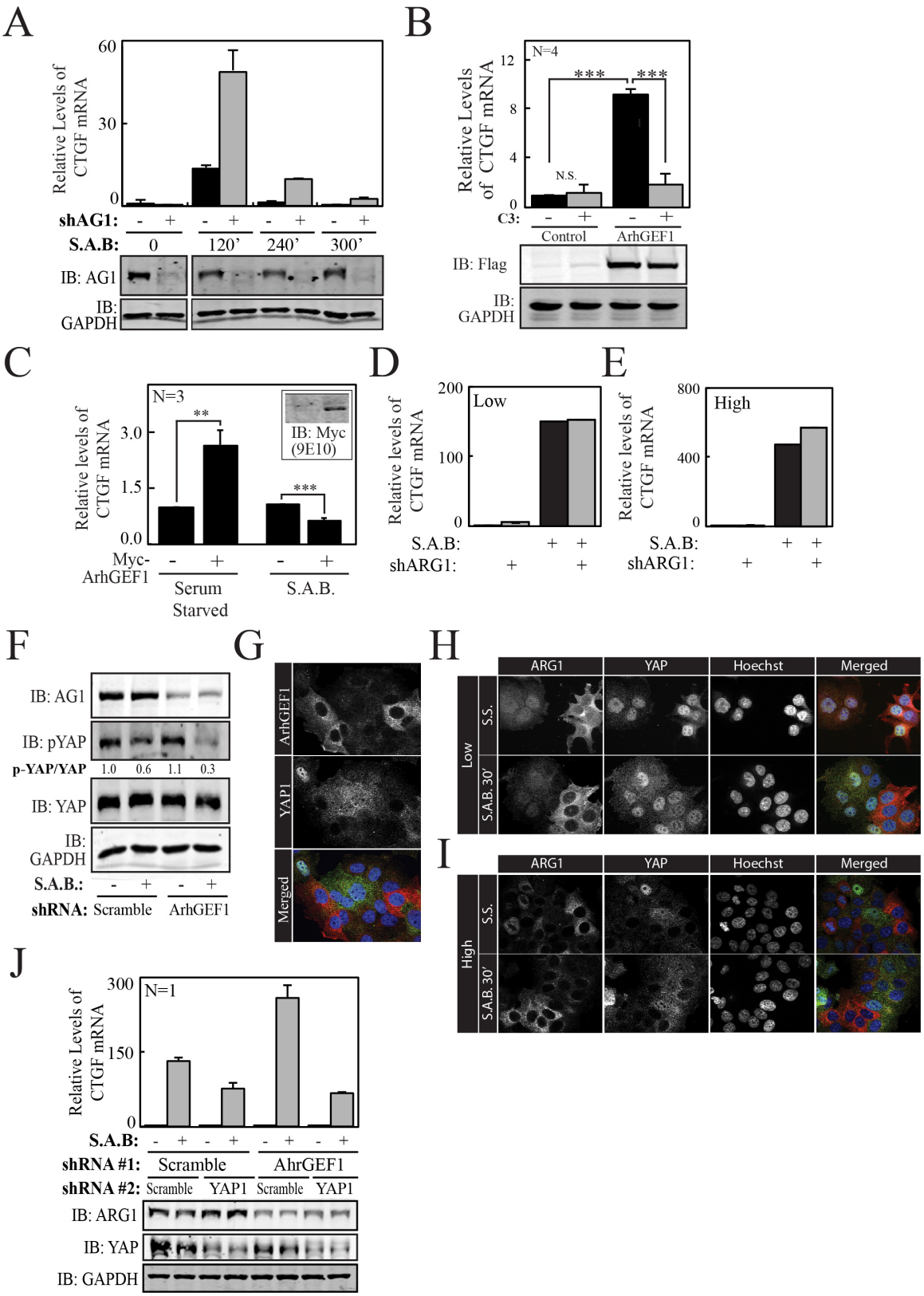
A
Relative Levels of CTGF mRNA
60
30
0
shAG1: - + - + - + - +
S.A.B: 0 120' 240' 300'
IB: AG1
IB: GAPDH
B
N=4
Relative Levels of CTGF mRNA
12
8
4
0
***
***
N.S.
C3: - + - +
Control
ArhGEF1
IB: Flag
IB: GAPDH
C
N=3
Relative levels of CTGF mRNA
3.0
1.5
0.0
**
***
IB: Myc (9E10)
Myc-ArhGEF1 - + - +
Serum Starved
S.A.B.
D
Low
Relative levels of CTGF mRNA
200
100
0
S.A.B: + +
shARG1: + +
E
High
Relative levels of CTGF mRNA
800
400
0
S.A.B: + +
shARG1: + +
F
IB: AG1
IB: pYAP
p-YAP/YAP 1.0 0.6 1.1 0.3
IB: YAP
IB: GAPDH
S.A.B.: - + - +
shRNA: Scramble ArhGEF1
G
ArhGEF1
YAP1
Merged
H
ARG1
YAP
Hoechst
Merged
Low
S.S.
S.A.B. 30'
I
High
S.S.
S.A.B. 30'
J
N=1
Relative Levels of CTGF mRNA
300
150
0
S.A.B: - + - + - + - +
shRNA #1: Scramble AhrGEF1
shRNA #2: Scramble YAP1 Scramble YAP1
IB: ARG1
IB: YAP
IB: GAPDH

**Figure 3-6: Loss of ARHGEF1 Expression Activates YAP1 in Cells After Prolonged Serum Treatment.**

**A**. CT value of CTGF mRNA transcript was measured by qRT-PCR in MCF7 cells stably silenced for ArhGEF1 (shAG1) or treated with shRNA control following serum starvation and then add back of media with 10 % FBS (S.A.B.) for the indicated times. Relative level of CTGF mRNA fold change (ΔΔCT) was then calculated for each sample compared to control expressing, serum starved MCF7 cells (Top Graph)(Replicates in Fig. S4A, B). Levels of ArhGEF1 and GAPDH were measured by immunoblot (Bottom Panel) **B.** CT value of CTGF mRNA transcript was measured by qRT-PCR in MCF7 cells expressing transient overexpression of Flag-tagged ArhGEF1 in MCF7 compared to control in combination with RhoA specific inhibitor C3 (Top Panel). Immunoblot of overexpressed Flag-tagged ArhGEF1 by M2 antibody. **C.** CT value of CTGF mRNA transcript was measured by qRT-PCR in MCF7 cells expressing myc-control or myc-ArhGEF1 after 24 hours serum starvation followed by treatment for 30 minutes with media alone or media with 10 % FBS (S.A.B.). Relative level of CTGF mRNA fold change (ΔΔCT) was then calculated for each sample compared to control serum-starved MCF7 cells. Furthermore, myc-ArhGEF1 that was subject to 10% FBS (S.A.B.), ΔΔCT, was normalized to control MCF7 cells subject to 10% FBS (S.A.B) ΔΔCT. **D**. Relative levels of CTGF transcript (measured by qRTPCR) in sparse cells stably silenced for ArhGEF1 (ARG1) or treated with shRNA control following serum starvation and then add back of media with 10 % FBS for 30 minutes. **E**. Relative levels of CTGF transcript (measured by qRTPCR) in confluent cells stably silenced for ArhGEF1 (ARG1) or treated with shRNA control following serum starvation and then add back of media with 10 % FBS for 30 minutes. **F** Levels of ArhGEF1, phospho-YAP1, total YAP1 and GAPDH were measured by immunoblot from lysates prepared from MCF7 silenced for ArhGEF1 following a 24-hour serum starvation and subsequent treatment for 30 min with media or media with 10% FBS (S.A.B.). **G.** MCF7 cells infected with shAG1 were serum starved and then fixed and immunostained for ArhGEF1 (Top Panel) and YAP1 (Middle Panel) merge with nuclei stained with Hoechst dye (Bottom Panel). **H.** MCF7 genetically silenced for ArhGEF1 through lentiviral delivered shRNA were plated at low density and were serum starved (Top panel) or serum starved and treated with 10% FBS for 30 minutes (Bottom Panel) then fixed and immunostained for ArhGEF1, YAP1, and Hoechst dye. **I.** MCF7 genetically silenced for ArhGEF1 through lentiviral delivered shRNA were plated at high density and were serum starved (Top panel) or serum starved and treated with 10% FBS for 30 minutes (Bottom Panel) then fixed and immunostained for ArhGEF1, YAP1, and Hoechst dye. **J.** CT value of CTGF mRNA transcript was measured by qRT-PCR in MCF7 cells stably silenced for ArhGEF1 or YAP1 alone or in combination that were then serum starved before being treated with media alone or media containing 10 % FBS (S.A.B.). Relative level of CTGF mRNA fold change (ΔΔCT) was then calculated for each sample compared to control serum-starved MCF7 cells. (Top Panel). The levels of ArhGEF1 (AG1), YAP1 and GAPDH were measured by immunoblot (Bottom Panels).

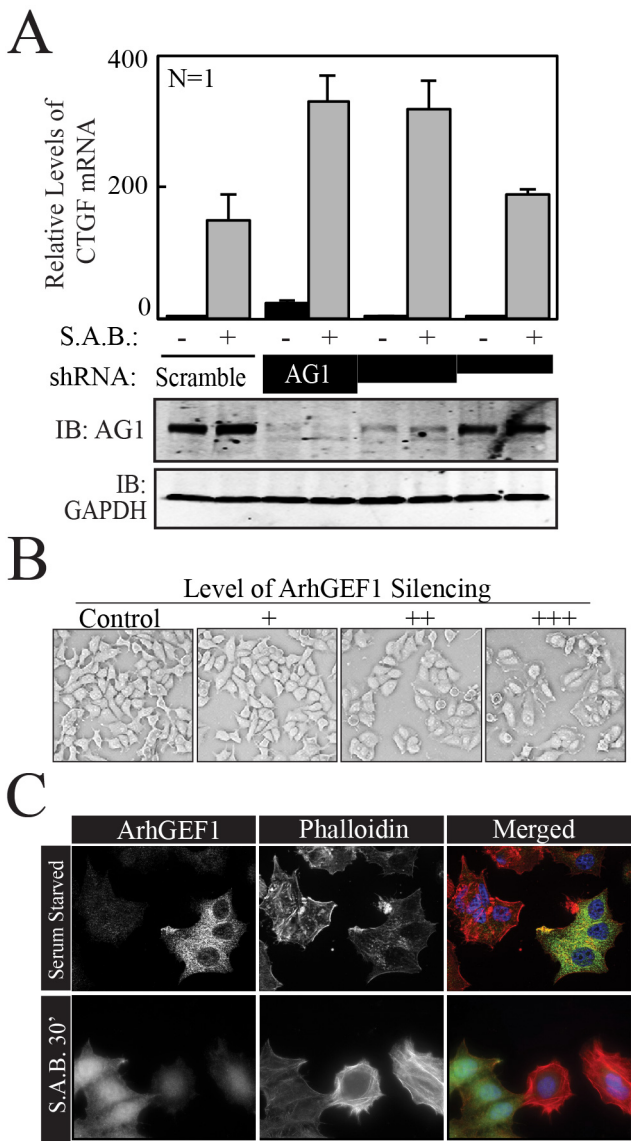


**Figure 3-7: Complete Loss of ArhGEF1 Expression Induces YAP1 Activation in Serum Starved Cells that also Exhibit a Dramatic Increase in F-Actin Fibers and Cell Flattening.**

**A.** CT value of CTGF mRNA transcript was measured by qRT-PCR in MCF7 cells with complete, high and moderate stable silencing of ArhGEF1 (AG1) MCF7 cells that were starved of serum before being treated for 30 min with media alone or media with 10% FBS (S.A.B.). Relative level of CTGF mRNA fold change (ΔΔCT) was then calculated for each sample compared to control expressing, serum starved MCF7 cells (Top Graph). ArhGEF1 (AG1) and GAPDH levels were measured by immunoblot (Bottom Panel). **B.** Brightfield images of cells from (A). **C.** Cells with differential stable silencing of AG1 after serum starvation and treatment with media alone or media with 10 % FBS (S.A.B.) were fixed and immunostained for ArhGEF1 (Left Panel) and phalloidin to visualize Actin (Middle Panel) and merged image with Nuclei stained with Hoechst (Right Panel).

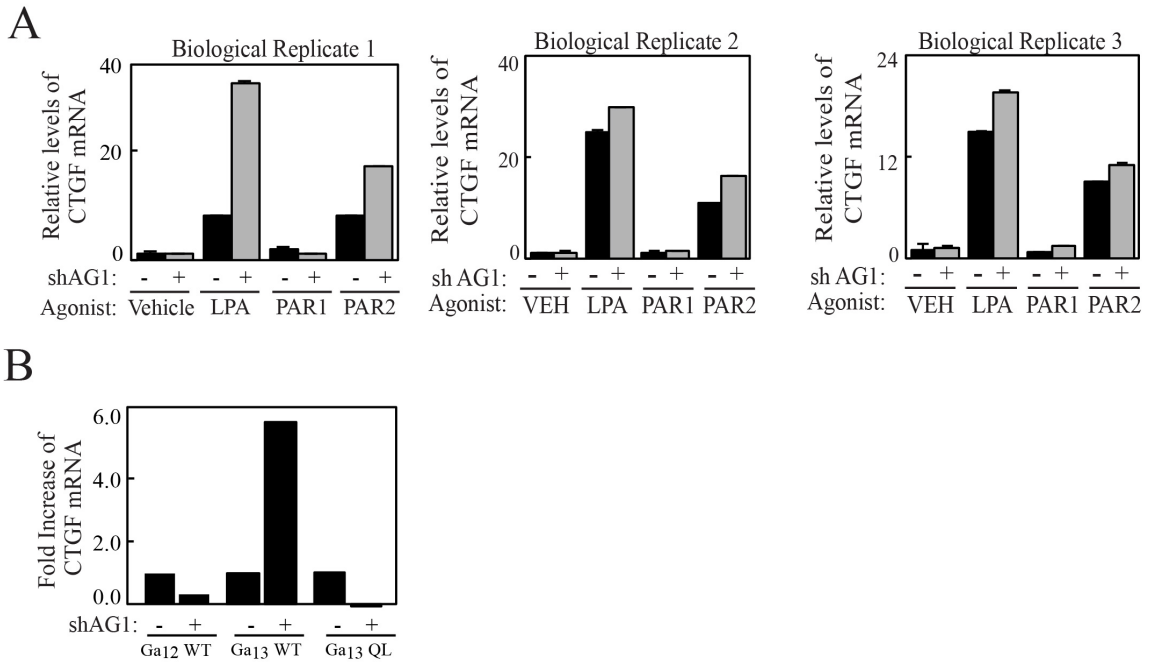


**Figure 3-8: ArhGEF1 Selectively Inhibits Signaling from Gα$_{13}$ and Transmits Signaling from Gα$_{12}$.**

**A.** CT value of CTGF mRNA transcript was measured by qRT-PCR in MCF7 cells stably silenced for ArhGEF1 or control that were serum starved before a 30 minute treatment with vehicle or agonists against the LPA (1uM), PAR1 (TFLLR-$NH_2$: 10 uM) or PAR2 receptors (2-furoyl-LIGRLO-$NH_2$ 5 uM). Relative level of CTGF mRNA fold change (ΔΔCT) was then calculated for each sample compared to control expressing, serum starved MCF7 cells. (3 Biological Replicates) **B.** CT value of CTGF mRNA transcript was measured by qRT-PCR in MCF7 cells stably expressing Flag-tagged Gα$_{12}$, Flag-tagged wild-type Gα$_{13}$ or a Flag-tagged mutant Gα$_{13}$ (QL) in combination with shRNA against ArhGEF1 or shScramble. Relative level of CTGF mRNA fold change (ΔΔCT) was then calculated for each sample compared to control expressing, serum starved MCF7 cells. Fold increase was further calculated by subtracting the ΔΔCT of the shScramble expressing vector blank control from those samples expressing the Gα subunit.

### 3.2.7 Model of RGS-RhoGEFs Regulation of YAP1

The requirements for ArhGEF11 and ArhGEF12 for the induction of CTGF by serum in a background of low ArhGEF1 activity were determined. The enhanced induction of CTGF following serum addition in MCF7 cells stably knocked down for ArhGEF1 expression was not evident if these cells were also silenced for expression of either ArhGEG11 or ArhGEF12 (Figure 3-9A). This further confirms that ArhGEF11 and ArhGEF12 both transmit signaling from $G\alpha_{13}$. It also indicates an essential non-redundant role for each exchange factor in serum induced $G\alpha_{12/13}$ to RhoA signaling. Overall, a model is proposed whereby cells under low pro-proliferation stimulation maximize $G\alpha_{13}$ signaling by promoting ArhGEF1 to have low GAP activity and to primarily function along with ArhGEF11 and ArhGEF12 to transmit signaling onto RhoA. This also seems to be the case during an Early Serum Response. However, in cells experiencing prolonged exposure to serum, the GAP activity of ArhGEF1 for $G\alpha_{13}$ becomes dominant and this is essential for limiting the ability of serum to further stimulate RhoA and in turn YAP1 dependent transcription (Figure 3-9B).

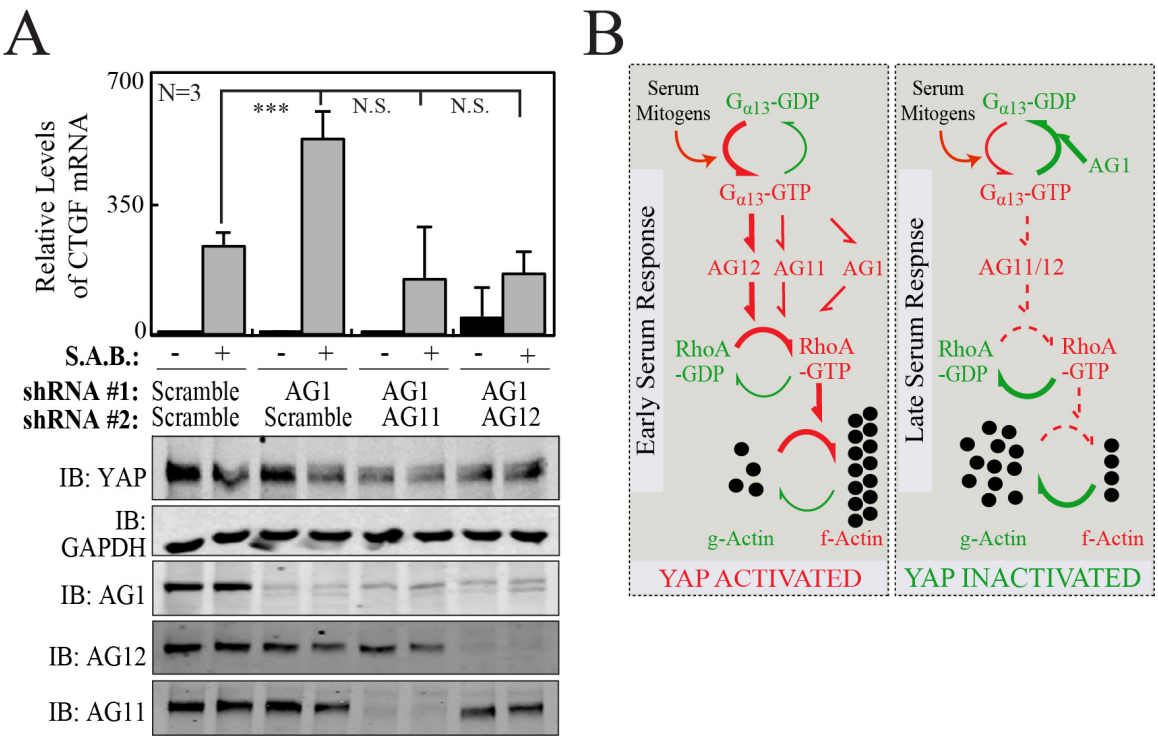


**Figure 3-9: Requirements for ArhGEF11 and ArhGEF12 for the Induction of CTGF by Serum in Cells with Reduced ArhGEF1.**

**A.** CT value of CTGF mRNA transcript was measured by qRT-PCR in MCF7 cells stably silenced for ArhGEF11 or ArhGEF12 alone or in combination with silencing of ArhGEF1 and were serum starved and then treated for 30 min with media or media containing 10 % FBS (S.A.B.). Relative level of CTGF mRNA fold change (ΔΔCT) was then calculated for each sample compared to control expressing, serum starved MCF7 cells (Top Graph). The levels of total YAP, GAPDH, ArhGEF1 (AG1), ArhGEF11 (AG11) and ArhGEF12 (AG12) were measured by immunoblot (Bottom panels) **B.** A model for the roles of ArhGEFs1/11/12 in the Early versus Late Serum Response onto the regulation of RhoA/Actin and YAP1/TEAD/CTGF.

## 3.3 DISCUSSION

### 3.3.1 Contributions of GEFs and GAPs to the Regulation YAP1

Defining how a sub-fraction of RhoGEFs and RhoGAPs regulate TEAD mediated transcription adds insight to their previously described functions. For instance, ArhGEF7 (aka β-PIX), has been shown to couple LATS1/2 to the phosphorylation of YAP1 and TAZ, to promote their exclusion from the nucleus through a mechanisms that is independent of its GEF domain (163). The ability of β-PIX to inhibit YAP1/TEAD dependent transcription upon its overexpression, functionally validated its role in mediating LATS1/2 dependent exclusion of YAP1 from the nucleus (163). Whereas, ArhGEF5 stimulation of YAP1/TEAD activity may explain its known functions in enhancing the proliferation and the malignant properties of breast (193) and lung (194) cancer cells. Interestingly, two of the best YAP1/TEAD activators, Ect2 (181) and PLEKHG6 (158) have key roles in cytokinesis, a process that is mediated by YAP1, independent of its transcriptional functionality (195). This would suggest that RhoA activation during cytokinesis also contributes to YAP1/TEAD dependent transcription. Alternatively, ArhGAP18 promotes actinomyosin-mediated tissue tension, as an effector of YAP1 (175), which is congruent with its inhibition of TEAD shown here and the well-established role of tension in activating YAP1. Along these lines of cytoskeleton regulation of YAP1, the cell rounding induced by STARD13 and DLC1 (175) is consistent with their ability to reduce both YAP1-dependent TEAD transcription and serum induced CTGF transcription. Conversely, GEFH1/ArhGEF2 is reported to inhibit YAP1 activity through activation of RhoB (196), whereas it strongly activated TEAD dependent transcription. This may be due to differences among the cellular backgrounds

or it may suggest, like ArhGEF1, ArhGEF2 can exhibit context dependent effects on YAP1.

### 3.3.2 RGS-RhoGEFs are Integral to Modulating the Signaling Flux of the Serum Response Network

The RGS-RhoGEFs are integral to mediating the serum response network, through the regulation of $G\alpha_{12/13}$ activation of RhoA induced stress fiber formation. The induction of stress fibers by RhoA in response to the activation of the serum response network, has been classically defined to promote the transcription of "immediate early" genes, such as Cyclin D1 and cFOS, inducing cell growth. However the relative physiological requirement of the RGS-RhoGEFs in this process have largely not been defined. Each member of the RGS-RhoGEFs has both a structural GAP domain and GEF domain for $G\alpha_{12/13}$ and RhoA, respectively. However, in vitro data would suggest that ArhGEF1 has the only functional GAP domain of the family, increasing the GTPase activity of $G\alpha_{12/13}$ when bound, whereas ArhGEF11 and ArhGEF12 cannot (99). Identified here using CTGF transcription as a primary readout, the RGS-RhoGEFs integrate external to internal signaling to regulate the serum response pathway. ArhGEF12, and to a lesser extent ArhGEF11, function to solely transmit signaling onto RhoA. Conversely, ArhGEF1 is a bi-directional switch, capable of mediating flux through the pathway. For example, ArhGEF1 transmits signaling from $G\alpha_{12/13}$ to GEF RhoA. However, in environments where growth is unwarranted, as in excessive signaling, ArhGEF1 function switches to GAP $G\alpha_{13}$ turning "off" the cascade. How these environments switch ArhGEF1 function is unknown, however recent studies highlight it is regulated by post-translational modifications. One study reveals that serine-330 is phosphorylated by an unknown kinase and that phosphorylation event increases its GEF activity (197). Further analysis of the ArhGEF1 amino acid sequence reveals consensus

LATS1/2 phosphorylation sites that fall within its DH/PH domain. These sites offer a potential regulatory mechanism in the times of high LATS1/2 activity that may inactivate its GEF function and prevent subsequent RhoA activity. The requirement of the RGS-RhoGEFs in regulating the serum response network highlights the importance of GEFs and GAPs in mediating GTPase activity and the role they play in maintaining cellular homeostasis.

Recently the activation of the serum response network was shown to induce YAP1 nuclear translocation, however the mechanism by which the RGS-RhoGEFs contribute to YAP1 activity is unclear. ArhGEF11 and ArhGEF12 seem to have non-redundant roles in regulating YAP1 activity, as the loss of either one prevents serum induced CTGF transcription with ArhGEF12 seemingly more potent. Their non-redundant roles in contributing to serum induced CTGF transcription may be a result of their individual requirements for the regulation of actin dynamics. Knockdown of ArhGEF11 shows no distinguishable cellular morphological difference compared to wild-type cells, whereas the knockdown of ArhGEF12 promotes cellular rounding. This rounding phenotype suggests that there is a global loss in RhoA dependent stress fiber formation, a required event for YAP1 nuclear translocation. The loss in actin as measured by phalloidin staining, may contribute to YAP1 degradation through the release of Angiomotin from filamentous actin and enhancing its associate with AIP4. This complex is well established to contribute to the ubiquitin mediated degradation of YAP1, and offers a potential mechanism to how ArhGEF12 may regulate YAP1 activity (124). Loss of ArhGEF1 promotes a sever actin phenotype, which could lead to the sequestration of Angiomotin on actin filaments, thereby uncoupling it from AIP4-dependent

ubiquitination and degradation of YAP1. This predicted mechanism would explain the hyper-induction of CTGF transcription in response to serum in MCF7 cells genetically inactivated for ArhGEF1. However, the mechanism by which ArhGEF11 loss contributes to YAP1 degradation is still up for speculation. These data suggest that $G\alpha_{13}$ is the primary driver of CTGF transcription in response to serum and the cyclic regulation of $G\alpha_{13}$ GDP/GTP cycle is important for YAP1 activity.

### 3.3.3 Biological Relevance of $G\alpha_{13}$ GDP/GTP Cycle

Serum signaling contains many growth factors and the ability of a cell to turn those growth-activating signals into precise transcriptional outputs is a coordinated process that is checked at many regulatory levels. Evidence suggests that prolonged signaling is not beneficial for cells. For instance, overexpression of a constitutive active RAS in a p53 wild type background creates a situation where excess MAP kinase signaling induces cellular senescence (198). Further evidence also suggests that chronic mitogenic signaling in the presence of activated RB pathway leads to an increase in Reactive Oxygen Species (ROS) and induces cellular senescence, rather than propagating growth (199). These "fail-safe" mechanisms are in place to prevent unwarranted cell growth and are often circumvented by cancer cells.

ArhGEF1, as suggested by this data, is a temporal regulator of the serum response network by maintaining proper down regulation of $G\alpha_{13}$. Until this study, the intracellular relevance of the cyclic regulation of $G\alpha_{13}$, by ArhGEF1 was not well understood. Knockout of $G\alpha_{13}$ but not $G\alpha_{12}$ is embryonic lethal in mice demonstrating the requirement for $G\alpha_{13}$ activity for survival and growth (200). Evidence would suggest that the cyclic regulation of the GTPases is a "fail-safe" mechanism to prevent excess growth signaling from propagating unwanted growth. As shown in this work, the loss of ArhGEF1 promotes the dephosphorylation, and nuclear accumulation of YAP1 leading to an increase in CTGF transcription in response to serum. Components of serum and an increase in actin stress fibers are *bona fide* regulators of YAP1 transcriptional activity, which is presumed to invoke a pro-growth phenotype That explains why elevated YAP1 activity has been found to drive a variety of cancers. The remaining work in this

dissertation looks to address whether or not activated YAP1 signaling induced by the chronic activation of $G\alpha_{13}$ promotes cellular growth or does the chronic activation engage senescence pathways, as described above, to promote a "fail-safe" mechanism preventing unwarranted growth.

# CHAPTER 4. ARHGEF1 CYCLIC REGULATION OF $G\alpha_{13}$ IS ESSENTIAL FOR MAINTAINING CELLULAR HOMEOSTASIS

## 4.1 INTRODUCTION

Cellular proliferation is a tightly coordinated process that is instigated by external biochemical and biophysical cues that are transduced onto the induction of transcriptional programs that eventually bring about mitosis. A key element in this process is the dynamic reorganization of the actin cytoskeleton. Actin dynamics are dictated by the Rho family of GTPase that are in turn spatially and temporally regulated by GEFs and GAPs. Recently, RhoA dependent actin stress fiber formation was shown to be required for the translocation YAP1 into the nucleus (142). This is essential for YAP1 to bind and co-activate multiple transcription factors, most notably TEAD1-4 (134); this results in levels of transcription of pro-growth and survival genes that are necessary to effect cellular state change. Here, the roles of the RGS-RhoGEFs identified in experiments described in Chapter 3 to mediate serum regulation of YAP1 activity in cell growth and survival were investigated.

YAP1/TEAD transcriptional activity is typically associated with pro-growth or pro-survival transcriptional programs. Overexpression of YAP1 in most cases leads to aberrant cell growth in culture systems and animal models (169, 201, 202). YAP1 expression is also elevated in a variety of cancers (203). In chapter 3, ArhGEF12 and ArhGEF11 were identified to be critical for transmitting $G\alpha_{12/13}$ activity onto YAP1 mediated transcription. ArhGEF1 was also found to be the primary GAP for $G\alpha_{13}$ during "Late Stage" serum response activity. This activity was further found to be sufficient to prevent RhoA and YAP1 activation. However, the impact of this regulation on cell growth and survival is not understood.

## 4.2 RESULTS

### 4.2.1 RGS-RhoGEFs Affects on MAPK Signaling

$G\alpha_{12/13}$ are well-established activators of YAP1-dependent transcription and MAPK cascades. Both $G\alpha_{12}$ and $G\alpha_{13}$ promote the activation of ERK1/2 and JNK1/2 via the activation of RAS and RhoA (115, 204-206). However, $G\alpha_{12}$ can under some circumstances inhibit both ERK1/2 and JNK1/2 activity (116). Consistently, individually, the RGS-RhoGEF have been found to promote MAPK signaling (115). However, it is unclear how all three RGS-RhoGEFs work coordinately to integrate $G\alpha_{12/13}$ signaling onto the regulation of RhoA.

The dephosphorylation of YAP1 at serine 127 is a surrogate measure for cells in growth inducing environments, e.g. cells that lack contacts with neighboring epithelial cells. (Figure 4-1A). As observed in Chapter 3, knockdown of ArhGEF1 in MCF7 cells also induces YAP1 dephosphorylation, but the affects on growth are unknown. The Serum Response Network is intricately linked to the activation of the MAPK pathway and in the regulation of HIPPO signaling. Understanding the role ArhGEF1 plays in this network may therefore provide insight into its ability to coordinately regulate cell growth via its control of MAPK and YAP1 activities. To more globally define the importance of ArhGEF1 in cell growth control signaling, the impact of silencing ArhGEF1 on the total and phospho-levels of proteins represented in the reverse phase protein analysis (RPPA) was determined. For this purpose, MCF7 cells that were stably silenced for ArhGEF1 were subjected to serum starvation for 24 hours and treated with 10% FBS for 30 minutes. Cell lysates were then collected and sent for analysis by the Reverse Phase

Protein Array (RPPA) core at the MD Anderson Cancer Center. RPPA utilizes nearly 350 different antibodies against different proteins or phospho-proteins to measure differences in their relative levels. Under serum add back conditions, MCF7 cells in which ArhGEF1 was silenced showed statistically significant increase in phosphorylation of threonine and tyrosine residues that are surrogate measures for the activation of MAPK, ERK, JNK, and p38 versus control MCF7 cells (Figure 4-1B). Levels of NRAS and MEK1 as well as the levels of phosphorylated cRAF (S338) and bRAF (S445), were significantly greater in ArhGEF1 silenced MCF7 cells (Figure 4-1B). Independent validation showed that serum induced ERK1/2 and JNK1/2 phosphorylation to a greater extent in ArhGEF1 silenced MCF7 cells versus cells expressing shScramble. Specifically, pERK1/2 levels were 3-fold higher at 120 minutes in ArhGEF1 silenced cells and at 300 minutes unlike control cells where p-ERK1/2 was not detectable (Figure 4-1C). Conversely, MCF7 cells silenced for ArhGEF12 showed a 70% reduction in ERK1/2 phosphorylation when treated with serum after 30 minutes. However, no discernable effects on the levels of phospho-ERK1/2 were seen when ArhGEF11 was knocked down (Figure 4-2A & 2B). Similar to results from the RPPA, ArhGEF1 knockdown in MCF7 cells enhanced JNK1 but not JNK2 phosphorylation at threonine 183 and tyrosine 185 (Figure 4-1D). The downstream target of JNK, cJUN, also had statistically greater levels of phosphorylation at serine 73, validating that JNK1/2 activity was elevated (Figure 4-1B). Interestingly, the effects of silencing the RGS-RhoGEFs on YAP1-dependent activity, were mirrored by the effects observed for MAPK signaling. These data highlight the importance of the RGS-RhoGEFs in the Serum Response Network for the activation of both YAP1 and MAPK cascades.

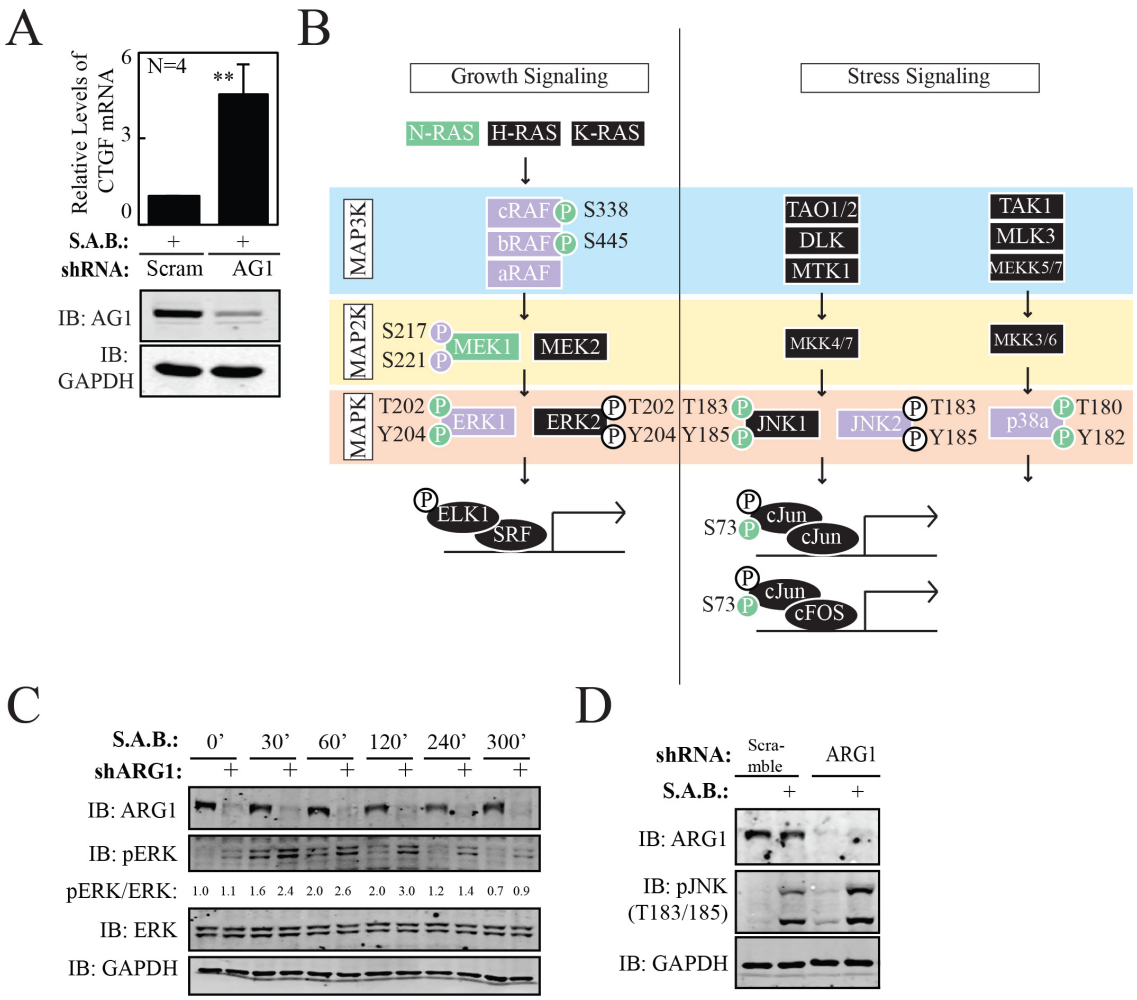


**Figure 4-1: ArhGEF1 is Essential for Maintaining Serum Response Activation of CTGF and Early Phase MAPK Activity.**

**A.** CT value of CTGF mRNA transcript was measured by qRT-PCR in MDA-MB-231 cells that genetically inactivated for ArhGEF1 expression using shRNA (AG1), and grown in 3D Matrigel for 2 days. Cells were then subjected to a 24 hours serum starvation and treated with 10% FBS for 30 minutes (Top Panel). Relative level of CTGF mRNA fold change (ΔΔCT) was then calculated for each sample compared to MDA-MB-231 transduced with the shRNA control. Immunoblot of total protein with either anti-ArhGEF1 (AG1) or anti-GAPDH (Bottom Panel). **B.** Relative changes in protein expression between MCF7 cells genetically silenced for ArhGEF1 by lenti viral transduction compared to shRNA control as measured by Reverse Phase Protein Array (RPPA). Samples were serum starved for 24 hours and treated for 30 minutes with serum. Colors: *Black* indicates protein was not present in array, *Purple* indicates no significance between shARG1 and control, *Red* indicates significant decrease (P <. 05) in expression, and *Green* indicates significant increase (P < .05) in expression. **C**. MCF7 cells were transduced with either a lentiviral shRNA directed towards ArhGEF1 or a control. MCF7 cells were serum starved for 24 hours and 10% FBS was added for the indicated time. The levels of total ArhGEF1 (ARG1), pERK, ERK and GAPDH were measured by immunoblot **D**. MCF7 cells were transduced with either a lentiviral shRNA directed towards ArhGEF1 or a control. MCF7 cells were serum starved for 24 hours and 10% FBS was added for 30 minutes. The levels of total ArhGEF1 (ARG1), pJNK, GAPDH were measured by immunoblot.

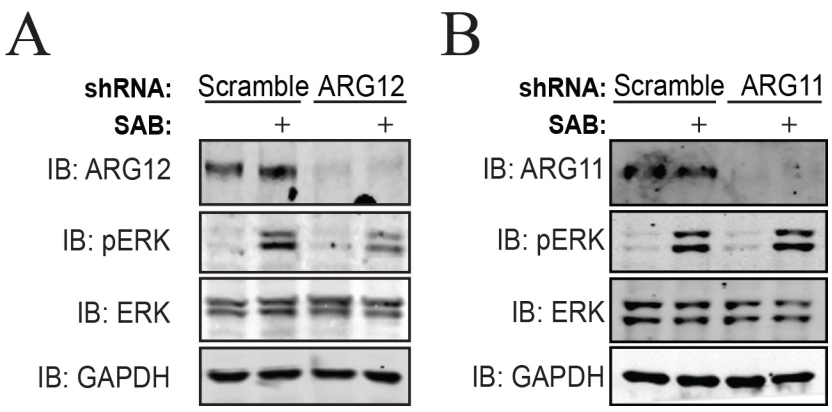


**Figure 4-2: ArhGEF12 is Essential for ERK1/2 Activity.**

**A.** MCF7 cells were transduced with either a lentiviral shRNA directed towards ArhGEF12 (shARG12) or a control. MCF7 cells were serum starved for 24 hours and 10% FBS was added for the indicated time. The levels of total ArhGEF12 (ARG12), pERK, ERK and GAPDH were measured by immunoblot. **B.** MCF7 cells were transduced with either a lentiviral shRNA directed towards ArhGEF11 (shARG11) or a control. MCF7 cells were serum starved for 24 hours and 10% FBS was added for 30 minutes. The levels of total ArhGEF11 (ARG11), pERK, ERK and GAPDH were measured by immunoblot.

4.2.2 Cell Growth Requires the RGS-RhoGEFs

Activation of ERK1/2, and YAP1 are strongly associated with committing a cell to proliferate (203). This study finds that the RGS-RhoGEFs are critical mediators of serum activation of both YAP1 and MAPK. Loss of ArhGEF11 or ArhGEF12 was therefore expected to reduce the growth of cells in serum as this retards the activation of YAP1 and MAPK by the mitogens in serum. Conversely, the loss of ArhGEF1 was anticipated to enhance cell growth especially under serum limiting conditions as its presence inhibited the activation of YAP1 and MAPK signaling by serum. In reality, the individual knockdown of each RGS-RhoGEF in MCF7 cells resulted in a similar inhibition of cell accumulation by ~40% over the course of 3 Days (Figure 4-3A). Similarly, the growth in size of colonies of ArhGEF1 silenced MCF7 and MDA-MB-231 cells in Matrigel over 5 Days was reduced by 35% and 60%, respectively, versus control cells (Figure 4-3B). The growth inhibiting effects of silencing ArhGEF1 was corroborated by a significant decrease in the reduction of MTT to formazan, a measure of mitochondrial respiration, by both ArhGEF1 silenced MCF7 (-50%) and MDA-MB-231 (-15%) cells (Figure 4-3C). This measure of cell viability was also significantly reduced by 20% in MCF7 cells knocked down for ArhGEF12 after 3 Days of growth (Figure 4-3E). Overexpression of the constitutively active $G\alpha_{13}QL$ mutant in MCF7 cells also reduced growth in 3D by 60% (Figure 4-3F), with a concurrent reduction of MTT to formazan when compared to control of ~20% (Figure 4-3G). These data demonstrate that all three RGS-RhoGEFs are required for the growth of multiple breast cancer cells lines in both 2D and 3D environments. The unexpected loss of growth in cells in which ArhGEF1 was silenced or $G\alpha_{13}QL$ was overexpressed, suggests that both hyper-

activation and hypo-activation of $G\alpha_{13}$ results in a loss of cell growth. Given the strong activation of MAPK and YAP1 signaling upon hyper $G\alpha_{13}$ activation, the mechanism that leads to a loss of growth was perplexing. The unraveling of this mechanism was consequently a major focus of the work that is presented in this dissertation.

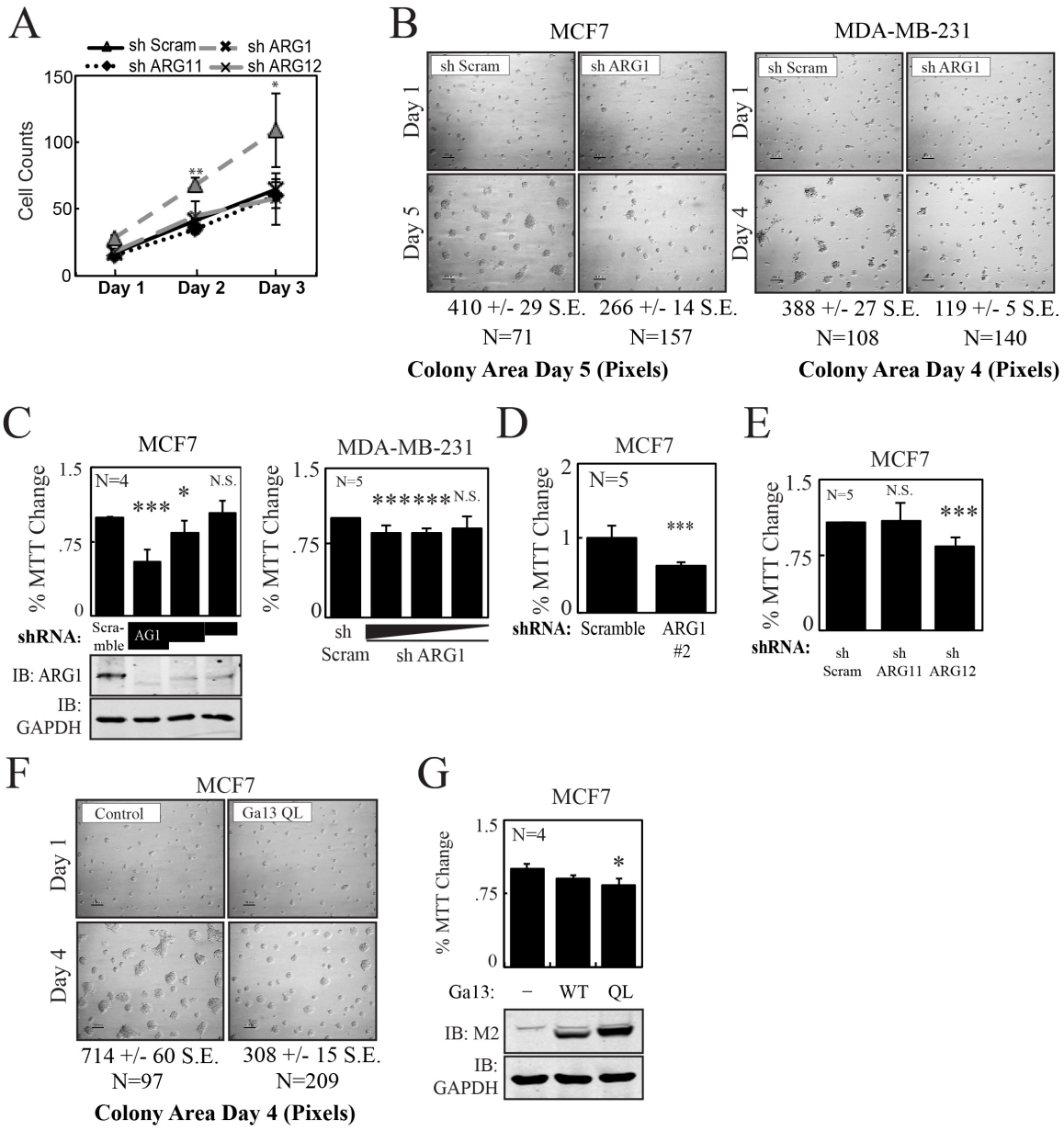


**Figure 4-3: RGS-RhoGEFs are Required for Cellular Growth.**

**A.** MCF7 cells stably silenced for the indicated RGS-RhoGEF through lentiviral transduction of the shRNA, were plated at 25,000 cells per 6 well plates and trypsinized on the indicated day and counted. Samples were done in biological triplicate and averaged together. **B.** Stereoimages of control MCF7 and MCF7 cells genetically inactivated for ArhGEF1 (shARG1) expression using shRNA. Pictures taken on Day 1 and Day 5. Colony area is measured in pixels using Adobe Photoshop (Left Panel), +/- the standard error (S.E.). Stereoimages of control MDA-MB-231 and MDA-MB-231 cells genetically inactivated for ArhGEF1 (shARG1) expression using shRNA. Pictures taken on Day1 and Day 4. Colony area is measured in pixels using Adobe Photoshop (Right Panel), +/- the standard error (S.E.). **C.** MCF7 (Left Panel) or MDA-MB-231 (Right Panel) cells stably silenced for ArhGEF1 (shAG1) were allowed to grow for 3 Days in a 96-well plate. On Day 3 15 uL of 5mg/mL of MTT was added for 4 hours, followed by the addition of

100 uL of MTT solvent for 1 hour. Cells were resuspended and absorbance at 570 nm was recorded and normalized to control. **D.** Using a second shRNA directed towards ArhGEF1, cells were allowed to grow for 3 Days in a 96-well plate. 15 uL of MTT solvent was added for 4 hours followed with MTT solvent for 1 hour. Cells were resuspended and absorbance at 570 nm was recorded and normalized to control. **E**. MCF7 cells stably silenced for ArhGEF11 (shARG11) or ArhGEF12 (shARG12) were allowed to grow for 3 Days in a 96-well plate. On Day 3 15 uL of 5mg/mL of MTT was added for 4 hours, followed by the addition of 100 uL of MTT solvent for 1 hour. Cells were resuspended and absorbance at 570 nm was recorded and normalized to control. **F.** Stereoimages of control MCF7 and MCF7 cells expressing stable $G\alpha_{13}$ QL. Pictures taken on Day1 and Day 4, acini area was calculated using pixels in Adobe Photoshop. **G.** MCF7 cells stably expressing $G\alpha_{13}$WT or $G\alpha_{13}$QL were allowed to grow for 3 Days in a 96-well plate. On Day 3 15 uL of 5mg/mL of MTT was added for 4 hours, followed by the addition of 100 uL of MTT solvent for 1 hour. Cells were resuspended and absorbance at 570 nm was recorded (Top Panel). Immunoblot of 3xFlag-tagged $G\alpha_{13}$WT and $G\alpha_{13}$QL using M2 antibody (Bottom Panel).

4.2.3 Loss of ArhGEF1 Results in Cell Cycle Arrest and a Reduction in Global Translation Elongation

The induction of transcription of Cyclin D1 is a major pro-growth event that is produced upon the activation of the serum response network by mitogenic lipids., Accumulation of Cyclin D1 is necessary to initiate the G1 phase of the cell cycle. Cyclin D1 transcription is facilitated by the AP-1 transcription factor complex, which consists of cFOS/cJUN or cJUN/cJUN dimers. The effects of silencing the RGS-RhoGEFs on the transcription of Cyclin D1 in MCF7 and MDA-MB-231 cells were therefore investigated. This revealed that MCF7 cells silenced for ArhGEF1, were desensitized to the induction of Cyclin D1 transcription by serum. Specifically, the levels of Cyclin D1 transcript were reduced by 90% ,as measured by qRTPCR, in MCF7 cells silenced for ArhGEF1 following serum add-back versus control cells (Figure 4-4A). While a reduction in basal Cyclin D1 levels in MCF7 cells was directly associated with the degree of AhrGEF1 silencing, even moderate (~50 %) ArhGEF1 silencing blocked the induction of CyclinD1 transcript levels by serum (Figure 4-1B). Furthermore, MCF7 cells with stable overexpression of $G\alpha_{13}QL$ had 40% less Cyclin D1 transcript levels when compared to control MCF7 cells (Figure 4-4C). Thus, ArhGEF1 silencing and heterologous expression of $G\alpha_{13}QL$ reduces cell growth and Cyclin D1 transcription while inducing YAP1 and MAPK activity. This strongly suggests that hyper activation of $G\alpha_{13}$ induces Cyclin D1 loss, which likely circumvents the pro-growth effects of both YAP1 and MAPK activation. Because MCF7 cells silenced for ArhGEF1 showed 2-fold higher levels of cJUN transcript after serum add-back and no difference in cFOS transcript versus control

cells, prolonged $G\alpha_{13}$ activation likely inhibits Cyclin D1 in a manner that is independent of AP1. (Figure 4-4D & 4E).

Consistent with ArhGEF1 silencing causing a loss of CyclinD1 activity, RPPA analysis of lysates from ArhGEF1 silenced cells showed a broad inhibition of proteins that control the cell cycle versus lysates from control cells. MCF7 cells with ArhGEF1 knockdown had significantly reduced levels of Cyclin E1, Cyclin Dependent Kinase 1 (CDK1), proliferating cell nuclear antigen (PCNA), and the Cyclin B1 phosphatase Cdc25 (Figure 4-4F). Overall, this is consistent with an inability of these cells to enter S phase from $G_1$ as the activation of Cyclin dependent kinase 2 (CDK2) by Cyclin E1 is required for this transition (20). Further, the loss of PCNA, which was validated by immunoblot (Figure 4-4G), indicates a defect in DNA synthesis due to its essential function as a DNA clamp during S-phase (207) The significant reduction in the levels of the Cdc25 phosphatase, as measured by RPPA (Figure 4-4F), presumably prevents dephosphorylation of its substrate Cyclin B1 at tyrosine residue 15. This is essential for Cyclin B1 to complex with CDK1 and thereby promote the transition of the cell into $G_2$/M (24).

As expected, the knockdown of ArhGEF11 or ArhGEF12 in MCF7 cells , results in a significant desensitization of these cells to being induced by serum to express Cyclin D1 as measured by qRTPCR (~10 fold decrease in Cyclin D1 transcript levels for both compared to control cells) (Figure 4-5A). Furthermore, MCF7 cells silenced for either ArhGEF11 or ArhGEF12 have significantly lower levels of PCNA protein (Figure 4-5D). The reduced levels of Cyclin D1 transcript and subsequent reduced rates of growth of MCF7 cells silenced for ArhGEF11 or ArhGEF12 may be explained by the observation

that they have significantly lower levels of cJUN mRNA versus control cells (Figure 4-5C). Further, ArhGEF12 silenced cells have significantly lower levels of cFOS transcript (Figure 4-5C). All together, the inhibition of these core regulators of the cell cycle upon inactivation of RGS-RhoGEFs that lead to either reduced or hyperactivated $G\alpha_{13}$ signaling underscore the importance of such signaling for cell growth control.

Early studies of cell growth identified nutrient availability as a major regulator of DNA transcription, mRNA translation and protein maturation (9). Both the initiation and elongation stages of protein translation are regulated by the mammalian target of rapamyacin (mTOR) pathway; which is itself controlled by the phosphoinositide 3 Kinase (PI3K) - AKT signaling network. Receptor Tyrosine Kinases (RTK)s are agonized by extracellular factors including Insulin Growth Factor (IGF), Epidermal Growth Factor (EGF), Platelet Derive Growth Factor (PDGF), etc. Ligand bound RTKs both homodimerize and heterodimerize with other RTKs to enable auto-phosphorylation at residues in the cytoplasmic C-terminal tail. The recruitment of downstream effectors to these phosphorylated motifs such as the catalytic subunit of P13K, p110, stimulates the conversion of $PIP_2$ to $PIP_3$ in the plasma membrane. $PIP_3$ activates PDK1 to phosphorylate AKT at threonine 308 (208). AKT is further phosphorylated at serine 473 by mTORC2 (209). Phosphorylated AKT then inhibits TSC1/2 (210), and thereby prevents their ability to turn off the GTPase, RHEB (211). The active GTP bound form of RHEB stimulates mTOR to facilitates the initialization of cap-dependent mRNA translation and to promote ribosomal elongation (212). Protein translation is required during the $G_1$ phase of the cell cycle to produce the machinery to duplicate the genome. Consequently, defects in this process block cell growth (11).

Consistent with ArhGEF1 expression being required for translation, RPPA analysis of ArhGEF1 silenced MCF7 cells finds that the core proteins that activate the initiation and elongation phases of translation are inhibited. However, activating phosphorylation events of PI3K/AKT are increased (Figure 4-6A). Specifically, the expression of the regulatory subunit of PI3K (p85) and the phosphorylation of threonine 308 of AKT were significantly increased (Figure 4-6A). This may be explained by the increases in NRAS levels and in the phosphorylation of ERRB3, an RTK that preferentially activates PI3K (213) (Figure 4-6A). Furthermore, a significant increase in AKT phosphorylation at serine 473, which is mediated by the mTORC2 complex, was also observed (Figure 4-6A). Dual phosphorylation of AKT maximizes its kinase activity (209). While surrogate events for the activation of the PI3K-Akt pathway was observed, downstream translation appears to be inhibited (Figure 4-6A) (211). For instance, there is a significant decrease in protein expression of RHEB in ArhGEF1 silenced MCF7 cells (Figure 4-6A). This inhibition of translation is also likely due to the observed increased levels of total AMPK as well as increased levels of its activated threonine phosphorylated form in ArhGEF1 silenced cells (Figure 4-6A). AMPK is activated by AMP to phosphorylate TSC1 and TSC2 which results in the inhibition of mTORC1 and consequently the initiation of protein translation (214). Overall ArhGEF1 in MCF7 cells is predicted to activate the mTORC1 complex and consequently mRNA translation.

Protein translation is a multi-step process involving an initiating step, elongation of the protein product and termination. For translation of an mRNA to be initiated, eIF4E must bind the 5' mRNA cap to allow engagement of the 60S ribosome . Subsequent elongation is then promoted by eIF2 (215). RPPA comparison of ArhGEF1 silenced

MCF7 cells to control cells shows significantly elevated levels of total and serine 209 phosphorylated eIF4E (Figure 4-6A). This suggests that ArhGEF1 may inhibit initiation. However, levels of the negative regulator of eIF4E, 4EBP1, are also significantly increased. Inhibitory activity induced by 4EBP1 is largely a product of stoichiometric interactions with eIF4E, so it's hard to determine if functional inhibition of translation initiation is achieved. However, Proteins involved in ribosomal elongation are almost uniformly significantly decreased in ArhGEF1 knockdown MCF7 cells in comparison to control cells. This includes p70S6K1, the negative regulator of eukaryotic elongation factor 2 kinase (eEF2K), and eukaryotic translation elongation factor 2 (eEF2) (Figure 4-6A). eEF2 promotes the GTP-dependent translocation of the ribosome and is inhibited through phosphorylation by eEF2K (Figure 4-6A). Together these data suggest that the initiation and elongation of translational may be perturbed in ArhGEF1 silenced MCF7 cells. However, the overall effects on translation and the molecular underpinnings of how prolonged serum signaling can contribute to such effects are unknown.

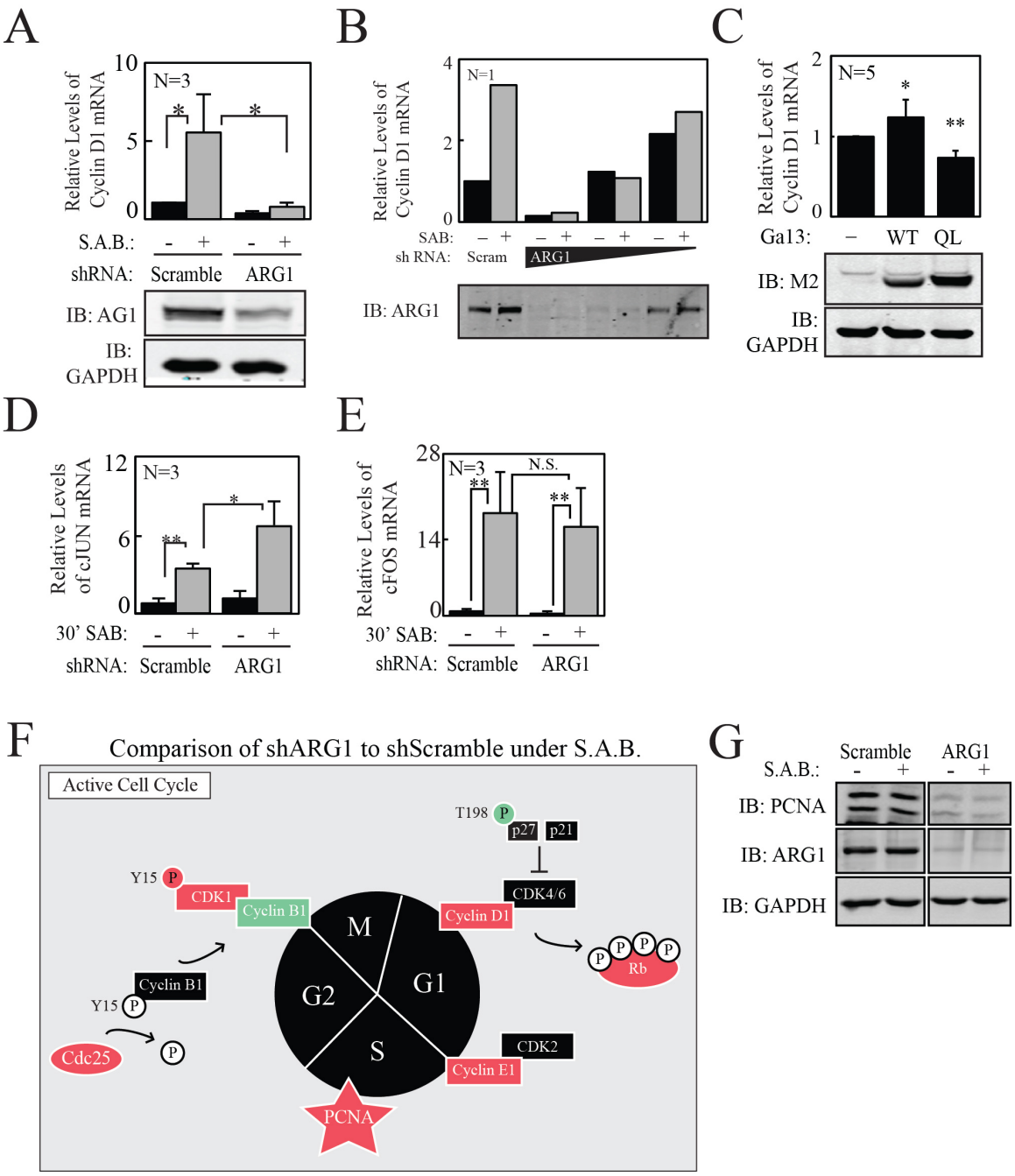


**Figure 4-4: ArhGEF1 is Intricately Involved in Global Cell Cycle Activity.**

**A.** CT value of Cyclin D1 mRNA transcript was measured by qRT-PCR in MCF7 cells silenced for expression of ArhGEF1 (ARG1) after serum starvation for 24 hours, followed with a 10 % FBS treatment for 30 minutes. Relative level of CTGF mRNA fold change (ΔΔCT) was then calculated for each sample compared to MCF7 transduced with the shRNA control and serum starved for 24 hours. (Top Graph). Total ArhGEF1 (AG1) and GAPDH endogenous protein levels were detected by immunoblot (Bottom Panel). **B.** CT value of Cyclin D1 mRNA transcript was measured in MCF7 cells with complete, high and moderate stable silencing of ArhGEF1 (AG1) were starved of serum before being treated for 30 min with media alone or media with

10% serum. Relative level of CTGF mRNA fold change (ΔΔCT) was then calculated for each sample compared to MCF7 transduced with the shRNA control and serum starved for 24 hours. **C.** CT value of Cyclin D1 mRNA transcript was measured by qRT-PCR in MCF7 cells expressing 3x-Flag $G\alpha_{13}$WT or $G\alpha_{13}$QL. Relative level of CTGF mRNA fold change (ΔΔCT) was then calculated for each sample compared to MCF7 expressing 3x-Flag control. (Top Graph). Detection of 3x-Flag $G\alpha_{13}$WT and 3x-Flag $G\alpha_{13}$QL using M2 antibody (Bottom Panel). **D.** CT value of cJUN mRNA transcript was measured by qRT-PCR in MCF7 cells silenced for expression of ArhGEF1 (ARG1) following serum starvation and then incubation with media containing or lacking 10 % FBS for 30 minutes. Relative level of CTGF mRNA fold change (ΔΔCT) was then calculated for each sample compared to MCF7 transduced with the shRNA control and serum starved for 24 hours. **E.** CT value of cFOS mRNA transcript was measured by qRT-PCR in MCF7 cells silenced for expression of ArhGEF1 (ARG1) following serum starvation and then incubation with media containing or lacking 10 % FBS for 30 minutes. Relative level of CTGF mRNA fold change (ΔΔCT) was then calculated for each sample compared to MCF7 transduced with the shRNA control and serum starved for 24 hours. **F.** Relative changes in protein expression between MCF7 control cells and MCF7 genetically inactivated for shArhGEF1 as measured by Reverse Phase Protein Array (RPPA). Samples were serum starved for 24 hours and treated for 30 minutes with serum. Colors: *Black* indicates protein was not present in array, *Purple* indicates no significance between shARG1 and control, *Red* indicates significant decrease (P <. 05) in expression, and *Green* indicates significant increase (P < .05) in expression. **G**. Immunoblot of endogenous total protein levels of PCNA, ARG1, and GAPDH in MCF7 cells knocked down for ARG1, using lentiviral transduction, compared to control upon a 24 hours serum starvation followed by a 30 minute serum add back.

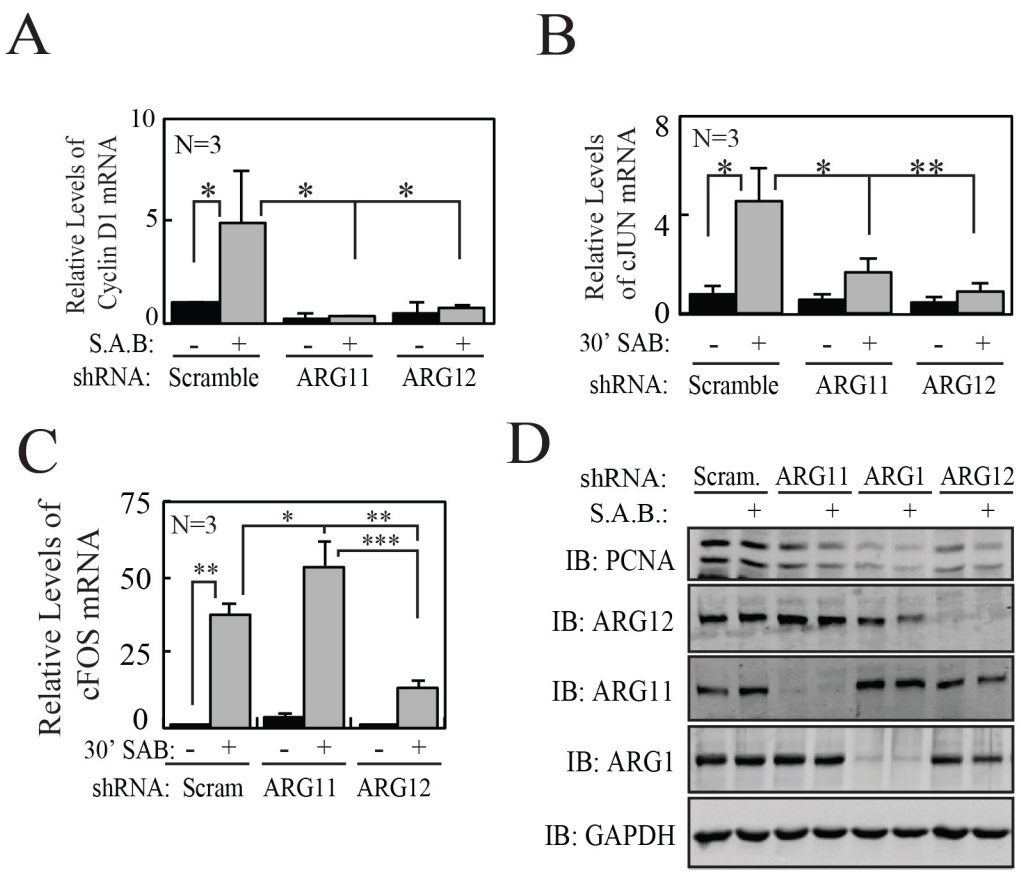


**Figure 4-5: ArhGEF11 and ArhGEF12 Contribute to Cell Cycle Activity.**

**A.** CT value of Cyclin D1 mRNA transcript was measured by qRT-PCR in MCF7 cells silenced for expression of ArhGEF11 (ARG11) or ArhGEF12 (ARG12) after serum starvation for 24 hours, followed with a 10 % FBS treatment for 30 minutes. Relative level of CTGF mRNA fold change (ΔΔCT) was then calculated for each sample compared to MCF7 transduced with the shRNA control and serum starved for 24 hours. (Top Graph). Total ArhGEF1 (AG1) and GAPDH endogenous protein levels were detected by immunoblot (Bottom Panel). **B.** CT value of cJUN mRNA transcript was measured by qRT-PCR in MCF7 cells silenced for expression of ArhGEF11 (ARG11) or ArhGGEF12 (ARG12) after serum starvation for 24 hours, followed with a 10 % FBS treatment for 30 minutes. Relative level of CTGF mRNA fold change (ΔΔCT) was then calculated for each sample compared to MCF7 transduced with the shRNA control and serum starved for 24 hours. (Top Graph). Total ArhGEF1 (AG1) and GAPDH endogenous protein levels were detected by immunoblot (Bottom Panel). **C.** CT value of cFOS mRNA transcript was measured by qRT-PCR in MCF7 cells silenced for expression of ArhGEF11 (ARG11) or ArhGEF12 (ARG12) after serum starvation for 24 hours, followed with a 10 % FBS treatment for 30 minutes. Relative level of CTGF mRNA fold change (ΔΔCT) was then calculated for each sample compared to MCF7 transduced with the shRNA control and serum starved for 24 hours. (Top Graph). Total ArhGEF1 (AG1) and GAPDH endogenous protein levels were detected by immunoblot (Bottom Panel). **D**. Immunoblot of endogenous total protein levels of PCNA, ArhGEF1 (ARG1), ArhGEF11 (ARG11), ArhGEF12 (ARG12) and GAPDH in cells knocked down for either ArhGEF1, ArhGEF11, or ArhGEF12 under serum starvation and 30 minute serum add back conditions.

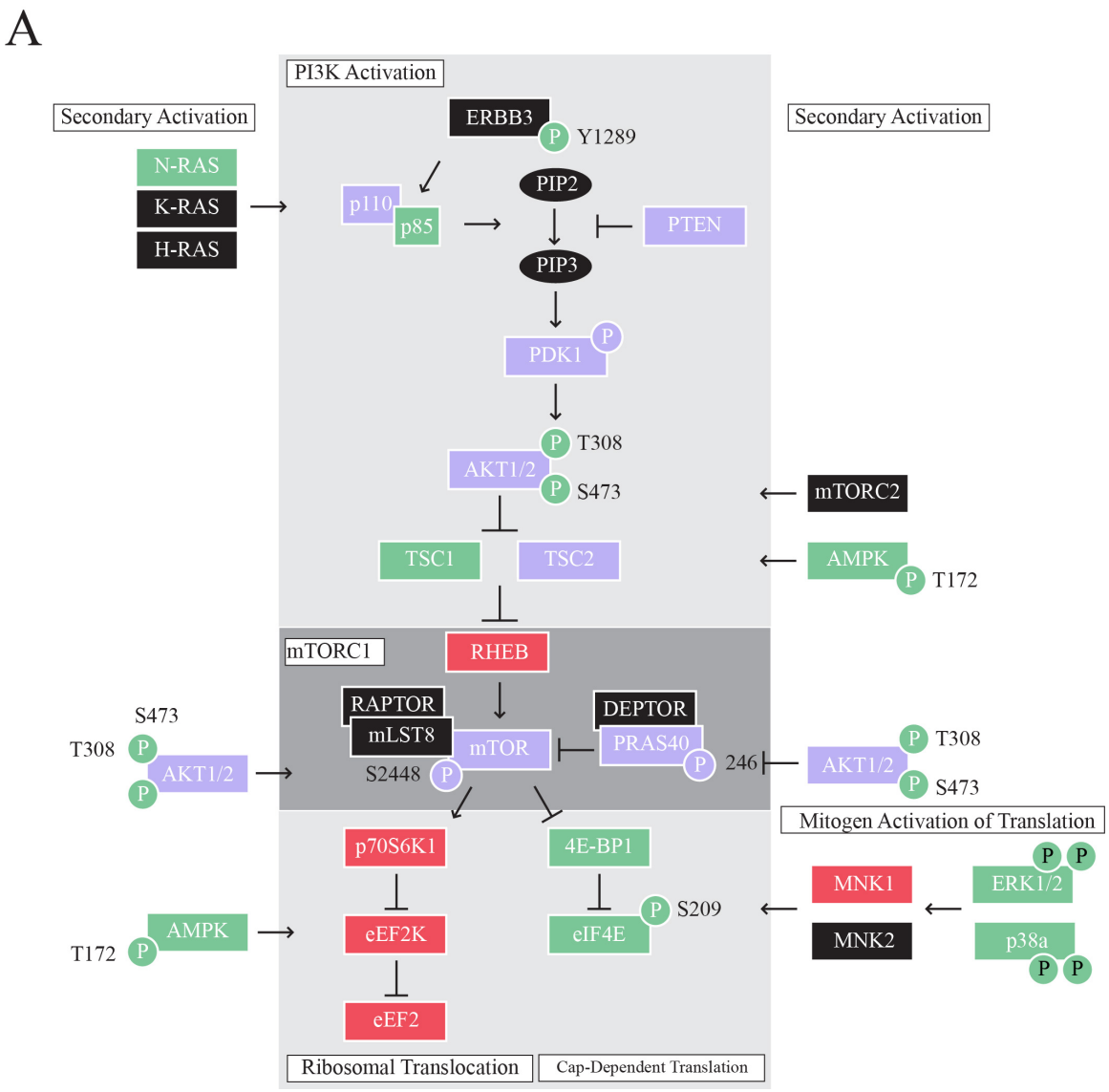


**Figure 4-6: ArhGEF1 is Required for Translation Elongation.**

**A.** Relative changes in protein expression between MCF7 control cells and MCF7 genetically inactivated for shArhGEF1 as measured by Reverse Phase Protein Array (RPPA). Samples were serum starved for 24 hours and treated for 30 minutes with serum. Colors: *Black* indicates protein was not present in array, *Purple* indicates no significance between shARG1 and control, *Red* indicates significant decrease (P <. 05) in expression, and *Green* indicates significant increase (P < .05) in expression.

4.2.4 Loss of ArhGEF1 Induces Aggregated Actin that Promotes Cellular Senescence

The loss of ArhGEF1 in MCF7 cells results in a hyper-actin stress fiber phenotype as visualized by phalloidin staining (Figure 4-7A). This likely explains the extreme flattening of these cells. The stable expression of $G\alpha_{13}QL$ in MCF7 cells similarly induces a flattening phenotype, suggesting that the effects of ArhGEF1 knockdown on actin occur from the prolonged activation of $G\alpha_{13}$ (Figure 4-7B). Further analysis of RPPA, suggest that cells stably knocked down for ArhGEF1 elevates RhoA activity, as ROCK1 protein expression is significantly increased. ROCK1 is a serine/threonine kinase that upon being activated by RhoA, it phosphorylates downstream effectors including Myosin Light Chain Kinase (MLC) (216,217), Lim domain kinase 1 (LIMK) (218), and mammalian Diaphanous-related formin-1 (mDia) (219). This typically results in promoting cell migration . This is due to the activation of Myosin IIa (MYOIIA), the heavy chain of the non-muscle myosin complex, that in conjunction with MLC, mediates contraction of the actinomyosin network. However, in ArhGEF1 knockdown MCF7 cells, the phosphorylation of serine 1943 of MYOIIA, when compared to control MCF7 cells, is significantly reduced, suggesting these cells lack migratory capacity (Figure 4-7C). Functional validation of a net reduction of cell migration is displayed by ArhGEF1 stably silenced MCF7 cells that only showed a 22% wound closure in a scratch wound assay compared to 66% wound closure by control cells over 24 hours (Figure 4-7D). Again, stable overexpression of $G\alpha_{13}QL$ recapitulated this ArhGEF1 phenotype, where MCF7 cells expressing $G\alpha_{13}QL$ showed less wound closure, 24% versus 52% for control cells (Figure 4-7D). These results highlight that ArhGEF1 in

MCF7 cells prevents the hyper-activation of $G\alpha_{13}$, and thereby the formation of excessive stress fibers that results in migration defects.

The increase in levels of actin stress fibers, the loss of migration, and an inability to grow, suggests that ArhGEF1 silenced cells may undergo senescence. Propidium iodide staining of cells allowed them to be sorted by flow cytometry on DNA content. This revealed that the ratio of $G_{1/0}/G_2$ for ArhGEF1 silenced cells was 2.8 versus control cells whose ratio was 1.8 (Figure 4-8A). These significant increases in $G_{1/0}/G_2$ for ArhGEF1 silenced MCF7 cells, suggest that they are aberrantly arresting in $G_{1/0}$. This aligns with their loss of Cyclin D1 transcription, as it is required for transition out of $G_0$. These same cells also exhibit a ~3-fold increase in nuclear staining of 53-binding protein 1 (53BP1), a marker for sustained double stranded breaks that is used as an indicator for cellular senescence (Figure 4-8B). Interestingly, knockdown of ArhGEF12 in MCF7 cells also locks cells in the $G_{1/0}$ phase, as the ratio of cells in $G_{1/0}/G_2$ is 4.8 compared to a ratio of 2.0 for control cells (Figure 4-8C). Overall, the hyperactivation of $G\alpha_{13}$ upon ArhGEF1 silencing is overwhelmingly and suggested to result in cellular senescence even though core pro-growth pathways are being activated. This suggests the existence of inherent fail-safe mechanisms to prevent cells from growing even under high levels of growth signaling in situations where ArhGEF1 fails to adequately dampen such signaling.

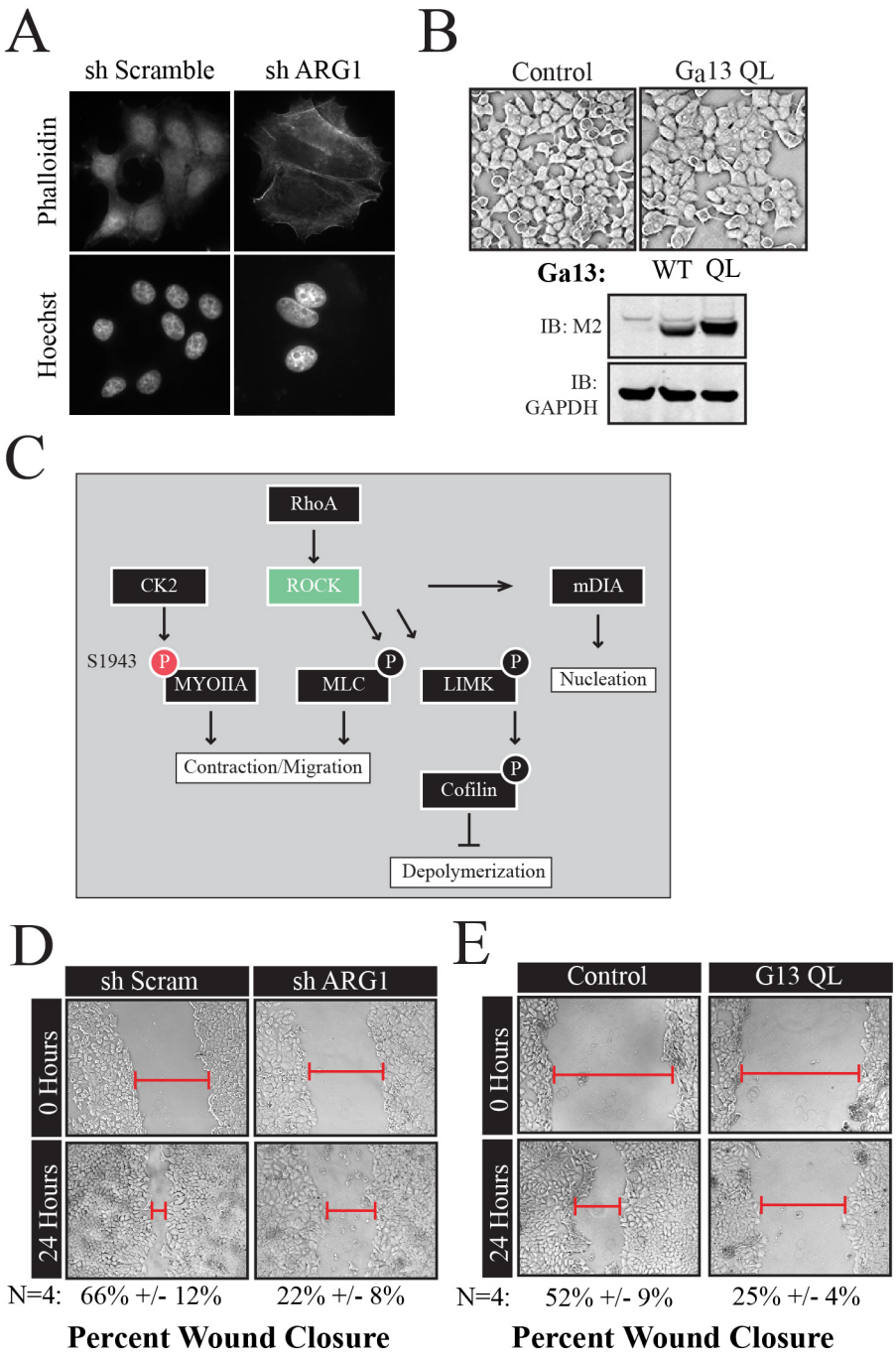


**Figure 4-7: Actin Dynamics are Disrupted in ArhGEF1 Knockout Cells.**

**A.** MCF7 cells infected with shArhGEF1 (shARG1) or shRNA and then fixed and immunostained for phalloidin (top panel) and Hoechst die (bottom panel). **B.** Brightfield imaging of live cells stably expressing 3x-Flag $G\alpha_{13}QL$ (Top Panel). Immunoblot of 3x-Flag $G\alpha_{13}QL$ using M2 antibody (Bottom Panel). **C.** Relative changes in protein expression between MCF7 control cells and MCF7 genetically inactivated for shArhGEF1 as measured by Reverse Phase Protein Array (RPPA). Samples were serum starved for 24 hours and treated for 30 minutes with

serum. Colors: *Black* indicates protein was not present in array, *Purple* indicates no significance between shARG1 and control, *Red* indicates significant decrease (P <. 05) in expression, and *Green* indicates significant increase (P < .05) in expression. **D.** MCF7 cells infected with either an shScramble or shArhGEF1 (shARG1) were plated to density and scratched 24 hours later. Brightfield images were taken at initial scratch and 24 hours later**.** Average area closed represents 4 individual experiments. (**P < .01). **E.** MCF7 cells stably expressing 3x-Flag $G\alpha_{13}QL$ were plated to density and scratched 24 hours later. Brightfield images were taken at initial scratch and 24 hours later**.** Average area closed represents 4 individual experiments. (**P < .01).

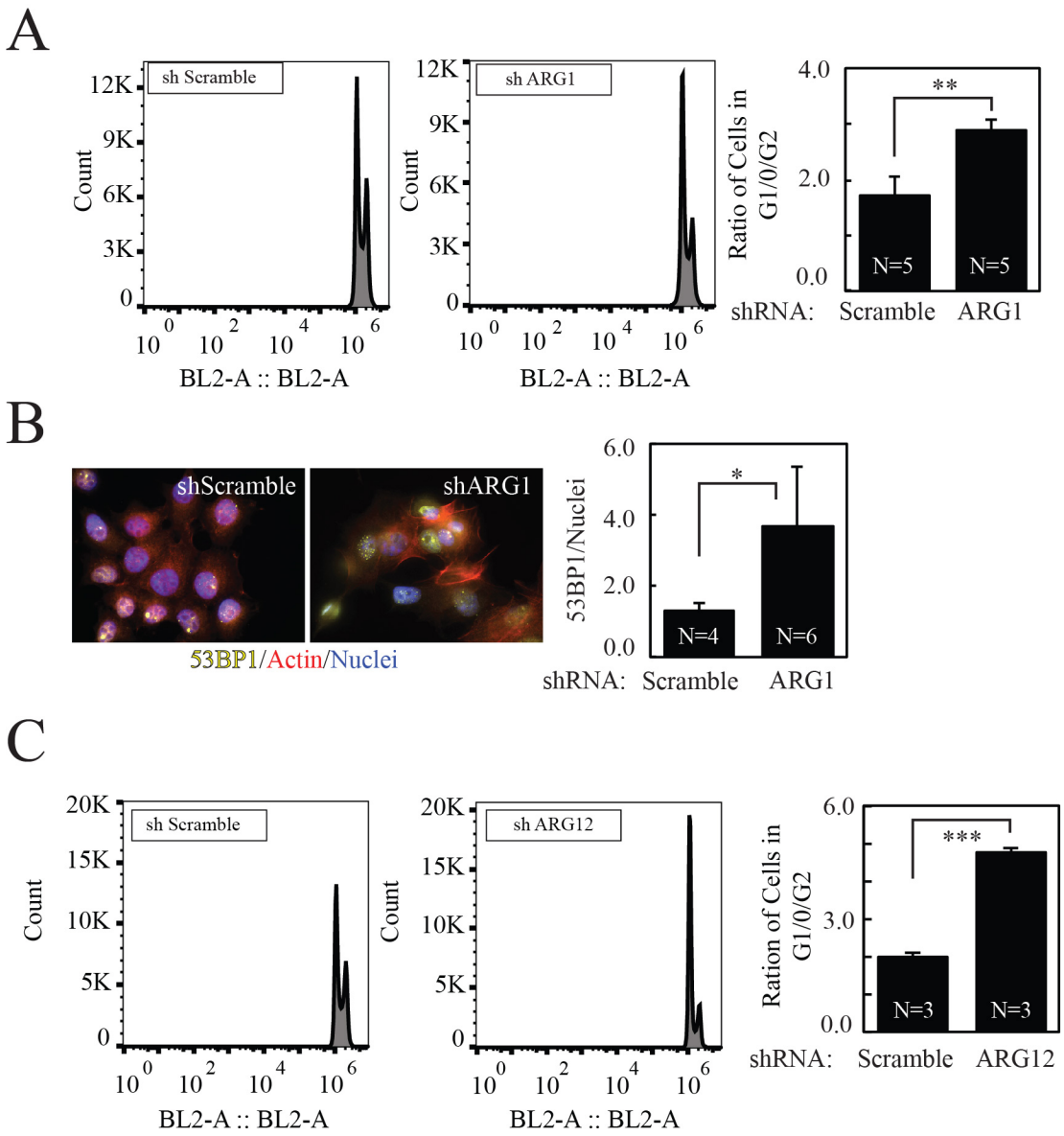


**Figure 4-8: ArhGEF1 and ArhGEF12 Knockout Result in $G_{1/0}$ Stacking.**

**A.** MCF7 cells were stably silenced for ArhGEF1 using lentiviral transduction, fixed, stained with propidium iodide and analyzed for DNA content. The first peak corresponds to $G_{1/0}$ phase and the second smaller peak corresponds to $G_2$ phase of the cell cycle. Control cells (Left Panel) and shArhGEF1 cells (Middle Panel). Ratio of $G_{1/0}$ to $G_2$ (Right Panel). **B.** MCF7 cells stably silenced for ArhGEF1 using lentiviral transduction were fixed and stained with 53BP1, Phalloidin, and Hoechst Dye (merged images) (Left two panels). The right panel is the average 53BP1 spots per nuclei **C.** MCF7 cells were stably silenced for ArhGEF12 using lentiviral transduction, fixed, stained with propidium iodide and analyzed for DNA content. The first peak corresponds to $G_{1/0}$ phase and the second smaller peak corresponds to $G_2$ phase of the cell cycle. Control cells (Left Panel), shArhGEF12 cells (Middle Panel). Ratio of $G_{1/0}$ to $G_2$ (Right Panel).

### 4.2.5 YAP1 Protects ArhGEF1 Senescent Cells from Apoptosis

YAP1 has been found to promote cell growth by both stimulating proliferation and by increasing the ability of cells to evade apoptosis (201). For instance, epithelial cells that detach from the basement membrane undergo cytoskeleton reorganization inducing anoikis. However, exogenous overexpression of YAP1 prevents anoikis in this context. Considering the strong activation of YAP1 that occurs with concomitant growth arrest upon ArhGEF1 silencing, the role of YAP1 in promoting survival mechanisms in senescent cells was investigated.

As seen by bright field microscopy, MCF7 cells stably silenced for ArhGEF1 exhibit a flattened morphology in comparison to control cells that exhibit a cuboidal epithelial phenotype (Figure 4-9A). The knockdown of YAP1 in MCF7 cells expressing shScramble produces no discernable affects on cellular morphology (Figure 4-9A). However, the silencing of YAP1 in cells that are already stably silenced for ArhGEF1, results in cell rounding and blebbing, indicative of apoptosis (Figure 4-9A). Tandem knockout of ArhGEF1 and YAP1 in MCF7 cells also significantly decreased cell viability when compared to YAP1 or ArhGEF1 individual knockouts, as measured by MTT assay following 60 hours of seeding (Figure 4-9B). Furthermore, 12 % of cells in which YAP1 or ArhGEF1 was silenced in isolation in isolation underwent death after 48 hours as measured by cell counting following Trypan blue staining (Figure 4-9C). However, 35% of MCF7 cells that were silenced for both ArhGEF1 and YAP1 were not viable after 48 hours (Figure 4-9C). These data suggest that YAP1 expression protects ArhGEF1 silenced cells from switching from a senescence to an apoptotic program.

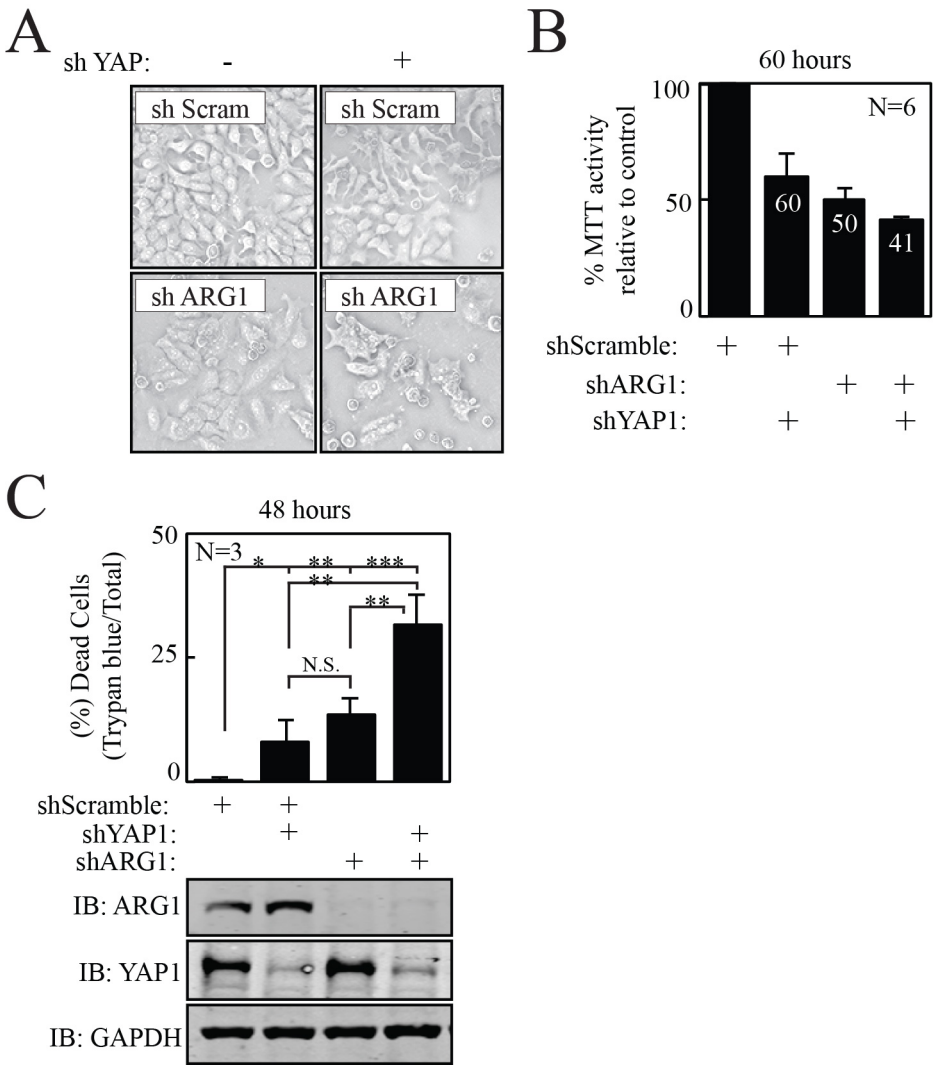


**Figure 4-9: Tandem Knockout of ArhGEF1 and YAP1 is Synthetically Lethal.**

**A.** Brightfield imaging of live MCF7 cells stably silenced for YAP1, ArhGEF1, or a combination YAP1 and ArhGEF1 by lentiviral transduction. **B.** MCF7 cells stably silenced for YAP1, ArhGEF1, or a combination YAP1 and ArhGEF1 through lentiviral transduction were allowed to grow for 3 Days in a 96-well plate. On Day 3 15 uL of 5mg/mL of MTT was added for 4 hours, followed by the addition of 100 uL of MTT solvent for 1 hour. Cells were resuspended and absorbance at 570 nm was recorded and normalized to control. **C.** MCF7 cells stably silenced for YAP1, ArhGEF1, or a combination YAP1 and ArhGEF1 through lentiviral transduction, were allowed to grow for 3 Days and stained with 1:1 dilution of Trypan blue.

## 4.3 DISCUSSION

### 4.3.1 $G\alpha_{13}$ Role in Growth and the Excessive Growth Signaling "fail-safe" Switch

The work in this chapter suggests that ArhGEF1 dictates a narrow range of $G\alpha_{13}$ activity that may stimulate cell growth. Loss of ARHGEF1 results in the hyper activation of $G\alpha_{13}$ that stimulates a broad activation of growth-signaling including YAP1, ERK1/2, JNK1/2 and PI3K/AKT pathways. However, cell cycle and cell migration are impaired likely from an inhibition of mRNA translation.

Chronic growth signaling in many contexts is linked to cellular senescence. For instance the overexpression of constitutive active RAS in NIH3T3 mouse fibroblast activates senescence pathways in the presence of wild type p53 (198). In more recent studies this was determined to require AKT, as cells that were deficient in AKT were resistant to replicative, oxidative, and oncogenic RAS induced senescence (220). Here, the aberrant activation of $G\alpha_{13}$ through the loss of ArhGEF1, a key GTPase activating protein for $G\alpha_{13}$, results in chronic growth signaling events that induce cellular senescence. This is accompanied by high levels of stress fibers that appear to aggregate and to lack a normal level of turnover. This may explain the reduced migratory capacity of ArhGEF1 silenced MCF7 cells. This suggests that if the actin dynamics of the cell are deregulated, then growth signaling is re-directed to promote a senescent phase. This work may also explain why senescent cells typically are observed to have a flattened morphology. This is proposed to be due to a structural "fail-safe" mechanism increased actin stress-fibers eventually physically limit the cell from proliferating, by uncoupling cell cycle activation from protein translation (221). Overall this "fail-safe mechanism appears to supersede all other signaling that also controls cell fate

4.3.2 The Role of YAP1 in Maintaining Cell Survival under JNK1/2 Activation

The chronic activation of JNK1/2 is associated with a variety of stresses, most notably DNA damage induced by UV irradiation (113). Cells that are UV-irradiated characteristically exhibit extreme flattening, increased actin stress fibers, the activation of JNK1/2 as measured by its phosphorylation, and senescence. Because MCF7 cells silenced for ArhGEF1 exhibit all of these characteristics, it is proposed that ARhGEF1 silencing induces senescence. Further, the synthetically lethal phenotype observed upon the combination of ArhGEF1 and YAP1 knockdown suggests that YAP1 mainly functions to maintain cell survival in senescent cells.

The ability of JNK1/2 to phosphorylate YAP1 presents a possible mechanism by which YAP1 may switch from acting as a pro-growth transcriptional co-activator to a manager of cell survival. Consistently, the JNK1/2 activator, anisomyocin, as well as UV-irradiation has been shown to induce the phosphorylation of YAP1 in a variety of cell types, including MCF7 breast cancer cells (222). Stimulation of JNK1/2 promotes YAP1 stabilization and association with Δp63α, as measured by IP, in HaCat and H357 cells. This prevents the E3 ubiquitin ligase, ITCH, from binding PPxY motifs of Δp63α and promoting its degradation. Furthermore in this study, the knockdown of YAP1 switched UV-irradiated cells from a Δp63α survival state to a p73 induced apoptotic state (222) (Figure 4-10A). Preliminary results in MCF7 breast cancer cells suggest the dual knockdown of YAP1 and ArhGEF1, increases the p73 dependent transcription of p53 upregulated modulator of apoptosis (PUMA), but not when either are independently knocked down (Figure 4-10B). More striking evidence that supports the idea that YAP1 promotes the survival of stressed or senescent cells is the observation that both p53 and

p63 pathways are predicted to be activated in cells silenced only for ArhGEF1 (Z score >2) by Ingenuity Pathway Analysis, whereas p73 is not (Figure 4-10C). These results in MCF7 cells mirror those found in this previous study and suggest in breast cancer cells that YAP1 may mediate cell survival under stressful conditions by toggling between stabilizing or contributing to the degradation of Δp63α in breast cancer cells. Overall, this suggests that the ability of YAP1 to protect stressed cells from engaging apoptotic pathways could contribute to the resistance of cancer cells to radiation or chemotherapeutic treatments.

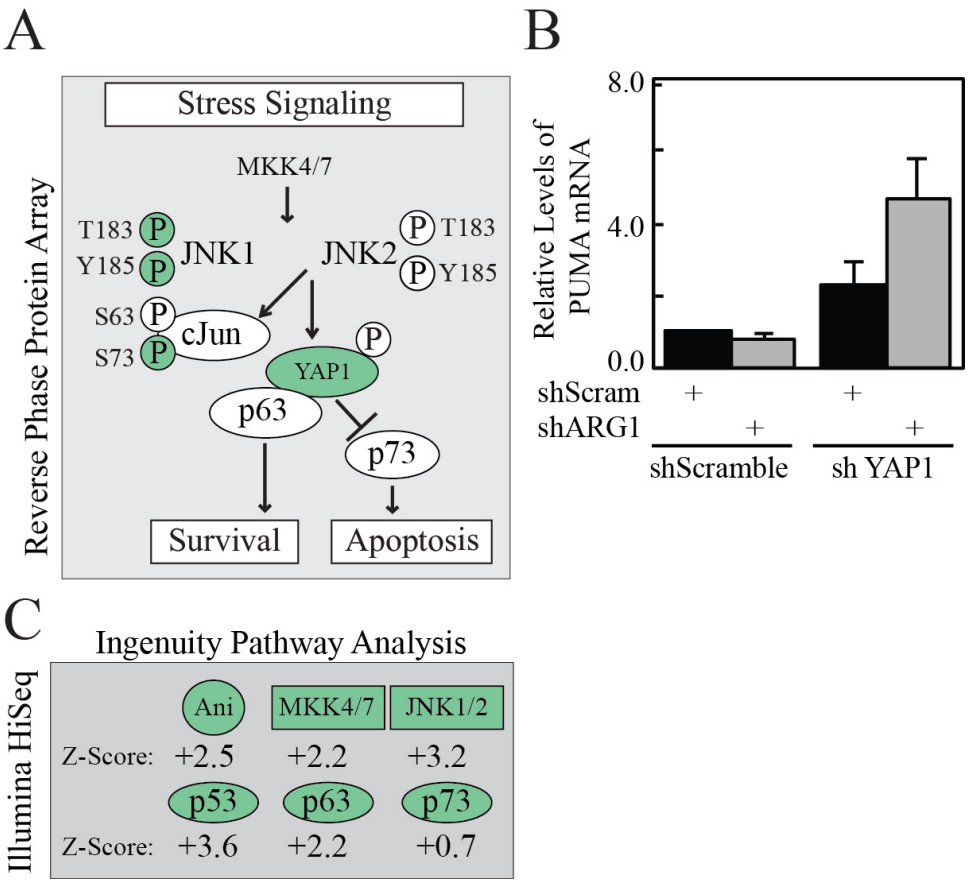


**Figure 4-10: YAP1 Protects ArhGEF1 Knockout Cells from Engaging Cell Death.**

**A.** Model of JNK1 phosphorylation and stabilization of YAP1/Δp63α to maintain cell survival under stress. *Green* indicates those proteins or post-translational modifications that are significantly increased in ArhGEF1 silenced MCF7 cells compared to control per RPPA. **B.** CT value of PUMA mRNA transcript was measured by qRT-PCR in MCF7 silenced for ArhGEF1 (shARG1) compared to control (shScram), with a knockout of YAP1 (shYAP1) in each condition as well, all delivered by lentiviral transduction. **C.** Ingenuity Pathway Analysis upon total transcriptome sequencing by Illumina HiSeq following a comparison of transcripts differences among MCF7 cells silenced for ArhGEF1 and control. A Z-score >2 indicate activation.

# CHAPTER 5. CONCLUDING REMARKS ON THE INTEGRATIN OF THE SERUM RESPONSE NETWORK, MAPK CASCADES, AND HIPPO IN CELLULAR HOMEOSTASIS

## 5.1 INTRODUCTION

The work presented in this dissertation elucidates intracellular roles of the RGS-RhoGEFs in mediating serum mitogen signaling onto regulating RhoA induced YAP1-TEAD dependent transcription. More specifically it defines how alterations in their regulation and function dictate YAP1 dependent cell fate decisions. The activity of the RGS-RhoGEFs mainly takes place at the plasma membrane, however they are known regulators of RhoA activity at focal adhesions (223). These variations in spatial activation of the RGS-RhoGEFs may have functionally different consequences in regards to YAP1 regulation. The functionality of the RGS-RhoGEFs is regulated by biophysical and biochemical stimuli as highlighted by data in Chapters 3 and 4. ArhGEF1 can switch from a GEF, in low serum, to a GAP when stimulated by serum. This binary switch is likely regulated by post-translational modifications. Furthermore, both ArhGEF11 and ArhGEF12 increase their proclivity to induce nucleotide exchange on RhoA upon tyrosine phosphorylation by focal adhesion kinase (FAK) (224). It is therefore imperative for future studies to identify spatial and temporal regulation of post-translational modifications of the RGS-RhoGEFs, in order to fully elucidate the mechanisms by which they regulate YAP1 activity. Understanding these modifications could be key in understanding how cancer cells circumvent "fail-safe" signaling mechanisms, like oncogene induced senescence, to continue to proliferate in times of unwarranted growth.

Also highlighted in this study is the requirement of the RGS-RhoGEFs for the integration of three prominent cell growth-signaling pathways: the Serum Response Network, Mitogen Activated Protein Kinase Cascades, and the HIPPO pathway. Cancer cells often utilize these pathways to propagate growth, and therefore further

understanding of how the RGS-RhoGEFs integrate these pathways is essential. In the data presented, we have physiologically identified a mechanism by which prolonged activation of the Serum response Network with concurrent activation of the MAPK cascades leads to growth retardation. The evidence suggest this rampant activation leads to cellular senescence, by inducing a hyper-actin stress fiber phenotype and by uncoupling the activation of growth signaling pathways from cell cycle progression. Also during this period of prolonged activation, and subsequent induction of cellular senescence, YAP1 is implicated in promoting cell survival. This function is essential, as the loss of YAP1 promotes a synthetically lethal phenotype. How exactly YAP1 maintains its survival functionality independent of its growth activating potential is unknown. Recent studies indicate YAP1 is subject to a variety of post-translational modifications via phosphorylation, sumoylation, ubiquitination, and acetylation in times of stress (120, 222, 225, 226). This study leaves open an area of future exploration into understanding how YAP1 functionality is switched under different types of stress, and when combined with hyper-activation of the Serum Response Network this may point to potential therapeutics targeting resistance to chemo and radiation therapies for cancers.

## 5.2 Determination of Cell Fate by Signaling Flux and Actin Dynamics

### 5.2.1 Role of Signaling Flux in Cell Growth and Cancer

Under normal physiological conditions, cells have numerous mechanisms that act as "fail-safes" to prevent unwarranted cellular growth. Mechanisms that typically facilitate growth control are core to cell cycle progression and also monitoring the integrity of the duplicating genome. The rapid proliferation of cancer cells often by-pass key cell cycle checkpoints and have genomic integrity issues, such a mutations in essential genes or double-stranded breaks. The introduction of double stranded breaks activates the tumor suppressive protein p53 that functions to limit cell cycle activity in order to repair the damage (227, 228). P53 can activate for a limited time cellular senescence, if the damage is manageable, or it can engage apoptotic pathways if the stress cannot be overcome (229, 230). The dominant role p53 plays in managing genomic integrity is primarily why many cancers harbor mutations (231) that disrupt its tumor suppressive function. This allows cancer cells to facilitate unregulated cellular growth that cannot be inhibited by faults in duplicating the genome.

Past studies identified the role p53 plays in facilitating oncogene-induced senescence. RAS is often altered in cancers by mutations that make it constitutively active (232). This is a prominent feature of a variety of pancreatic and breast cancers. However, in cell model systems, the introduction of constitutive active RAS in mouse fibroblast, that maintain wild type p53, initiates oncogene-induced senescence (198). This is also the case for constitutive active and RAF (233). The two cell lines in this study that characterize the prolonged activation of the serum response network and MAPK cascade, by knockdown of ArhGEF1, resulting in cellular senescence, one MCF7, has wild-type

p53 (234), and the other MDA-MB-231 (235), has a gain of function mutant p53. This suggests that the "fail-safe" mechanism instigated by prolonged activation of the serum response network, concurrent MAPK signaling, and YAP1 hyper transcriptional activity is p53 independent (Figure 5-1A). This therefore suggests a universal mechanism for inhibiting growth in a variety of tumors that maintain high levels of MAPK signaling and mutated p53, many of which are inherently resistant or develop resistance to current treatments.

5.2.2 Role of Actin in Determining Cell Fate

Actin fibers form major structural components of cells that that are subject to drastic reorganization in response to microenvironmental conditions. These changes are core to relaying outward-inward signaling to mediate cell fate decisions. The ability of a cell to adapt to its environment is critical for survival, and conversely if it cannot adapt, the cell may engage cell death signaling pathways. Core to these cell fate decisions is the ability of actin cytoskeletal structures to be dynamic (236). Under these transitions, cells break down cortical actin structures, and repurpose that actin into stress fibers and adhesive structures (236). As this occurs, genes tied to the activation of the cell cycle are activated to propagate cell growth (172, 237, 238). However if the cell experiences extreme stress, actin structures become aggregated and then static. This stasis of actin fibers initiates cellular senescence and under extreme stresses apoptosis (236). Because the mechanism(s) by which this stabilized, aggregated actin induces senescence is not known, I will speculate how this may occur based on the data in this dissertation.

The loss of ArhGEF1 promotes a dominant stress fiber phenotype. This phenotype is thought to exceed the normal physiological range of actin polymerization for a couple of reasons. First, actin polymerization typically elicits growth signaling, however in MCF7 cells with ArhGEF1 knockdown, actin polymerization is uncoupled from promoting cell proliferation. Second, the dominant actin phenotype in ArhGEF1 knockdown MCF7 cells, also restricts cells from migrating correctly, which is supported by the loss of MYOIIA serine 1943 phosphorylation (Appendix C). These data suggest that ArhGEF1 is critical for maintaining actin turnover, and that too much signaling flux through the GTPase, $G\alpha_{13}$, locks actin into a static form, leading to cellular senescence.

However, the mechanistic details of how actin dictates cellular senescence in this scenario are unknown.

Secondly, actin is a major source of ATP consumption. Actin filament formation involves the addition of ATP-G-actin monomers to the barbed (+) end of an active filament. Conversely, the breakdown of filaments involves the release of ADP-F-actin-monomers from the pointed (-) end. The release of ADP from the pointed end is then converted back into ATP and the cycle continues if necessary. This cycle of addition and subtraction is known as actin tread-milling and is the dynamic mechanism for motility (236). Changes in environmental cues or the subjection of a cell to a stress, causes actin to be repurposed to stress fibers, which inherently alters the transcriptional programming and cellular ATP/ADP levels to change to respond to that stress. However if actin is static, it is hypothesized that ADP would be trapped in the filaments, creating a structural, "actin sink" for ATP. Recent work suggest the depletion of ATP in neurons is reduced by nearly 50% by slowing down actin turnover using drugs targeted toward filament turnover, jasplakinolide (targets disassembly) or latrunculin A (prevents assembly) (239). When these two drugs are applied together they prevent ATP loss in a background where ATP synthesis is inhibited. This study implies that actin filaments are major reservoirs for ATP/ADP in the cell and actin aggregates that are no longer dynamic reduce the levels of ADP available. This essentially starves the cell of energy, preventing basic cellular functions such as transcription, translation, protein synthesis, etc. Mechanistically this could explain how cells become senescent as they show a flattened phenotype with high levels of actin filaments, suggesting a structural "fail-safe" mechanism for unwarranted prolonged signaling.

The mechanism by which ArhGEF1 knockdown contributes to the loss of cell growth is not known. However, knockdown of ArhGEF1 contributes to global losses in cell cycle progression and translation even in the presence of activated growth pathways such as the MAPK cascades and YAP1 transcriptional activity. These global cellular programs require a great deal of energy, from both ATP and GTP. The enhanced actin phenotype in ArhGEF1 knockdown cells, facilitated by activated $G\alpha_{13}$-RhoA-Rock signaling, may suggest that actin is being aggregated and serves as an "actin sink" for cellular ATP, reducing energy reserves. This "actin sink" hypothesis is supported by the notion that MYOIIA serine 1943 phosphorylation is significantly decreased, consistent with actin turnover being reduced as migration is inhibited. Further, the activation of the nutrient sensor AMPK, via its phosphorylation at tyrosine 172, indicates that there is disproportional amount of AMP compared to ATP in the cell. Studies are needed to further prove that the loss of actin turnover is detrimental to maintaining a proper balance of cellular AMP, ADP, and ATP levels. Rescue experiments to show the liberation of ADP from the actin in ArhGEF1 knockdown MCF7 cells, for example by expressing a constitutive active cofillin that can potentially rescue the loss of cell growth, may help test this hypothesis. Such data might further indicate that actin dynamics supersedes the activity of even the most potent oncogenes like YAP1 or MAPK cascades.

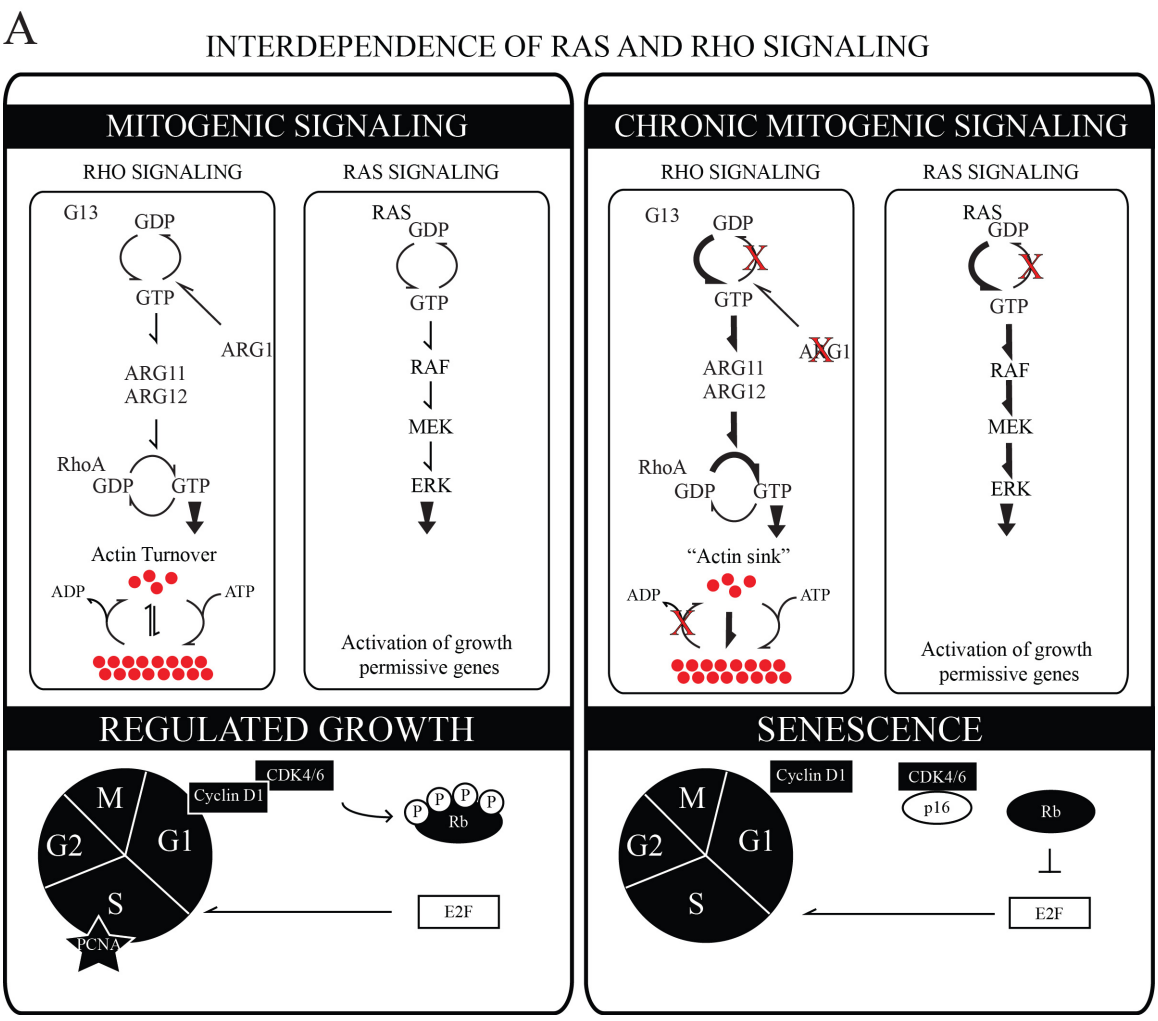


**Figure 5-1: Interdependence of Ras and Rho Signaling on Cell Fate; "Actin-sink" Model.**

**A.** Schematic of the dependence of Ras and Rho Signaling in response to mitogens. Maintained mitogenic signaling leads to regulated growth, whereas prolonged or unregulated mitogenic signaling results in cellular senescence.

5.2.3 RGS-RhoGEFs Regulate YAP1 Stability Through Actin Dynamics

The nuclear translocation of YAP1 is essential for it to bind and co-activate transcription factors to influence transcriptional programs that control cell fate. The regulation of YAP1 nuclear translocation is completely dependent on the cells having a certain level of biomechanical loading. Canonical sequestration of YAP1 from the nucleus involves its phosphorylation at serine 127 by the upstream kinase LATS1/2 in response to cell-to-cell contact (120). 14-3-3 then binds this phosphorylation motif and YAP1 is retained in the cytosol. Furthermore, a LATS1/2-independent event was discovered that involves YAP1 mediated stabilization and nuclear translocation by filamentous actin fiber formation, the disruption of which caused YAP1 degradation and nuclear exclusion (142). However controversy still exists on to whether the dominant regulation of YAP1 nuclear translocation and stability is LATS1/2 dependent or independent.

Previous studies from the Wells laboratory delineated a role for Angiomotin members in YAP1 protein stabilization (Figure 5-2A). In response to serum deprivation, Angiomotin is phosphorylated at serine 175 by LATS1/2 (125). This phosphorylation site lies in the middle of an actin-binding domain (240). Phosphorylation dislodges Angiomotin from the actin cytoskeleton, freeing the N-terminal PPxY motifs to interact with YAP1. Subsequently, 14-3-3 can bind Angiomotin and sequester the Amot-YAP1 complex in the cytosol or it can recruit an Amot-AIP4 complex. The dimerization of the Angiomotin complexes brings YAP1 into the proximity of AIP4, leading to YAP1 ubiquitination and degradation (124). Conversely, in situation where there are high levels of actin stress fibers, which is indicative of low intercellular contact, LATS1/2 is

inactivated and Angiomotin binds to the actin cytoskeleton. This prevents the association of Amot with AIP4 and therefore YAP1 is not subject to ubiquitination and subsequent degradation. The RGS-RhoGEFs are key mediators of actin dynamics and therefore they are likely able to alter YAP1 stability, nuclear translocation, and activity by altering actin-Angiomotin complex dynamics.

The knockdown of ArhGEF12 and ArhGEF1 in MCF7 cells show appreciable changes in the overall actin structure and consequently cell morphology. Concurrent, with changes in actin dynamics, there is also an associative change in YAP1 protein stability and function. In MCF7 cells silenced for ArhGEF12, cells morphologically round, and their actin structures are reduced. Concurrently, there is a loss of YAP1 protein transcriptional activity. Conversely, when ArhGEF1 is knocked down, cells flatten and acquire prominent stress fibers. YAP1 phosphorylation is also reduced, whereas YAP1 nuclear translocation and transcriptional activity are enhanced. In cells inactivated for ArhGEF1, it is proposed that the flattened, aggregated actin increases Angiomotin binding to the filament to inhibit the interaction of Angiomotin-AIP4 and Angiomotin-YAP1 complexes, allowing nuclear translocation of YAP1 (Figure 5-2B). The loss in YAP1 protein in ArhGEF12 knockdown MCF7 cells is hypothesized to result from the formation of Angiomotin/YAP1-Angiomotin/AIP4 complexes (Figure 5-2C). The formation of these complexes in ArhGEF12 knockdown MCF7 cells is expected to be dominant, as the cells have reduced levels of actin, therefore promoting the release of Angiomotin from actin fibers and consequently its coupling of ubiquitin mediated degradation to YAP1. This complete restriction of YAP1 from the nucleus may suggest why cells silenced for ArhGEF12, when compared to ArhGEF1 and ArhGEF11 silenced

MCF7 cells, have lower proliferation rates, and higher cell death. If these hypotheses are true it would suggest a dominant role for the actin cytoskeleton, and its regulators, to the regulation of LATS1/2 interactions with YAP1 to control its stability and functionality.

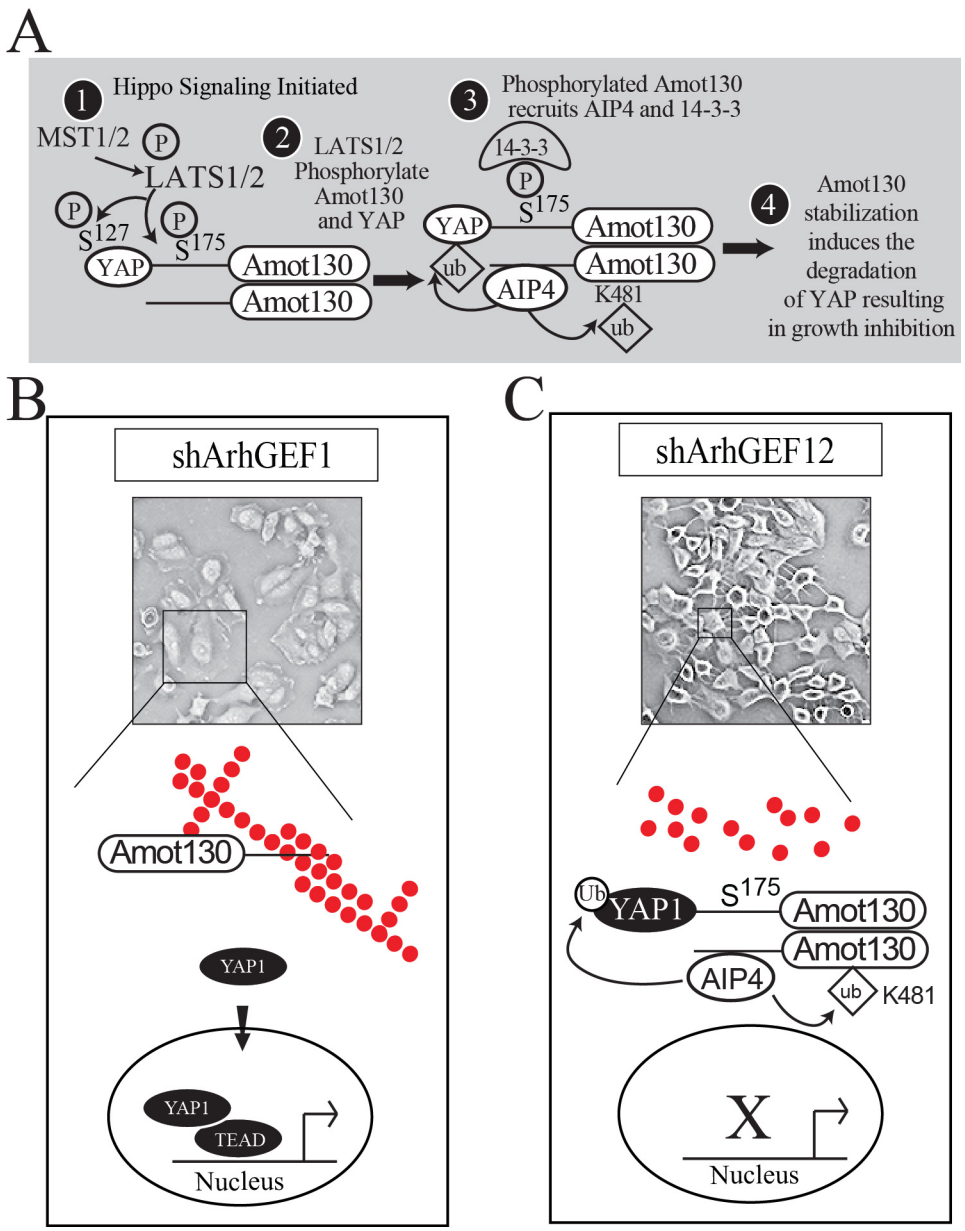


**Figure 5-2: Angiomotin's Potential Role in Regulating YAP1 in Cells Silenced for ArhGEF1 or ArhGEF12.**

**A.** Schematic of known role Angiomotin plays in adapting YAP1 to AIP4 for ubiquitin mediated degradation. (Figure Adopted from Adler 2013). **B.** A model of the potential role Angiomotin plays in facilitating YAP1 nuclear translocation in shArhGEF1 cells. **C.** A model of the potential role Angiomotin plays in facilitating YAP1 nuclear exclusion in shArhGEF1 cells. *Red* dots are G-actin, *Red* fibers are f-actin.

## 5.3 Regulation of RGS-RhoGEFs and YAP1 by Localization and Post-Translational Modifications

### 5.3.1. Role of RGS-RhoGEFs Localization Implications on Regulating YAP1

This work identified the requirement of the RGS-RhoGEFs in regulating YAP1-TEAD dependent transcription in response to biochemical signals at the plasma membrane, however the RhoGEFs also contribute to baso-lateral biomechanical signaling. How this baso-lateral signaling regulates YAP1 activity is still an area for future exploration. Biomechanical regulation of YAP1 is product of the cells asymmetric interactions with both the basement membrane and sites of cell-to-cell cohesion. Intercellular interactions are cadherin based and supported by the underlying cortical actin structures. The cell facilitates interaction with the basement membrane through integrin linked stress fibers at focal adhesion complex. The underlying regulation of actin/focal adhesion complexes involves the cyclic activity of RhoA mediated by the RGS-RhoGEFs, independently of their function at the plasma membrane (223, 224). The contradictory regulation of YAP1 by RhoA induced stress fibers and RhoA induced cortical actin; suggest that the localized activity of the RGS-RhoGEFs may contribute differentially to YAP1 localization and functionality.

Focal adhesions independently regulate YAP1 activity and therefore understanding how the RGS-RhoGEFs contribute to the regulation of stress fiber/focal adhesion complexes together may explain what ultimately influences YAP1 functionality. Focal adhesion dynamics play a major role in the motility of the cell, and alter transcriptional growth propagating programs. The small GTPases, RhoA and Rac1, each are required and work in a temporal manner to regulate cell adhesion (223). Initially,

during early stage adhesion, Rac1-dependent activity drives lamellapodia formation and cell flattening (241). Conversely, during this time, RhoA activity is retarded in a GAP-dependent manner, mainly through p190RhoGAP (242). During the late stage maturation of focal adhesion complexes, Rac1 activity is diminished and RhoA facilitates stress fiber formation (241). The GEFs responsible for RhoA activity are ArhGEF1 and ArhGEF12 (223). At the plasma membrane, upon serum stimulation, the GAP activity of ArhGEF1 is elevated, while under these same conditions, at focal adhesions its GEF activity is enhanced. This evidence strongly supports the notion that ArhGEF1 function is dependent of its localization within the cell. These reciprocal functions of ArhGEF1 could potentially have opposing roles in mediating YAP1 nuclear translocation and functionality.

Further complicating matters, the RGS-RhoGEFs also contribute to the regulation of cortical actin at cellular junctions and this regulation could further affect YAP1 activity in a cell density manner. Evidence for this is highlighted in MCF7 cells, as the knockdown of ArhGEF1 results in the loss of E-cadherin complexes at intercellular junctions, which is likely due to a loss in the cortical actin network (243). $G\alpha_{12/13}$ are known to stimulate actin filamentation at cell junctions, ArhGEF1 would presumably act as a GEF for RhoA in this context if the GTPases were working through it. If ArhGEF1 is working independently of heterotrimeric proteins, this would define a new avenue for its regulation and function and add another layer to our understanding of how actin network regulation is coupled to YAP1 localization. These data also support the notion that ArhGEF1 may have dual functions that are context dependent. Conversely, knockdown of ArhGEF11 drastically enhances E-cadherin attachments whereas the knockdown of

ArhGEF12 has no discernible effect (243). Again, ArhGEF11, like ArhGEF1, exhibits contradictory functionalities that are dependent on its localization within the cell. The RGS-RhoGEFs are also differentially required in response to serum to regulate YAP1 as highlighted by the differential activation of TEAD transcription under different cellular densities. These data suggest a rheostat role for the RGS-RhoGEFs, as they are uniquely capable of dialing "up" or "down" the actin cytoskeleton, which directly dictates YAP1 nuclear translocation and activation. Further understanding of how these GEFs utilize their functional domains at each locale, and how the cell mediates the activation of these seemingly opposing domains will be important to understanding the intercalated crosstalk between cell density and the basement membrane attachments that facilitate epithelial cell fate decisions.

The RGS-RhoGEFs also differentially localize between the cytosolic and nuclear compartments of the cell (Figure 5-3A & 3B). Nuclear fractionation data suggest that ArhGEF1 is found mainly in the cytosol fraction, ArhGEF11 is distributed among the cytosol and nuclear fraction, whereas ArhGEF12 is found mainly in the nuclear fraction. This complicates the notion that RGS-RhoGEFs function only at the plasma membrane, focal adhesions, and at sites of cell-to-cell contacts. The ability of ArhGEF11 and ArhGEF12 to distribute to the nucleus may be important in controlling subpopulations of RhoA that directly impinge on YAP1 nuclear activity. Consistently, RhoA is required for cellular division, and recently actin has been shown to integrate into the RNA Polymerase II complex to facilitate transcription (221). Understanding how ArhGEF11 and ArhGEF12 contribute to RhoA nuclear activity may provide insight into how they regulate cell fate decisions.

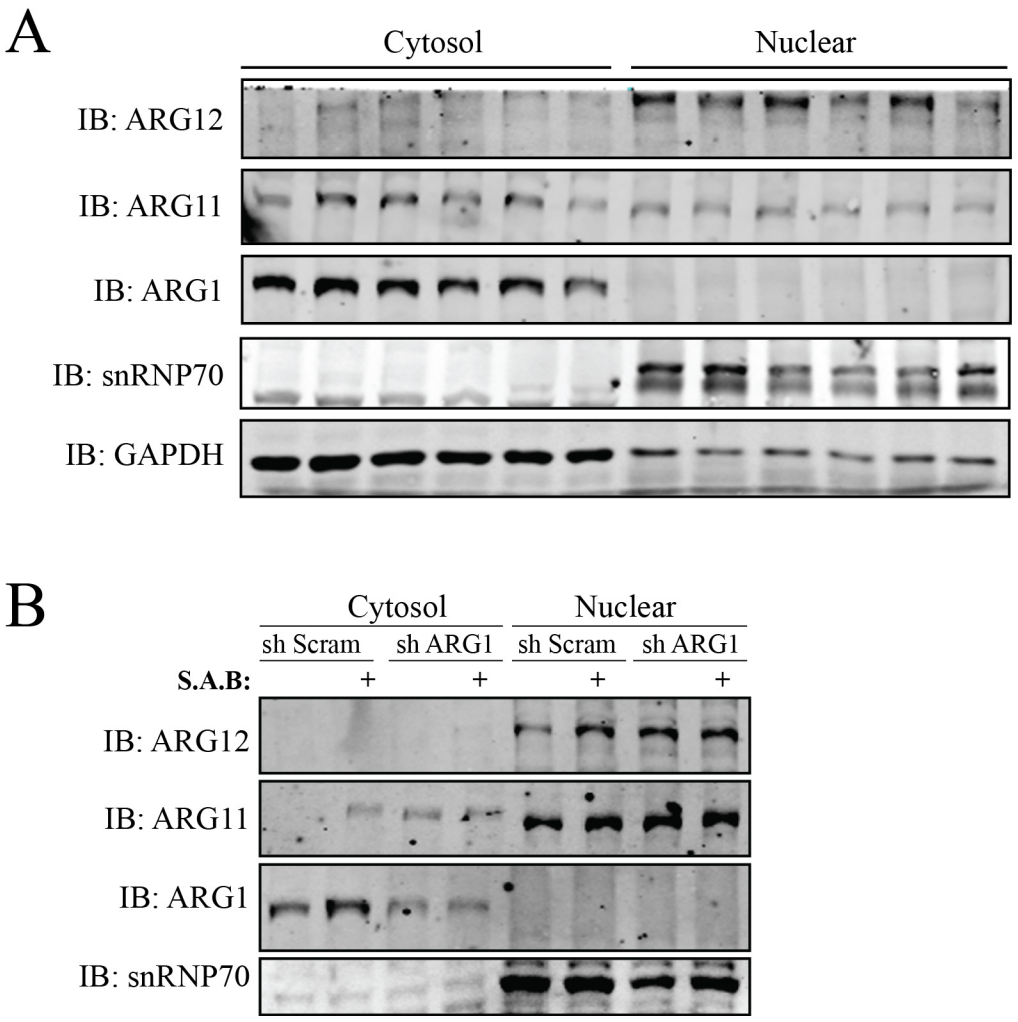


**Figure 5-3: Cytosolic vs. Nuclear Localization of the RGS-RhoGEFs.**

**A.** Immunoblot of endogenous ArhGEF1 (ARG1), ArhGEF11 (ARG11), ArhGEF12 (ARG12), snRNP70, and GAPDH in MCF7 cells. Cells were lysed in Nuclear Fractionation Buffer and fractionated, into nuclear and cytosolic fractions based on method 2.6. **B.** Immunoblot of endogenous ArhGEF1 (ARG1), ArhGEF11 (ARG11), ArhGEF12 (ARG12), and snRNP70 in MCF7 infected with shScramble (shScram) or shArhGEF1 (shARG1) following a 24 hours serum starvation and 30 minute treatment with 10% FBS. Cells were lysed in Nuclear Fractionation Buffer and fractionated, into nuclear and cytosolic fractions based on method 2.6.

5.3.2 Regulation of RGS-RhoGEFs Function by Post-translational Modifications

Post-translational modifications alter functionality, localization and stabilization of many proteins. All three members of the RGS-RhoGEF family can be post-translationally modified by phosphorylation at serine/threonine residues as well as tyrosine residues by a variety of kinases. These events typically lead to the activation of their GEF function independent of $G\alpha_{12/13}$. How these manipulations regulate YAP1 activity is largely unknown, and thus they are an area for further study.

Besides the direct activation of the exchange activity of ArhGEF1 by $G\alpha_{12/13}$, ArhGEF1 is independently activated by tyrosine and serine phosphorylation. In hematopoietic cells the angiostensin II receptor type-I (AT-1) Janus Kinase2 (JAK2) phosphorylates ArhGEF1 at tyrosine 738 to positively regulate its GEF activity (244). Positive regulation of GEF activity also occurs through tyrosine phosphorylation on an unknown residue by proline rich tyrosine kinase2 (Pyk2) following PAR-1 activation (197). It is not known if this increases GEF activity independently of $G\alpha_{12/13}$ activation. Serine phosphorylation at residue 330 promotes the unhinging of the inhibitory linker region from the DH/PH domain, freeing it, and empowering its functionality (197) (Figure 5-4A). These post-translational modifications activate RhoA and therefore it is hypothesized that they would facilitate YAP1 nuclear localization.

While post-translational modifications that activate exchange activity are known, an analysis of the ArhGEF1 sequence finds canonical LATS1/2 phosphorylation sites that are predicted to inhibit GEF activity. Of the three potential canonical LATS1/2 phosphorylation sequence motifs, HxRxxS/T, the ones located at serine 631 and tyrosine 695 in ArhGEF1 (Figure 5-4A) fall within the DH and PH domains,. It is predicted that

phosphorylation of these sites negatively regulate GEF function because they are not present in ArhGEF11 and ArhGEF12, which exclusively transmit activated $G\alpha_{12/13}$ signaling to RhoA. Specifically, the tyrosine residue of ArhGEF1 that is part of the LATS1/2 phosphorylation motif is a nonpolar valine and alanine in ArhGEF11 and ArhGEF12, respectively. Furthermore, this tyrosine phosphorylation site in ArhGEF1 may explain how ArhGEF1 flips its GEF activity under serum starved and serum add back conditions which strongly influences LATS1/2 activity. Previous work from our lab identified that serum deprivation activates LATS1/2 to phosphorylate the adaptor protein Angiomotin to facilitate YAP1 degradation. The negative regulation of ArhGEF1 GEF activity by LATS1/2 may therefore be a complimentary mechanism to inhibit YAP1 activity. The concurrent loss of RhoA activity would effectively eliminate the formation of stress fibers necessary for YAP1 nuclear translocation. Furthermore, activation of LATS1/2 by cell-to-cell contacts explain the differentially effects of ArhGEF1 silencing observed in cells at different densities. If the phosphorylation of ArhGEF1 by LATS1/2 is density dependent, it may also define how the GEF/GAP activity of ArhGEF1 could be fine-tuned to regulate the migratory capacity of individual's cells in a population (Figure 5-4B). This is important because it suggests that in non-pathological conditions, such as wound healing, ArhGEF1 is a key driver of cellular differentiation through its ability to manipulate the actin cytoskeleton. If this is true, ArhGEF1 is a critical rheostat to integrate biochemical signals released by platelets that induce migratory and proliferative events required to close a wound and to turn off those functions upon wound closure, even in the presence of excess biochemical stimuli. LATS1/2 activity is therefore hypothesized to control the impact of RGS-RhoGEFs on YAP1 activity.

While post-translational modifications of ArhGEF11 and ArhGEF12 have been extensively characterized, they encode only one canonical LATS1/2 phosphorylation site. However, focal Adhesion Kinase phosphorylates both ArhGEF11 and ArhGEF12 upon PAR-1 activation on a tyrosine residue in the c-terminus of each protein (224). This phosphorylation enhances GEF activity independently of $G\alpha_{12/13}$. The prevailing thought on why this increases GEF activity is the phosphorylation event promotes the dissociation of inhibitory homo- and hetero-dimers of the RGS-RhoGEFs (245). This suggests the localized activation of ArhGEF11 and ArhGEF12 at focal adhesions could activate RhoA independent of $G\alpha_{12/13}$, to facilitate YAP1-TEAD dependent transcription. Located in the N-terminus of ArhGEF11 is a canonical LATS1/2 phosphorylation site, however it's not located within a known functional domain and thus it is likely to play a role in altering localization. The N-terminal domain is required for recruitment of ArhGEF11 to the plasma membrane upon activation of GPCR through $G\alpha_{12/13}$. Speculation would arise at the idea that phosphorylation at this LATS1/2 canonical site, in a growth inhibitory environment, may interrupt the $G\alpha_{12/13}$-ArhGEF11 interaction and further inhibit its recruitment to the plasma membrane. This would decisively limit the activation of RhoA by $G\alpha_{12/13}$. Understanding how these post-translational modifications contribute to the functionality of the RGS-RhoGEFs and further how those contribute to YAP1 activity may provide key insights into our understanding of actin mediated cell fate decision.

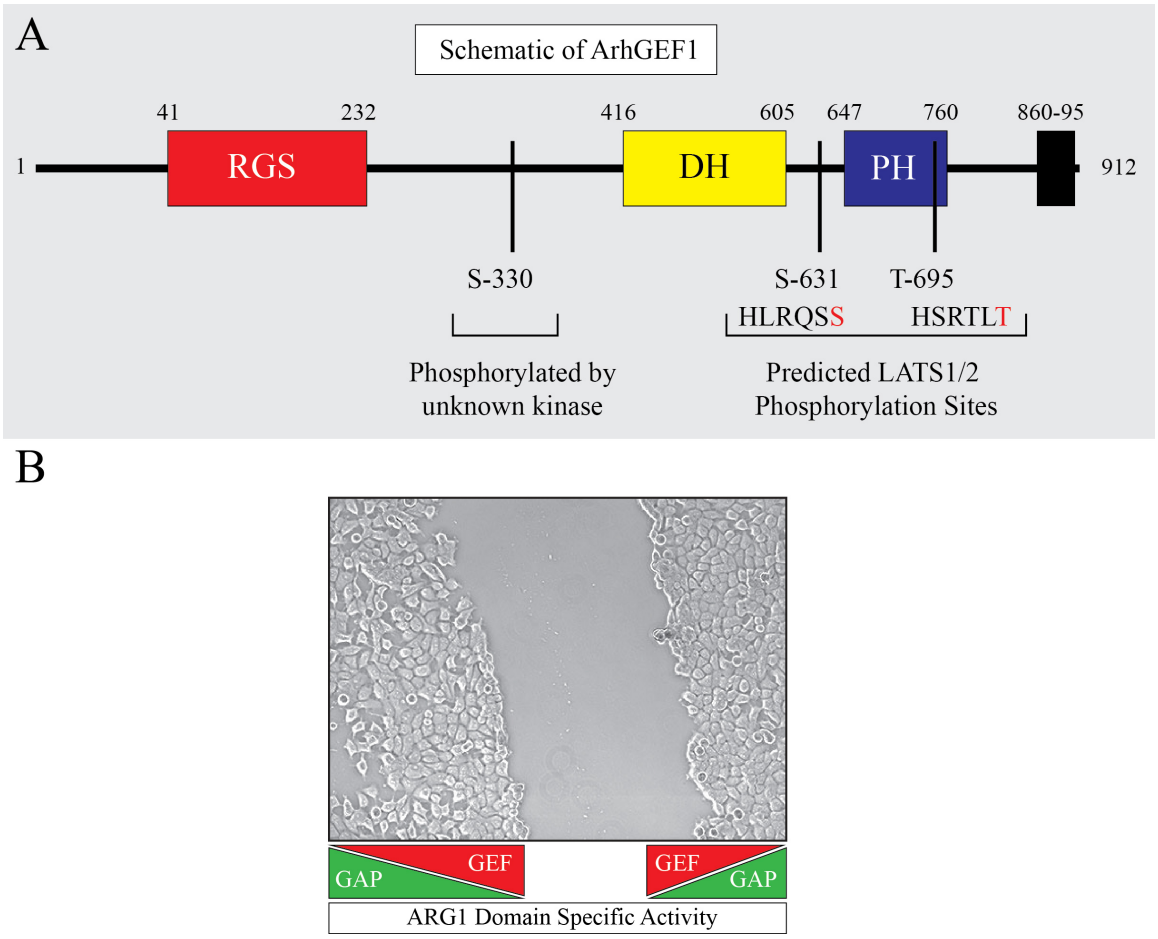


**Figure 5-4: Post-Translational Modifications that Alter ArhGEF1 Functionality in Biochemical and Biophysical Stimuli.**

**A.** Schematic of ArhGEF1 domains as well as sites of known phosphorylation events (S330) and predicted LATS1/2 phosphorylation sites (S631 & T695). **B.** Model of how ArhGEF1 may respond to cell density among a population of cells to alter the activity of its functional domains to mediate cell fate decisions.

### 5.3.3 Nuclear YAP1 Post-Translational Modifications And Cell Fate

YAP1, being a transcriptional co-activator facilitates most of its growth activating potential through the TEAD family of transcription factors. YAP1 has also been shown to promote cell survival by resisting anoikis (201) as well as inducing an apoptotic response through binding the p73 family of transcription factors (246). The data in this dissertation suggest that nuclear YAP1 is required for cell survival and not growth activation in response to chronic serum signaling. Also in this work the loss of ArhGEF1 activates cellular senescence whereas the tandem knockout with YAP1 activates cell death. The mechanisms by which YAP1 oscillates among these opposing roles for mediating cellular fate is still an area under investigation, but recent work implicates post-translational modifications.

In times of stress, YAP1 is preferentially post-translational modified. For instance, when cells are exposed to biochemical energy stress, the activation of AMPK facilitates phosphorylation of serine 94 of YAP1 (247). The phosphorylation of serine 94 disrupts the interaction of YAP1 with its transcriptional co-activator TEAD, preventing oncogenic transformation of LATS1/2 null cells (247). Furthermore when cells are exposed to SN2 alkylating agent, YAP1 is acetylated by the CREB binding protein and p300 (225). This acetylation event is specific to stress induced by alkylating agents, not DNA damage, and can be reversed by SIRT1 deacetylation. In response to DNA damage, YAP1 is sumoylated and stabilized by promyelocytic leukemia (PML), enhancing its association with p73 to induce an apoptotic response (226). Understanding the role post-translational modifications play in directing YAP1 dependent cell fate determination is critical to understanding growth control in cells.

As highlighted previously, biochemical stress can alter nuclear YAP1 post-translational modifications, so it is hypothesized that biophysical stress, such as stress fibers can do the same. Previous studies highlight the necessity of stress fibers to mediate YAP1 nuclear translocation, independent of LATS1/2 regulation. A scenario has been described where YAP1 promotes cell survival in response to the biophysical stress of a cell detaching from its basement membrane. However, there is no evidence to date that suggest how stress fibers influence YAP1 induced cell fate decisions. Here we provide evidence that under high levels of stress fibers, YAP1 functionality is switched to promote survival, as its knockdown is synthetically lethal. Further studies are needed in high stress fiber environments to elucidate exactly how nuclear YAP1 promotes transcriptional programs that favor survival mechanisms rather than growth. It is likely that nuclear YAP1 is further post-transnationally modified. These alterations in post-translational modifications likely dictate YAP1 transcriptional co-activator binding partners, which in turn preferentially activate genetic programs for survival, growth or apoptosis. Identifying how nuclear YAP1 post-translational modifications lead to corresponding cellular fate decisions could be critical to understanding why YAP1 is required for some cancers that have inherent or developed resistance to treatments.

## 5.4 Therapeutic Potential of the Serum Response Network

### 5.4.1 ArhGEF1 and YAP1 Synthetic Lethality

YAP1's ability to mediate cellular survival under stress may be critical for the survival of cancers cells subject to low oxygen, low nutrient, or toxic treatment conditions. In cancer, traditional therapeutics involves invoking a cellular stress on rapidly proliferating cells or blocking key growth activating pathways that then engage cell death pathways. However, some cancers are inherently averse to treatment, or can develop resistance overtime as a result of mutational selection. The development of resistance typically involves the engagement of survival pathways until the cells can re-integrate signaling networks to continue to grow. YAP1 is thought to be key factor in promoting survival-induced resistance, with which many cancers utilize (128, 248).

Recent work has highlighted YAP1's role in promoting resistance to treatments in both pancreatic carcinomas as well as melanoma (128, 248). Roughly 95% pancreatic cancers harbor a mutation that promotes the translation of a constitutive active KRAS (147). This activation leads to the oncogenic addiction of pancreatic tumors to KRAS. The reliance of the tumors on the mutant KRAS signaling for initiation and maintenance is thus the basis of targeted MAPK therapies (248). However, many of these tumors develop resistance upon targeted treatments, and begin to grow in a KRAS-independent manner (248). These KRAS-independent tumors require YAP1 to facilitate growth through the transcription of cFOS or E2F (249), a component of the AP-1 progrowth transcription factor complex. However, knocking down YAP1 in cell lines that no longer depend on KRAS for growth was shown to inhibit their colony formation capacity and proliferation (248). This also holds true in melanoma cell lines that typically harbor an

activating mutant of BRAF. Using Vemurafenib, a RAF inhibitor, or Trametinib, a MEK inhibitor only garners cell from proliferation, it does not engage cell death in the presence of YAP1 (250). In this context, YAP1 activity facilitates the transcription of BCl-xL to prevent apoptosis. It is only when YAP1 is genetically inactivated with simultaneous treatment of MAPK inhibitors that causes BRAF mutant melanoma cell lines to engage cell death pathways (250). These studies suggest the requirement of YAP1 in cell survival and conversely, the need to co-target it in RAF-MEK-ERK driven cancers that utilize YAP1 to program survival genetic programs.

In this study we have also uncovered the dual requirement of YAP1 and the serum response pathway for cell survival. The knockdown of ArhGEF1 surrenders cells in a $G_1/G_0$ phase of the cell cycle. This is thought to occur due to the constitutive activation of $G\alpha_{13}$, which produces a hyper-activated RhoA stress fiber phenotype, leading to prolonged/chronic MAPK signaling. The sensitization to growth signaling is a cellular stress, as the energy and macromolecule demands outweigh the capabilities of the cell, and in a reactionary measure the cell induces senescence. The induction of stress fibers, promotes YAP1 nuclear localization and evidence would suggest this is a survival signal, as ArhGEF1 knockout cells have limited growth capacity in both 2D and 3D. Further evidence that this is a survival signaling is that the tandem knockdown of ArhGEF1 and YAP1 induce a synthetic lethality in breast cancer cells. Therefore co-targeting the serum response pathway along with YAP1/TEAD interaction is potentially another therapeutic angle for tumors that are resistant to current treatments, such as MAPK inhibitors.

Developing compounds that inhibit the functionality of the RGS-RhoGEFs may prove effective in combination with YAP1/TEAD to limit cellular growth. ArhGEF1's

ability to turn off $G\alpha_{12/13}$ signaling and transmit activity to RhoA is based on its recruitment to the plasma membrane by activated $G\alpha_{12/13}$. Therefore disrupting its ability to dominantly GAP, by targeting its known interaction domains with $G\alpha_{13}$, is a potential mechanism to achieve prolonged activation of the serum sensitive heterotrimeric GTPase and induce cellular senescence. Hypothetically, as guided by these discoveries, compounds that target disruption in localization or the functionality of the RGS domain, combined with a molecule that would disrupt YAP1/TEAD interactions would produce a synthetically lethal phenotype. Of potentially more significant interest, targeting the DH/PH domain of ArhGEF12 could be more critical for preventing YAP1 mediated cell survival. ArhGEF12 seems to be dominantly required for YAP1 stability and stress fiber formation. The requirement of stress fibers for YAP1 nuclear translocation has already been well established. Therefore, by inhibiting the ability of ArhGEF12 to activate RhoA, YAP1 would remain cytosolic and negate its ability to activate any genetic program whether it is for survival or growth. Targeting the serum response pathway in tandem with YAP1/TEAD interactions may provide a new avenue for therapeutics, especially in cancers that are inherently resistant or develop resistance to MAPK inhibitors.

Albeit the synthetic lethal effects were witnessed in 2D tissue culture, these hard tensile surfaces are not typical of 3D physiological environments. These environments are rich in an array of nutrients and ECM interactions that may contribute to alternative reactionary mechanisms when targeting the GEFs or YAP1/TEAD interactions. For instance, promoting stress fibers, such as eliminating the GAP activity of ArhGEF1, to initiate cellular stress in 2D, potentially, could backfire under physiological conditions, as these structures are needed for cell motility and migration. These are mechanisms and

structures that are utilized by cancers cells to disseminate throughout the body, and therefore validation in relevant 3D model systems will be critical for evaluating the effectiveness of targeting the RGS-RhoGEFs.

5.4.2 Targeting Triple Negative Breast Cancer Subtypes

Triple negative breast cancers represent 10-20% of all diagnosed breast cancers, and tend to have a higher rate of recurrence that results in increased dissemination throughout the body (151). This phenotype is resistant to anti-estrogen treatments, such as Tamoxifen, and anti-HER2 monoclonal antibodies, like Trastuzumab, as they do not express the receptors to antagonize. This results in poor prognosis with a relative 5 year survival rate of an abysmal 22%, according to the American Cancer Society. Therefore a need for identifying new molecular targets for therapeutic treatment is needed.

Recent work has identified the correlation between elevated ROCK1 and RhoA and poor patient prognosis for women with breast cancer (251-253). Work by the Bissel group further characterized that the inhibition of ROCK using a small molecule inhibitor could revert the metastatic phenotype of the highly invasive MDA-MB-231 cancer cell line in 3D tissue culture environments (254). Not only could ROCK inhibition revert the metastatic phenotype but it could also sensitize aggressive breast to apoptosis with concurrent overexpression of E-cadherin (254). Analysis of aberrant signal transduction pathways found in many breast cancers revealed the inhibition of ROCK suppressed the activation of AKT, MAPK, FAK, and the expression of GLUT3 and LDHA (254). These data suggest that intricate network of cell-cell contacts and cell to ECM contacts, which are mediated by changes in the actin cytoskeleton, are important for cell fate decisions through the regulation of signal transduction cascades.

MCF7 breast cancer cells are estrogen receptor and progesterone receptor positive, suggesting current antagonist for these receptors would be ideal candidates to administer to limit their growth potential. Interestingly, in this study we observed that

when ArhGEF1 is knocked down in relative comparison to control MCF7 cells, the expression of both these receptors, as analyzed by RPPA were statistically decreased (Appendix C). Under these same conditions ROCK1 protein expression as well as a majority of canonical MAPK and AKT proteins had elevated expression. It would be interesting to see if the inhibition of ROCK1 resulted in the down regulation of the MAPK and AKT protein expression, as the Bissel group discovered. This transition from an estrogen receptor and progesterone receptor positive breast cancer cell line to a more triple negative type cell line, as MCF7 are negative for HER2, suggest ArhGEF1 may be a critical component to establishing sensitivity to current treatments. This also suggest that the extreme actin phenotypes, that results in the uncoupling of cell growth from the hyper activation of MAPK and the serum response pathway, is likely important for this transition as well.

A vast array of new treatments for cancer in general are targeting components of the MAPK pathway using RAS, RAF and ERK inhibitors (90). Unfortunately, if these pathways are not utilized to facilitate growth, as we have shown in this study, these treatment strategies for triple negative breast cancers may be futile. This study provides evidence that an affective treatment would be to inhibit YAP1 transcriptional activity in triple negative breast cancers, as the knockout in the more triple negative like MCF7 cells (ArhGEF1 knockdown with a decrease in estrogen and progesterone receptors) would engage cell death pathways. The complications with this strategy are the transcriptional programs driven by YAP1 are not defined in the ArhGEF1 knockout MCF7 cells, which mimics cells in an extreme tensile environment. It is likely that under progrowth situations YAP1 is binding the TEAD family of transcription factors to drive growth,

however the transcription factors and survival genetic programs YAP1 is driving when cells exert a hyper-actin, senescent phenotype are not known much beyond its interaction with p73. Therefore studies need to be conducted to identify the YAP1 interactome of stressed cells and the concurrent transcriptome. Upon this characterization, strategies can be guided to disrupt the relevant and specific YAP1 interactions, preventing the transcriptional activation of these survival programs. Furthermore, ROCK inhibition could potentially revert triple negative cancers back to a positive receptor status, which is suggestive of data in this study and from the Bissel team (254). This could potentially sensitize them to current receptor antagonist treatments. Utilizing this re-sensitization strategy along with defining the YAP1 interactome that is maintaining cell survival could become powerful future treatments in the fight against those breast cancers that have the poorest prognosis.

## 5.5 Conclusion

The entirety of this work contributes to the body of knowledge trying to understand how cells integrate biomechanical and biochemical stimuli to determine cell fate decisions. Central to these decisions, as highlighted here, is the manipulation of the cellular architecture, which has an underappreciated role in regulating transcriptional programs that determine cellular fate. YAP1 is a key transcription factor that is regulated by changes in RhoA dependent actin dynamics as previously shown (142). Here we have identified the relative physiological role for the RGS-RhoGEFs in contributing to $G\alpha_{12/13}$-RhoA actin mediated YAP1 activity. Members of the RGS-RhoGEFs, ArhGEF1, ArhGEF11, and ArhGEF12 function in opposing roles to maintain a delicate cycle of activation of the $G\alpha_{12/13}$-RhoA signaling axis, that can be quickly tuned in response to mitogens and tensile interactions with the microenvironment. ArhGEF1 mainly functions, in a physiological role, as described in this work as, a GAP for $G\alpha_{13}$ whereas ArhGEF11 and ArhGEF12 function to transmit signaling from $G\alpha_{12/13}$ to RhoA. Defining the roles of the individual RGS-RhoGEFs in facilitating signaling through the serum response network to activate YAP1, further provided insight into the functional crosstalk between the Rho and RAS signaling networks. The loss of ArhGEF1, disrupted cellular homeostasis, and contributed to prolonged $G\alpha_{13}$ signaling. We have demonstrated this prolonged activation results in stress fiber aggregation leading to the shutdown of the cell cycle and global translation elongation machinery to enact cellular senescence. Furthermore, this aggregated actin dominantly directed YAP1 into the nucleus, enhancing its transcriptionally activity. However, nuclear YAP1 in this context did not facilitate cellular growth, and mainly functioned to protect cells from engaging cell death during

this oncogene induced senescence. The critical requirement of the RGS-RhoGEFs in temporally regulating the $G\alpha_{12/13}$-RhoA signaling axis, in response to biochemical and biophysical stimuli, provides insight into how cells maintain signaling homeostasis under physiological conditions. This insight into how cellular signaling pathways integrate can further be utilized to understand how cancers re-wire themselves to circumvent these inherent "fail-safe" mechanisms to propagate unmitigated growth.

# APPENDICES

## -APPENDIX A-
## PLASMIDS USED IN YAP1/TEAD SCREEN (ALPHABETICAL LISTING)

| Protein | Human or Mouse | Accession # | V# |
|---|---|---|---|
| ALS2 | Human | BC031479 | V2681 |
| ARAP1 | Human | AB018325 | V2713 |
| ARHGAP 1 | Human | BC018118 | V2661 |
| ARHGAP 11A | Human | D87717 | V2693 |
| Arhgap 17 | Mouse | BC003259 | V2744 |
| ARHGAP 2 | Human | BC011393 | V2649 |
| ARHGAP 20 | Human | AB037845 | V159 |
| ARHGAP 25 | Human | D29642 | V2694 |
| ARHGAP 26 | Human | AB014521 | V2708 |
| ARHGAP 28 | Human | BC033668 | V2687 |
| ARHGAP 31 | Human | AB033030 | V2721 |
| ARHGAP 35 | Human | AB051509 | V2732 |
| ARHGAP 4 | Human | D50921 | V2695 |
| ARHGAP 9 | Human | BC006107 | V2745 |
| Arhgap12 | Mouse | BC024633 | V2667 |
| Arhgap15 | Mouse | BC034881 | V2688 |
| Arhgap18 | Mouse | BC030858 | V2678 |
| Arhgap24 | Mouse | BC027070 | V2672 |
| ArhGAP29 | Mouse | BC040387 | V2691 |
| ARHGAP39 | Human | AB051510 | V2733 |
| Arhgap8 | Mouse | BC010306 | V2647 |
| ARHGEF 1 | Human | BC034013 | V2747 |
| ARHGEF 10 | Human | AB002292 | V2699 |
| ARHGEF 10L | Human | AB046846 | V2731 |
| ARHGEF 11 | Human | AB002378 | V2703 |
| ARHGEF 12 | Human | AB002380 | V2704 |
| ARHGEF 15 | Human | AB020722 | V2716 |
| ARHGEF 16 | Human | BC002681 | V2633 |
| ARHGEF 17 | Human | AB002335 | V2701 |
| ARHGEF 2 | Human | AB014551 | V2709 |
| ARHGEF 25 | Human | BC012860 | V2655 |
| ARHGEF 4 | Human | AB029035 | V2718 |
| ARHGEF 5 | Human | BC010046 | V2645 |
| ARHGEF 6 | Human | D25304 | V2692 |

| | | | |
|---|---|---|---|
| ARHGEF 7 | Human | D63476 | V2696 |
| ARHGEF 9 | Human | AB007884 | V2706 |
| ARHGEF39 | Human | BC033666 | V2686 |
| ARHGEF8 | Human | BC010285 | V2646 |
| DNMBP | Human | AB023227 | V2746 |
| DOCK 4 | Human | AB018259 | V2710 |
| DOCK6 | Human | AB037816 | V2727 |
| DOCK7 | Human | AB051558 | V2734 |
| Ect2 | Mouse | BC025565 | V2668 |
| Fam13b | Mouse | BC031465 | V2680 |
| Farp1 | Mouse | BC030329 | V2676 |
| FARP2 | Human | AB018336 | V2714 |
| FGD1 | Human | BC034530 | V290 |
| FGD2 | Human | BC023645 | V2665 |
| FGD6 | Human | AB037783 | V2725 |
| Fgd6 | Mouse | BC026860 | V2671 |
| HMHA1 | Human | D86976 | V2613 |
| Inpp5B | Mouse | BC028864 | V2674 |
| INTERSECTIN 2 | Human | AB033082 | V2722 |
| NGEF | Human | BC031573 | V2682 |
| P-REX1 | Human | AB037836 | V2728 |
| Plekhg6 | Mouse | BC026778 | V2670 |
| RACGAP1 | Human | BC032754 | V2685 |
| RALBP1 | Human | BC013126 | V2656 |
| SH3BP1 | Human | BC008282 | V2642 |
| SRGAP3 | Human | BC039300 | V2705 |
| Stard13 | Mouse | BC027830 | V2673 |
| STARD8 | Human | D80011 | V2697 |
| SYDE1 | Human | BC029926 | V2675 |
| TAGAP | Human | BC015859 | V2659 |
| VAV1 | Human | BC013361 | V2657 |

**-APPENDIX B-**
**Nucleotide Sequences for Primers**

## Primers for Cloning CTGF Promoter

| Promoter | Mutations | Sense | Antisense | gBlock |
|---|---|---|---|---|
| Short | WT | X | X | |
| Short | TEAD Mut | X | X | 3x TEAD gblock |
| Short | TEAD/SRF Mut | CCTACCCAGGATGTATGTCAGTGGACAGAACAGGGCAAACTTATT | CATCCTGGGTAGGAAGTAGGTAGCTGAAAGAGGCAAACAGCAG | 3x TEAD gblock |
| Short | SRF Mutant | CCTACCCAGGATGTATGTCAGTGGACAGAACAGGGCAAACTTATT | CATCCTGGGTAGGAAGTAGGTAGCTGAAAGAGGCAAACAGCAG | |
| Long | WT | | | |
| Long | 1st SRF Mut | | | |
| Long | 1st & 2nd SRF Mut | CATACCTGGGATAGCTTGGTAAACAGGACTCAGTGGCCAGC | GCTATCCCAGGTATGTGTGTGTGTCTACTAGGGCATCATTTGTACTGG | |
| Long | 1, 2, and 3 SRF Mutant | CCTACCCAGGATGTATGTCAGTGGACAGAACAGGGCAAACTTATT | CATCCTGGGTAGGAAGTAGGTAGCTGAAAGAGGCAAACAGCAG | |
| Long | 1, 2, and 3 SRF and TEAD Mutant | GAGGGCGGCGAGGGCGGTCCCTGTTTGTGTAGGAC | GGGACCGCCTCGCCGCCCTCC | 3x TEAD gblock |
| Long | WT TEAD Mutants | GAGGGCGGCGAGGGCGGTCCCTGTTTGTGTAGGAC | GGGACCGCCTCGCCGCCCTCC | 3x TEAD gBlock |

## qRTPCR Primers

CTGF Sense: AGGAGTGGGTGTGTGACGA (142)
CTGF Antisense: CCAGGCAGTTGGCTCTAATC (142)

Cyr61 Sense: AAGGAGCTGGGATTCGATG
Cyr61 Antisense: TCTGGCCTTGTAAAGGGTTG

Cyclin D1 Sense: GCCTGTGATGCTGGGCACTTCATC
Cyclin D1 Antisense: TTTGGTTCGGCAGCTTGCTAGGTG

cMyc Sense: CTTCTCTCCGTCCTCGGATTCT
cMyc Antisense: GAAGGTGATCCAGACTCTGACCTT

FOS Sense: CACTCCAAGCGGAGACAGAC
FOS Antisense: AGGTCATCAGGGATCTTGCAG

cFOS Sense: CTGGCGTTGTGAAGACCAT
cFOS Antisense: TCCCTTCGGATTCTCCTTTT

cJUN Sense: ATCAAGGCGGAGAGGAAGCG
cJUN Antisense: TGAGCATGTTGGCCGTGGAC

GAPDH Sense: CTCCTGCACCACCAACTGCT (142)
GAPDH Antisense: GGGCCATCCACAGTCTTCTG (142)

**shRNA Sequences**

**ARHGEF1 shRNA:**

Sequence #1:
CCGGCCATCTCTACCGACGAAGAAACTCGAGTTTCTTCGTCGGTAGAGATGG
TTTTTG
in pLKO.1 (Sigma, TRCN0000033566)

Sequence #2:
CCGGTCCCTGAAGCAGCTTCTGTTTCTCGAGAAACAGAAGCTGCTTCAGGGA
TTTTTG
in pLKO.1 (Sigma, TRCN0000033568)

**ARHGEF11 shRNA:**
CCGGCCTGATCTTCTACCAGCGAATCTCGAGATTCGCTGGTAGAAGATCAGG
TTTTTG
in pLKO.1 (Sigma, TRCN0000047465)

**ARHGEF12 shRNA:**

Sequence #1:
CCGGGCGAGTATCCAGAGAAGGAATCTCGAGATTCCTTCTCTGGATACTCGC
TTTTTG in pLKO.1 (Sigma, TRCN0000298941)

Sequence #2:
CCGGGCGTTGCGTAATCATCCAGAACTCGAGTTCTGGATGATTACGCAACGC
TTTTTG

in pLKO.1 (Sigma, TRCN0000298942)

**YAP1 shRNA:**

Sequence #1:
CCGGCAGGTCATACTATCAACCAAATCGAGTTTGGTTGATAGTATCACCTGTT
TTTG
in pLKO.1 (Sigma, TRCN0000107267)

**Scramble shRNA**: shControl pLKO.1 plasmid #1864 (Addgene)

**-APPENDIX C-**
**COMPLETE RESULTS OF RPPA COMPARING CONTROL TO ARHGEF1 KNOCKDOWN MCF7 CELLS UNDER SERUM ADD BACK CONDITIONS**
(Red=Negative Relative Change, Green=Positive Relative Change, Yellow=statistical significance p<.05)

| Antibody Name | Gene Name | Probabilities (QC Score) | Change (shARG1-shScramble) | TTEST |
|---|---|---|---|---|
| eEF2K | EEF2K | 0.924519781 | -0.782621396 | 3.35703E-06 |
| EMA | EMA | 0.914941009 | -1.105142864 | 1.59682E-05 |
| ER | ESR1 | 0.929650338 | -0.846927639 | 2.67886E-05 |
| AR | AR | 0.921837285 | -0.241715676 | 7.7882E-05 |
| Notch1 | NOTCH1 | 0.929029422 | -0.313420198 | 0.000130004 |
| MSH6 | MSH6 | 0.906915983 | -0.338250909 | 0.000176417 |
| INPP4b | INPP4B | 0.934027466 | 0.250212379 | 0.000186785 |
| c-Myc | MYC | 0.915134137 | -0.174266509 | 0.000211574 |
| GATA3 | GATA3 | 0.919524235 | -0.445368492 | 0.000217064 |
| PAR | PAR | 0.93363016 | 0.914029681 | 0.000244503 |
| Src_pY527 | SRC | 0.952998946 | 0.276528602 | 0.000250872 |
| C-Raf_pS338 | RAF1 | 0.946611448 | 0.214033161 | 0.000410915 |
| PEA-15 | PEA15 | 0.955663775 | 0.172199353 | 0.000460139 |
| c-Met | MET | 0.89813279 | -0.13751199 | 0.00047324 |
| YB1_pS102 | YBX1 | 0.960910762 | 0.18401262 | 0.00070258 |
| Bcl-xL | BCL2L1 | 0.958356756 | 0.120570735 | 0.000712437 |
| Bcl2 | BCL2 | 0.808674126 | -0.538587251 | 0.000745317 |
| IGFRb | IGF1R | 0.935735234 | -0.270319874 | 0.000839395 |
| Hexokinase-II | HK2 | 0.891190246 | 0.168319917 | 0.000895323 |
| p90RSK_pT573 | RPS6K | 0.949836221 | 0.243232403 | 0.000906354 |
| Gys_pS641 | GYS1 | 0.924796756 | -0.372546612 | 0.001056583 |
| Connexin-43 | CNST43 | 0.859682344 | 0.455075848 | 0.001148287 |
| eIF4E | EIF4E | 0.961295801 | 0.27433424 | 0.001196745 |
| AMPKa | PRKAA1 | 0.959336434 | 0.181942408 | 0.00150417 |
| Gab2 | GAB2 | 0.950630467 | 0.269791066 | 0.001566279 |
| Sox2 | SOX2 | 0.913202868 | -0.663688552 | 0.001608348 |
| Cyclin-E1 | CCNE1 | 0.871957271 | -0.140108497 | 0.001613403 |
| Myt1 | MYT1 | 0.857764605 | -0.289923126 | 0.001956314 |
| MEK1 | MAP2K1 | 0.886200842 | 0.199482807 | 0.00203358 |
| HSP27_pS82 | HSBP1 | 0.899115019 | 0.365067834 | 0.002301855 |

| | | | | |
|---|---|---|---|---|
| XRCC1 | XRCC1 | 0.857350386 | -0.169676472 | 0.00257914 |
| Caspase-7-cleaved | CASP7 | 0.937727913 | 0.317513856 | 0.002628117 |
| N-Ras | NRAS | 0.863343194 | 0.233849693 | 0.002695515 |
| c-Jun_pS73 | JUN | 0.932273615 | 0.237057804 | 0.002892938 |
| TWIST | TWIST1 | 0.902995015 | -0.141273591 | 0.002958416 |
| eEF2 | EEF2 | 0.948364345 | -0.562100593 | 0.003148213 |
| Glutamate-D1-2 | GLUD | 0.89358631 | 0.094160607 | 0.003148498 |
| Pdcd4 | PDCD4 | 0.96278045 | -0.341885465 | 0.003275396 |
| p70-S6K1 | RPS6KB1 | 0.895390777 | -0.441223929 | 0.003612783 |
| Bcl2A1 | BCL2A1 | 0.921555341 | 0.20540552 | 0.003926516 |
| Akt_pT308 | AKT1 | 0.948259669 | 0.398833285 | 0.004084158 |
| GAPDH | GAPDH | 0.900778605 | -0.501460948 | 0.004126068 |
| Histone-H3 | HIST3H3 | 0.926741302 | 0.207552795 | 0.004329081 |
| Granzyme-B | GZMB | 0.901817951 | -0.279645869 | 0.004418429 |
| VHL-EPPK1 | EPPK1 | 0.832274939 | -0.313052939 | 0.004445258 |
| Rock-1 | ROCK1 | 0.918664058 | 0.188136496 | 0.004732761 |
| Shc_pY317 | SHC1 | 0.936181355 | -0.196832646 | 0.005708169 |
| PI3K-p85 | PIK3R1 | 0.962347653 | 0.127388943 | 0.006148226 |
| UGT1A | UGT1A | 0.876595017 | -0.1530747 | 0.006288289 |
| TFAM | TFAM | 0.948567989 | -0.277189577 | 0.006302088 |
| PREX1 | PREX1 | 0.92958986 | 0.503393676 | 0.00655734 |
| IR-b | INSRB | 0.943488106 | 0.278906242 | 0.006796991 |
| NDUFB4 | NDUFB4 | 0.858149039 | -0.232000177 | 0.006946234 |
| Merlin | NF2 | 0.945224176 | -0.261442211 | 0.007033182 |
| Rb | RB1 | 0.883650129 | -0.101731273 | 0.007074228 |
| NF-kB-p65_pS536 | NFKB1 | 0.939374736 | 0.187314413 | 0.00744387 |
| p38_pT180_Y182 | MAPK14 | 0.890124822 | 0.172153206 | 0.007494262 |
| WIPI2 | WIPI2 | 0.918360838 | -0.096231581 | 0.007630346 |
| VEGFR-2 | KDR | 0.950805083 | 0.333532908 | 0.007778599 |
| SHP-2_pY542 | PTPN11 | 0.923015974 | 0.337762112 | 0.008014248 |
| Bad_pS112 | BAD | 0.940912945 | 0.100642852 | 0.00828807 |
| PAK1 | PAK1 | 0.932634371 | 0.271228572 | 0.00832206 |
| Akt_pS473 | AKT1 | 0.953916425 | 0.310225272 | 0.009247238 |
| Rheb | RHEB | 0.88538088 | -0.291261079 | 0.009294377 |
| XBP-1 | XBP1 | 0.843554622 | -0.254647345 | 0.009308097 |

| | | | | |
|---|---|---|---|---|
| ERCC1 | ERCC1 | 0.916758163 | -0.207225395 | 0.009481168 |
| Vimentin | VIM | 0.834682978 | -0.348780319 | 0.009854836 |
| SOD1 | SOD1 | 0.898228044 | 0.102803733 | 0.010104901 |
| Bim | BCL2L11 | 0.947598357 | -0.180317834 | 0.010138904 |
| SF2 | SRSF1 | 0.866495597 | -0.149575816 | 0.010476214 |
| PLK1 | PLK1 | 0.954160701 | -0.274038184 | 0.010720303 |
| RSK | RPS6KA1 | 0.958876303 | -0.047131196 | 0.011508911 |
| Src | SRC | 0.917964385 | 0.192983015 | 0.011851271 |
| JNK_pT183_Y185 | MAPK8 | 0.942058938 | 0.253104874 | 0.011978805 |
| 4E-BP1 | EIF4EBP1 | 0.952266644 | 0.125927025 | 0.012848913 |
| Notch3 | NOTCH3 | 0.934675677 | 0.246661931 | 0.013233998 |
| HER3_pY1289 | ERBB3 | 0.949816823 | 0.064189238 | 0.013278873 |
| PR | PGR | 0.946083442 | -0.15580807 | 0.014303927 |
| FoxM1 | FOXM1 | 0.952676375 | -0.150507069 | 0.014334351 |
| YAP | YAP1 | 0.914399036 | 0.16538202 | 0.015051339 |
| Glutaminase | GLS | 0.8498355 | 0.183686896 | 0.015534934 |
| Cyclin-B1 | CCNB1 | 0.951700371 | 0.099013621 | 0.015633424 |
| Rab25 | RAB25 | 0.939933499 | -0.136221419 | 0.016299154 |
| RPA32 | RPA2 | 0.856768809 | -0.233789701 | 0.016548547 |
| DUSP4 | DUSP4 | 0.944212494 | 0.214034523 | 0.016727482 |
| Myosin-IIa_pS1943 | MYO2A | 0.952525218 | -0.880903283 | 0.016893503 |
| Paxillin | PXN | 0.927748675 | 0.148363234 | 0.017594558 |
| GSK-3a-b | GSK3A/GSK3B | 0.906663031 | -0.295144992 | 0.017907573 |
| eIF4E_pS209 | EIF4E | 0.868939199 | 0.125220692 | 0.018604887 |
| CDK1 | CDK1 | 0.951631851 | -0.322012811 | 0.018818812 |
| SDHA | SDHA | 0.892025112 | -0.160590202 | 0.019598368 |
| PCNA | PCNA | 0.842402773 | -0.343000615 | 0.019704058 |
| Smad3 | SMAD3 | 0.94453799 | -0.168654923 | 0.02077896 |
| cdc25C | CDC25C | 0.919016188 | -0.195843504 | 0.020988399 |
| Tyro3 | TYRO3 | 0.941358517 | -0.137863265 | 0.022191518 |
| UBAC1 | UBAC1 | 0.94114427 | 0.237706027 | 0.02318527 |
| eIF4G | EIF4G1 | 0.952669274 | -0.353566321 | 0.023289049 |
| MAPK_pT202_Y204 | MAPK3 | 0.928607995 | 0.184030645 | 0.025817529 |
| MIF | MIF | 0.82208949 | -0.232734761 | 0.027198972 |

| | | | | |
|---|---|---|---|---|
| NDRG1_pT346 | NDRG1 | 0.951074961 | 0.289844423 | 0.027366161 |
| DJ1 | PARK7 | 0.950115095 | 0.161094411 | 0.028159697 |
| YAP_pS127 | YAP1 | 0.946591374 | 0.15888396 | 0.029974363 |
| Creb | CREB1 | 0.875291335 | 0.083641547 | 0.029997469 |
| XPF | XPF | 0.933202227 | -0.115256815 | 0.030394708 |
| Jagged1 | JAG1 | 0.831790996 | 0.081704815 | 0.031816515 |
| Mnk1 | MKNK1 | 0.887836465 | -0.200027256 | 0.032050539 |
| Rad50 | RAD50 | 0.907297712 | -0.214392988 | 0.032518741 |
| CD171 | L1CAM | 0.932042728 | -0.195789821 | 0.032804193 |
| NAPSIN-A | NAPSA | 0.936579493 | 0.134452801 | 0.03335449 |
| TTF1 | TTF1 | 0.813439498 | -0.246792511 | 0.03639674 |
| ER-a_pS118 | ESR1 | 0.912913145 | -0.188051014 | 0.037890997 |
| Cdc2_pY15 | CDK1 | 0.849876978 | -0.088677843 | 0.037937422 |
| MIG6 | ERRFI1 | 0.91816802 | -0.17862004 | 0.04235988 |
| Bax | BAX | 0.942631041 | -0.184153319 | 0.042765705 |
| p27_pT198 | CDKN1B | 0.932786303 | 0.10023564 | 0.04309231 |
| ATR_pS428 | ATR | 0.929656614 | -0.063068585 | 0.043295185 |
| B-Raf_pS445 | BRAF | 0.954040186 | 0.107698233 | 0.043459997 |
| EGFR | EGFR | 0.919463542 | -0.263588572 | 0.044431986 |
| Axl | AXL | 0.947576346 | -0.230220886 | 0.044444839 |
| IGFBP2 | IGFBP2 | 0.92540376 | -0.16506233 | 0.048505241 |
| ENY2 | ENY2 | 0.901109421 | -0.231765819 | 0.048929918 |
| AMPKa_pT172 | PRKAA1 | 0.952965502 | 0.184527599 | 0.049349929 |
| TSC1 | TSC1 | 0.963610314 | 0.20330725 | 0.049815456 |
| Aurora-B | AIM1 | 0.866944489 | -0.105147554 | 0.052259317 |
| WIPI1 | WIPI1 | 0.91578778 | 0.166329917 | 0.052327523 |
| DM-K9-Histone-H3 | H3K9ME2 | 0.882757271 | 0.07355292 | 0.052963546 |
| PDGFR-b | PDGFR | 0.94195543 | -0.171377826 | 0.055992339 |
| 14-3-3-epsilon | YWHAE | 0.86868706 | -0.084709291 | 0.059041118 |
| 14-3-3-beta | YWHAB | 0.920483668 | -0.150620842 | 0.059993357 |
| SCD | SCD | 0.878472238 | -0.262215931 | 0.060430983 |
| PKM2 | PKM2 | 0.904517888 | 0.152802392 | 0.060432321 |
| Stat5a | STAT5A | 0.956448437 | -0.137054617 | 0.060884504 |
| PI3K-p110-b | PIK3BC | 0.905149746 | -0.080582595 | 0.062736036 |
| ADAR1 | ADAR | 0.937891587 | 0.164095685 | 0.06274368 |
| 53BP1 | TP53BP1 | 0.959850837 | 0.202305759 | 0.063120814 |

| | | | | |
|---|---|---|---|---|
| P-Cadherin | CDH3 | 0.92082188 | -0.203364647 | 0.066290214 |
| IRS1 | IRS1 | 0.951272039 | -0.154304637 | 0.066607342 |
| Beclin | BECN1 | 0.85952359 | -0.102981655 | 0.066936511 |
| CD31 | PECAM1 | 0.818729862 | 0.114517446 | 0.067672546 |
| HER2 | ERBB2 | 0.899754615 | -0.113233302 | 0.068517136 |
| RBM15 | RBM15 | 0.96366825 | 0.117453852 | 0.069223194 |
| Rictor_pT1135 | RICTOR | 0.959884739 | 0.152722955 | 0.072408382 |
| Ets-1 | ETS1 | 0.800760225 | -0.240927924 | 0.076692461 |
| N-Cadherin | CDH2 | 0.890046222 | 0.071761586 | 0.077595229 |
| PARP1 | PARP1 | 0.92900004 | 0.197575271 | 0.078465625 |
| PAK4 | PAK4 | 0.911743213 | 0.091602625 | 0.079049907 |
| H2AX_pS140 | H2AFX | 0.88516782 | 0.181127134 | 0.079255777 |
| Chk1 | CHEK1 | 0.895271108 | -0.11542644 | 0.079517173 |
| G6PD | G6PD | 0.855824293 | -0.232303075 | 0.081226646 |
| C-Raf | RAF1 | 0.944673349 | 0.12802346 | 0.08513827 |
| c-Met_pY1234_Y1235 | MET | 0.910119508 | -0.097540817 | 0.086051782 |
| GSK-3a-b_pS21_S9 | GSK3A GSK3B | 0.962506153 | -0.159349906 | 0.088483228 |
| TAZ | TAZ | 0.940228008 | -0.081285639 | 0.089788131 |
| LDHA | LDHA | 0.860015649 | -0.15594994 | 0.091662805 |
| PI3K-p110-a | PIK3C2A | 0.936300542 | 0.085212101 | 0.092662683 |
| VASP | VASP | 0.894157385 | 0.135495612 | 0.093129859 |
| Wee1 | WEE1 | 0.902240853 | -0.108097973 | 0.093925575 |
| PDK1_pS241 | PDK1 | 0.964036888 | -0.079178356 | 0.095295107 |
| JNK2 | MAPK9 | 0.861215193 | -0.251178667 | 0.101728265 |
| ULK1_pS757 | ULK1 | 0.940440661 | 0.131226996 | 0.10544179 |
| Rictor | RICTOR | 0.96480466 | 0.167691517 | 0.105989431 |
| SOD2 | SOD2 | 0.826950876 | 0.055441929 | 0.105999049 |
| Bak | BAK1 | 0.915375136 | 0.079488036 | 0.110441497 |
| S6 | RPS6 | 0.878278211 | 0.26111214 | 0.110520108 |
| PDK1 | PDK1 | 0.941446581 | -0.061994401 | 0.116199395 |
| IRF-1 | IRF1 | 0.9193 | -0.166715084 | 0.116334889 |
| Wee1_pS642 | WEE1 | 0.925881034 | 0.077561702 | 0.116585043 |
| FRA-1 | FOSL1 | 0.928100641 | -0.14678341 | 0.117982713 |
| SLC1A5 | SLC1A5 | 0.948444961 | 0.083905567 | 0.119681717 |
| Cox2 | CMC2 | 0.926941734 | 0.14674027 | 0.122245869 |

| | | | | |
|---|---|---|---|---|
| TFRC | TFRC | 0.956537825 | 0.059570894 | 0.125733258 |
| Chk2 | CHEK2 | 0.890084389 | -0.168637941 | 0.126140028 |
| PKC-b-II_pS660 | PRKCB | 0.962128936 | 0.140796089 | 0.128146909 |
| CD44 | CD44 | 0.869158542 | 0.090777669 | 0.128663756 |
| p70-S6K_pT389 | RPS6KB1 | 0.904492601 | 0.16421419 | 0.134782616 |
| Annexin-VII | ANXA7 | 0.845780423 | -0.173776928 | 0.135151085 |
| Raptor | RPTOR | 0.96285984 | -0.131030454 | 0.136520874 |
| HER3 | ERBB3 | 0.948379117 | -0.138336148 | 0.139704432 |
| LRP6_pS1490 | LRP6 | 0.878015944 | -0.071822475 | 0.141472281 |
| CD49b | ITGA2 | 0.892866427 | -0.08534928 | 0.142610639 |
| TRIM25 | TRIM25 | 0.948126764 | -0.191413818 | 0.143395563 |
| CD29 | CD29 | 0.84550005 | -0.133250143 | 0.146261011 |
| FoxO3a_pS318_S321 | FOXO3 | 0.941110072 | 0.055713016 | 0.149162356 |
| E2F1 | E2F1 | 0.876652917 | -0.035569727 | 0.159680906 |
| RIP | RIP | 0.895510946 | -0.095582261 | 0.161875739 |
| ATRX | ATRX | 0.879463378 | 0.132874702 | 0.16280821 |
| HSP70 | HSPA1A | 0.936139482 | -0.068204694 | 0.164155807 |
| Syk | SYK | 0.923145899 | 0.091520742 | 0.169209623 |
| Jak2 | JAK2 | 0.927379868 | 0.121786811 | 0.183152809 |
| Chk2_pT68 | CHEK2 | 0.912454656 | 0.06564456 | 0.183172056 |
| Stat3_pY705 | STAT3 | 0.947819279 | 0.073086942 | 0.183286675 |
| TUFM | TUFM | 0.867157233 | -0.113544183 | 0.190918747 |
| Atg7 | ATG7 | 0.92429845 | 0.069468196 | 0.19954523 |
| Src_pY416 | SRC | 0.927365842 | 0.084248858 | 0.20227887 |
| Cox-IV | PTGS3 | 0.891645109 | -0.075649151 | 0.202693438 |
| Chk1_pS296 | CHEK1 | 0.901064164 | 0.053996826 | 0.203612968 |
| p21 | CDKN1A | 0.922240971 | 0.070909188 | 0.203793333 |
| Ubq-Histone-H2B | H2BFM | 0.869110765 | -0.165300796 | 0.217115153 |
| Tuberin_pT1462 | TSC2 | 0.941491547 | 0.034403663 | 0.22001039 |
| DM-Histone-H3 | HISTH3 | 0.907659435 | 0.071109227 | 0.220139584 |
| AMPK-a2_pS345 | PRKAA2 | 0.883373786 | 0.03606149 | 0.221502406 |
| PEA-15_pS116 | PEA15 | 0.862043142 | 0.070836236 | 0.231739731 |

| | | | | |
|---|---|---|---|---|
| RPA32_pS4_S8 | RPA2 | 0.93219595 | 0.15379532 | 0.238452935 |
| PDHK1 | PDHK1 | 0.896612896 | 0.037463225 | 0.242201332 |
| PAX8 | PAX8 | 0.93775019 | -0.078990506 | 0.24683624 |
| 4E-BP1_pS65 | EIF4EBP1 | 0.955001119 | 0.050815246 | 0.254687284 |
| HSP27 | HSBP1 | 0.865317061 | -0.083318041 | 0.256383724 |
| MDM2_pS166 | MDM2 | 0.962828399 | -0.081818993 | 0.279129147 |
| B7-H4 | VTCN1 | 0.879510237 | 0.047922452 | 0.283262844 |
| Fibronectin | FN1 | 0.90112857 | 0.081143207 | 0.296132628 |
| Gys | GYS1 | 0.930619549 | -0.090914535 | 0.306914165 |
| PRAS40 | AKT1S1 | 0.890769068 | -0.085718459 | 0.30748265 |
| LC3A-B | LC3AB | 0.866665392 | 0.092702538 | 0.32385153 |
| Collagen-VI | COL6A1 | 0.903121728 | 0.067763918 | 0.324036703 |
| PAICS | PAICS | 0.949686294 | 0.056134794 | 0.324076048 |
| ACC1 | ACACA | 0.96067722 | -0.07038547 | 0.330557222 |
| TIGAR | TIGAR | 0.940998046 | -0.061000471 | 0.331138269 |
| b-Catenin_pT41_S45 | CTNNB1 | 0.921505538 | -0.063245475 | 0.345073385 |
| HES1 | HES1 | 0.948686722 | -0.03557233 | 0.346115152 |
| MSI2 | MSI2 | 0.878007368 | 0.031268456 | 0.346858054 |
| Heregulin | NRG1 | 0.935422005 | 0.047776099 | 0.350299196 |
| Smad4 | SMAD4 | 0.877720431 | -0.050294471 | 0.355127746 |
| Myosin-11 | MYH11 | 0.929613212 | -0.063824105 | 0.359468708 |
| Pdcd-1L1 | PDCD1 | 0.838939896 | 0.055163274 | 0.362122961 |
| Rab11 | RAB11A | 0.911237331 | -0.043199324 | 0.373065664 |
| Snail | SNAI2 | 0.88186091 | 0.050881088 | 0.375925091 |
| b-Catenin | CTNNB1 | 0.945816291 | 0.044272554 | 0.387149585 |
| IGF1R_pY1135_Y1136 | IGF1R | 0.940709673 | 0.078640903 | 0.39548314 |
| b-Actin | ACTB | 0.826466747 | -0.043202374 | 0.398360203 |
| mTOR | MTOR | 0.964167593 | -0.031872844 | 0.400274648 |
| HER2_pY1248 | ERBB2 | 0.940032967 | 0.074404441 | 0.401927975 |
| FASN | FASN | 0.954931529 | 0.097855572 | 0.405552788 |
| c-IAP2 | BIRC3 | 0.895640062 | -0.046504338 | 0.406474581 |
| GCLM | GCLM | 0.860156054 | -0.025531823 | 0.417873877 |
| PTEN | PTEN | 0.950865773 | -0.033696168 | 0.418400134 |

| | | | | |
|---|---|---|---|---|
| PMS2 | PMS2 | 0.895510682 | -0.045718438 | 0.422351463 |
| Rb_pS807_S811 | RB1 | 0.961853551 | -0.048798626 | 0.447247241 |
| Rad51 | RAD51 | 0.907398227 | -0.026953154 | 0.451311288 |
| 14-3-3-zeta | YWHAZ | 0.932699104 | -0.046460678 | 0.455905364 |
| ZAP-70 | ZAP70 | 0.898087037 | -0.032301943 | 0.476534123 |
| PKC-delta_pS664 | PRKCD | 0.89969306 | -0.039953166 | 0.477919093 |
| ACC_pS79 | ACACA | 0.956825154 | 0.060103487 | 0.483903042 |
| Bid | BID | 0.914385664 | 0.027587174 | 0.491554516 |
| FAK_pY397 | PTK2 | 0.924612769 | 0.037384011 | 0.492452207 |
| Stathmin-1 | STMN1 | 0.933044668 | 0.012666531 | 0.495780976 |
| Stat3 | STAT3 | 0.957852539 | 0.052929938 | 0.496723404 |
| p38-MAPK | MAPK14 | 0.962348377 | 0.057750032 | 0.497022718 |
| p16INK4a | CDKN2A | 0.897591442 | 0.063810701 | 0.505003302 |
| ARID1A | ARID1A | 0.965111926 | -0.053831361 | 0.505985899 |
| Smad1 | SMAD1 | 0.912781418 | 0.041021259 | 0.512729061 |
| Akt | AKT1 | 0.906913806 | 0.050207676 | 0.51467867 |
| c-Abl | ABL1 | 0.895417672 | 0.040017239 | 0.523156713 |
| GCN5L2 | KAT2A | 0.937620567 | -0.059756601 | 0.533352324 |
| ATM | ATM | 0.958305597 | 0.024491231 | 0.537314206 |
| BiP-GRP78 | HSPA5 | 0.825035489 | 0.042065791 | 0.546420097 |
| Caspase-3 | CASP3 | 0.929047996 | -0.036698153 | 0.547138959 |
| Oct-4 | OCT4 | 0.906201348 | 0.027768839 | 0.551222257 |
| MCT4 | SLC16A4 | 0.930072269 | -0.150716267 | 0.563820403 |
| S6_pS240_S244 | RPS6 | 0.955767997 | -0.102079387 | 0.567999411 |
| COG3 | COG3 | 0.956201463 | -0.036456211 | 0.575623369 |
| PLC-gamma2_pY759 | PLCG2 | 0.893114005 | -0.028117768 | 0.578116216 |
| p27-Kip-1 | CDKN1B | 0.876353548 | -0.048682106 | 0.580042357 |
| Cyclin-D3 | CCND3 | 0.893231558 | 0.034238183 | 0.591909174 |
| PKA-a | PRKAR1A | 0.964364548 | 0.05082469 | 0.603484526 |
| CD26 | DPP4 | 0.921168287 | 0.013316176 | 0.605314033 |
| FAK | PTK2 | 0.895871854 | -0.026334968 | 0.614446626 |
| PKCa | PRKCA | 0.959382438 | 0.02780146 | 0.62495743 |
| EGFR_pY1173 | EGFR | 0.946716206 | -0.011448577 | 0.626387624 |
| MEK1_pS217_S221 | MAP2K1 | 0.926137202 | 0.034950157 | 0.62699941 |

| | | | | |
|---|---|---|---|---|
| Caveolin-1 | CAV1 | 0.945889174 | -0.084582541 | 0.636178994 |
| BAP1 | BAP1 | 0.90552614 | -0.054427727 | 0.649145325 |
| A-Raf | ARAF | 0.957599003 | 0.057640456 | 0.652539135 |
| Atg3 | ATG3 | 0.940925825 | -0.017440376 | 0.659174592 |
| c-Kit | KIT | 0.915589662 | -0.023933221 | 0.674046647 |
| Smac | DIABLO | 0.932136808 | 0.02024953 | 0.681584421 |
| D-a-Tubulin | TUBA1A | 0.908841788 | -0.025107787 | 0.684235821 |
| ERCC5 | ERCC5 | 0.965449096 | -0.029318375 | 0.71054704 |
| Transglutaminase | TGM2 | 0.922737728 | -0.014435034 | 0.712842183 |
| MERIT40_pS29 | BABAM1 | 0.930816455 | -0.015964806 | 0.727602324 |
| PAI-1 | SERPINE1 | 0.919700611 | -0.015335085 | 0.731211036 |
| Cyclophilin-F | PPIF | 0.944362008 | -0.051308613 | 0.775126281 |
| FoxO3a | FOX3 | 0.885258515 | 0.010442903 | 0.775847866 |
| B-Raf | BRAF | 0.924694841 | -0.010589111 | 0.781796069 |
| Caspase-8 | CASP8 | 0.906354255 | 0.022215457 | 0.792627355 |
| mTOR_pS2448 | MTOR | 0.959819881 | -0.012794421 | 0.793089893 |
| PD-L1 | CD274 | 0.897957206 | 0.011099223 | 0.804683043 |
| E-Cadherin | CDH1 | 0.938221099 | -0.012375217 | 0.80502146 |
| S6_pS235_S236 | RPS6 | 0.962743168 | -0.029753045 | 0.820538846 |
| Mcl-1 | MCL1 | 0.949925576 | 0.01198075 | 0.837527452 |
| Lck | LCK | 0.909992033 | 0.013076019 | 0.880510559 |
| Tuberin | TSC2 | 0.942642367 | -0.008287769 | 0.882289599 |
| Elk1_pS383 | ELK1 | 0.93342207 | -0.006031659 | 0.885403148 |
| Annexin-I | ANXA1 | 0.850489364 | 0.022988764 | 0.887456953 |
| XPA | XPA | 0.913097595 | -0.007662482 | 0.906198506 |
| Cyclin-D1 | CCND1 | 0.942241131 | -0.007475434 | 0.90639671 |
| PRAS40_pT246 | AKT1S1 | 0.959921709 | 0.00660596 | 0.92077878 |
| Tau | MAPT | 0.872948242 | 0.008939546 | 0.944788388 |
| p44-42-MAPK | MAPK3 | 0.954227863 | -0.00490989 | 0.949928155 |
| Claudin-7 | CLDN7 | 0.941950888 | -0.00476762 | 0.969660842 |
| ATM_pS1981 | ATM | 0.855016859 | 0.001174199 | 0.970904381 |
| Hif-1-alpha | HIF1A | 0.863310684 | 0.001884145 | 0.972337185 |
| MMP2 | MMP2 | 0.910304447 | -0.001349593 | 0.983460951 |
| BRD4 | BRD4 | 0.934794426 | 0.00252552 | 0.986316871 |

| | | | | |
|---|---|---|---|---|
| p53 | TP53 | 0.856310474 | 0.001528984 | 0.987480401 |
| Porin | VDAC1 | 0.913176636 | 0.00019121 | 0.996632734 |

## REFERENCES


1. Nelson, C. M., and Bissell, M. J. (2006) Of Extracellular Matrix, Scaffolds, and Signaling: Tissue Architecture Regulates Development, Homeostasis, and Cancer. *Annual Review of Cell and Developmental Biology* **22**, 287-309

2. Bissell, M. J., Rizki, A., and Mian, I. S. (2003) Tissue architecture: the ultimate regulator of breast epithelial function. *Current Opinion in Cell Biology* **15**, 753-762

3. Russo, J., and Russo, I. H. (2004) Development of the human breast. *Maturitas* **49**, 2-15

4. Neville, M. C., McFadden, T. B., and Forsyth, I. (2002) Hormonal Regulation of Mammary Differentiation and Milk Secretion. *Journal of Mammary Gland Biology and Neoplasia* **7**, 49-66

5. Going, J. J., and Moffat, D. F. (2004) Escaping from Flatland: clinical and biological aspects of human mammary duct anatomy in three dimensions. *The Journal of Pathology* **203**, 538-544

6. Hassiotou, F., and Geddes, D. (2013) Anatomy of the human mammary gland: Current status of knowledge. *Clinical Anatomy* **26**, 29-48

7. Cowell, C. F., Weigelt, B., Sakr, R. A., Ng, C. K. Y., Hicks, J., King, T. A., and Reis-Filho, J. S. (2013) Progression from ductal carcinoma in situ to invasive breast cancer: Revisited. *Molecular Oncology* **7**, 859-869

8. Pardee, A. B. (1974) A Restriction Point for Control of Normal Animal Cell Proliferation. *Proceedings of the National Academy of Sciences of the United States of America* **71**, 1286-1290

9. Tobey, R. A., and Ley, K. D. (1970) REGULATION OF INITIATION OF DNA SYNTHESIS IN CHINESE HAMSTER CELLS : I. Production of Stable, Reversible G(1)-Arrested Populations in Suspension Culture. *The Journal of Cell Biology* **46**, 151-157

10. Bürk, R. R. (1970) One-step growth cycle for BHK21/13 hamster fibroblasts. *Experimental Cell Research* **63**, 309-316

11. Wiebel, F., and Baserga, R. (1969) Early alterations in amino acid pools and protein synthesis of diploid fibroblasts stimulated to synthesize DNA by addition of serum. *Journal of Cellular Physiology* **74**, 191-202

12. Temin, H. M. (1971) Stimulation by serum of multiplication of stationary chicken cells. *Journal of Cellular Physiology* **78**, 161-170

13. Campisi, J., and d'Adda di Fagagna, F. (2007) Cellular senescence: when bad things happen to good cells. *Nat Rev Mol Cell Biol* **8**, 729-740

14. Johnson, D. G., and Walker, C. L. (1999) CYCLINS AND CELL CYCLE CHECKPOINTS. *Annual Review of Pharmacology and Toxicology* **39**, 295-312

15. Elledge, S. J. (1996) Cell Cycle Checkpoints: Preventing an Identity Crisis. *Science* **274**, 1664-1672

16. Collins, K., Jacks, T., and Pavletich, N. P. (1997) The cell cycle and cancer. *Proceedings of the National Academy of Sciences* **94**, 2776-2778

17. Rosenthal, E. T., Hunt, T., and Ruderman, J. V. (1980) Selective translation of mRNA controls the pattern of protein synthesis during early development of the surf clam, Spisula solidissima. *Cell* **20**, 487-494

18. Baldin, V., Lukas, J., Marcote, M. J., Pagano, M., and Draetta, G. (1993) Cyclin D1 is a nuclear protein required for cell cycle progression in G1. *Genes & Development* **7**, 812-821

19. Hinds, P. W., Mittnacht, S., Dulic, V., Arnold, A., Reed, S. I., and Weinberg, R. A. (1992) Regulation of retinoblastoma protein functions by ectopic expression of human cyclins. *Cell* **70**, 993-1006

20. Ohtsubo, M., Theodoras, A. M., Schumacher, J., Roberts, J. M., and Pagano, M. (1995) Human cyclin E, a nuclear protein essential for the G1-to-S phase transition. *Molecular and Cellular Biology* **15**, 2612-2624

21. Schulze, A., Zerfass, K., Spitkovsky, D., Middendorp, S., Bergès, J., Helin, K., Jansen-Dürr, P., and Henglein, B. (1995) Cell cycle regulation of the cyclin A gene promoter is mediated by a variant E2F site. *Proceedings of the National Academy of Sciences of the United States of America* **92**, 11264-11268

22. Girard, F., Strausfeld, U., Fernandez, A., and Lamb, N. J. C. (1991) Cyclin a is required for the onset of DNA replication in mammalian fibroblasts. *Cell* **67**, 1169-1179

23. Walker, D. H., and Maller, J. L. (1991) Role for cyclin A in the dependence of mitosis on completion of DMA replication. *Nature* **354**, 314-317

24. King, R. W., Jackson, P. K., and Kirschner, M. W. (1994) Mitosis in transition. *Cell* **79**, 563-571

25. Castor, L. N. (1972) Contact Inhibitions of Cell Division and Cell Movement. *Journal of Investigative Dermatology* **59**, 27-32

26. Stoker, M. G. P., and Rubin, H. (1967) Density Dependent Inhibition of Cell Growth in Culture. *Nature* **215**, 171-172

27. Todaro, G. J., Lazar, G. K., and Green, H. (1965) The initiation of cell division in a contact-inhibited mammalian cell line. *Journal of Cellular and Comparative Physiology* **66**, 325-333

28. Martin-Belmonte, F., and Perez-Moreno, M. (2012) Epithelial cell polarity, stem cells and cancer. *Nat Rev Cancer* **12**, 23-38

29. Karp, C. M., Tan, T. T., Mathew, R., Nelson, D., Mukherjee, C., Degenhardt, K., Karantza-Wadsworth, V., and White, E. (2008) Role of the Polarity Determinant Crumbs in Suppressing Mammalian Epithelial Tumor Progression. *Cancer Research* **68**, 4105-4115

30. Bilder, D., and Perrimon, N. (2000) Localization of apical epithelial determinants by the basolateral PDZ protein Scribble. *Nature* **403**, 676-680

31. Noatynska, A., Tavernier, N., Gotta, M., and Pintard, L. (2013) Coordinating cell polarity and cell cycle progression: what can we learn from flies and worms? *Open Biology* **3**, 130083

32. Anderson, J. M., and Van Itallie, C. M. (2009) Physiology and Function of the Tight Junction. *Cold Spring Harbor Perspectives in Biology* **1**, a002584

33. Yang, C. C., Graves, H. K., Moya, I. M., Tao, C., Hamaratoglu, F., Gladden, A. B., and Halder, G. (2015) Differential regulation of the Hippo pathway by adherens junctions and apical- Basal cell polarity modules. *Proceedings of the National Academy of Sciences of the United States of America* **112**, 1785-1790

34. Meng, W., and Takeichi, M. (2009) Adherens Junction: Molecular Architecture and Regulation. *Cold Spring Harbor Perspectives in Biology* **1**, a002899

35. Hsu, S.-C., Galceran, J., and Grosschedl, R. (1998) Modulation of Transcriptional Regulation by LEF-1 in Response to Wnt-1 Signaling and Association with β-Catenin. *Molecular and Cellular Biology* **18**, 4807-4818

36. Shtutman, M., Zhurinsky, J., Simcha, I., Albanese, C., D'Amico, M., Pestell, R., and Ben-Ze'ev, A. (1999) The cyclin D1 gene is a target of the β-catenin/LEF-1 pathway. *Proceedings of the National Academy of Sciences* **96**, 5522-5527

37. Capaldo, C. T., Koch, S., Kwon, M., Laur, O., Parkos, C. A., and Nusrat, A. (2011) Tight function zonula occludens-3 regulates cyclin D1–dependent cell proliferation. *Molecular Biology of the Cell* **22**, 1677-1685

38. Huerta, M., Muñoz, R., Tapia, R., Soto-Reyes, E., Ramírez, L., Recillas-Targa, F., González-Mariscal, L., and López-Bayghen, E. (2007) Cyclin D1 Is Transcriptionally Down-Regulated by ZO-2 via an E Box and the Transcription Factor c-Myc. *Molecular Biology of the Cell* **18**, 4826-4836

39. Motokura, T., Bloom, T., Kim, H. G., Juppner, H., Ruderman, J. V., Kronenberg, H. M., and Arnold, A. (1991) A novel cyclin encoded by a bcl1-linked candidate oncogene. *Nature* **350**, 512-515

40. Bodrug, S. E., Warner, B. J., Bath, M. L., Lindeman, G. J., Harris, A. W., and Adams, J. M. (1994) Cyclin D1 transgene impedes lymphocyte maturation and collaborates in lymphomagenesis with the myc gene. *The EMBO Journal* **13**, 2124-2130

41. Lovec, H., Grzeschiczek, A., Kowalski, M. B., and Möröy, T. (1994) Cyclin D1/bcl-1 cooperates with myc genes in the generation of B-cell lymphoma in transgenic mice. *The EMBO Journal* **13**, 3487-3495

42. Wang, T. C., Cardiff, R. D., Zukerberg, L., Lees, E., Arnold, A., and Schmidt, E. V. (1994) Mammary hyperplasia and carcinoma in MMTV-cyclin D1 transgenic mice. *Nature* **369**, 669-671

43. Leach, F. S., Elledge, S. J., Sherr, C. J., Willson, J. K. V., Markowitz, S., Kinzler, K. W., and Vogelstein, B. (1993) Amplification of Cyclin Genes in Colorectal Carcinomas. *Cancer Research* **53**, 1986

44. Easton, J., Wei, T., Lahti, J. M., and Kidd, V. J. (1998) Disruption of the Cyclin D/Cyclin-dependent Kinase/INK4/Retinoblastoma Protein Regulatory Pathway in Human Neuroblastoma. *Cancer Research* **58**, 2624

45. Rutherford, R., and Ross, R. (1976) Platelet factors stimulate fibroblasts and smooth muscle cells quiescent in plasma serum to proliferate. *The Journal of Cell Biology* **69**, 196-203

46. Yatomi, Y., Ruan, F., Hakomori, S., and Igarashi, Y. (1995) Sphingosine-1-phosphate: a platelet-activating sphingolipid released from agonist-stimulated human platelets. *Blood* **86**, 193

47. Eichholtz, T., Jalink, K., Fahrenfort, I., and Moolenaar, W. H. (1993) The bioactive phospholipid lysophosphatidic acid is released from activated platelets. *Biochemical Journal* **291**, 677-680

48. Boucharaba, A., Serre, C.-M., Gr, xE, s, S., Saulnier-Blache, J. S., xE, bastien, Bordet, J.-C., Guglielmi, J., Cl, xE, zardin, P., and Peyruchaud, O. Platelet-derived lysophosphatidic acid supports the progression of osteolytic bone metastases in breast cancer. *The Journal of Clinical Investigation* **114**, 1714-1725

49. Panupinthu, N., Lee, H. Y., and Mills, G. B. (2010) Lysophosphatidic acid production and action: critical new players in breast cancer initiation and progression. *Br J Cancer* **102**, 941-946

50. Pyne, N. J., and Pyne, S. (2010) Sphingosine 1-phosphate and cancer. *Nat Rev Cancer* **10**, 489-503

51. Yin, Y.-J., Katz, V., Salah, Z., Maoz, M., Cohen, I., Uziely, B., Turm, H., Grisaru-Granovsky, S., Suzuki, H., and Bar-Shavit, R. (2006) Mammary Gland Tissue Targeted Overexpression of Human Protease-Activated Receptor 1 Reveals a Novel Link to β-Catenin Stabilization. *Cancer Research* **66**, 5224

52. Hernández, N. A., Correa, E., Avila, E. P., Vela, T. A., and Pérez, V. M. (2009) PAR1 is selectively over expressed in high grade breast cancer patients: a cohort study. *Journal of Translational Medicine* **7**, 47-47

53. Kamath, L., Meydani, A., Foss, F., and Kuliopulos, A. (2001) Signaling from Protease-activated Receptor-1 Inhibits Migration and Invasion of Breast Cancer Cells. *Cancer Research* **61**, 5933

54. Pierce, K. L., Premont, R. T., and Lefkowitz, R. J. (2002) Seven-transmembrane receptors. *Nat Rev Mol Cell Biol* **3**, 639-650

55. Palczewski, K., Kumasaka, T., Hori, T., Behnke, C. A., Motoshima, H., Fox, B. A., Trong, I. L., Teller, D. C., Okada, T., Stenkamp, R. E., Yamamoto, M., and Miyano, M. (2000) Crystal Structure of Rhodopsin: A G Protein-Coupled Receptor. *Science* **289**, 739-745

56. Dixon, R. A. F., Kobilka, B. K., Strader, D. J., Benovic, J. L., Dohlman, H. G., Frielle, T., Bolanowski, M. A., Bennett, C. D., Rands, E., Diehl, R. E., Mumford, R. A., Slater, E. E., Sigal, I. S., Caron, M. G., Lefkowitz, R. J., and Strader, C. D. (1986) Cloning of the gene and cDNA for mammalian [beta]-adrenergic receptor and homology with rhodopsin. *Nature* **321**, 75-79

57. Kleuss, C., Raw, A. S., Lee, E., Sprang, S. R., and Gilman, A. G. (1994) Mechanism of GTP hydrolysis by G-protein alpha subunits. *Proceedings of the National Academy of Sciences of the United States of America* **91**, 9828-9831

58. Strathmann, M. P., and Simon, M. I. (1991) G alpha 12 and G alpha 13 subunits define a fourth class of G protein alpha subunits. *Proceedings of the National Academy of Sciences of the United States of America* **88**, 5582-5586

59. Xu, N., Bradley, L., Ambdukar, I., and Gutkind, J. S. (1993) A mutant alpha subunit of G12 potentiates the eicosanoid pathway and is highly oncogenic in NIH 3T3 cells. *Proceedings of the National Academy of Sciences* **90**, 6741-6745

60. Xu, N. Z., Voynoyasenetskaya, T., and Gutkind, J. S. (1994) Potent Transforming Activity of the G13 α Subunit Defines a Novel Family of Oncogenes. *Biochemical and Biophysical Research Communications* **201**, 603-609

61. Kelly, P., Stemmle, L. N., Madden, J. F., Fields, T. A., Daaka, Y., and Casey, P. J. (2006) A Role for the G12 Family of Heterotrimeric G Proteins in Prostate Cancer Invasion. *Journal of Biological Chemistry* **281**, 26483-26490

62. Gan, C. P., Patel, V., Mikelis, C. M., Zain, R. b., Molinolo, A. A., Abraham, M. T., Teo, S.-H., Abdul Rahman, Z. A., Gutkind, J. S., and Cheong, S. C. (2014) *Heterotrimeric G-protein alpha-12 (Gα12) subunit promotes oral cancer metastasis*,

63. Yagi, H., Asanoma, K., Ohgami, T., Ichinoe, A., Sonoda, K., and Kato, K. (2016) GEP oncogene promotes cell proliferation through YAP activation in ovarian cancer. *Oncogene*

64. Kelly, P., Moeller, B. J., Juneja, J., Booden, M. A., Der, C. J., Daaka, Y., Dewhirst, M. W., Fields, T. A., and Casey, P. J. (2006) The G12 family of heterotrimeric G proteins promotes breast cancer invasion and metastasis. *Proceedings of the National Academy of Sciences* **103**, 8173-8178

65. Wells, C. D., Gutowski, S., Bollag, G., and Sternweis, P. C. (2001) Identification of Potential Mechanisms for Regulation of p115 RhoGEF through Analysis of Endogenous and Mutant Forms of the Exchange Factor. *Journal of Biological Chemistry* **276**, 28897-28905

66. Chen, Z., Singer, W. D., Wells, C. D., Sprang, S. R., and Sternweis, P. C. (2003) Mapping the Gα13 Binding Interface of the rgRGS Domain of p115RhoGEF. *Journal of Biological Chemistry* **278**, 9912-9919

67. Grabocka, E., and Wedegaertner, P. B. (2005) Functional consequences of Gα(13) mutations that disrupt interaction with p115RhoGEF. *Oncogene* **24**, 2155-2165

68. Wells, C. D., Liu, M. Y., Jackson, M., Gutowski, S., Sternweis, P. M., Rothstein, J. D., Kozasa, T., and Sternweis, P. C. (2002) Mechanisms for reversible regulation between G13 and Rho exchange factors. *Journal of Biological Chemistry* **277**, 1174-1181

69. Ron, D., Graziani, G., Aaronson, S. A., and Eva, A. (1989) The N-terminal region of proto-dbl down regulates its transforming activity. *Oncogene* **4**, 1067-1072

70. Eva, A., Vecchio, G., Durga Rao, C., Tronick, S. R., and Aaronson, S. A. (1988) The predicted DBL oncogene product defines a distinct class of transforming proteins. *Proceedings of the National Academy of Sciences of the United States of America* **85**, 2061-2065

71. Eva, A., and Aaronson, S. A. (1985) Isolation of a new human oncogene from a diffuse B-cell lymphoma. *Nature* **316**, 273-275

72. Hart, M. J., Eva, A., Evans, T., Aaronson, S. A., and Cerione, R. A. (1991) Catalysis of guanine nucleotide exchange on the CDC42Hs protein by the dbloncogene product. *Nature* **354**, 311-314

73. Hart, M. J., Eva, A., Zangrilli, D., Aaronson, S. A., Evans, T., Cerione, R. A., and Zheng, Y. (1994) Cellular transformation and guanine nucleotide exchange

activity are catalyzed by a common domain on the dbl oncogene product. *Journal of Biological Chemistry* **269**, 62-65

74. Hart, M. J., Sharma, S., elMasry, N., Qiu, R.-G., McCabe, P., Polakis, P., and Bollag, G. (1996) Identification of a Novel Guanine Nucleotide Exchange Factor for the Rho GTPase. *Journal of Biological Chemistry* **271**, 25452-25458

75. Reuther, G. W., Lambert, Q. T., Booden, M. A., Wennerberg, K., Becknell, B., Marcucci, G., Sondek, J., Caligiuri, M. A., and Der, C. J. (2001) Leukemia-associated Rho Guanine Nucleotide Exchange Factor, a Dbl Family Protein Found Mutated in Leukemia, Causes Transformation by Activation of RhoA. *Journal of Biological Chemistry* **276**, 27145-27151

76. Kourlas, P. J., Strout, M. P., Becknell, B., Veronese, M. L., Croce, C. M., Theil, K. S., Krahe, R., Ruutu, T., Knuutila, S., Bloomfield, C. D., and Caligiuri, M. A. (2000) Identification of a gene at 11q23 encoding a guanine nucleotide exchange factor: Evidence for its fusion with MLL in acute myeloid leukemia. *Proceedings of the National Academy of Sciences of the United States of America* **97**, 2145-2150

77. Kranenburg, O., Poland, M., van Horck, F. P. G., Drechsel, D., Hall, A., and Moolenaar, W. H. (1999) Activation of RhoA by Lysophosphatidic Acid and Gα(12/13) Subunits in Neuronal Cells: Induction of Neurite Retraction. *Molecular Biology of the Cell* **10**, 1851-1857

78. Nobes, C. D., Hawkins, P., Stephens, L., and Hall, A. (1995) Activation of the small GTP-binding proteins rho and rac by growth factor receptors. *Journal of Cell Science* **108**, 225-233

79. Sotiropoulos, A., Gineitis, D., Copeland, J., and Treisman, R. (1999) Signal-regulated activation of serum response factor is mediated by changes in actin dynamics. *Cell* **98**, 159-169

80. Sahai, E., Alberts, A. S., and Treisman, R. (1998) RhoA effector mutants reveal distinct effector pathways for cytoskeletal reorganization, SRF activation and transformation. *EMBO Journal* **17**, 1350-1361

81. Hill, C. S., Wynne, J., and Treisman, R. (1995) The Rho family GTPases RhoA, Racl , and CDC42Hsregulate transcriptional activation by SRF. *Cell* **81**, 1159-1170

82. Miralles, F., Posern, G., Zaromytidou, A. I., and Treisman, R. (2003) Actin dynamics control SRF activity by regulation of its coactivator MAL. *Cell* **113**, 329-342

83. Posern, G., Sotiropoulos, A., and Treisman, R. (2002) Mutant Actins Demonstrate a Role for Unpolymerized Actin in Control of Transcription by Serum Response Factor. *Molecular Biology of the Cell* **13**, 4167-4178

84. Cen, B., Selvaraj, A., Burgess, R. C., Hitzler, J. K., Ma, Z., Morris, S. W., and Prywes, R. (2003) Megakaryoblastic leukemia 1, a potent transcriptional coactivator for serum response factor (SRF), is required for serum induction of SRF target genes. *Molecular and Cellular Biology* **23**, 6597-6608

85. Norman, C., Runswick, M., Pollock, R., and Treisman, R. (1988) Isolation and properties of cDNA clones encoding SRF, a transcription factor that binds to the c-fos serum response element. *Cell* **55**, 989-1003

86. Treisman, R. (1986) Identification of a protein-binding site that mediates transcriptional response of the c-fos gene to serum factors. *Cell* **46**, 567-574

87. Gilman, M. Z., Wilson, R. N., and Weinberg, R. A. (1986) Multiple protein-binding sites in the 5'-flanking region regulate c-fos expression. *Molecular and Cellular Biology* **6**, 4305-4316

88. Prywes, R., and Roeder, R. G. (1986) Inducible binding of a factor to the c-fos enhancer. *Cell* **47**, 777-784

89. Dorsam, R. T., and Gutkind, J. S. (2007) G-protein-coupled receptors and cancer. *Nat Rev Cancer* **7**, 79-94

90. Saini, K. S., Loi, S., de Azambuja, E., Metzger-Filho, O., Saini, M. L., Ignatiadis, M., Dancey, J. E., and Piccart-Gebhart, M. J. (2013) Targeting the PI3K/AKT/mTOR and Raf/MEK/ERK pathways in the treatment of breast cancer. *Cancer Treatment Reviews* **39**, 935-946

91. Meloche, S., Seuwen, K., Pagès, G., and Pouysségur, J. (1992) Biphasic and synergistic activation of p44mapk (ERK1) by growth factors: correlation between late phase activation and mitogenicity. *Molecular Endocrinology* **6**, 845-854

92. Courtois-Cox, S., Jones, S. L., and Cichowski, K. (2008) Many roads lead to oncogene-induced senescence. *Oncogene* **27**, 2801-2809

93. Cargnello, M., and Roux, P. P. (2011) Activation and Function of the MAPKs and Their Substrates, the MAPK-Activated Protein Kinases. *Microbiology and Molecular Biology Reviews* **75**, 50-83

94. Ferrell, J. E. (1996) Tripping the switch fantastic: how a protein kinase cascade can convert graded inputs into switch-like outputs. *Trends in Biochemical Sciences* **21**, 460-466

95. Jelinek, T., Dent, P., Sturgill, T. W., and Weber, M. J. (1996) Ras-induced activation of Raf-1 is dependent on tyrosine phosphorylation. *Molecular and Cellular Biology* **16**, 1027-1034

96. Alessi, D. R., Saito, Y., Campbell, D. G., Cohen, P., Sithanandam, G., Rapp, U., Ashworth, A., Marshall, C. J., and Cowley, S. (1994) Identification of the sites in

MAP kinase kinase-1 phosphorylated by p74raf-1. *The EMBO Journal* **13**, 1610-1619

97. Zheng, C. F., and Guan, K. L. (1994) Activation of MEK family kinases requires phosphorylation of two conserved Ser/Thr residues. *The EMBO Journal* **13**, 1123-1131

98. Payne, D. M., Rossomando, A. J., Martino, P., Erickson, A. K., Her, J. H., Shabanowitz, J., Hunt, D. F., Weber, M. J., and Sturgill, T. W. (1991) Identification of the regulatory phosphorylation sites in pp42/mitogen-activated protein kinase (MAP kinase). *The EMBO Journal* **10**, 885-892

99. Jaiswal, M., Gremer, L., Dvorsky, R., Haeusler, L. C., Cirstea, I. C., Uhlenbrock, K., and Ahmadian, M. R. (2011) Mechanistic insights into specificity, activity, and regulatory elements of the regulator of G-protein signaling (RGS)-containing Rho-specific guanine nucleotide exchange factors (GEFs) p115, PDZ-RhoGEF (PRG), and leukemia-associated RhoGEF (LARG). *Journal of Biological Chemistry* **286**, 18202-18212

100. Boulton, T., Yancopoulos, G., Gregory, J., Slaughter, C., Moomaw, C., Hsu, J., and Cobb, M. (1990) An insulin-stimulated protein kinase similar to yeast kinases involved in cell cycle control. *Science* **249**, 64-67

101. Lenormand, P., Brondello, J.-M., Brunet, A., and Pouysségur, J. (1998) Growth Factor–induced p42/p44 MAPK Nuclear Translocation and Retention Requires Both MAPK Activation and Neosynthesis of Nuclear Anchoring Proteins. *The Journal of Cell Biology* **142**, 625-633

102. Nye, J. A., Petersen, J. M., Gunther, C. V., Jonsen, M. D., and Graves, B. J. (1992) Interaction of murine ets-1 with GGA-binding sites establishes the ETS domain as a new DNA-binding motif. *Genes & Development* **6**, 975-990

103. Karim, F. D., Urness, L. D., Thummel, C. S., Klemsz, M. J., McKercher, S. R., Celada, A., Van Beveren, C., Maki, R. A., Gunther, C. V., and Nye, J. A. (1990) The ETS-domain: a new DNA-binding motif that recognizes a purine-rich core DNA sequence. *Genes & Development* **4**, 1451-1453

104. Janknecht, R., Ernst, W. H., Pingoud, V., and Nordheim, A. (1993) Activation of ternary complex factor Elk-1 by MAP kinases. *The EMBO Journal* **12**, 5097-5104

105. Dalton, S., and Treisman, R. (1992) Characterization of SAP-1, a protein recruited by serum response factor to the c-fos serum response element. *Cell* **68**, 597-612

106. Hipskind, R. A., Roa, V. N., Muller, C. G. F., Raddy, E. S. P., and Nordheim, A. (1991) Ets-related protein Elk-1 is homologous to the c-fos regulatory factor p62TCF. *Nature* **354**, 531-534

107. Pagès, G., Lenormand, P., L'Allemain, G., Chambard, J. C., Meloche, S., and Pouysségur, J. (1993) Mitogen-activated protein kinases p42mapk and p44mapk are required for fibroblast proliferation. *Proceedings of the National Academy of Sciences of the United States of America* **90**, 8319-8323

108. Lavoie, J. N., L'Allemain, G., Brunet, A., Müller, R., and Pouysségur, J. (1996) Cyclin D1 Expression Is Regulated Positively by the p42/p44MAPK and Negatively by the p38/HOGMAPK Pathway. *Journal of Biological Chemistry* **271**, 20608-20616

109. Ventura, J.-J., Hübner, A., Zhang, C., Flavell, R. A., Shokat, K. M., and Davis, R. J. (2006) Chemical Genetic Analysis of the Time Course of Signal Transduction by JNK. *Molecular Cell* **21**, 701-710

110. Chang, L., Kamata, H., Solinas, G., Luo, J.-L., Maeda, S., Venuprasad, K., Liu, Y.-C., and Karin, M. (2006) The E3 Ubiquitin Ligase Itch Couples JNK Activation to TNFα-induced Cell Death by Inducing c-FLIPL Turnover. *Cell* **124**, 601-613

111. Lu, C., Zhu, F., Cho, Y.-Y., Tang, F., Zykova, T., Ma, W.-y., Bode, A. M., and Dong, Z. (2006) Cell Apoptosis: Requirement of H2AX in DNA Ladder Formation, but Not for the Activation of Caspase-3. *Molecular Cell* **23**, 121-132

112. Maki, Y., Bos, T. J., Davis, C., Starbuck, M., and Vogt, P. K. (1987) Avian sarcoma virus 17 carries the jun oncogene. *Proceedings of the National Academy of Sciences of the United States of America* **84**, 2848-2852

113. Hibi, M., Lin, A., Smeal, T., Minden, A., and Karin, M. (1993) Identification of an oncoprotein- and UV-responsive protein kinase that binds and potentiates the c-Jun activation domain. *Genes & Development* **7**, 2135-2148

114. Kovary, K., and Bravo, R. (1991) The jun and fos protein families are both required for cell cycle progression in fibroblasts. *Molecular and Cellular Biology* **11**, 4466-4472

115. Lee, Y.-N., Malbon, C. C., and Wang, H.-y. (2004) Gα13 Signals via p115RhoGEF Cascades Regulating JNK1 and Primitive Endoderm Formation. *Journal of Biological Chemistry* **279**, 54896-54904

116. Voyno-Yasenetskaya, T. A., Faure, M. P., Ahn, N. G., and Bourne, H. R. (1996) Gα12 and Gα13 Regulate Extracellular Signal-regulated Kinase and c-Jun Kinase Pathways by Different Mechanisms in COS-7 Cells. *Journal of Biological Chemistry* **271**, 21081-21087

117. Dhillon, A. S., Hagan, S., Rath, O., and Kolch, W. (0000) MAP kinase signalling pathways in cancer. *Oncogene* **26**, 3279-3290

118. Lian, I., Kim, J., Okazawa, H., Zhao, J., Zhao, B., Yu, J., Chinnaiyan, A., Israel, M. A., Goldstein, L. S. B., Abujarour, R., Ding, S., and Guan, K.-L. (2010) The role of YAP transcription coactivator in regulating stem cell self-renewal and differentiation. *Genes & Development* **24**, 1106-1118

119. Cordenonsi, M., Zanconato, F., Azzolin, L., Forcato, M., Rosato, A., Frasson, C., Inui, M., Montagner, M., Parenti, Anna R., Poletti, A., Daidone, Maria G., Dupont, S., Basso, G., Bicciato, S., and Piccolo, S. (2011) The Hippo Transducer TAZ Confers Cancer Stem Cell-Related Traits on Breast Cancer Cells. *Cell* **147**, 759-772

120. Zhao, B., Wei, X., Li, W., Udan, R. S., Yang, Q., Kim, J., Xie, J., Ikenoue, T., Yu, J., Li, L., Zheng, P., Ye, K., Chinnaiyan, A., Halder, G., Lai, Z.-C., and Guan, K.-L. (2007) Inactivation of YAP oncoprotein by the Hippo pathway is involved in cell contact inhibition and tissue growth control. *Genes & Development* **21**, 2747-2761

121. Huang, J., Wu, S., Barrera, J., Matthews, K., and Pan, D. (2005) The Hippo Signaling Pathway Coordinately Regulates Cell Proliferation and Apoptosis by Inactivating Yorkie, the Drosophila Homolog of YAP. *Cell* **122**, 421-434

122. Yu, F. X., Zhao, B., Panupinthu, N., Jewell, J. L., Lian, I., Wang, L. H., Zhao, J., Yuan, H., Tumaneng, K., Li, H., Fu, X. D., Mills, G. B., and Guan, K. L. (2012) Regulation of the Hippo-YAP pathway by G-protein-coupled receptor signaling. *Cell* **150**, 780-791

123. Fan, R., Kim, N.-G., and Gumbiner, B. M. (2013) Regulation of Hippo pathway by mitogenic growth factors via phosphoinositide 3-kinase and phosphoinositide-dependent kinase-1. *Proceedings of the National Academy of Sciences* **110**, 2569-2574

124. Adler, J. J., Heller, B. L., Bringman, L. R., Ranahan, W. P., Cocklin, R. R., Goebl, M. G., Oh, M., Lim, H. S., Ingham, R. J., and Wells, C. D. (2013) Amot130 adapts atrophin-1 interacting protein 4 to inhibit yes-associated protein signaling and cell growth. *Journal of Biological Chemistry* **288**, 15181-15193

125. Adler, J. J., Johnson, D. E., Heller, B. L., Bringman, L. R., Ranahan, W. P., Conwell, M. D., Sun, Y., Hudmon, A., and Wells, C. D. (2013) Serum deprivation inhibits the transcriptional co-activator YAP and cell growth via phosphorylation of the 130-kDa isoform of Angiomotin by the LATS1/2 protein kinases. *Proceedings of the National Academy of Sciences of the United States of America* **110**, 17368-17373

126. Feng, X., Degese, M., Iglesias-Bartolome, R., Vaque, J., Molinolo, A., Rodrigues, M., Zaidi, M. R., Ksander, B. R., Merlino, G., Sodhi, A., Chen, Q., and Gutkind, J. S. (2014) Hippo-independent activation of YAP by the GNAQ uveal melanoma oncogene through a Trio-regulated Rho GTPase Signaling Circuitry. *Cancer Cell* **25**, 831-845

127. Azzolin, L., Panciera, T., Soligo, S., Enzo, E., Bicciato, S., Dupont, S., Bresolin, S., Frasson, C., Basso, G., Guzzardo, V., Fassina, A., Cordenonsi, M., and Piccolo, S. (2014) YAP/TAZ Incorporation in the β-Catenin Destruction Complex Orchestrates the Wnt Response. *Cell* **158**, 157-170

128. Zhang, W., Nandakumar, N., Shi, Y., Manzano, M., Smith, A., Graham, G., Gupta, S., Vietsch, E. E., Laughlin, S. Z., Wadhwa, M., Chetram, M., Joshi, M., Wang, F., Kallakury, B., Toretsky, J., Wellstein, A., and Yi, C. (2014) Downstream of Mutant KRAS, the Transcription Regulator YAP Is Essential for Neoplastic Progression to Pancreatic Ductal Adenocarcinoma. *Science Signaling* **7**, ra42-ra42

129. Mohseni, M., Sun, J., Lau, A., Curtis, S., Goldsmith, J., Fox, V. L., Wei, C., Frazier, M., Samson, O., Wong, K. K., Kim, C., and Camargo, F. D. (2014) A genetic screen identifies an LKB1-MARK signalling axis controlling the Hippo-YAP pathway. *Nature Cell Biology* **16**, 108-117

130. Altomare, D. A., Vaslet, C. A., Skele, K. L., De Rienzo, A., Devarajan, K., Jhanwar, S. C., McClatchey, A. I., Kane, A. B., and Testa, J. R. (2005) A Mouse Model Recapitulating Molecular Features of Human Mesothelioma. *Cancer Research* **65**, 8090-8095

131. Kaneko, K. J., and DePamphilis, M. L. (1998) Regulation of gene expression at the beginning of mammalian development and the TEAD family of transcription factors. *Developmental Genetics* **22**, 43-55

132. Vassilev, A., Kaneko, K. J., Shu, H., Zhao, Y., and DePamphilis, M. L. (2001) TEAD/TEF transcription factors utilize the activation domain of YAP65, a Src/Yes-associated protein localized in the cytoplasm. *Genes & Development* **15**, 1229-1241

133. Wu, S., Liu, Y., Zheng, Y., Dong, J., and Pan, D. (2008) The TEAD/TEF Family Protein Scalloped Mediates Transcriptional Output of the Hippo Growth-Regulatory Pathway. *Developmental Cell* **14**, 388-398

134. Zhao, B., Ye, X., Yu, J., Li, L., Li, W., Li, S., Yu, J., Lin, J. D., Wang, C.-Y., Chinnaiyan, A. M., Lai, Z.-C., and Guan, K.-L. (2008) TEAD mediates YAP-dependent gene induction and growth control. *Genes & Development* **22**, 1962-1971

135. Tian, W., Yu, J., Tomchick, D. R., Pan, D., and Luo, X. (2010) Structural and functional analysis of the YAP-binding domain of human TEAD2. *Proceedings of the National Academy of Sciences* **107**, 7293-7298

136. Li, Z., Zhao, B., Wang, P., Chen, F., Dong, Z., Yang, H., Guan, K.-L., and Xu, Y. (2010) Structural insights into the YAP and TEAD complex. *Genes & Development* **24**, 235-240

137. Larkin, S. B., Farrance, I. K., and Ordahl, C. P. (1996) Flanking sequences modulate the cell specificity of M-CAT elements. *Molecular and Cellular Biology* **16**, 3742-3755

138. Zhao, B., Kim, J., Ye, X., Lai, Z.-C., and Guan, K.-L. (2009) Both TEAD-Binding and WW Domains Are Required for the Growth Stimulation and Oncogenic Transformation Activity of Yes-Associated Protein. *Cancer Research* **69**, 1089-1098

139. Zizer, E., Beilke, S., Buerle, T., Schilling, K., Mhnle, U., Adler, G., Fischer, K., and Wagner, M. (2010) Loss of Lsc/p115 protein leads to neuronal hypoplasia in the esophagus and an achalasia-like phenotype in mice. *Gastroenterology* **139**, 1344-1354

140. Graness, A., Giehl, K., and Goppelt-Struebe, M. (2006) Differential involvement of the integrin-linked kinase (ILK) in RhoA-dependent rearrangement of F-actin fibers and induction of connective tissue growth factor (CTGF). *Cellular Signalling* **18**, 433-440

141. Aktories, K., Braun, U., Rösener, S., Just, I., and Hall, A. (1989) The rho gene product expressed in E. Coli is a substrate of botulinum ADP-ribosyltransferase C3. *Biochemical and Biophysical Research Communications* **158**, 209-213

142. Dupont, S., Morsut, L., Aragona, M., Enzo, E., Giulitti, S., Cordenonsi, M., Zanconato, F., Le Digabel, J., Forcato, M., Bicciato, S., Elvassore, N., and Piccolo, S. (2011) Role of YAP/TAZ in mechanotransduction. *Nature* **474**, 179-183

143. Yu, O. M., Miyamoto, S., and Brown, J. H. (2016) Myocardin-Related Transcription Factor A and Yes-Associated Protein Exert Dual Control in G Protein-Coupled Receptor- and RhoA-Mediated Transcriptional Regulation and Cell Proliferation. *Molecular and Cellular Biology* **36**, 39-49

144. Zanconato, F., Forcato, M., Battilana, G., Azzolin, L., Quaranta, E., Bodega, B., Rosato, A., Bicciato, S., Cordenonsi, M., and Piccolo, S. (2015) Genome-wide association between YAP/TAZ/TEAD and AP-1 at enhancers drives oncogenic growth. *Nat Cell Biol* **17**, 1218-1227

145. Reddy, B., and Irvine, K. D. (2013) Regulation of Hippo signaling by EGFR-MAPK signaling through Ajuba family proteins. *Developmental cell* **24**, 459-471

146. Rauskolb, C., Sun, S., Sun, G., Pan, Y., and Irvine, K. D. (2014) Cytoskeletal tension inhibits Hippo signaling through an Ajuba-Warts complex. *Cell* **158**, 143-156

147. Eser, S., Schnieke, A., Schneider, G., and Saur, D. (2014) Oncogenic KRAS signalling in pancreatic cancer. *Br J Cancer* **111**, 817-822

148. de Waard, F. (1969) The epidemiology of breast cancer; Review and prospects. *International Journal of Cancer* **4**, 577-586

149. Simpson, P. T., Reis-Filho, J. S., Gale, T., and Lakhani, S. R. (2005) Molecular evolution of breast cancer. *The Journal of Pathology* **205**, 248-254

150. Neve, R. M., Chin, K., Fridlyand, J., Yeh, J., Baehner, F. L., Fevr, T., Clark, L., Bayani, N., Coppe, J.-P., Tong, F., Speed, T., Spellman, P. T., DeVries, S., Lapuk, A., Wang, N. J., Kuo, W.-L., Stilwell, J. L., Pinkel, D., Albertson, D. G., Waldman, F. M., McCormick, F., Dickson, R. B., Johnson, M. D., Lippman, M., Ethier, S., Gazdar, A., and Gray, J. W. (2006) A collection of breast cancer cell lines for the study of functionally distinct cancer subtypes. *Cancer Cell* **10**, 515-527

151. Foulkes , W. D., Smith , I. E., and Reis-Filho , J. S. (2010) Triple-Negative Breast Cancer. *New England Journal of Medicine* **363**, 1938-1948

152. DuBridge, R. B., Tang, P., Hsia, H. C., Leong, P. M., Miller, J. H., and Calos, M. P. (1987) Analysis of mutation in human cells by using an Epstein-Barr virus shuttle system. *Molecular and Cellular Biology* **7**, 379-387

153. Graham, F. L., Smiley, J., Russell, W. C., and Nairn, R. (1977) Characteristics of a Human Cell Line Transformed by DNA from Human Adenovirus Type 5. *Journal of General Virology* **36**, 59-72

154. Bissell, M. J., Hall, H. G., and Parry, G. (1982) How does the extracellular matrix direct gene expression? *Journal of Theoretical Biology* **99**, 31-68

155. Petersen, O. W., Rønnov-Jessen, L., Howlett, A. R., and Bissell, M. J. (1992) Interaction with basement membrane serves to rapidly distinguish growth and differentiation pattern of normal and malignant human breast epithelial cells. *Proceedings of the National Academy of Sciences of the United States of America* **89**, 9064-9068

156. Pan, D. (2007) Hippo signaling in organ size control. *Genes & Development* **21**, 886-897

157. Maddox, A. S., and Burridge, K. (2003) RhoA is required for cortical retraction and rigidity during mitotic cell rounding. *Journal of Cell Biology* **160**, 255-265

158. Wu, D., Asiedu, M., Adelstein, R., and Wei, Q. (2006) A Novel Guanine Nucleotide Exchange Factor, MYOGEF, is Required for Cytokinesis. *Cell Cycle* **5**, 1234-1239

159. Kuner, R., Swiercz, J. M., Zywietz, A., Tappe, A., and Offermanns, S. (2002) Characterization of the expression of PDZ-RhoGEF, LARG and Gα12/Gα13 proteins in the murine nervous system. *European Journal of Neuroscience* **16**, 2333-2341

160. Rümenapp, U., Blomquist, A., Schwörer, G., Schablowski, H., Psoma, A., and Jakobs, K. H. (1999) Rho-specific binding and guanine nucleotide exchange catalysis by KIAA0380, a Dbl family member. *FEBS Letters* **459**, 313-318

161. Xue, W., Krasnitz, A., Lucito, R., Sordella, R., VanAelst, L., Cordon-Cardo, C., Singer, S., Kuehnel, F., Wigler, M., Powers, S., Zender, L., and Lowe, S. W. (2008) DLC1 is a chromosome 8p tumor suppressor whose loss promotes hepatocellular carcinoma. *Genes & Development* **22**, 1439-1444

162. Ching, Y.-P., Wong, C.-M., Chan, S.-F., Leung, T. H.-Y., Ng, D. C.-H., Jin, D.-Y., and Ng, I. O.-l. (2003) Deleted in Liver Cancer (DLC) 2 Encodes a RhoGAP Protein with Growth Suppressor Function and Is Underexpressed in Hepatocellular Carcinoma. *Journal of Biological Chemistry* **278**, 10824-10830

163. Heidary Arash, E., Song, K. M., Song, S., Shiban, A., and Attisano, L. (2014) Arhgef7 promotes activation of the Hippo pathway core kinase Lats. *The EMBO Journal* **33**, 2997-3011

164. Besson, A., Gurian-West, M., Schmidt, A., Hall, A., and Roberts, J. M. (2004) p27Kip1 modulates cell migration through the regulation of RhoA activation. *Genes and Development* **18**, 862-876

165. Muehlich, S., Cicha, I., Garlichs, C. D., Krueger, B., Posern, G., and Goppelt-Struebe, M. (2007) Actin-dependent regulation of connective tissue growth factor. *American Journal of Physiology - Cell Physiology* **292**, C1732-C1738

166. Mo, J.-S., Yu, F.-X., Gong, R., Brown, J. H., and Guan, K.-L. (2012) Regulation of the Hippo–YAP pathway by protease-activated receptors (PARs). *Genes & Development* **26**, 2138-2143

167. Miller, E., Yang, J., Deran, M., Wu, C., Su, A. I., Bonamy, G. M. C., Liu, J., Peters, E. C., and Wu, X. (2012) Identification of serum-derived sphingosine-1-phosphate as a small molecule regulator of YAP. *Chemistry and Biology* **19**, 955-962

168. Chen, D., Sun, Y., Wei, Y., Zhang, P., Rezaeian, A. H., Teruya-Feldstein, J., Gupta, S., Liang, H., Lin, H.-K., Hung, M.-C., and Ma, L. (2012) LIFR is a breast cancer metastasis suppressor upstream of the Hippo-YAP pathway and a prognostic marker. *Nature medicine* **18**, 1511-1517

169. Dong, J., Feldmann, G., Huang, J., Wu, S., Zhang, N., Comerford, S. A., Gayyed, Mariana F., Anders, R. A., Maitra, A., and Pan, D. (2007) Elucidation of a Universal Size-Control Mechanism in Drosophila and Mammals. *Cell* **130**, 1120-1133

170. Aragona, M., Panciera, T., Manfrin, A., Giulitti, S., Michielin, F., Elvassore, N., Dupont, S., and Piccolo, S. (2013) A Mechanical Checkpoint Controls

Multicellular Growth through YAP/TAZ Regulation by Actin-Processing Factors. *Cell* **154**, 1047-1059

171. Yu, F.-X., Zhao, B., Panupinthu, N., Jewell, Jenna L., Lian, I., Wang, Lloyd H., Zhao, J., Yuan, H., Tumaneng, K., Li, H., Fu, X.-D., Mills, Gordon B., and Guan, K.-L. (2012) Regulation of the Hippo-YAP Pathway by G-Protein-Coupled Receptor Signaling. *Cell* **150**, 780-791

172. Chrzanowska-Wodnicka, M., and Burridge, K. (1996) Rho-stimulated contractility drives the formation of stress fibers and focal adhesions. *The Journal of Cell Biology* **133**, 1403-1415

173. Ridley, A. J., and Hall, A. (1992) Distinct patterns of actin organization regulated by the small GTP- binding proteins Rac and Rho. *Cold Spring Harbor Symposia on Quantitative Biology* **57**, 661-672

174. Reginensi, A., Scott, R. P., Gregorieff, A., Bagherie-Lachidan, M., Chung, C., Lim, D.-S., Pawson, T., Wrana, J., and McNeill, H. (2013) Yap- and Cdc42-Dependent Nephrogenesis and Morphogenesis during Mouse Kidney Development. *PLoS Genetics* **9**, e1003380

175. Porazinski, S., Wang, H., Asaoka, Y., Behrndt, M., Miyamoto, T., Morita, H., Hata, S., Sasaki, T., Krens, S. F. G., Osada, Y., Asaka, S., Momoi, A., Linton, S., Miesfeld, J. B., Link, B. A., Senga, T., Castillo-Morales, A., Urrutia, A. O., Shimizu, N., Nagase, H., Matsuura, S., Bagby, S., Kondoh, H., Nishina, H., Heisenberg, C.-P., and Furutani-Seiki, M. (2015) YAP is essential for tissue tension to ensure vertebrate 3D body shape. *Nature* **521**, 217-221

176. Liu-Chittenden, Y., Huang, B., Shim, J. S., Chen, Q., Lee, S.-J., Anders, R. A., Liu, J. O., and Pan, D. (2012) Genetic and pharmacological disruption of the TEAD–YAP complex suppresses the oncogenic activity of YAP. *Genes & Development* **26**, 1300-1305

177. Wells, C. D., Fawcett, J. P., Traweger, A., Yamanaka, Y., Goudreault, M., Elder, K., Kulkarni, S., Gish, G., Virag, C., Lim, C., Colwill, K., Starostine, A., Metalnikov, P., and Pawson, T. (2006) A Rich1/Amot Complex Regulates the Cdc42 GTPase and Apical-Polarity Proteins in Epithelial Cells. *Cell* **125**, 535-548

178. Booden, M. A., Siderovski, D. P., and Der, C. J. (2002) Leukemia-associated Rho guanine nucleotide exchange factor promotes Gαq-coupled activation of RhoA. *Molecular and Cellular Biology* **22**, 4053-4061

179. Fukuhara, S., Murga, C., Zohar, M., Igishi, T., and Gutkind, J. S. (1999) A Novel PDZ Domain Containing Guanine Nucleotide Exchange Factor Links Heterotrimeric G Proteins to Rho. *Journal of Biological Chemistry* **274**, 5868-5879

180. Hart, M. J., Jiang, X., Kozasa, T., Roscoe, W., Singer, W. D., Gilman, A. G., Sternweis, P. C., and Bollag, G. (1998) Direct Stimulation of the Guanine Nucleotide Exchange Activity of p115 RhoGEF by Gα13. *Science* **280**, 2112-2114

181. Kimura, K., Tsuji, T., Takada, Y., Miki, T., and Narumiya, S. (2000) Accumulation of GTP-bound RhoA during Cytokinesis and a Critical Role of ECT2 in This Accumulation. *Journal of Biological Chemistry* **275**, 17233-17236

182. Crespo, P., Schuebel, K. E., Ostrom, A. A., Gutkind, J. S., and Bustelo, X. R. (1997) Phosphotyrosine-dependent activation of Rac-1 GDP/GTP exchange by the vav proto-oncogene product. *Nature* **385**, 169-172

183. Welch, H. C. E., Coadwell, W. J., Ellson, C. D., Ferguson, G. J., Andrews, S. R., Erdjument-Bromage, H., Tempst, P., Hawkins, P. T., and Stephens, L. R. (2002) P-Rex1, a PtdIns(3,4,5)P3- and Gβγ-Regulated Guanine-Nucleotide Exchange Factor for Rac. *Cell* **108**, 809-821

184. Ren, Y., Li, R., Zheng, Y., and Busch, H. (1998) Cloning and Characterization of GEF-H1, a Microtubule-associated Guanine Nucleotide Exchange Factor for Rac and Rho GTPases. *Journal of Biological Chemistry* **273**, 34954-34960

185. Hussain, N. K., Jenna, S., Glogauer, M., Quinn, C. C., Wasiak, S., Guipponi, M., Antonarakis, S. E., Kay, B. K., Stossel, T. P., Lamarche-Vane, N., and McPherson, P. S. (2001) Endocytic protein intersectin-l regulates actin assembly via Cdc42 and N-WASP. *Nat Cell Biol* **3**, 927-932

186. Durkin, M. E., Ullmannova, V., Guan, M., and Popescu, N. C. (2007) Deleted in liver cancer 3 (DLC-3), a novel Rho GTPase-activating protein, is downregulated in cancer and inhibits tumor cell growth. *Oncogene* **26**, 4580-4589

187. Kozasa, T., Jiang, X., Hart, M. J., Sternweis, P. M., Singer, W. D., Gilman, A. G., Bollag, G., and Sternweis, P. C. (1998) p115 RhoGEF, a GTPase Activating Protein for Gα12 and Gα13. *Science* **280**, 2109-2111

188. Gohla, A., Harhammer, R., and Schultz, G. (1998) The G-protein G13 but Not G12 Mediates Signaling from Lysophosphatidic Acid Receptor via Epidermal Growth Factor Receptor to Rho. *Journal of Biological Chemistry* **273**, 4653-4659

189. Wells, C. D., Liu, M. Y., Jackson, M., Gutowski, S., Sternweis, P. M., Rothstein, J. D., Kozasa, T., and Sternweis, P. C. (2002) Mechanisms for reversible regulation between G13 and Rho exchange factors. *J Biol Chem* **277**, 1174-1181

190. Wells, C. D., Gutowski, S., Bollag, G., and Sternweis, P. C. (2001) Identification of potential mechanisms for regulation of p115 RhoGEF through analysis of endogenous and mutant forms of the exchange factor. *J Biol Chem* **276**, 28897-28905

191. Carter, A. M., Gutowski, S., and Sternweis, P. C. (2014) Regulated Localization Is Sufficient for Hormonal Control of Regulator of G Protein Signaling Homology Rho Guanine Nucleotide Exchange Factors (RH-RhoGEFs). *Journal of Biological Chemistry* **289**, 19737-19746

192. Siehler, S., and Manning, D. R. (2002) Pathways of transduction engaged by sphingosine 1-phosphate through G protein-coupled receptors. *Biochimica et Biophysica Acta (BBA) - Molecular and Cell Biology of Lipids* **1582**, 94-99

193. Debily, M. A., Camarca, A., Ciullo, M., Mayer, C., El Marhomy, S., Ba, I., Jalil, A., Anzisi, A., Guardiola, J., and Piatier-Tonneau, D. (2004) Expression and molecular characterization of alternative transcripts of the ARHGEF5/TIM oncogene specific for human breast cancer. *Hum Mol Genet* **13**, 323-334

194. He, P., Wu, W., Yang, K., Tan, D., Tang, M., Liu, H., Wu, T., Zhang, S., and Wang, H. (2015) Rho Guanine Nucleotide Exchange Factor 5 Increases Lung Cancer Cell Tumorigenesis via MMP-2 and Cyclin D1 Upregulation. *Mol Cancer Ther* **14**, 1671-1679

195. Bui, D. A., Lee, W., White, A. E., Harper, J. W., Schackmann, R. C., Overholtzer, M., Selfors, L. M., and Brugge, J. S. (2016) Cytokinesis involves a nontranscriptional function of the Hippo pathway effector YAP. *Sci Signal* **9**, ra23

196. Dubois, F., Keller, M., Calvayrac, O., Soncin, F., Hoa, L., Hergovich, A., Parrini, M.-C., Mazieres, J., Vaisse-Lesteven, M., Camonis, J., Levallet, G., and Zalcman, G. (2016) RASSF1A suppresses the invasion and metastatic potential of human non-small cell lung cancer cells by inhibiting YAP activation through the GEF-H1/RhoB pathway. *Cancer Research*

197. Chow, C. R., Suzuki, N., Kawamura, T., Hamakubo, T., and Kozasa, T. (2013) Modification of p115RhoGEF Ser330 regulates its RhoGEF activity. *Cellular Signalling* **25**, 2085-2092

198. Serrano, M., Lin, A. W., McCurrach, M. E., Beach, D., and Lowe, S. W. (1997) Oncogenic ras Provokes Premature Cell Senescence Associated with Accumulation of p53 and p16INK4a. *Cell* **88**, 593-602

199. Imai, Y., Takahashi, A., Hanyu, A., Hori, S., Sato, S., Naka, K., Hirao, A., Ohtani, N., and Hara, E. (2014) Crosstalk between the Rb Pathway and AKT Signaling Forms a Quiescence-Senescence Switch. *Cell Reports* **7**, 194-207

200. Offermanns, S., Mancino, V., Revel, J.-P., and Simon, M. I. (1997) Vascular System Defects and Impaired Cell Chemokinesis as a Result of Gα13 Deficiency. *Science* **275**, 533-536

201. Zhao, B., Li, L., Wang, L., Wang, C.-Y., Yu, J., and Guan, K.-L. (2012) Cell detachment activates the Hippo pathway via cytoskeleton reorganization to induce anoikis. *Genes & Development* **26**, 54-68

202. Zhao, B., Li, L., Lei, Q., and Guan, K.-L. (2010) The Hippo–YAP pathway in organ size control and tumorigenesis: an updated version. *Genes & Development* **24**, 862-874

203. Steinhardt, A. A., Gayyed, M. F., Klein, A. P., Dong, J., Maitra, A., Pan, D., Montgomery, E. A., and Anders, R. A. (2008) Expression of Yes-associated protein in common solid tumors. *Human Pathology* **39**, 1582-1589

204. Burbelo, P. D., Miyamoto, S., Utani, A., Brill, S., Yamada, K. M., Hall, A., and Yamada, Y. (1995) p190-B, a new member of the Rho GAP family, and Rho are induced to cluster after integrin cross-linking. *Journal of Biological Chemistry* **270**, 30919-30926

205. Wang, H.-y., Kanungo, J., and Malbon, C. C. (2002) Expression of Gα13 (Q226L) Induces P19 Stem Cells to Primitive Endoderm via MEKK1, 2, or 4. *Journal of Biological Chemistry* **277**, 3530-3536

206. Collins, L. R., Minden, A., Karin, M., and Brown, J. H. (1996) Gα12 Stimulates c-Jun NH2-terminal Kinase through the Small G Proteins Ras and Rac. *Journal of Biological Chemistry* **271**, 17349-17353

207. Essers, J., Theil, A. F., Baldeyron, C., van Cappellen, W. A., Houtsmuller, A. B., Kanaar, R., and Vermeulen, W. (2005) Nuclear Dynamics of PCNA in DNA Replication and Repair. *Molecular and Cellular Biology* **25**, 9350-9359

208. Alessi, D. R., James, S. R., Downes, C. P., Holmes, A. B., Gaffney, P. R. J., Reese, C. B., and Cohen, P. (1997) Characterization of a 3-phosphoinositide-dependent protein kinase which phosphorylates and activates protein kinase Bα. *Current Biology* **7**, 261-269

209. Sarbassov, D. D., Guertin, D. A., Ali, S. M., and Sabatini, D. M. (2005) Phosphorylation and Regulation of Akt/PKB by the Rictor-mTOR Complex. *Science* **307**, 1098-1101

210. Dan, H. C., Sun, M., Yang, L., Feldman, R. I., Sui, X.-M., Ou, C. C., Nellist, M., Yeung, R. S., Halley, D. J. J., Nicosia, S. V., Pledger, W. J., and Cheng, J. Q. (2002) Phosphatidylinositol 3-Kinase/Akt Pathway Regulates Tuberous Sclerosis Tumor Suppressor Complex by Phosphorylation of Tuberin. *Journal of Biological Chemistry* **277**, 35364-35370

211. Zhang, Y., Gao, X., Saucedo, L. J., Ru, B., Edgar, B. A., and Pan, D. (2003) Rheb is a direct target of the tuberous sclerosis tumour suppressor proteins. *Nat Cell Biol* **5**, 578-581

212. Long, X., Lin, Y., Ortiz-Vega, S., Yonezawa, K., and Avruch, J. (2005) Rheb Binds and Regulates the mTOR Kinase. *Current Biology* **15**, 702-713

213. Prigent, S. A., and Gullick, W. J. (1994) Identification of c-erbB-3 binding sites for phosphatidylinositol 3'-kinase and SHC using an EGF receptor/c-erbB-3 chimera. *The EMBO Journal* **13**, 2831-2841

214. Inoki, K., Zhu, T., and Guan, K.-L. (2003) TSC2 Mediates Cellular Energy Response to Control Cell Growth and Survival. *Cell* **115**, 577-590

215. Ma, X. M., and Blenis, J. (2009) Molecular mechanisms of mTOR-mediated translational control. *Nat Rev Mol Cell Biol* **10**, 307-318

216. Kimura, K., Ito, M., Amano, M., Chihara, K., Fukata, Y., Nakafuku, M., Yamamori, B., Feng, J., Nakano, T., Okawa, K., Iwamatsu, A., and Kaibuchi, K. (1996) Regulation of Myosin Phosphatase by Rho and Rho-Associated Kinase (Rho-Kinase). *Science* **273**, 245-248

217. Amano, M., Ito, M., Kimura, K., Fukata, Y., Chihara, K., Nakano, T., Matsuura, Y., and Kaibuchi, K. (1996) Phosphorylation and Activation of Myosin by Rho-associated Kinase (Rho-kinase). *Journal of Biological Chemistry* **271**, 20246-20249

218. Ohashi, K., Nagata, K., Maekawa, M., Ishizaki, T., Narumiya, S., and Mizuno, K. (2000) Rho-associated Kinase ROCK Activates LIM-kinase 1 by Phosphorylation at Threonine 508 within the Activation Loop. *Journal of Biological Chemistry* **275**, 3577-3582

219. Nakano, K., Takaishi, K., Kodama, A., Mammoto, A., Shiozaki, H., Monden, M., and Takai, Y. (1999) Distinct Actions and Cooperative Roles of ROCK and mDia in Rho Small G Protein-induced Reorganization of the Actin Cytoskeleton in Madin–Darby Canine Kidney Cells. *Molecular Biology of the Cell* **10**, 2481-2491

220. Astle, M. V., Hannan, K. M., Ng, P. Y., Lee, R. S., George, A. J., Hsu, A. K., Haupt, Y., Hannan, R. D., and Pearson, R. B. (2012) AKT induces senescence in human cells via mTORC1 and p53 in the absence of DNA damage: implications for targeting mTOR during malignancy. *Oncogene* **31**, 1949-1962

221. Hofmann, W. A., Stojiljkovic, L., Fuchsova, B., Vargas, G. M., Mavrommatis, E., Philimonenko, V., Kysela, K., Goodrich, J. A., Lessard, J. L., Hope, T. J., Hozak, P., and de Lanerolle, P. (2004) Actin is part of pre-initiation complexes and is necessary for transcription by RNA polymerase II. *Nat Cell Biol* **6**, 1094-1101

222. Tomlinson, V., Gudmundsdottir, K., Luong, P., Leung, K. Y., Knebel, A., and Basu, S. (2010) JNK phosphorylates Yes-associated protein (YAP) to regulate apoptosis. *Cell Death & Disease* **1**, e29

223. Dubash, A. D., Wennerberg, K., García-Mata, R., Menold, M. M., Arthur, W. T., and Burridge, K. (2007) A novel role for Lsc/p115 RhoGEF and LARG in regulating RhoA activity downstream of adhesion to fibronectin. *Journal of Cell Science* **120**, 3989-3998

224. Chikumi, H., Fukuhara, S., and Gutkind, J. S. (2002) Regulation of G protein-linked guanine nucleotide exchange factors for Rho, PDZ-RhoGEF, and LARG by tyrosine phosphorylation: Evidence of a role for focal adhesion kinase. *Journal of Biological Chemistry* **277**, 12463-12473

225. Hata, S., Hirayama, J., Kajiho, H., Nakagawa, K., Hata, Y., Katada, T., Furutani-Seiki, M., and Nishina, H. (2012) A Novel Acetylation Cycle of Transcription Co-activator Yes-associated Protein That Is Downstream of Hippo Pathway Is Triggered in Response to SN2 Alkylating Agents. *Journal of Biological Chemistry* **287**, 22089-22098

226. Lapi, E., Di Agostino, S., Donzelli, S., Gal, H., Domany, E., Rechavi, G., Pandolfi, P. P., Givol, D., Strano, S., Lu, X., and Blandino, G. PML, YAP, and p73 Are Components of a Proapoptotic Autoregulatory Feedback Loop. *Molecular Cell* **32**, 803-814

227. El-Deiry, W. S., Tokino, T., Velculescu, V. E., Levy, D. B., Parsons, R., Trent, J. M., Lin, D., Mercer, W. E., Kinzler, K. W., and Vogelstein, B. (1993) WAF1, a potential mediator of p53 tumor suppression. *Cell* **75**, 817-825

228. Tang, W., Willers, H., and Powell, S. N. (1999) p53 Directly Enhances Rejoining of DNA Double-Strand Breaks with Cohesive Ends in γ-Irradiated Mouse Fibroblasts. *Cancer Research* **59**, 2562-2565

229. Iyer, N. G., Chin, S.-F., Ozdag, H., Daigo, Y., Hu, D.-E., Cariati, M., Brindle, K., Aparicio, S., and Caldas, C. (2004) p300 regulates p53-dependent apoptosis after DNA damage in colorectal cancer cells by modulation of PUMA/p21 levels. *Proceedings of the National Academy of Sciences of the United States of America* **101**, 7386-7391

230. Yu, J., Wang, Z., Kinzler, K. W., Vogelstein, B., and Zhang, L. (2003) PUMA mediates the apoptotic response to p53 in colorectal cancer cells. *Proceedings of the National Academy of Sciences* **100**, 1931-1936

231. Hanahan, D., and Weinberg, R. A. (2000) The Hallmarks of Cancer. *Cell* **100**, 57-70

232. Fernández-Medarde, A., and Santos, E. (2011) Ras in Cancer and Developmental Diseases. *Genes & Cancer* **2**, 344-358

233. Zhu, J., Woods, D., McMahon, M., and Bishop, J. M. (1998) Senescence of human fibroblasts induced by oncogenic Raf. *Genes & Development* **12**, 2997-3007

234. Lu, X., Errington, J., Curtin, N. J., Lunec, J., and Newell, D. R. (2001) <div xmlns="http://www.w3.org/1999/xhtml Impact of p53 Status on Cellular Sensitivity to Antifolate Drugs . *Clinical Cancer Research* **7**, 2114-2123

235. Olivier, M., Eeles, R., Hollstein, M., Khan, M. A., Harris, C. C., and Hainaut, P. (2002) The IARC TP53 database: New online mutation analysis and recommendations to users. *Human Mutation* **19**, 607-614

236. Posey, S. C., and Bierer, B. E. (1999) Actin Stabilization by Jasplakinolide Enhances Apoptosis Induced by Cytokine Deprivation. *Journal of Biological Chemistry* **274**, 4259-4265

237. Esnault, C., Stewart, A., Gualdrini, F., East, P., Horswell, S., Matthews, N., and Treisman, R. (2014) Rho-actin signaling to the MRTF coactivators dominates the immediate transcriptional response to serum in fibroblasts. *Genes & Development* **28**, 943-958

238. Machesky, L. M., and Hall, A. (1997) Role of Actin Polymerization and Adhesion to Extracellular Matrix in Rac- and Rho-induced Cytoskeletal Reorganization. *The Journal of Cell Biology* **138**, 913-926

239. Bernstein, B. W., and Bamburg, J. R. (2003) Actin-ATP Hydrolysis Is a Major Energy Drain for Neurons. *The Journal of Neuroscience* **23**, 1-6

240. Mana-Capelli, S., Paramasivam, M., Dutta, S., and McCollum, D. (2014) Angiomotins link F-actin architecture to Hippo pathway signaling. *Molecular Biology of the Cell* **25**, 1686-1697

241. Parsons, J. T., Horwitz, A. R., and Schwartz, M. A. (2010) Cell adhesion: integrating cytoskeletal dynamics and cellular tension. *Nature reviews. Molecular cell biology* **11**, 633-643

242. Noren, N. K., Arthur, W. T., and Burridge, K. (2003) Cadherin engagement inhibits RhoA via p190RhoGAP. *Journal of Biological Chemistry* **278**, 13615-13618

243. Kher, S. S., Struckhoff, A. P., Alberts, A. S., and Worthylake, R. A. (2014) A novel role for p115RhoGEF in regulation of epithelial plasticity. *PLoS ONE* **9**

244. Guilluy, C., Bregeon, J., Toumaniantz, G., Rolli-Derkinderen, M., Retailleau, K., Loufrani, L., Henrion, D., Scalbert, E., Bril, A., Torres, R. M., Offermanns, S., Pacaud, P., and Loirand, G. (2010) The Rho exchange factor Arhgef1 mediates the effects of angiotensin II on vascular tone and blood pressure. *Nat Med* **16**, 183-190

245. Chikumi, H., Barac, A., Behbahani, B., Gao, Y., Teramoto, H., Zheng, Y., and Gutkind, J. S. (2004) Homo- and hetero-oligomerization of PDZ-RhoGEF, LARG and p115RhoGEF by their C-terminal region regulates their in vivo Rho GEF activity and transforming potential. *Oncogene* **23**, 233-240

246. Levy, D., Adamovich, Y., Reuven, N., and Shaul, Y. (2006) The Yes-associated protein 1 stabilizes p73 by preventing Itch-mediated ubiquitination of p73. *Cell Death Differ* **14**, 743-751

247. Mo, J.-S., Meng, Z., Kim, Y. C., Park, H. W., Hansen, C. G., Kim, S., Lim, D.-S., and Guan, K.-L. (2015) Cellular energy stress induces AMPK-mediated regulation of YAP and the Hippo pathway. *Nat Cell Biol* **17**, 500-510

248. Kapoor, A., Yao, W., Ying, H., Hua, S., Liewen, A., Wang, Q., Zhong, Y., Wu, C.-J., Sadanandam, A., Hu, B., Chang, Q., Chu, Gerald C., Al-Khalil, R., Jiang, S., Xia, H., Fletcher-Sananikone, E., Lim, C., Horwitz, Gillian I., Viale, A., Pettazzoni, P., Sanchez, N., Wang, H., Protopopov, A., Zhang, J., Heffernan, T., Johnson, Randy L., Chin, L., Wang, Y. A., Draetta, G., and DePinho, Ronald A. (2014) Yap1 Activation Enables Bypass of Oncogenic Kras Addiction in Pancreatic Cancer. *Cell* **158**, 185-197

249. Shao, D., Zhai, P., Del Re, D. P., Sciarretta, S., Yabuta, N., Nojima, H., Lim, D.-S., Pan, D., and Sadoshima, J. (2014) A functional interaction between Hippo-YAP signalling and FoxO1 mediates the oxidative stress response. *Nat Commun* **5**

250. Lin, L., Sabnis, A. J., Chan, E., Olivas, V., Cade, L., Pazarentzos, E., Asthana, S., Neel, D., Yan, J. J., Lu, X., Pham, L., Wang, M. M., Karachaliou, N., Cao, M. G., Manzano, J. L., Ramirez, J. L., Torres, J. M. S., Buttitta, F., Rudin, C. M., Collisson, E. A., Algazi, A., Robinson, E., Osman, I., Munoz-Couselo, E., Cortes, J., Frederick, D. T., Cooper, Z. A., McMahon, M., Marchetti, A., Rosell, R., Flaherty, K. T., Wargo, J. A., and Bivona, T. G. (2015) The Hippo effector YAP promotes resistance to RAF- and MEK-targeted cancer therapies. *Nat Genet* **47**, 250-256

251. Bottino, J., Gelaleti, G. B., Maschio, L. B., Jardim-Perassi, B. V., and de Campos Zuccari, D. A. P. (2014) Immunoexpression of ROCK-1 and MMP-9 as prognostic markers in breast cancer. *Acta Histochemica* **116**, 1367-1373

252. Gilkes, D. M., Xiang, L., Lee, S. J., Chaturvedi, P., Hubbi, M. E., Wirtz, D., and Semenza, G. L. (2014) Hypoxia-inducible factors mediate coordinated RhoA-ROCK1 expression and signaling in breast cancer cells. *Proceedings of the National Academy of Sciences* **111**, E384-E393

253. Ma, L., Liu, Y.-p., Geng, C.-z., Wang, X.-l., Wang, Y.-j., and Zhang, X.-h. (2010) Over Expression of RhoA is Associated with Progression in Invasive Breast Duct Carcinoma. *The Breast Journal* **16**, 105-107

254. Matsubara, M., and Bissell, M. J. (2016) *Inhibitors of Rho kinase (ROCK) signaling revert the malignant phenotype of breast cancer cells in 3D context*,

# CURRICULUM VITAE

**Brandon S. Lane**

## EDUCATION:

| | | |
|---|---|---|
| 2017 | Ph.D. | Indiana University, Indianapolis, Indiana<br>Department of Biochemistry and Molecular Biology<br>Dissertation: The Regulation of the Serum Response Network by the RGS-RhoGEFs is Critical for YAP1 Activity and Cell Fate Decisions |
| 2010 | B.S. | University of Indianapolis<br>Indianapolis, Indiana |

## RESEARCH POSITIONS:

| | |
|---|---|
| 2010-2016 | Doctoral Research: Breast Cancer Researcher, Indiana University School of Medicine<br>Defined the role of RGS-RhoGEFs in contributing to YAP1 activity |
| 2010 | Post baccalaureate Research: Methodist Research Institute, Indianapolis, Indiana |
| 2009-2010 | Undergraduate Research: Eli Lilly Company, Indianapolis, Indiana<br>Developed an in vivo social competition model to screen preclinical antidepressants |

## PUBLICATIONS:

**Lane BS**, Heller B, Wells CD. "The RGS-RhoGEFs Coordinate Serum Initiated Signaling onto the Regulation of RhoA Dependent YAP1 Activity." (Manuscript under review).

**Lane BS,** Heller B, Wells CD**. "**ArhGEF1 Cyclic Regulation of $G\alpha_{13}$ is essential for maintaining cellular homeostasis." (Manuscript in preparation).

He R, Yu ZH, Zhang RY, Wu L, Gunawan AM, **Lane BS**, Shim JS, Zeng LF, He Y, Chen L, Wells CD, Liu JO, Zhang ZY. "Exploring the Existing Drug Space for Novel pTyr Mimetic and SHP2 Inhibitors." *American Chemical Society Medicinal Chemistry Letters*. 6 (June 2015), 782-786.

Zeng LF, Zhang RY, Yu ZH, Li S, Wu L, Gunawan AM, **Lane BS**, Mali RS, Li X, Chan RJ, Kapur R, Wells CD, Zhang ZY. "Therapeutic potential of targeting the oncogenic SHP2 phosphatase." *Journal of Medicinal Chemistry*. 57 (August 2014), 6594-609.

Thyagarajan-Sahu, A, **Lane BS**, Silva D. "ReishiMax, mushroom based dietary supplement, inhibits adipocyte differentiation, stimulates glucose uptake and activates AMPK." *BMC Complement Alternative Medicine.* 74 (September 2011).

## PROFESSIONAL PRESENTATIONS:

American Society for Cell Biology. **Poster**: "rgsRhoGEFs coordinately mediate serum induced YAP-dependent growth" (December 2016).

Department of Biochemistry & Molecular Biology Research Day. **Poster**. "rgsRhoGEFs coordinately mediate serum induced YAP-dependent growth" (September 2014).

## RESEARCH BASED SKILLS:

2D & 3D Mammalian Cell Culture
Transfections & Reverse Transfections
Gene Expression and knockdown using lenti viral system
Genome Editing using CRISPR/Cas9
SDS resolution of proteins from both 2D & 3D cell cultures
Immunoprecipitations
Cellular fractionations including both nuclear and actin sedimentation
RNA Extraction & qRTPCR from both 2D and 3D cell cultures
RNASeq Analysis
RPPA Analysis
Fixed Cell and live cell imaging
Dual Luciferase Reporter Systems
Cloning/Subcloning using PCR and gBlock based techniques
PCR based site directed mutagenesis
Microsoft: Word, Excel, and PowerPoint
Adobe: Photoshop, Illustrator, Acrobat Pro